UNIVERSITÉ DE STRASBOURG

ÉCOLE DOCTORALE DES SCIENCES CHIMIQUES

Institut de Chimie et Procédés pour l'Énergie, l'Environnement et la Santé

THÈSE présentée par :

Diego RUA GONZALEZ

soutenue le : **9 février 2024**

pour obtenir le grade de : **Docteur de l'université de Strasbourg**

Discipline/Spécialité : Chimie/Catalyse hétérogène

Synthèse de matériaux catalytiques de type oxydes mixtes pour la production de méthanol par la précipitation en flux continu en système microfluidique

THÈSE dirigée par :

Mme ROGER Anne-Cécile	Professeur, Université de Strasbourg (ICPEES)

RAPPORTEURS :

Mme BATIOT-DUPEYRAT Catherine	Professeur, Université de Poitiers (IC2MP)
M. VARGAS Julio César	Professeur, Université Nationale de Colombie

---

AUTRES MEMBRES DU JURY :

M. PAUL Sébastien	Professeur, Centrale Lille (UCCS)
Mme PARKHOMENKO Ksenia	Chargée de Recherche, Université de Strasbourg (ICPEES)

Acknowledgements

I would like to thank all of the people that I met who helped me during this unforgettable stage of my life. I also acknowledge the financial support of the Ministry of Sciences of Colombia, which allowed me to follow PhD studies and also to live for a few years in a beautiful country with an admirable culture and way of living. It was a learning experience from all points of view.

I'd like to express my gratitude to professor Anne-Cécile Roger and Dr. Ksenia Parkhomenko for their guidance and teachings during these 3 years and for receiving me in their laboratory.

I would also like to thank Clémence Aun for her support during all the thesis. Her help was indispensable to make all the equipment work correctly. The support of the personnel in charge of the materials characterizations is also greatly appreciated: Thierry Dintzer for XRD, Fabrice Vigneron for N_2-physisorption analysis, Thierry Romero for the SEM-EDS, Christophe Mélart for TGA and FT-IR, Christophe Sutter for technical support and Sécou Sall for CO_2-TPD analysis.

I'm also grateful to my colleagues in the laboratory and the people I met in Strasbourg for their help and support both at the lab and outside of it: Zama, Camila, Chaimae, Arno, Zinab, Camille, François, Morvan, Vincent, Murad, Xiong, Qianwen, Yu, Senlin, Xi.

And last but not least, the support and love of my family and friends in Colombia, even from a long distance, were indispensable to finish this work.

Contents

List of figures

List of tables

List of equations

Chapter 1 General introduction and thesis objectives

1.1. Context

1.1.1. Energy consumption and climate change

Climate change and global warming have been on the world agenda for several decades, but recently, society has become more concerned about them, as there's a growing body of evidence about drastic weather changes in the world, and a mounting occurrence of natural disasters and other phenomena that affect the environment, societies and economies, especially in developing countries.

It is thought that the magnitude of these events will increase, as more greenhouse gases are released into the atmosphere. These are mainly released during human activities, such as the burning of fossil fuels for transport and energy purposes (i.e. electricity production, heating and cooling, etc.), during agricultural and industrial activities and to a lesser extent because of the decomposition of solid and liquid organic wastes [1].

The most representative greenhouse gases are carbon dioxide, methane, nitrous oxide and many different fluorinated gases [1]. They have different impacts on the environment, the atmosphere chemistry and contribute differently to the greenhouse effect. The global warming potential (GWP) is the property used to measure the impact of any of these substances on the greenhouse effect, and it takes into account the amount of energy that a substance can absorb compared to that of carbon dioxide, and also how much time the substance persists in the atmosphere [2]. This property is shown in Table 1.1 for some known greenhouse gases.

Table 1.1 Global warming potential of different greenhouse gases.

Substance name	Global warming potential (GWP)		
	20 years	100 years	500 years
Carbon dioxide	1	1	1
Methane	56	21	6.5
Nitrous oxide	280	310	170
Hydrofluorocarbon-23	9100	11700	9800

Sources: [1], [2].

Even though CO_2 is shown as the reference value in the above table, this gas persists in the atmosphere for a long time, therefore its emissions are concerning. Other gases such as Chlorofluorocarbons, hydrofluorocarbons, hydrochlorofluorocarbons, among other similar substances have very high GWP values, which make them very contaminating and they can also interact with the atmosphere ozone.

The atmospheric CO_2 concentration has been increasing steadily since many decades. It has increased from a value of 212 ppm in 1958 to a value of 408 ppm in 2019, and 445 ppm in 2021 [3]–[5]. These high CO_2 concentrations exceed the

maximum level of 300 ppm of CO_2 occurring on earth since millennia [6]. Therefore, the use and recycling of CO_2 can be considered as an important alternative to help tackle the climate change [4], [7].

In 2018 the global consumption of energy increased due to economic growth and higher heating and cooling needs, which also caused an increase in the demand for natural gas and other sources of energy [8]. That year, the increase in electricity demand was responsible for over half of the growth in energy needs [8]. According to the International Energy Agency, in 2020 the total final consumption of energy in the world was 9938 tons of oil equivalent (Mtoe) [9]. In the same year, most of the world energy demand was met by the use of fossil fuels, namely crude oil with a share of 40.8%, natural gas with a share of 16.2%, and coal with a share of 10% [9], which sum up to 67% of the world energy demand. The remaining percentage corresponds to electricity with a share of 19.3%, biofuels and waste with a share of 10.2%, and a 3.5% share corresponding to other energy sources, which include heat, solar thermal and geothermal energy [9]. Moreover, a 64.2% of the aforementioned electricity share is generated mostly by the use of fossil fuels too (i.e. 38.2% coal, 23.1% natural gas and 2.9% oil) while 15.8% is generated by the use of hydroelectric plants, 10.2% by nuclear and 9.8% of non-hydro renewables and waste [9]. It is clear that the emissions of CO_2 from fossil fuels are a significant contributor to climate change and global warming [10]. These statistics also show that societies around the world are strongly dependent on fossil fuels, which are a polluting and non-renewable source of energy. Figure 1.1 shows the share of energy sources used to satisfy the global energy demand in 2020.

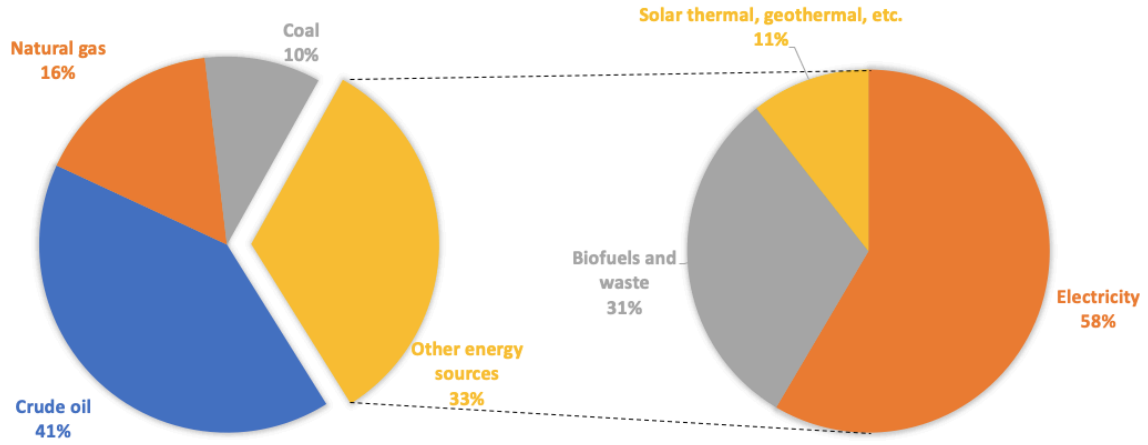

Figure 1.1 Share of energy sources used to satisfy the global energy demand in 2020 on the left and composition of the “Other energy sources” on the right [9].

The consumption of energy is expected to increase worldwide, in part as a consequence of the growing global population, the change in people’s consumption habits and the improvement in the quality of life in certain countries. Higher consumption of goods and services by the global population, will undoubtedly increase the energy consumption of factories and businesses. Statistical data shows the world CO_2-equivalent emissions by sector [11] for the year 2020, based on a total emissions

value of 4.84×10^{10} tons of CO_2-equivalent emissions. This data is presented in Figure 1.2.

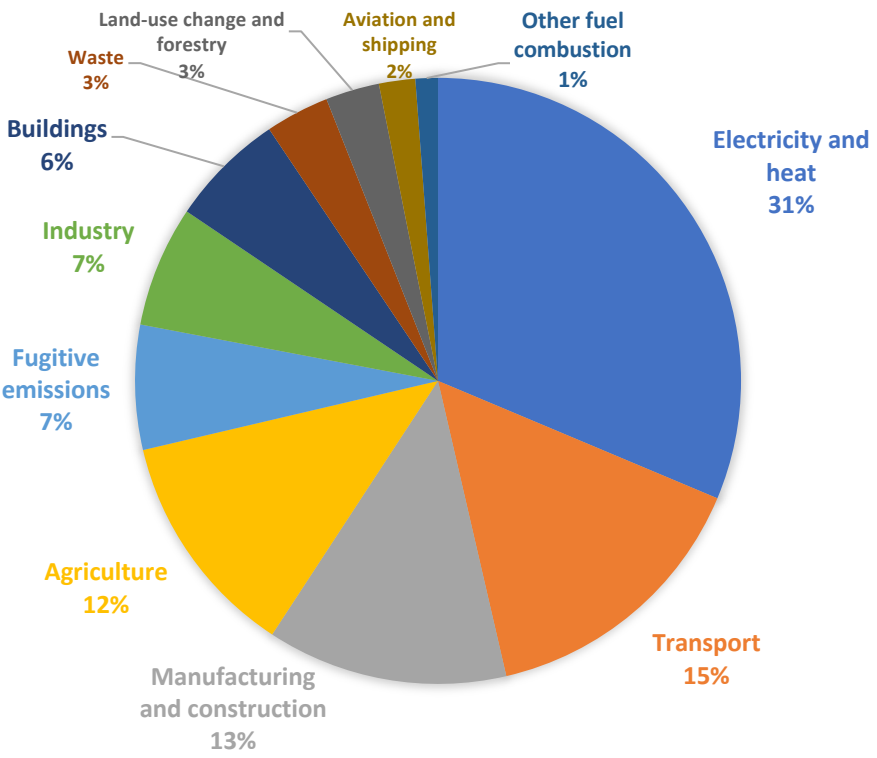

Figure 1.2 Percentage of the tonnes of CO_2-equivalent emissions of the world by sector in 2020 [11].

As can be observed, the electricity and heat sector together with the transport and the manufacturing and construction sector contribute to more than half of the total CO_2-equivalent emissions in 2020 in the world. This highlights the need of reducing the environmental impact of these three sectors by using renewable sources of energy.

In order to delay climate change, many efforts are being made by governments and the private sector. Among them are those focused to transitioning to more environmentally friendly sources of energy for supplying homes, businesses and factories. Other efforts are those focused on improving energy efficiency in the abovementioned sectors, designing more energy efficient production processes and transport means, among others.

Given the importance of electricity for supplying energy needs, renewable electricity sources such as solar and wind have been gaining importance, given their potential to decrease harmful emissions like sulfur oxides (SOx) and nitrogen oxides (NOx) as well as CO_2. Although renewable and more environmentally friendly, these sources of energy suffer from intermittency, which causes the energy supply to be higher or lower than the energy demand, generating excesses of electricity that cannot be stored or deficits in the electric grids.

One way to avoid the loss and waste of electricity due to mismatches between the electricity supply and demand in the electrical grids, is using the so called Power-to-X concept. This way of managing energy consists in converting energy surpluses into various chemicals, heating and cooling, and/or other means to store and use electricity. This concept will be explained more deeply in the next section.

1.1.2. Power-to-X concept

The intermittent nature of renewable energies, such as solar and wind, has led to the conception and development of technologies and strategies capable of using or storing electricity in periods where electricity supply surpasses the demand [12]. Such technologies or strategies could be beneficial due to a reduced waste of energy, and also for economic reasons. The Power-to-X concept aims at converting the energy surpluses from intermittent sources of energy, into chemicals, storing it in different media or giving them other final uses, such as heating and cooling, etc., contributing to reducing the dependence on fossil fuels [10], [13].

Among the chemicals that can be used as energy reservoirs, gases such as hydrogen and methane are desirable due to their interesting properties as fuels. In the case of hydrogen, it could be produced by water electrolysis [14], which can then be used to produce methane via the Sabatier process (i.e. $CO_2 + 4H_2 \rightarrow 2H_2O + CH_4$) [13]. Moreover, both methane and hydrogen could be integrated into the existing gas distribution systems, while hydrogen to a lesser extent [13]. Hydrogen is generally not considered a suitable medium for energy storage because of its undesirable storage properties and difficulty to handle [15].

Methanol can also be produced by the hydrogenation of CO_2. Some researchers sustain that storing energy in the form of methanol can reduce the world's dependence on fossil fuels [16]. Besides its possible use as a fuel, methanol is also a very important chemical due to its interesting properties as a chemical synthesis feedstock. It can be used in mixtures with gasoline, it can be used in fuel cells and a wide variety of commodities and added value chemicals with different uses can be synthesized from it [4], [17]–[21]. Some of the most important chemicals typically produced from it include formaldehyde, methyl tert-butyl ether, acetic acid, methyl methacrylate, dimethyl terephthalate, and methylamines. In turn, these chemicals are used to produce polymers, paints, plastics, resins, among other important products [15][22][23]. More recently, the olefins production (i.e. ethylene and propylene) from methanol has been gaining increasing importance, especially in the Chinese market [23].

According to other researchers [12], the transportation sector is responsible for 80% of the total energy consumption, so integrating the Power-to-X concept to the transport

sector by integrating chemicals such as methanol could be an attractive strategy to increase the efficiency of energy systems and also to reduce emissions of GHG.

The next section deals with the thermodynamics of the production of methanol and discusses the conditions that are favorable for producing this compound.

1.2. Thermodynamics of methanol production

The synthesis of methanol from carbon monoxide and from carbon dioxide are both exothermic reactions that involve a decrease in the number of moles. The other reaction that takes place in the process is the reverse water-gas shift (RWGS) reaction which is endothermic and doesn't present a change in the number of moles of reactants and products [24]. These 3 chemical reactions are shown in Equations 1.1 to 1.3.

Equation 1.1 Methanol synthesis from CO reaction.

$$CO(g) + 2H_2(g) \leftrightarrow CH_3OH\ (g) \quad \Delta rH_{298K} = -90.7\ kJ/mol$$

Equation 1.2 Methanol synthesis from CO_2 reaction.

$$CO_2\ (g) + 3H_2\ (g) \leftrightarrow CH_3OH\ (g) + H_2O(g) \quad \Delta rH_{298K} = -49.5\ kJ/mol$$

Equation 1.3 Reverse water-gas shift reaction (RWGS).

$$CO_2\ (g) + H_2\ (g) \leftrightarrow CO\ (g) + H_2O\ (g) \quad \Delta rH_{298K} = 41.2\ kJ/mol$$

Normally, when using catalysts composed of Cu, Zn, Al, and or Zr, no other carbon containing species such as CH_4 are formed in important quantities. So, the chemistry that occurs during the methanol synthesis process is well represented by the above three chemical equations.

According to Le Chatelier's principle, the equilibrium conversions of the methanol production reactions are favored at low temperatures and high pressures, while the equilibrium conversion of the RWGS reaction is favored at high temperatures with no effect from the reaction pressure [22], [24], [25]. Figure 1.3 shows the effect of the temperature on the equilibrium conversions of H_2 and CO_2 and on the methanol selectivity. These values were calculated by the minimization of the Gibbs free energy of the system by using a process simulator. The results show that the H_2 and CO_2 equilibrium conversions decrease with increasing temperature, while the CO_2 conversion attains a minimum value at approximately 280ºC and then increases again. The occurrence of this minimum can be explained by the decrease of the CO_2 conversion due to the formation of methanol and by the increase of the production of CO from CO_2 via the RWGS reaction. The above also explains the behavior of the methanol selectivity, which decreases with increasing temperatures. The appropriate

temperatures for the production of methanol from CO_2 hydrogenation seem to lie between 200ºC and 300ºC, where the methanol selectivity has values between 95% and 24%, respectively.

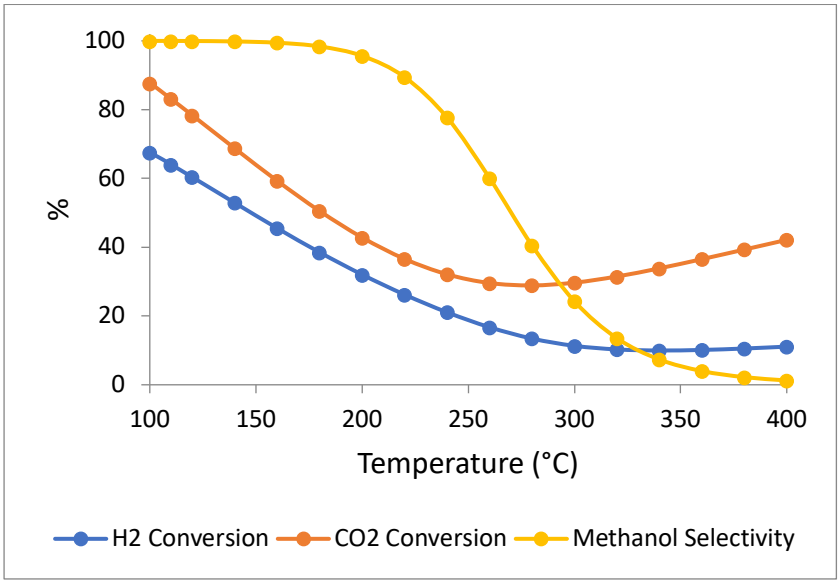

Figure 1.3 Effect of the temperature on the H_2 and CO_2 conversions and on the methanol selectivity at 50 bar.

The effect of the pressure on the equilibrium conversion of a reaction occurs when there's a change in the number of moles on one side of the chemical equation. For instance, in the case of the methanol production reactions presented above, the product side presents the least number of moles, which indicates that the production of methanol is favored at higher pressures. The RWGS reaction doesn't present a change in the number of moles, which indicates that this reaction is unaffected by pressure, as mentioned above.

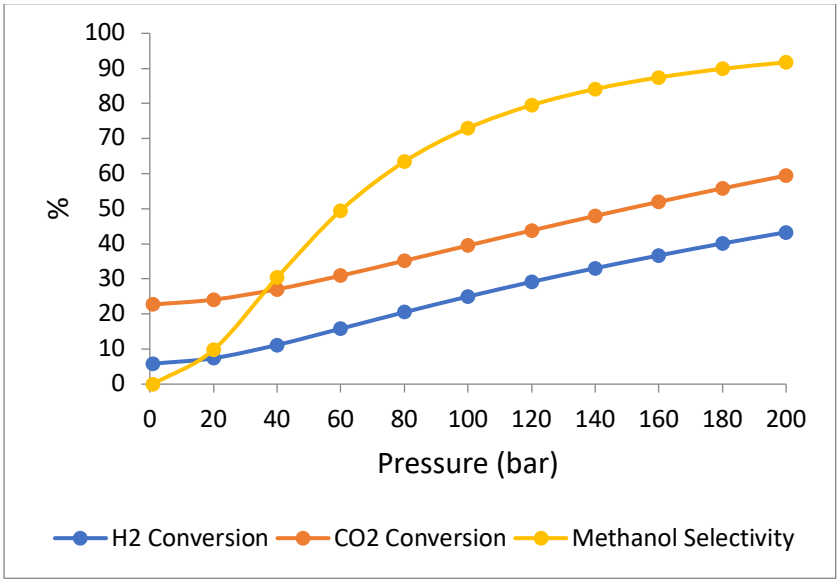

Figure 1.4 Effect of the pressure on the H_2 and CO_2 conversions and on the methanol selectivity at 280ºC.

Figure 1.4 shows that both the H_2 and CO_2 conversions increase with increasing pressure, as well as the methanol selectivity. In the industry, pressures between 50 and 100 bar are typically employed.

The methanol synthesis reactions are considered thermodynamically limited [26]. CO_2 presents the highest oxidation state of the carbon element which makes it a thermodynamically stable compound with low reactivity and a formation enthalpy of -396 kJ/mol [5], [19]. Given the stability of the CO_2 molecule, a large amount of energy is necessary for its reduction or transformation [27].

For instance, the Gibbs free-energy changes are positive above 150ºC for the reaction in Equation 1.1 and above 180ºC for the reaction in Equation 1.2 [24], so it is important to choose the operating conditions with care, in order to obtain an acceptable conversion. Typical operating conditions for these reactions are between 250 and 300ºC, and thanks to the advances in the catalyst development, pressures around 50-80 bar are used industrially.

1.3. Catalysts for methanol production

1.3.1. Catalysts for methanol production from syngas and from carbon dioxide

Methanol production has been traditionally based on the steam reforming of hydrocarbons, typically methane, into synthesis gas and then by the reaction of synthesis gas using a solid catalyst during an exothermic process [19], [28]. The methanol production process has evolved from the use of $ZnO\text{-}Cr_2O_3$ catalysts conceived during the 1920s, which operated at very high temperatures and pressures [29][30], to the modern $CuO\text{-}ZnO\text{-}Al_2O_3$ catalysts that allow the methanol synthesis at milder conditions [18], [24], [31]. Today, alumina is widely employed in the ternary $Cu\text{-}ZnO\text{-}Al_2O_3$ catalysts used in the industry, which are typically prepared by coprecipitation [32][33].

Copper is considered as an abundant and cheap metal, which favors its utilization as a material for catalysis. This metal has been extensively used in the industry and in research, and can be used along with many different types of support, which influence importantly its catalytic activity [7]. Despite the importance of copper in the catalysis for the production of methanol, using only this element as a catalyst is not possible because copper alone does not catalyze the methanol formation reaction [30][32]. Also, copper oxide is more easily reduced under certain conditions and in a dispersed form [30] so, having a mixed oxide system is important for the production of methanol. It is known that zinc oxide can improve copper dispersion of Cu-based catalysts and that it is a good hydrogenation catalyst that activates hydrogen by heterogeneous dissociation, giving rise to ZnH and OH species [28].

The reduction of the operating temperature and pressure in the reactor that has occurred gradually, has resulted in lower capital and operating costs, as well as lower CO_2 emissions. Table 1.2 shows some of the main catalysts that have been developed for methanol production since the first catalysts conceived for this process. It shows the process conditions and some advantages and disadvantages that they presented.

Table 1.2 Evolution of catalysts for methanol synthesis from synthesis gas.

Catalyst composition	**Year of development and/or commercialization**	**Process conditions of the catalyst**	**Catalysts advantages and disadvantages**	**Source**
No catalyst before 1920's	Until 1920's	Methanol was produced by dry distillation of wood	-	[25]
$ZnO\text{-}Cr_2O_3$	Developed and commercialized in the 1920s decade by BASF.	25-38MPa, 300-450ºC	**Pros:** Highly stable to S and Cl compounds. **Cons:** Byproducts such as dimethyl ether, higher alcohols, carbonyl compounds and methane. Very high T and P.	[29], [32], [34]
CuO-ZnO	Developed in the 1920s decade. Imperial Chemical Industries.	15MPa, 300ºC	**Cons:** This catalyst was not commercialized because H_2S and Cl compounds deactivated it.	[25], [29]
$CuO\text{-}ZnO\text{-}Al_2O_3$	Developed and commercialized in 1966 for the ICI low pressure process.	6-7MPa, 250-300ºC	**Pros:** The formation of undesirable byproducts was also reduced. Alumina was used as a stabilizer and its high activity allowed the synthesis at 220-230ºC and 5MPa, avoiding also the sintering of copper. **Cons:** Cannot be used above 300ºC and are sensitive to sulfur poisoning.	[29], [32], [35]
$CuO\text{-}ZnO\text{-}Al_2O_3$	Currently used for syngas	230-240ºC, 40-100 bar, Less than	**Pros:** Established process	[18], [36]

	hydrogenation to methanol	6v/v% of CO_2 in the syngas.	**Cons:** Low activity for the CO_2 hydrogenation to methanol.	

Besides the catalysts mentioned above, many variations have been developed and can be found in the literature, patents and research articles, and they differ mostly in the composition, the use of different stabilizers or promoters, and the synthesis method.

The production of methanol from synthesis gas makes use of fossil fuels such as methane and consumes large amounts of energy [15]. For such reasons, alternatives to the classical process that don't use methane, should be considered, in order to improve the energy efficiency of the process and to reduce its dependence on fossil fuels.

Instead of producing methanol from syngas, it can be produced from CO_2 and H_2 alone. The CO_2 hydrogenation to methanol has gained increased attention, as it is a promising way of converting the CO_2 into methanol while reducing GHG emissions. In fact, the capture and use of CO_2 and the use of green hydrogen such as that produced by water electrolysis, would create a process with much less GHG emissions. Unfortunately, these cleaner process alternatives are not extensively commercialized mostly due to high costs reasons [37]. For the CO_2 hydrogenation to methanol, the use of supports such as zirconia instead of alumina is necessary due to the unfavorable properties of alumina during this reaction. The classical catalyst containing Al_2O_3 presents different disadvantages when using CO_2 and H_2 mixtures for the production of methanol, such as lower activity and selectivity for methanol production, the inhibiting effect of the water byproduct and reduced catalyst stability due to sintering favored by water [17], [38]–[40].

Despite the above, the production of methanol from CO_2/H_2 mixtures has been gaining increased attention since decades ago [28] and the utilization of ZrO_2 containing copper-catalysts for CO_2/H_2 mixtures is well known [41]. Cu-ZrO_2 catalysts are interesting because ZrO_2 itself has catalytic activity and also because this system presents good adsorption properties, as well as good mechanical and thermal stability [7]. ZrO_2 presents different advantages compared to Al_2O_3, such as its less hydrophilic character, its promotion of the copper dispersion and a higher surface basicity, which can affect the CO_2 adsorption properties and the methanol selectivity [42]–[44]. The hydrogenation of CO_2 into methanol, has also become an increasingly important field of research due to its possible role in the valorization and the reduction of CO_2 emissions.

1.3.2. Supports and promoters of copper based catalysts

Support materials and promoters are utilized in the synthesis of solid catalysts to improve the stability, the surface properties and the interactions of the species in a catalyst to produce materials with desirable catalytic performance. Many of the promoters and modifiers used in the hydrogenation of carbon dioxide to methanol belong to the alkali, alkaline-earth, rare-earth, transition metals, metalloids and main group metals elements [4]. Metal oxides such as Fe_2O_3, Nb_2O_5, Ga_2O_3, ZrO_2, CeO_2, In_2O_3, Cr_2O_3, Al_2O_3, Y_2O_3 have been used as promoters to obtain materials with better properties, such as higher copper dispersion, higher Cu surface area, better CuO reducibility, among others [45].

To further increase the activity and stability of the Cu/ZnO catalysts, different modifiers are used as promoters and supports [46]. Many modifications to the classical CuO-ZnO-Al_2O_3 catalyst have been tested, such as promoting with boron, cerium, chromium, magnesium among other elements [29], [39]. The goal of promoting the catalysts for methanol synthesis includes improving Cu dispersion and surface area, adjusting the adsorption properties and also improves the reduction of the CuO to metallic Cu [4], [18].

Promoters such as B (as boric acid or borax), Si (as silicon oxides, precursors of silicon oxides, sodium silicate and diatomaceous earth), and for instance the oxides or salts of Mg, Zr, La, Mn, Cr, P have been used to improve the catalytic activity and mechanical properties of methanol production catalysts [25], [47], [48]. For instance, the use of Mn as a promoter of CuO-ZnO-ZrO_2 catalysts at low concentrations (2 wt%) can increase methanol production rates [19]. In the case of Al_2O_3, it acts as a structural promoter in the industrial catalyst [49], increasing the dispersion of Cu, the total surface area and the mechanical stability of the material [50].

Ba and K improve the CO_2 adsorption capacity compared to the unpromoted catalysts [4], while, CeO_2 and CeO_2-containing materials have superior chemical and physical stability, high oxygen mobility and high oxygen vacancy concentrations [51][52]. CeO_2 also favors the production of methanol, allows controlling the growth of Cu crystallites and improves surface basicity for CO_2 adsorption [4][52].

It has been shown that Cu-Zn-based catalysts are among the most useful systems for the catalytic hydrogenation of CO_2 to methanol [53]. Many other metal oxides can be used as a support or promoters for the CO_2 hydrogenation into methanol [54], which may include ZrO_2, SiO_2, TiO_2, CeO_2, Ga_2O_3, MgO, Cr_2O_3, Nb_2O_5, La_2O_3, Y_2O_3 , etc.)[3], [50], [54]. The use of these components can increase the Cu dispersion, modify the acid–base properties and redox properties, and enhance the catalytic performance and stability. ZnO improves the Cu dispersion, and both ZrO_2 and ZnO improve the adsorption of CO_2, thanks to their surface basicity [33], [50]. The works of different researchers [19], [41], [54] suggest that ZrO_2 presents a weak hydrophilic character,

which benefits the desorption of produced water, enhancing both the methanol production rate and the selectivity and making the catalyst more resistant to water. Also, the work of L'hospital *et al* [55] indicates that ZrO_2 has a basic character and that allows improving the dispersion of copper, which improves its surface area. Zr can also stabilize the Cu^+ species, and increase the basicity of the catalyst [46][56]. According to other articles [18][50], Cu/ZnO catalysts containing ZrO_2 instead of Al_2O_3 present a higher thermal and mechanical stability under the typical reaction conditions of reduction and oxidation, and also high specific surface area.

According to the work of Li *et al*. [54], Cu, Pd, Au, Pt, Re, and Rh supported-metals show high performance for CO_2 hydrogenation into methanol. Also, the work of Wambach *et al*. [7] suggests that catalysts with Cu and Ag have the highest selectivities to methanol, while other transition metals such as Ru, Rh, Au, Pd, Pt, Re and Ni produce methanol along with methane and carbon monoxide, making them less selective [4].

Several works have discussed the performance of different metals supported on zirconia for the hydrogenation of carbon dioxide into methanol [7], [38], [54]. Moreover, [38] also pointed out that Cu/ZrO_2 catalysts, especially with 40% CuO, showed high conversion and selectivity to methanol. For the above reasons, Cu-ZnO-ZrO_2 based catalysts are among the most suitable catalysts for the hydrogenation of CO_2 to methanol using H_2 and CO_2 rich feedstocks.

1.3.3. Catalyst synthesis methods for methanol production

Different catalyst preparation methods such as impregnation, coprecipitation, sol-gel synthesis, ion exchange, deposition precipitation, controlled oxidation of amorphous metal alloys for the production of metal/ZrO_2 catalysts, etc. have been tried and are known to produce catalysts with different properties [7], [16], [38]. Despite the process complexity during the synthesis of a catalyst, it is known that the synthesis methods that encourage an intimate mixing between the metal and support, are those that produce materials with the best catalytic performances [7], [16], [32].

Wambach *et al*. [7], explain the differences in the structures formed of a metal supported on ZrO_2 catalyst in Figure 1.5. This figure shows the arrangement of metal and support particles for (a) the impregnation, (b) coprecipitation and sol-gel and (c) the oxidation of glassy metal-zirconium alloy methods. White circles represent ZrO_2 particles while dark circles represent the metal particles. The (c) structure are disk shaped particles that contain both metal and support.

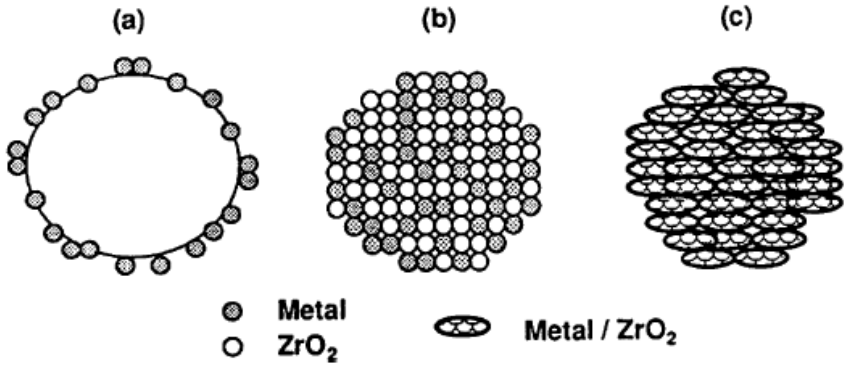

Figure 1.5 Structural features of catalysts prepared by different methods [7].

As shown above, the catalysts prepared by coprecipitation and by controlled oxidation of amorphous metal alloys are the ones that have a higher degree of interfacial contact and homogeneity, whereas the material prepared by impregnation presents lower interfacial contact [7]. According to different researchers [25][57], the materials prepared by coprecipitation are one of the best in terms of catalytic properties.

Many variables influence the final performance of a solid catalyst. From its chemical composition, to its preparation procedure and processing conditions, many factors influence the final surface and bulk properties of the material, as well as its catalytic performance. Schuth *et al*. [58] presented a diagram shown in Figure 1.6 that explains how some conditions during the coprecipitation reaction affect the final properties of a catalyst.

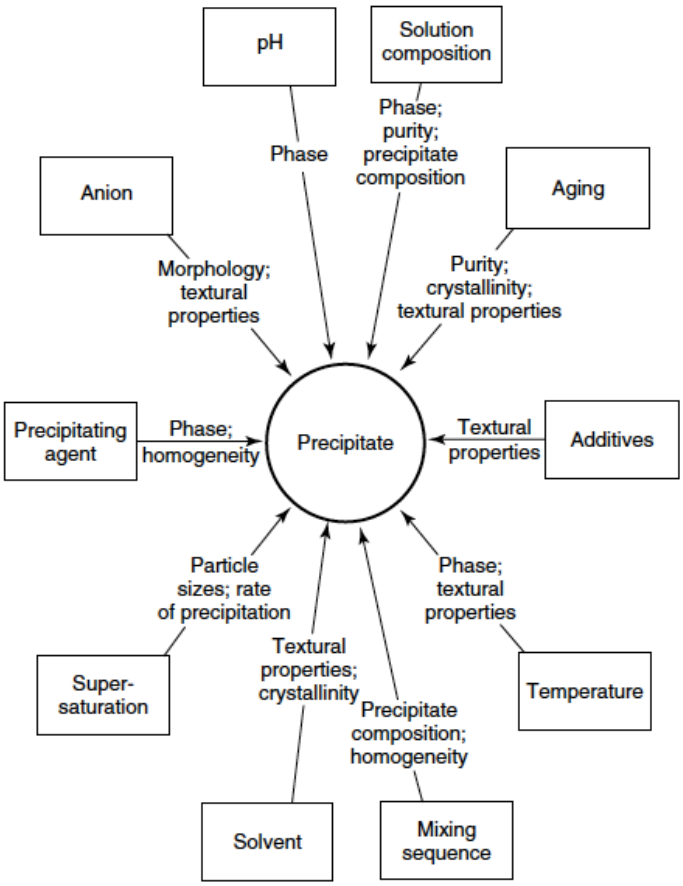

Figure 1.6 Parameters that affect the properties of a catalyst produced by coprecipitation. Taken from [58].

As seen in Figure 1.6, the aging pH, the aging time, the temperature and the mixing conditions, have a direct effect on the catalyst properties such as the composition, the material's crystallinity, the phases formed and the textural properties.

In the case of Cu-Zn-Al catalysts, small and stable crystallites are desirable for a good catalytic performance of the catalyst [59] and those characteristics are achieved through the formation of malachite and other hydroxycarbonates during the precipitation step [25], [26], [59]. These desirable catalyst properties also apply to other catalysts such as the Cu-ZnO-ZrO_2 used for the hydrogenation of CO_2 to methanol.

Other catalyst preparation methods such as a novel coprecipitation method from the work of An *et al*. [39], have allowed the production of Cu-Zn-Al-Zr catalysts with fibrous morphology and high catalytic activity, selectivity and thermal stability thanks to higher Cu-Zn crystallites dispersion.

Despite the availability of many catalyst synthesis techniques, the coprecipitation of metal salts is one of the preferred and most common methods for the production of Cu-ZnO-ZrO_2 mixed oxides catalysts [55], [60]. This method allows to produce a solid precipitate that contains the desired metallic species, usually in the form of hydroxides

or hydroxycarbonates of the metal. One of the main advantages of the coprecipitation technique, is that it allows to obtain materials in which all the elements are mixed at the atomic level [32].

The catalyst synthesis steps (i.e. precipitation, aging, washing, drying, and calcination) are known to influence the final properties of the catalyst [38]. Coprecipitation temperatures between 60-70ºC are considered favorable to obtain a material with optimum properties [36]. In the case of pH, pHs around 6 and 7 favor the formation of small catalyst particles, while acid and alkaline pHs favor the formation of large particles [36], [59]. The ageing of the precipitated material before filtration and washing was also found to be an important step to obtain catalysts of high activity and stability [59]. A calcination step in the range of 300 to 400ºC is considered beneficial for the formation of nanostructures during the formation of the mixed metal oxides [36]. According to the work of Jadhav *et al*. [19], the highest activity for the CuO-ZnO-ZrO_2 catalyst was obtained when the material was calcined at 400ºC.

The properties of the solvent selected for the catalyst synthesis, also plays a role in the final properties of the formed material [38]. According to Ma *et al*. [38], the viscosity, surface tension, and boiling point of the solvent affect significantly the structure of the precipitates and calcined catalysts.

For a catalyst containing copper, different copper sources can be used, such as copper nitrate, copper sulfate, copper acetate, etc. [47]. As for the precipitating agent, some of them include sodium carbonate, ammonium carbonate, sodium hydroxide, aqueous ammonia and also carbon dioxide [47]. Ultimately, the choice of the reactants will take into account technical and economic reasons.

Some of the most utilized precipitating agents are sodium and ammonium carbonates. Ammonium carbonate is attractive for the production of catalysts because the byproduct ammonium salt decomposes at temperatures between 200 and 260ºC [61]. This temperature range is typically below the calcination temperature of the precursor materials, therefore, ammonium residues that may deactivate or reduce the activity of the catalysts are eliminated by thermal decomposition during the calcination step. On the other hand, sodium carbonate, is one of the most utilized precipitating agents because of its availability and low cost. However, the material resulting from the precipitation reaction must be washed to ensure that no sodium remains in the solid. Sodium is known to act as a catalyst poison and it can alter the morphology and surface properties of the catalyst by reducing the Cu surface area and increasing Cu crystallite size, but also inhibiting the interaction between Cu and ZnO [62], [63]. The presence of these residual compounds is undesirable, as they can cause particle sintering and agglomeration during the subsequent thermal treatment steps, which causes a loss in the surface area and therefore a reduction in the catalytic activity [64].

The synthesis route for the preparation of Cu-ZnO-ZrO_2 catalysts follows a multistep procedure [49]. The coprecipitation process starts when both metal salts and precipitating agent solutions get in contact. After the first contact, the reaction between the species gives rise to the formation of nuclei, a process that's called nucleation. Then, as these nuclei continue to grow, the solid material is formed and different phases are formed depending on the process conditions [64]. The rates of nucleation, crystal growth and agglomeration of the particles are affected by the temperature, the concentration, the pH, among other variables. These have an effect on the final particle sizes and the morphology of the material [60].

After the solid is formed, it can be aged for a determined amount of time, and then it is washed. After washing, the catalysts are dried, then calcined and finally activated by reduction of the CuO to metallic Cu. Some of the variables that affect the characteristics of the resulting catalyst are the reaction pH, temperature, the solvent used, the mixing sequence, among others [22][64]. Precipitation temperatures from 20 to 90ºC can be used, with temperatures from 50 to 70ºC more common for this operation [47]. Behrens *et al*. [65] also suggest that the optimum coprecipitation temperature is between 60 and 70ºC and pHs between 6 and 7.

The knowledge of the effect of all of these parameters is essential to produce a catalyst that has the desired characteristics [22]. It is important that these variables are well controlled to obtain materials with the desired composition and properties. According to different research works [25], [32], the conditions during coprecipitation and aging steps are of great importance to obtain the desired catalyst. There's in fact a phenomenon called "chemical memory" which causes the final properties of the catalyst to depend on the conditions of the coprecipitation and aging steps during the synthesis process [25], [66].

Many other different catalytic systems, can be produced by this method. For example, Ni supported on Al_2O_3 for methane steam reforming, and the iron, copper, potassium catalyst for Fischer−Tropsch synthesis are produced by coprecipitation. Morales *et al*. [67] studied a catalyst made up of copper and manganese oxides prepared by coprecipitation. According to them, this method allows obtaining materials with highly desirable properties, such as high inter-dispersion of the metallic elements, and the formation of different morphologies such as solid solutions, mixed compounds and the arrangement of phases over another [67]. According to other works [35], [47], the intimate mixing of the metal salts with the precipitating agent is important to obtain good catalytic properties.

Some of the crystalline phases identified after the coprecipitation of a metal solution containing Cu, Zn and Zr for the production of methanol are shown in Table 1.3 [22][32][68].

Table 1.3 Hydroxycarbonates and other phases that can form during the coprecipitation process

Name of the compound	Chemical formula
Aurichalcite	$Zn_3Cu_2(OH)_6(CO_3)_2$
Baddeleyite	ZrO_2
Malachite	$Cu_2(OH)_2CO_3$
Georgeite	$Cu_2(OH)_2CO_3 \cdot 6H_2O$
Gerhardtite	$Cu_2(OH)_3NO_3$
Hydrozincite	$Zn_5(CO_3)_2(OH)_6$
Rosasite or zincian malachite	$CuZn(OH)_2\ CO_3$

The phases that are more often identified in the literature for the catalyst precursor include malachite, georgeite, hydrozincite, rosasite and aurichalcite. Copper oxide and zinc oxide develop after the calcination step.

Some research works suggest that the desired phases are thin needles of rosasite, malachite and zincian malachite [49], [59], [68]. Moreover, malachite, is usually obtained in its amorphous form which is called georgeite [65]. The incorporation of Zn in the malachite favors the nanostructuring of aggregates formed during calcination, which gives a material with a good distribution of metallic species [49]. A good distribution of the metallic species will give higher metal surface areas and higher levels of copper dispersion as well as small particle sizes. All of these characteristics are crucial to obtain catalysts with high catalytic activity [69].

The chemistry during the coprecipitation process can be very complex and involve many species and compounds and it is also considered a dynamic process [36]. The work of Tofighi *et al*. [36] presents different reactions that occur during the coprecipitation process and during the aging of the precipitate, as will be shown next.

Reactions occurring during the coprecipitation process:

Equation 1.4 Malachite formation reaction.

$$2Cu^{2+} + CO_3^{2-} + 2OH^- \rightarrow Cu_2(CO_3)(OH)_2$$

Equation 1.5 Hydrozincite formation reaction.

$$5Zn^{2+} + 2CO_3^{2-} + 6OH^- \rightarrow Zn_5(CO_3)_2(OH)_6$$

Equation 1.6 Nitrogen containing Cu hydroxide formation.

$$2Cu^{2+} + NO_3^- + 3OH^- \rightarrow Cu_2(NO_3)(OH)_3$$

Reactions occurring during the aging process:

Equation 1.7 Formation of Cu malachite from nitrogen containing precursor.

$$Cu_2(NO_3)(OH)_3 + CO_3^{2-} \rightarrow Cu_2(CO_3)(OH)_2 + NO_3^- + OH^-$$

Equation 1.8 Formation of rosasite from Cu malachite.

$$Cu_2(CO_3)(OH)_2 + xZn^{2+} \rightarrow (Cu_{2-x}, Zn_x)(CO_3)(OH)_2 + xCu^{2+}$$

Equation 1.9 Aurichalcite formation from hydrozincite.

$$Zn_5(CO_3)_2(OH)_6 + xCu^{2+} \rightarrow (Zn_{5-x}, Cu_x)(CO_3)_2(OH)_6 + xZn^{2+}$$

Where $Cu_2(CO_3)(OH)_2$ is malachite, $Zn_5(CO_3)_2(OH)_6$ is hydrozincite, $(Cu, Zn)_2(CO_3)(OH)_2$ is rosasite, $(Zn_{5-x}, Cu_x)(CO_3)_2(OH)_6$ is aurichalcite and $Cu_2(NO_3)(OH)_3$ a copper hydroxide compound with nitrogen.

1.4. Microfluidic synthesis of solid catalysts

1.4.1. General aspects of the synthesis of catalysts by coprecipitation using microreactors

The coprecipitation reaction for the synthesis of Cu-ZnO-Al_2O_3 and Cu-ZnO-ZrO_2 type of catalysts is usually conducted with a batch process using a stirred tank (or beaker at a laboratory scale), which has disadvantages such as the occurrence of concentration, pH and temperature gradients as well as different residence times, affecting the repeatability and consequently the properties of the final catalysts [60], [70]. The use of stirred tanks can also cause spatial and temporal variations in the concentrations of reagents and products because of the simultaneous presence of precipitate and dissolved ions [66].

Batch synthesis doesn't allow a precise control of the materials properties, which results in large particle sizes, wide particle size distribution, inhomogeneous morphologies and poor repeatability [60]. During the coprecipitation process it is very important that fluctuations of the conditions are avoided, like for example temperature and concentration gradients and also unfavorable mixing conditions, which can cause undesired growth patterns, the precipitation of undesirable species, among others [64]. A fast and homogeneous mixing of the reactants during the coprecipitation reaction is necessary to obtain catalysts with uniform properties. This cannot be achieved easily in stirred batch reactors, where the precipitation starts before the components have been well mixed, causing spatial and temporal concentration gradients [36], [66] which can have an effect on the properties of the catalysts.

For such reasons, alternatives to the traditional batch process have gained increasing importance. One such alternative is microfluidic synthesis, which as the name implies, deals with reactors, mixers and other devices that handle very small flowrates of

substances in channels of millimeter or micrometer scales [71], [72]. These types of devices offer advantages over large scale batch systems, such as higher mass and heat transfer area to volume ratio, higher speed of mixing, and constant product quality [60], [70], [71], [73], [74]. In this way, more reproducible conditions of nucleation and crystals growth can be achieved during the coprecipitation reaction [66]. The advantages of the synthesis using microreactors include their higher mass and heat transfer areas to volume ratio, which translates into a more effective exchange of mass and heat and also an increase in the speed of mixing due to a smaller diffusional path, unlike large scale processes [71], [73], [74]. Higher productivity can be achieved by connecting a common large feed stream to a number of microchannels [75].

As the name implies, microfluidic synthesis deals with reactors, mixers and other kind of devices that handle very small flowrates of substances in channels of millimeter or micrometer scales [71], [72]. Microreactors have found different applications in fields such as the pharmaceutical, medical and chemical, besides academic research [60], [72], [76]. In fact some of these applications can be found in daily life devices such as ink jet printer heads, surgical instruments, microsensors in automobiles, etc. [73]. The synthesis of materials using microreactors has been gaining attention since the 80's and 90's, mostly in Europe and the United States, where research has focused on applications related to biology, chemistry, analytical chemistry, the energy sector, among others [71], [74], [75].

1.4.2. Type of microreactors and fabrication methods

Microreactors can be produced by using different kinds of materials and techniques. The choice of material and production technique is based on the process conditions and on the nature of the chemicals that the device will handle. Examples of materials include polymers, silicon, stainless steel, among others [76]. According to Yao *et al*. [76], there are essentially two types of microreactors, namely chip-type microreactors and microcapillary reactors. Chip-type microreactors are adaptations from the microelectronic industry [76], and they allow an efficient integration of several unit operations in one single small device. Many different processes exist to produce chip-type microreactors, and they include dry or wet etching, photolithography, lithography, injection molding, embossing, among others [76]. The final choice of the production method will depend on the material of the microreactor and the desired characteristics of the structure. Moreover, microcapillary reactors consist in the adaptation of capillaries with very small internal diameters to a mixing device of the appropriate dimensions such as a mixing tee. For example, fused silica capillaries can be employed for this end with internal and external diameters of 50 and 150 micrometers, respectively.

1.4.3. Application of microfluidic devices to the synthesis of catalysts for the production of methanol

The application of microfluidic devices to the synthesis of catalysts for the production of methanol has been gaining importance in the recent years as an innovative and alternative approach for the synthesis of Cu based catalysts for methanol production and for CO_2 valorization and abatement.

Tofighi *et al*. [36] found that the Cu-ZnO-Al_2O_3 catalysts produced by the microfluidic method presented smaller CuO crystallites, higher specific surface areas, more uniform morphology as well as better Cu-Zn dispersion than the catalysts synthesized by coprecipitation in a batch reactor. Similarly, the work of Zhang *et al*. [77] on the synthesis of Cu-ZnO-Al_2O_3 catalysts using a microfluidic device, allowed them to obtain catalysts with smaller crystallite sizes, better Cu-Zn dispersion, higher BET surface area and specific Cu surface area compared to a catalyst synthesized by the classical batch method. All of these properties had a positive effect on the catalytic performance.

Wang *et al*. [78] synthesized ZnO/ZrO_2 catalysts by physical blending, impregnation and by a coprecipitation method using a microreactor and found that the catalyst synthesized with the microfluidic device developed properties such as a higher amount of oxygen vacancies compared to the other catalysts and a solid solution which gave a better catalytic activity.

Y. Wang *et al*. [79] prepared a Cu-Ce-ZrO_x solid solution catalyst by a microfluidic method coupled with ultrasounds. The catalyst synthesized by such method presented smaller particle size, higher specific surface area and higher methanol productivity and stability than the catalyst prepared by a classical batch method. According to the authors, the reason why the catalyst prepared by the microfluidic method presented an improved catalytic activity was based on a synergistic effect of smaller particle size, higher Cu dispersion and higher amount of oxygen vacancies.

Angelo *et al*. [80] investigated the synthesis of a Cu-ZnO-ZrO_2 catalyst by the microfluidic method and found that this method allowed the synthesis of a catalyst with better Cu surface area and better catalytic activity.

The work of L'hospital *et al*. [55] addressed the optimization of the synthesis parameters (i.e. carrier fluid nature, residence time, reagents flowrate and coprecipitation pH) during the synthesis of Cu-ZnO-ZrO_2 catalysts with a microfluidic device. They found that water as a carrier fluid gave better results than silicon oil, and determined the optimum residence time, the optimum reagents flowrates of the metal nitrates and the precipitating agent and the optimal coprecipitation pH.

Based on the research works discussed above it is clear that the investigation of process conditions during the microfluidic synthesis such as the aging time and the catalysts composition deserve more attention to help to better understand the microfluidic technique and to find optimal conditions for the synthesis of Cu-ZnO-ZrO_2 catalysts. Also, comparing the properties of catalysts synthesized by the batch and microfluidic methods, such as the surface properties could allow to know better the differences between both types of catalysts. The addition of the oxides CeO_2 or In_2O_3 as promoters could also be interesting given the potential benefits that these compounds could give to the methanol production catalysts from CO_2 hydrogenation. The following sections present a brief review about the reaction mechanisms of methanol synthesis and some of the state of the art regarding the works on the effect of the aging time and the catalysts composition on the properties of Cu-ZnO-ZrO_2 catalysts.

1.5. Reaction mechanisms of methanol synthesis on solid catalysts

Since decades ago, many studies have addressed the question of the reaction mechanisms and the active sites for the production of methanol from syngas and more recently from the hydrogenation of carbon dioxide. The nature of the active sites and the reaction mechanism of the hydrogenation of carbon dioxide into methanol have been a subject of intense research and continue to be a subject of debate [4], [28], [81], [82].

Despite this debate, the dual-site mechanism has been proposed and demonstrated as a good representation of what occurs during this process. Many references [83]–[87] point out that the methanol production reaction on Cu based catalysts occurs in two different active sites. One is the Cu where H_2 is adsorbed and dissociated, and the other is the support (e.g. ZnO and ZrO_2) on which CO_2 is adsorbed and converted into other carbon containing species by reaction with H. After adsorption on the Cu surface, H_2 is dissociated into H on partially oxidized Cu sites and then it is transported to the support by hydrogen spillover. Simultaneously, the adsorption of CO_2 on the partially reduced support and the production of other carbon containing species is followed by the interaction of H and C containing species at the Cu-ZnO interface to produce a formate species, which is subsequently hydrogenated to methoxy and then to methanol. Some reaction mechanisms may include the formate, RWGS pathway, or trans-COOH* pathway, as shown in Figure 1.7 [88].

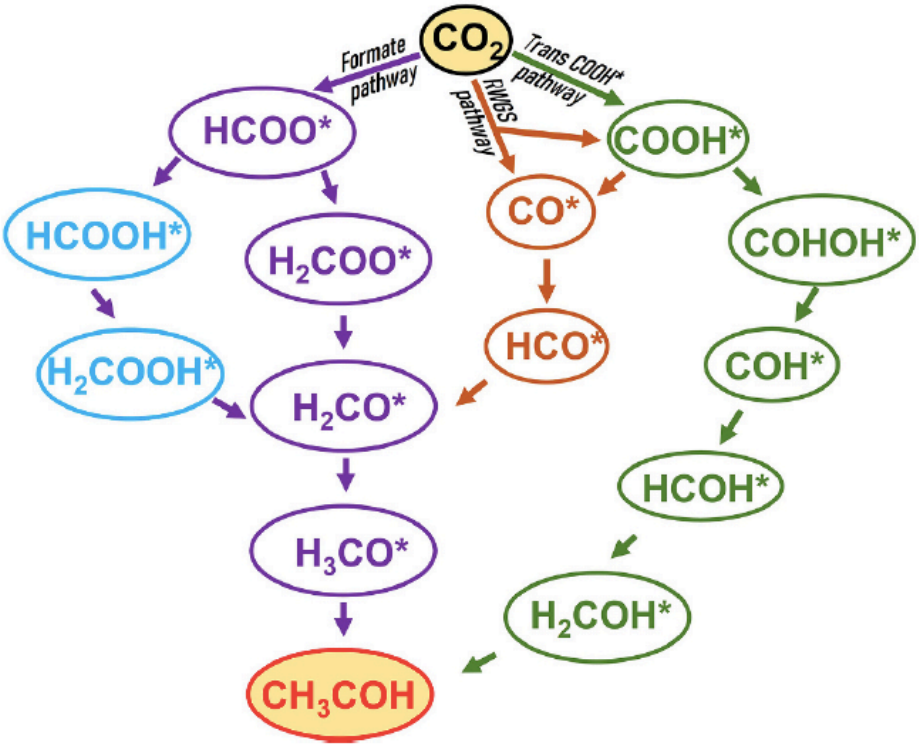

Figure 1.7 Several proposed reaction mechanisms of CO_2 hydrogenation into methanol. Taken from [88].

A dual-site reaction pathway is also widely accepted over Cu/ZrO_2 based catalysts for CO_2 hydrogenation [50]. As shown in Figure 1.8, the adsorption and dissociation of hydrogen take place on the Cu sites, and the adsorption of CO_2 as bicarbonate and carbonate species occurs on the basic sites of ZnO and ZrO_2 [50]. Then, the atomic hydrogen spills over from the Cu surface to the surface of the $ZnO\text{-}ZrO_2$ support and hydrogenates the adsorbed carbon-containing species to formate HCO_2^-, methoxide species CH_3O^- and methanol [48], [50]. The role of ZrO_2 during this reaction may cause an improved adsorption of CO_2 due to its high basicity and an increased adsorption at the $Cu\text{-}ZrO_2$ interface or on copper particles close to the ZrO_2 support [41].

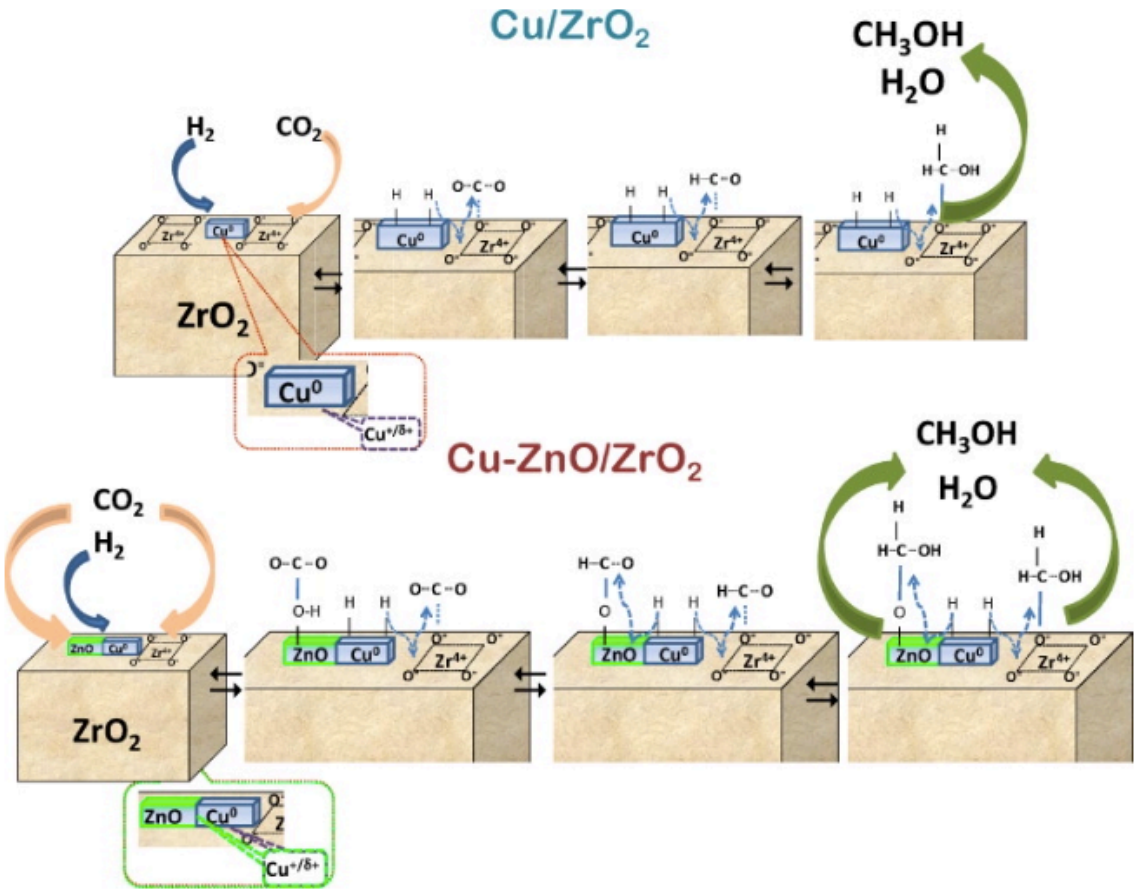

Figure 1.8 Catalysts surface and reaction paths for CO_2 hydrogenation on Cu based ZrO_2 containing catalysts. Taken from [89].

Other two types of active sites are proposed for the CO_2 hydrogenation into methanol reaction. The first active site consists of a synergy between Cu and ZnO at the interface [4], [82] and the second a Cu-Zn alloy on the surface of the catalyst [4], [28], [82] in which the Cu allows the hydrogenation of C species during the methanol synthesis. Furthermore, the roles of ZnO include the stabilization of the Cu^+ species by the ZnO moieties on the Cu surface, hydrogen reservoir, stabilization of key intermediates such as formate, and promotion of the hydrogenation of formate species [4]. ZnO can act as a structural and electronic promoter for Cu-based catalysts. It can serve as a promoter and improve Cu dispersion and Cu surface area by preventing the agglomeration of Cu particles, and it can also neutralize the acidity of the catalyst, improving the adsorption of CO_2 [50], [90].

In the case of catalysts containing CeO_2 and/or ZrO_2, one of the oxygen atoms of CO_2 is attracted to the oxygen vacancies created by these compounds or by their solid solution, while the dissociative adsorption of H_2 occurs on the Cu^0 sites [91]. Then, the adsorbed H reacts with C by the formate route [91].

More recently, the In_2O_3 containing catalysts have been investigated for the hydrogenation of CO_2 to methanol. The reaction mechanisms occurring on In_2O_3 during this reaction involve the participation of oxygen vacancies which adsorb and

activate the CO_2 mainly through the pathway CO_2 → HCOO* → H_2CO* → H_3CO* → CH_3OH but can also occur through the COOH* and RWGS pathways [92].

1.6. Effect of the synthesis conditions and the composition on Cu based catalysts for the production of methanol

A review of the effects of different catalyst synthesis parameters and compositions on the properties of Cu based catalysts for the hydrogenation of CO_2 to methanol is given next.

1.6.1. Effect of the aging time

The aging time of the precipitate formed during the coprecipitation step has important effects on the formation of crystalline phases, on the textural properties and on the homogeneity of the catalyst [58].

The work of Schimpf *et al*. [32] describes some of the phenomena that occur during the aging step after the coprecipitation reaction for the production of Cu-ZnO-Al_2O_3 catalysts. According to their work, after the addition of the metal precursors solution and the precipitating agent, the mixture experienced first a reduction in the pH accompanied by a change of color, which indicated a change in the solid material. After the pH drop, the mixture experienced a progressive increase in the pH due to the incorporation of carbonate into the solid, releasing hydroxide and accompanied by the crystallization of the material [32], [93]. Bems *et al*. [93] also found that immediately after the coprecipitation, the solid material was amorphous, and that it became more crystalline with increasing aging time, as determined by XRD. During aging, the amorphous precipitate converts into a crystalline material, which is considered as beneficial for the properties of the catalyst [68].

According to the work of Mota *et al*. [94], the aging of the precipitates is important to obtain Cu-ZnO-Al_2O_3 catalysts with high catalytic activity. Their work indicates that the thermal decomposition profiles of Cu-Zn-Al catalyst precursors vary with the aging time [94]. Furthermore, their research also provided an explanation on the aging process, in which the initially formed solids after coprecipitation are amorphous hydroxycarbonates that become more crystalline during the aging time due to different processes such as Ostwald ripening, dissolution and precipitation or agglomeration [94].

Zhang *et al*. [77] found that increasing the aging time of the Cu-ZnO-Al_2O_3 precursors (i.e. from 0 to 1 hour) resulted in a material with uniform microstructures, with higher Cu surface area and higher catalytic performance. They also found that after 1 hour of aging, an undesirable growth of the crystallite sizes occurred, lowering the activity of the catalysts.

Raudaskoski *et al*. [95] studied the effect of aging time in the coprecipitation of Cu-ZnO-ZrO_2 catalysts and found that longer aging times are favorable for the CO_2 conversion and the selectivity to methanol. Their work also indicated that longer aging times favor the removal of sodium from the catalyst, which may act as a catalyst poison and inhibitor in the CO_2 hydrogenation to methanol reaction. Some other research works [68], [96] point out that the formation of particular phases determines the final properties of the catalysts, such as the case of zincian malachite, derived from transient amorphous zincian georgeite.

Most of the research works discussed above address the effects of aging time on Cu-ZnO-Al_2O_3 catalysts for the production of methanol, and the synthesis method they employed was a batch coprecipitation in a stirred flask. The above highlights the need to investigate the effect of aging time on Cu-ZnO-ZrO_2 catalysts prepared by coprecipitation using a microfluidic technique.

1.6.2. Effect of the catalyst's composition

1.6.2.1. Effect of CuO content

The CuO content of Cu based catalysts for the hydrogenation of CO_2 to methanol is an important parameter that can affect the properties and catalytic performance of a catalyst, given its role as an active metal during the H_2 splitting step of the methanol synthesis reaction.

Witoon *et al*. [97] prepared different Cu-ZnO-ZrO_2 catalysts by the reverse coprecipitation method and found that the optimum catalyst composition was 38.2, 28.6 and 33.2 mole% of Cu, Zn and Zr respectively. Such catalyst gave the best CO_2 conversion and space-time yield of methanol.

In their work, Chang *et al*. [98] synthesized different Cu-Zn-Ce-Ti catalysts by the coprecipitation of metal nitrates with sodium hydroxide and they found that the optimum CuO content and Zn/Cu molar ratio was 30wt% and 1.2 respectively. These conditions allowed to obtain an optimal CO_2 conversion value and a maximum methanol yield, respectively.

Huang *et al*. [99] studied Cu-ZnO-ZrO_2 catalysts of different CuO and ZnO contents for the hydrogenation of CO_2 to methanol prepared by the citrate method. They found that the optimal composition of the catalysts they tested was 20% CuO, 70% ZnO and 10% ZrO_2. This composition gave the catalyst with the best copper dispersion, textural properties, CO_2 conversion, selectivity and methanol productivity. Furthermore, according to their research, the adsorption properties of H_2 and CO_2 on the catalyst surface can be influenced by the catalyst composition, which can have an important effect on the catalytic performance of the material [99].

Wang *et al*. [100] studied the effect of different Cu contents of Cu/Ce-ZrO_2 catalysts prepared by oxalate coprecipitation method and found an CuO optimal loading of 35 wt%, which gave the catalyst an optimal CO_2 conversion and methanol selectivity. This catalyst also presented an optimal number of Cu species which gave a high copper surface area and good adsorption and activation of CO_2 by a Cu-Ce-Zr solid solution.

Li *et al*. [101] prepared a catalyst with a copper content of 60wt% by coprecipitation and they studied the use of Al, Ce, and AlCeO as supports of metallic copper for the hydrogenation of carbon dioxide to methanol. The results of their work indicate that the presence of Al_2O_3 enhances the BET surface area of the catalyst, while the presence of Ce has the opposite effect. It is known that higher BET surface areas favor the copper surface area as well as the copper dispersion in the catalyst. Their results also indicate a synergy or strong interactions between the metal species when using both supports, which translates into higher CO_2 conversions and higher selectivity to methanol.

As observed in the works presented above, the study of the effect of the CuO content in catalysts for the CO_2 hydrogenation to methanol has been investigated before. This is not the case for catalysts synthesized by a microfluidic technique. This represents a good opportunity to study more in depth the use of this catalyst technique applied to the synthesis of Cu-ZnO-ZrO_2 catalysts.

1.6.2.2. Effect of CeO_2 as a component of Cu based catalysts

Cerium is an abundant and inexpensive rare earth element with excellent redox properties and oxygen storage capacity [3]. Its oxide, CeO_2, is a very important material used in heterogeneous catalysis [102].

Some of the advantages of CeO_2 as a catalyst and of metals supported on CeO_2 are the physical stability of the material as well as its high oxygen mobility, oxygen vacancies of fluorite-type oxides and the highly active Ce^{4+}/Ce^{3+} redox pair [4], [50], [51], [102]–[104]. Also, the use of CeO_2 as a support for the CO_2 hydrogenation to methanol reduces the sintering of metal particles, which results in higher metal dispersion and copper surface area, compared to other supports [3]. Different parameters affect the catalytic properties of CeO_2 when used as a catalyst or as a promoter, such as its particle size, its morphology and the exposed facets [105].

The work of Wang *et al*. [52] showed that Cu/ZrO_2 and Cu/CeO_2 catalysts presented similar CO_2 conversions for the hydrogenation of carbon dioxide into methanol, while the Cu/CeO_2 catalyst presented a higher methanol selectivity under the conditions of their experiments. The addition of ZrO_2 and CeO_2 as catalyst supports also improved the reducibility of both systems separately, and the catalyst with the CeO_2 support was better at reducing the copper particle size [52]. Furthermore, the addition of ceria can increase the surface basicity of the catalysts, which is considered beneficial for the

CO_2 hydrogenation to methanol reaction [101]. CeO_2-ZrO_2 mixed oxides have also been considered attractive due to properties such as redox potential and oxygen storage capacity [91].

Bonura *et al*. [106] investigated the effect of the addition of CeO_2 on the properties and the catalytic performance of Cu-ZnO and Cu-ZnO-ZrO_2 catalysts. Among the results they obtained, they found that the addition CeO_2 to the catalysts reduced the surface area and that this effect became stronger with the further addition of CeO_2. In their work they also found that the substitution of ZrO_2 by CeO_2 reduced the copper dispersion of the catalysts and in consequence the copper surface area. The wt% of CeO_2 that the authors tested ranged from 9% to 54%.

The work of Ouyang *et al*. [102] indicated that the morphology of CeO_2 in the Cu catalyst affects the conversion and selectivity of the catalysts for CO_2 hydrogenation to methanol. In their work they demonstrated that the nanorods morphology presented the best CuO-CeO_2 interaction, as well as better metal copper dispersion, selectivity and catalytic activity, compared to other morphologies [4].

The different research works summarized above indicate that CeO_2 could possibly give interesting properties to Cu based catalysts for the hydrogenation of CO_2 to methanol. Therefore, combining the use of CeO_2 with an alternative catalyst synthesis approach such as the coprecipitation using a microfluidic reactor seems like an interesting alternative to study more in depth, in order to obtain catalysts with more attractive properties and better catalytic performance.

1.6.2.3. Effect of In_2O_3 as a component of Cu based catalysts and as active metal

In_2O_3, a semiconductor material, has been used as a catalyst promoter for copper based catalysts and also as a catalyst by itself, promoted or not with other elements for the hydrogenation of CO_2 to methanol [33], [107]. Indium based catalysts benefit from high methanol selectivity in a wide range of temperatures, and high stability [27], [33], [108].

Martin *et al*. [40] synthesized an In_2O_3 catalyst for the hydrogenation of CO_2 to methanol supported on ZrO_2 with high activity and stability under industrially relevant conditions. They also found through extensive characterization that the reaction mechanism consisted in the creation and annihilation of oxygen vacancies, which serve as active sites [40].

Sharma *et al*. [109] investigated a Cu/CeO_2 catalyst promoted with 1% indium loading. The catalyst was synthesized by the separate preparation of the CeO_2 support by a hydrothermal method and then deposition of the In and Cu on the CeO_2 support. After testing, the material experienced an increase in copper dispersion and a decrease in

Cu particle size, as well as higher activity and methanol selectivity compared to the unpromoted material [5], [109].

Wang *et al*. [110] prepared a pure In_2O_3 and a Rh/In_2O_3 catalysts by coprecipitation and by deposition-precipitation methods, respectively. The rhodium supported catalyst presented a methanol selectivity of 100% for temperatures below 225ºC and a methanol selectivity of 56% at 300ºC. This catalyst presented a negligible production of methane and exhibited high dispersion of Rh as well as oxygen vacancies, which according to the authors was responsible for the high catalytic activity of the material. Although the $Rh\text{-}In_2O_3$ catalyst presented a better catalytic activity than the pure In_2O_3 catalyst, the latter presented a higher methanol selectivity.

Salomone *et al*. [108] investigated an In_2O_3 catalyst prepared with different ZrO_2 and CeO_2 proportions by a gel-oxalate coprecipitation and found that CeO_2 didn't improve the catalytic performance, while ZrO_2 stabilized the structure and had an electronic promotion effect.

Shi *et al*. [107] investigated the effect of the reduction temperature (i.e. from 250 to 500ºC) on a Cu-In intermetallic compound used for the hydrogenation of CO_2 to methanol and prepared by coprecipitation in a stirred beaker. They found that the detection of metallic indium by XRD occurred above a reduction temperature of 400ºC and became very evident at 500ºC. Their work also reported the formation of a $Cu_{11}In_9$ compound above reduction temperatures of 350ºC. According to their work, a reduction temperature of 350ºC maximizes the interaction between the intermetallic compound $Cu_{11}In_9$ and the oxide In_2O_3, which means a higher amount of actives sites for the CO_2 hydrogenation to methanol, which in the end means higher conversions and methanol productivity. The reaction mechanism proposed in their work [107] consists in the adsorption of the H_2 on the surface of the $Cu_{11}In_9$ intermetallic compound and the adsorption of CO_2 on the oxygen vacancies of In_2O_3. After adsorption, the dissociated H* and the CO_2 migrate to the $Cu_{11}In_9\text{-}In_2O_3$ interface, where CO_2 reacts with H* forming HCOO*, then H_2COO*, then H_2CO* and H_3CO*. Finally, H_3CO* reacts with H* to form H_3COH* giving H_2COH upon desorption.

In the work of Sun *et al*. [5], [111] a catalyst made up entirely of In_2O_3 was prepared by a simple calcination in air at 500ºC for 5 hours. This catalyst showed activities compared to those of Cu based catalysts.

The work of Frei *et al*. [112] investigated the role of monoclinic zirconia as a support of In_2O_3 catalysts and obtained a promotion effect due to better activation of the reactants due to the oxygen vacancies generated by both In_2O_3 and ZrO_2. Different works point out that the CO_2 activation and H_2 splitting during the CO_2 hydrogenation to methanol reaction on In_2O_3 catalysts involve the creation and annihilation of oxygen vacancies surrounded by indium atoms [27], [40].

None of the above research works involves the use of a microfluidic device for the synthesis of In_2O_3 containing catalysts. Therefore, the investigation of In_2O_3 as a promoter and as active metal prepared with a microfluidic technique becomes interesting given the improved properties and catalytic performance that can be achieved with this catalyst synthesis technique.

1.7. Novel catalysts for methanol production

Today there are many alternatives to the classical Cu based catalysts used for the production of methanol, even if this metal continues to be the most used in the industry. According to some review works [26], [87], methanol catalysts can be mainly classified into different categories, which include: metal-based catalysts, such as those that have supported copper and noble metals such as palladium, oxygen deficient materials, metal oxides with semiconductor properties, such as In_2O_3 catalysts which present good activity, selectivity, and stability [4], and other materials with novel catalytic structure, such as metal-organic frameworks and zeolitic imidazolate frameworks [4]. Intermetallic compounds are also attractive due to the ability to control the formation of active sites and their structural stability [4].

The review works of [5] and [50] also provide a classification of catalysts that have been used for the hydrogenation of carbon dioxide into methanol. Such classification is presented in Figure 1.9.

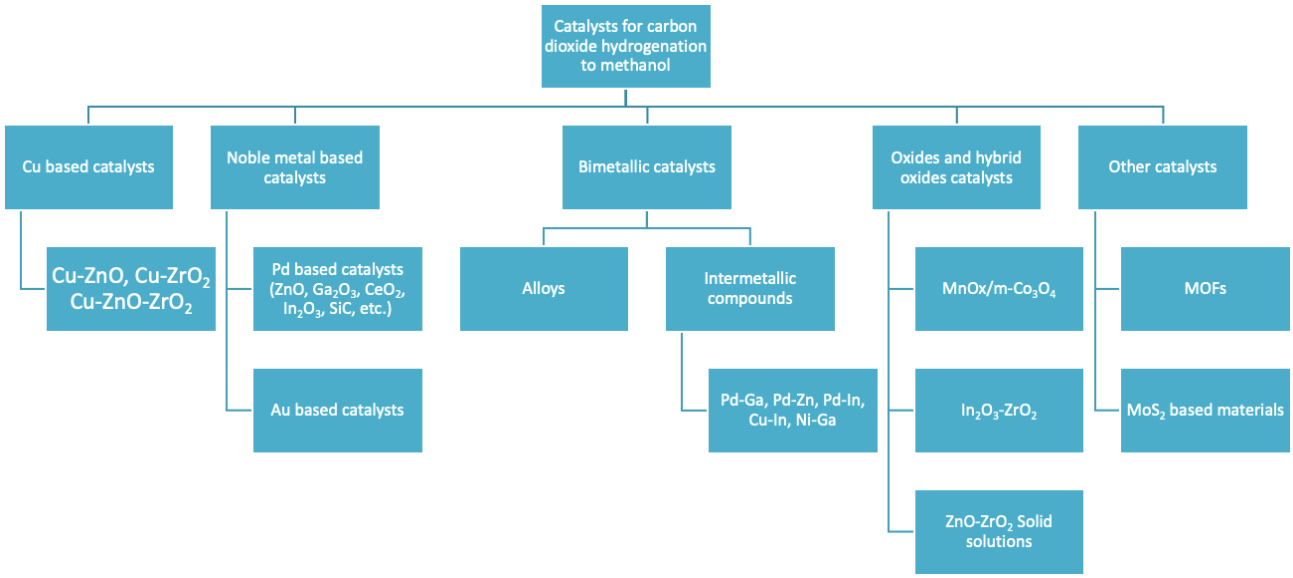

Figure 1.9 Classification of catalysts used for carbon dioxide hydrogenation into methanol. Information taken from [5] and [50].

Bimetallic catalysts including metal pairs such as Pd-Cu, Pd-Ga, Pd-In, among others have also been used successfully for the hydrogenation of CO_2 to methanol [27]. Solid solutions such as the reducible $ZnO\text{-}ZrO_2$ or $Cd\text{-}ZrO_x$ and $Ga\text{-}ZrO_x$ have also been used for the production of methanol [27].

Metal−organic frameworks (MOFs) are crystalline, nanoporous materials that are tailorable through large accessible surface areas, tunable pore functionalities, and reactive open metal sites [4]. The use of MOFs can increase importantly the catalytic activity of metallic copper in the carbon dioxide hydrogenation to methanol [21]. Also, the electronic properties of metal catalysts can be tuned by modifying a MOF support [21], which in the end affects the catalyst activity and selectivity. Since the CO_2 hydrogenation to methanol reaction is structure sensitive, MOFs may prove good catalysts due to their tuning capability [4].

Indium containing catalysts have been gaining increasing attention due to their high methanol selectivity and different reaction mechanism and are viewed as an alternative to the classical Cu based catalysts for the production of methanol. Based on the research results presented before about the catalytic performance of Cu based catalysts promoted with In and In containing catalysts, it is clear that the addition of this element to catalysts for the hydrogenation of CO_2 to methanol is interesting and should be investigated to a deeper extent, for example, by employing other catalyst synthesis techniques, such as using a microfluidic reactor.

1.8. Thesis objectives

This thesis deals mainly with the synthesis of Cu-ZnO-ZrO_2 catalysts for the hydrogenation of CO_2 into methanol, by performing the coprecipitation reaction using a microfluidic device. The experiments conducted during this thesis will allow to understand better the effects of the synthesis method, the coprecipitation parameters (i.e. aging time and coprecipitation temperature) and the catalyst composition on the crystalline structure, morphology, reducibility and other properties of the catalysts, as well as on the catalytic performance. These effects haven't been studied before in the synthesis of Cu-ZnO-ZrO_2 catalysts by the microfluidic method.

Chapter 2 will present the materials and methods employed during this thesis, which includes the reagents and chemicals used in the experiments, the different catalyst synthesis procedures used to synthesize the catalytic materials, some theory and methodology of the characterization techniques, the reaction setup description as well as the methodology used to calculate the performance of the catalysts. Also, the catalysts densities and the catalyst synthesis yields are given in this chapter.

Chapter 3 will deal with the study of the properties and catalytic performance of two Cu-ZnO-ZrO_2 catalysts synthesized by the microfluidic and by the batch methods. In this chapter, an explanation of which synthesis method produces the catalysts with the best catalytic performance will be given, based on the characterization results and the catalytic tests.

In Chapter 4, the effect of the aging time and the coprecipitation temperature on the properties of the catalysts and their catalytic performance will be examined, in order to explore other microfluidic synthesis conditions that may allow producing improved Cu-ZnO-ZrO_2 catalysts.

In Chapter 5, the composition of Cu based catalysts prepared by the microfluidic method for the hydrogenation of CO_2 to methanol will be studied. The effect of different CuO contents and the effect of the addition of CeO_2 or In_2O_3 to Cu-ZnO-ZrO_2 catalysts will be examined. An In_2O_3 containing catalyst without copper was also prepared and characterized to study the use of In as an active metal.

Finally, in Chapter 6 the general conclusions are presented as well as the perspectives for future work.

1.9. Bibliography of chapter 1

[1] United States Environmental Protection Agency, “Overview of Greenhouse Gases | Greenhouse Gas (GHG) Emissions | US EPA,” EPA. Accessed: Mar. 19, 2021. [Online]. Available: https://www.epa.gov/ghgemissions/overview-greenhouse-gases

[2] UNFCCC, “Global Warming Potentials (IPCC Second Assessment Report).” Accessed: Sep. 09, 2021. [Online]. Available: https://unfccc.int/process/transparency-and-reporting/greenhouse-gas-data/greenhouse-gas-data-unfccc/global-warming-potentials

[3] K. Chang, H. Zhang, M. J. Cheng, and Q. Lu, “Application of Ceria in CO_2 Conversion Catalysis,” *ACS Catal.*, vol. 10, no. 1, pp. 613–631, 2020, doi: 10.1021/acscatal.9b03935.

[4] X. Jiang, X. Nie, X. Guo, C. Song, and J. G. Chen, “Recent Advances in Carbon Dioxide Hydrogenation to Methanol via Heterogeneous Catalysis,” *Chem. Rev.*, vol. 120, no. 15, pp. 7984–8034, 2020, doi: 10.1021/acs.chemrev.9b00723.

[5] M. Ren, Y. Zhang, X. Wang, and H. Qiu, “Catalytic Hydrogenation of CO_2 to Methanol: A Review,” *Catalysts*, vol. 12, no. 4, 2022, doi: 10.3390/catal12040403.

[6] Climate NASA, “Carbon dioxide.” Accessed: Nov. 23, 2023. [Online]. Available: https://climate.nasa.gov/vital-signs/carbon-dioxide/

[7] J. Wambach, A. Baiker, and A. Wokaun, “CO_2 hydrogenation over metal / zirconia catalysts” *Phys. Chem. Chem. Phys.*, vol. 1, pp. 5071–5080, 1999.

[8] IEA, “Global Energy & CO_2 Status Report 2019, IEA Paris,” Paris, 2019. [Online]. Available: https://www.iea.org/reports/global-energy-co2-status-report-2019

[9] IEA, “Key World Energy Statistics 2020,” *Int. Energy Agency*, vol. 33, no. August, p. 4649, 2020, [Online]. Available: https://www.iea.org/reports/key-world-energy-statistics-2020

[10] M. Aneke and M. Wang, “Energy storage technologies and real life applications – A state of the art review,” *Appl. Energy*, vol. 179, pp. 350–377, 2016, doi: 10.1016/j.apenergy.2016.06.097.

[11] H. Ritchie, P. Rosado, and M. Roser, “Emissions by sector,” *Our world data*, 2020, [Online]. Available: https://ourworldindata.org/emissions-by-sector

[12] F. Severin, E. Rüdiger-A, C. Izaak, and G. Lambertus, “Power-to-Syngas - an enabling technology for the transition of the energy system? Production of tailored synfuels and chemicals using renewably generated electricity.,” *Angew. Chem. Int. Ed. Engl.*, 2016, doi: 10.1002/anie.201607552.

[13] P. D. Lund, J. Lindgren, J. Mikkola, and J. Salpakari, “Review of energy system flexibility measures to enable high levels of variable renewable electricity,” *Renew. Sustain. Energy Rev.*, vol. 45, pp. 785–807, 2015, doi: 10.1016/j.rser.2015.01.057.

[14] J. F. Portha, K. Parkhomenko, K. Kobl, A. C. Roger, S. Arab, J. M. Commenge, and L. Falk, “Kinetics of Methanol Synthesis from Carbon Dioxide Hydrogenation over Copper-Zinc Oxide Catalysts,” *Ind. Eng. Chem. Res.*, vol. 56, no. 45, pp. 13133–13145, 2017, doi: 10.1021/acs.iecr.7b01323.

[15] S. Olah, George; Prakash, “Efficient and selective conversion of carbon dioxide to methanol, dimethyl ether and derived products,” 2006 [Online]. Available: https://patents.google.com/patent/CA2604569C/en?oq=2604569

[16] A. M. Hengne, D. J. Yuan, N. S. Date, Y. Saih, S. P. Kamble, C. V. Rode, and

K. W. Huang, “Preparation and Activity of Copper-Gallium Nanocomposite Catalysts for Carbon Dioxide Hydrogenation to Methanol,” *Ind. Eng. Chem. Res.*, vol. 58, no. 47, pp. 21331–21340, 2019, doi: 10.1021/acs.iecr.9b04083.

[17] M. Lachowska and J. Skrzypek, “Methanol synthesis from carbon dioxide and hydrogen over Mn-promoted copper/zinc/zirconia catalysts,” *React. Kinet. Catal. Lett.*, vol. 83, no. 2, pp. 269–273, 2004, doi: 10.1023/B:REAC.0000046086.93121.36.

[18] S. Natesakhawat, J. W. Lekse, J. P. Baltrus, P. R. Ohodnicki, B. H. Howard, X. Deng, and C. Matranga, “Active sites and structure-activity relationships of copper-based catalysts for carbon dioxide hydrogenation to methanol,” *ACS Catal.*, vol. 2, no. 8, pp. 1667–1676, 2012, doi: 10.1021/cs300008g.

[19] S. G. Jadhav, P. D. Vaidya, B. M. Bhanage, and J. B. Joshi, “Catalytic carbon dioxide hydrogenation to methanol: A review of recent studies,” *Chem. Eng. Res. Des.*, vol. 92, no. 11, pp. 2557–2567, 2014, doi: 10.1016/j.cherd.2014.03.005.

[20] X. Jiang, N. Koizumi, X. Guo, and C. Song, “Bimetallic Pd-Cu catalysts for selective CO_2 hydrogenation to methanol,” *Appl. Catal. B Environ.*, vol. 170–171, pp. 173–185, 2015, doi: 10.1016/j.apcatb.2015.01.010.

[21] H. Kobayashi, J. M. Taylor, Y. Mitsuka, N. Ogiwara, T. Yamamoto, T. Toriyama, S. Matsumura, and H. Kitagawa, “Charge transfer dependence on CO_2 hydrogenation activity to methanol in Cu nanoparticles covered with metal-organic framework systems,” *Chem. Sci.*, vol. 10, no. 11, pp. 3289–3294, 2019, doi: 10.1039/c8sc05441j.

[22] J. B. Hansen and P. E. Højlund Nielsen, “Methanol Synthesis,” in *Handbook of Heterogeneous Catalysis*, 2008, pp. 2920–2949. doi: https://doi.org/10.1002/9783527610044.hetcat0148.

[23] IRENA, *INNOVATION OUTLOOK RENEWABLE METHANOL*. 2021. [Online]. Available: www.irena.org

[24] J. Skrzypek, M. Lachowska, M. Grzesik, J. Słoczyński, and P. Nowak, “Thermodynamics and kinetics of low pressure methanol synthesis,” *Chem. Eng. J. Biochem. Eng. J.*, vol. 58, no. 2, pp. 101–108, 1995, doi: 10.1016/0923-0467(94)02955-5.

[25] M. Behrens and R. Schlögl, “How to prepare a good Cu/ZnO catalyst or the role of solid state chemistry for the synthesis of nanostructured catalysts,” *Zeitschrift fur Anorg. und Allg. Chemie*, vol. 639, no. 15, pp. 2683–2695, 2013, doi: 10.1002/zaac.201300356.

[26] S. Dang, H. Yang, P. Gao, H. Wang, X. Li, W. Wei, and Y. Sun, “A review of research progress on heterogeneous catalysts for methanol synthesis from carbon dioxide hydrogenation,” *Catal. Today*, vol. 330, no. March 2018, pp. 61–75, 2019, doi: 10.1016/j.cattod.2018.04.021.

[27] P. Gao, L. Zhang, S. Li, Z. Zhou, and Y. Sun, “Novel Heterogeneous Catalysts for CO_2 Hydrogenation to Liquid Fuels,” *ACS Cent. Sci.*, vol. 6, no. 10, pp. 1657–1670, Oct. 2020, doi: 10.1021/acscentsci.0c00976.

[28] X. M. Liu, G. Q. Lu, Z. F. Yan, and J. Beltramini, “Recent Advances in Catalysts for Methanol Synthesis via Hydrogenation of CO and CO_2,” *Ind. Eng. Chem. Res.*, vol. 42, no. 25, pp. 6518–6530, 2003, doi: 10.1021/ie020979s.

[29] E. Fiedler, G. Grossmann, D. B. Kersebohm, and C. Witte, “Methanol,” in *Ullmann’s Encyclopedia of Industrial Chemistry*, 2012. [Online]. Available: https://doi.org/10.1002/14356007.a16_465.pub3

[30] E. Magoon, “Production of Methanol from Biomass,” 2006 doi:

10.1201/9781420020700.sec1.
[31] J. Nakamura, T. Fujitani, S. Kuld, S. Helveg, I. Chorkendorff, and J. Sehested, “Comment on ‘Active sites for CO_2 hydrogenation to methanol on Cu/ZnO catalysts,’” *Science (80-.).*, vol. 357, no. 6354, pp. 1296–1299, 2017, doi: 10.1126/science.aan8074.
[32] Schimpf and Muhler, “Synthesis of Solid Catalysts,” in *Synthesis of Solid Catalysts*, K. P. de Jong, Ed., Wiley-VCH, 2009, pp. 1–401. doi: 10.1002/9783527626854.
[33] K. Stangeland, H. Li, and Z. Yu, “CO_2 hydrogenation to methanol: the structure–activity relationships of different catalyst systems,” *Energy, Ecol. Environ.*, vol. 5, no. 4, pp. 272–285, 2020, doi: 10.1007/s40974-020-00156-4.
[34] S. S. Iyer, T. Renganathan, S. Pushpavanam, M. Vasudeva Kumar, and N. Kaisare, “Generalized thermodynamic analysis of methanol synthesis: Effect of feed composition,” *J. CO_2 Util.*, vol. 10, pp. 95–104, 2015, doi: 10.1016/j.jcou.2015.01.006.
[35] M. Behrens, “Coprecipitation: An excellent tool for the synthesis of supported metal catalysts - From the understanding of the well known recipes to new materials,” *Catal. Today*, vol. 246, pp. 46–54, 2015, doi: 10.1016/j.cattod.2014.07.050.
[36] G. Tofighi, H. Lichtenberg, A. Gaur, W. Wang, S. Wild, K. Herrera Delgado, S. Pitter, R. Dittmeyer, J.-D. Grunwaldt, and D. E. Doronkin, “ Continuous synthesis of Cu/ZnO/Al_2O_3 nanoparticles in a co-precipitation reaction using a silicon based microfluidic reactor ,” *React. Chem. Eng.*, 2022, doi: 10.1039/d1re00499a.
[37] S. Sollai, A. Porcu, V. Tola, F. Ferrara, and A. Pettinau, “Renewable methanol production from green hydrogen and captured CO_2: A techno-economic assessment,” *J. CO_2 Util.*, vol. 68, no. December 2022, p. 102345, 2023, doi: 10.1016/j.jcou.2022.102345.
[38] Y. Ma, Q. Sun, D. Wu, W. H. Fan, Y. L. Zhang, and J. F. Deng, “A practical approach for the preparation of high activity Cu/ZnO/ZrO_2 catalyst for methanol synthesis from CO_2 hydrogenation,” *Appl. Catal. A Gen.*, vol. 171, no. 1, pp. 45–55, 1998, doi: 10.1016/S0926-860X(98)00079-9.
[39] X. An, J. Li, Y. Zuo, Q. Zhang, D. Wang, and J. Wang, “A Cu/Zn/Al/Zr fibrous catalyst that is an improved CO_2 hydrogenation to methanol catalyst,” *Catal. Letters*, vol. 118, no. 3–4, pp. 264–269, 2007, doi: 10.1007/s10562-007-9182-x.
[40] O. Martin, A. J. Martín, C. Mondelli, S. Mitchell, T. F. Segawa, R. Hauert, C. Drouilly, D. Curulla-Ferré, and J. Pérez-Ramírez, “Indium oxide as a superior catalyst for methanol synthesis by CO_2 hydrogenation,” *Angew. Chemie - Int. Ed.*, vol. 55, no. 21, pp. 6261–6265, 2016, doi: 10.1002/anie.201600943.
[41] S. Polierer, D. Guse, S. Wild, K. H. Delgado, T. N. Otto, T. A. Zevaco, M. Kind, J. Sauer, F. Studt, and S. Pitter, “Enhanced direct dimethyl ether synthesis from CO_2-rich syngas with Cu/ZnO/ZrO_2 catalysts prepared by continuous co-precipitation,” *Catalysts*, vol. 10, no. 8, pp. 1–18, 2020, doi: 10.3390/catal10080816.
[42] F. Arena, G. Italiano, K. Barbera, G. Bonura, L. Spadaro, and F. Frusteri, “Basic evidences for methanol-synthesis catalyst design,” *Catal. Today*, vol. 143, no. 1–2, pp. 80–85, 2009, doi: 10.1016/j.cattod.2008.11.022.
[43] X. Dong, F. Li, N. Zhao, F. Xiao, J. Wang, and Y. Tan, “CO_2 hydrogenation to methanol over Cu/ZnO/ZrO_2 catalysts prepared by precipitation-reduction

method," *Appl. Catal. B Environ.*, vol. 191, pp. 8–17, 2016, doi: 10.1016/j.apcatb.2016.03.014.
[44] Y. Wang, S. Kattel, W. Gao, K. Li, P. Liu, J. G. Chen, and H. Wang, "Exploring the ternary interactions in Cu–ZnO–ZrO_2 catalysts for efficient CO_2 hydrogenation to methanol," *Nat. Commun.*, vol. 10, no. 1, 2019, doi: 10.1038/s41467-019-09072-6.
[45] C. S. Santana, L. F. Rasteiro, F. C. F. Marcos, E. M. Assaf, J. F. Gomes, and J. M. Assaf, "Influence of Al, Cr, Ga, or Zr as promoters on the performance of Cu/ZnO catalyst for CO_2 hydrogenation to methanol," *Mol. Catal.*, vol. 528, no. July, 2022, doi: 10.1016/j.mcat.2022.112512.
[46] H. Yang, C. Zhang, P. Gao, H. Wang, X. Li, L. Zhong, W. Wei, and Y. Sun, "A review of the catalytic hydrogenation of carbon dioxide into value-added hydrocarbons," *Catal. Sci. Technol.*, vol. 7, no. 20, pp. 4580–4598, 2017, doi: 10.1039/c7cy01403a.
[47] K. Y. Y. Yamagishi, "Process for manufacturing methanol and process for manufacturing catalyst for methanol synthesis," 1996 [Online]. Available: https://patents.google.com/patent/US5767039A/en?oq=5767039
[48] Z. Shi, Q. Tan, and D. Wu, "Ternary copper-cerium-zirconium mixed metal oxide catalyst for direct CO_2 hydrogenation to methanol," *Mater. Chem. Phys.*, vol. 219, no. July, pp. 263–272, 2018, doi: 10.1016/j.matchemphys.2018.08.038.
[49] S. Zander, E. L. Kunkes, M. E. Schuster, J. Schumann, G. Weinberg, D. Teschner, N. Jacobsen, R. Schlögl, and M. Behrens, "The role of the oxide component in the development of copper composite catalysts for methanol synthesis," *Angew. Chemie - Int. Ed.*, vol. 52, no. 25, pp. 6536–6540, 2013, doi: 10.1002/anie.201301419.
[50] J. Zhong, X. Yang, Z. Wu, B. Liang, Y. Huang, and T. Zhang, "State of the art and perspectives in heterogeneous catalysis of CO_2 hydrogenation to methanol," *Chem. Soc. Rev.*, vol. 49, no. 5, pp. 1385–1413, 2020, doi: 10.1039/c9cs00614a.
[51] A. Pintar, J. Batista, and S. Hoevar, "TPR, TPO and TPD Examination of Cu0.15Ce0.85O_2-y Mixed Oxide Catalyst Prepared by Co-precipitation Synthesis," *Micromeritics*, vol. 2, pp. 1–4, 2011.
[52] W. Wang, Z. Qu, L. Song, and Q. Fu, "CO_2 hydrogenation to methanol over Cu/CeO_2 and Cu/ZrO_2 catalysts: Tuning methanol selectivity via metal-support interaction," *J. Energy Chem.*, vol. 40, no. xxxx, pp. 22–30, 2020, doi: 10.1016/j.jechem.2019.03.001.
[53] C. Li, X. Yuan, and K. Fujimoto, "Development of highly stable catalyst for methanol synthesis from carbon dioxide," *Appl. Catal. A Gen.*, vol. 469, pp. 306–311, 2014, doi: 10.1016/j.apcata.2013.10.010.
[54] K. Li and J. G. Chen, "CO_2 Hydrogenation to Methanol over ZrO_2-Containing Catalysts: Insights into ZrO_2 Induced Synergy," *ACS Catal.*, vol. 9, no. 9, pp. 7840–7861, 2019, doi: 10.1021/acscatal.9b01943.
[55] V. L'hospital, S. Heyte, S. Paul, K. Parkhomenko, and A.-C. Roger, "Optimization of the continuous coprecipitation in a microfluidic reactor: Cu-based catalysts for CO_2 hydrogenation into methanol," *Fuel*, vol. 319, no. February, p. 123689, Jul. 2022, doi: 10.1016/j.fuel.2022.123689.
[56] R. Guil-López, N. Mota, J. Llorente, E. Millán, B. Pawelec, J. L. G. Fierro, and R. M. Navarro, "Methanol synthesis from CO_2: A review of the latest developments in heterogeneous catalysis," *Materials (Basel).*, vol. 12, no. 23, 2019, doi: 10.3390/ma122333902.

[57] G. Bonura, M. Cordaro, C. Cannilla, F. Arena, and F. Frusteri, “The changing nature of the active site of Cu-Zn-Zr catalysts for the CO_2 hydrogenation reaction to methanol,” *Appl. Catal. B Environ.*, vol. 152–153, pp. 152–161, 2014, doi: 10.1016/j.apcatb.2014.01.035.

[58] F. Schuth, M. Hesse, and K. K. Unger, “Precipitation and Coprecipitation,” in *Handbook of Heterogeneous Catalysis*, John Wiley & Sons, Ltd, 2008, pp. 100–119. doi: 10.1002/9783527610044.HETCAT0008.

[59] M. S. Spencer, “The role of zinc oxide in Cu/ZnO catalysts for methanol synthesis and the water-gas shift reaction,” *Top. Catal.*, vol. 8, no. 3–4, pp. 259–266, 1999, doi: 10.1023/a:1019181715731.

[60] H. Chen, Z. Dong, and J. Yue, “Advances in Microfluidic Synthesis of Solid Catalysts,” *Powders*, vol. 1, no. 3, pp. 155–183, 2022, doi: 10.3390/powders1030011.

[61] W. M. Haynes, *CRC Handbook of Chemistry and Physics*. CRC Press, 2016. [Online]. Available: https://books.google.fr/books?id=VVezDAAAQBAJ

[62] K. W. Jun, W. J. Shen, K. S. Rama Rao, and K. W. Lee, “Residual sodium effect on the catalytic activity of $Cu/ZnO/Al_2O_3$ in methanol synthesis from CO_2 hydrogenation,” *Appl. Catal. A Gen.*, vol. 174, no. 1–2, pp. 231–238, 1998, doi: 10.1016/S0926-860X(98)00195-1.

[63] S. A. Kondrat, P. J. Smith, J. H. Carter, J. S. Hayward, G. J. Pudge, G. Shaw, M. S. Spencer, J. K. Bartley, S. H. Taylor, and G. J. Hutchings, “The effect of sodium species on methanol synthesis and water-gas shift Cu/ZnO catalysts: Utilising high purity zincian georgeite,” *Faraday Discuss.*, vol. 197, pp. 287–307, 2017, doi: 10.1039/c6fd00202a.

[64] P. Munnik, P. E. De Jongh, and K. P. De Jong, “Recent Developments in the Synthesis of Supported Catalysts,” *Chem. Rev.*, vol. 115, no. 14, pp. 6687–6718, 2015, doi: 10.1021/cr500486u.

[65] M. Behrens, D. Brennecke, F. Girgsdies, S. Kißner, A. Trunschke, N. Nasrudin, S. Zakaria, N. F. Idris, S. B. A. Hamid, B. Kniep, R. Fischer, W. Busser, M. Muhler, and R. Schlögl, “Understanding the complexity of a catalyst synthesis: Co-precipitation of mixed Cu,Zn,Al hydroxycarbonate precursors for $Cu/ZnO/Al_2O_3$ catalysts investigated by titration experiments,” *Appl. Catal. A Gen.*, vol. 392, no. 1–2, pp. 93–102, 2011, doi: 10.1016/j.apcata.2010.10.031.

[66] M. Schur, B. Bems, A. Dassenoy, I. Kassatkine, J. Urban, H. Wilmes, O. Hinrichsen, M. Muhler, and R. Schlögl, “Continuous coprecipitation of catalysts in a micromixer: Nanostructured Cu/ZnO composite for the synthesis of methanol,” *Angew. Chemie - Int. Ed.*, vol. 42, no. 32, pp. 3815–3817, 2003, doi: 10.1002/anie.200250709.

[67] M. R. Morales, B. P. Barbero, and L. E. Cadús, “Evaluation and characterization of Mn-Cu mixed oxide catalysts for ethanol total oxidation: Influence of copper content,” *Fuel*, vol. 87, no. 7, pp. 1177–1186, 2008, doi: 10.1016/j.fuel.2007.07.015.

[68] P. J. Smith, S. A. Kondrat, P. A. Chater, B. R. Yeo, G. M. Shaw, L. Lu, J. K. Bartley, S. H. Taylor, M. S. Spencer, C. J. Kiely, G. J. Kelly, C. W. Park, and G. J. Hutchings, “A new class of Cu/ZnO catalysts derived from zincian georgeite precursors prepared by co-precipitation,” *Chem. Sci.*, vol. 8, no. 3, pp. 2436–2447, 2017, doi: 10.1039/c6sc04130b.

[69] S. Sá, H. Silva, L. Brandão, J. M. Sousa, and A. Mendes, “Catalysts for methanol steam reforming—A review,” *Appl. Catal. B Environ.*, vol. 99, no. 1–2, pp. 43–57, Aug. 2010, doi: 10.1016/j.apcatb.2010.06.015.

[70] S. G. Robles Macias L, Curulla-Ferre D, Ferreira C, Santiago Redondo M, “Process for manufacturing a methanol synthesis catalyst,” WO2013/120711 Al, 2013 [Online]. Available: https://patentimages.storage.googleapis.com/94/2c/3b/d73feaab0591c1/WO2013120711A1.pdf
[71] K. Jähnisch, V. Hessel, H. Löwe, and M. Baerns, “Chemistry in Microstructured Reactors,” *Angew. Chemie Int. Ed.*, vol. 43, no. 4, pp. 406–446, Jan. 2004, doi: 10.1002/anie.200300577.
[72] Y. Song, J. Hormes, and C. S. S. R. Kumar, “Microfluidic synthesis of nanomaterials,” *Small*, vol. 4, no. 6, pp. 698–711, 2008, doi: 10.1002/smll.200701029.
[73] W. Ehrfeld, V. Hessel, and V. Haverkamp, “Microreactors,” in *Ullmann’s Encyclopedia of Industrial Chemistry*, Weinheim, Germany: Wiley-VCH Verlag GmbH & Co. KGaA, 2000. doi: 10.1002/14356007.b16_b37.
[74] K. Mae, “Advanced chemical processing using microspace,” *Chem. Eng. Sci.*, vol. 62, no. 18–20, pp. 4842–4851, 2007, doi: 10.1016/j.ces.2007.01.012.
[75] W. Ehrfeld, V. Hessel, and H. Lehr, “Microreactors for Chemical Synthesis and Biotechnology --- Current Developments and Future Applications,” in *Microsystem Technology in Chemistry and Life Science*, A. Manz and H. Becker, Eds., Berlin, Heidelberg: Springer Berlin Heidelberg, 1998, pp. 233–252. doi: 10.1007/3-540-69544-3_10.
[76] X. Yao, Y. Zhang, L. Du, J. Liu, and J. Yao, “Review of the applications of microreactors,” *Renew. Sustain. Energy Rev.*, vol. 47, pp. 519–539, 2015, doi: 10.1016/j.rser.2015.03.078.
[77] Q. C. Zhang, K. P. Cheng, L. X. Wen, K. Guo, and J. F. Chen, “A study on the precipitating and aging processes of $CuO/ZnO/Al_2O_3$ catalysts synthesized in micro-impinging stream reactors,” *RSC Adv.*, vol. 6, no. 40, pp. 33611–33621, 2016, doi: 10.1039/c6ra02512a.
[78] X. Wang, Y. Wang, C. Yang, Y. Yi, X. Wang, F. Liu, J. Cao, and H. Pan, “A novel microreaction strategy to fabricate superior hybrid zirconium and zinc oxides for methanol synthesis from CO_2,” *Appl. Catal. A Gen.*, vol. 595, no. March, p. 117507, 2020, doi: 10.1016/j.apcata.2020.117507.
[79] Y. Wang, H. Yu, Q. Hu, Y. Huang, X. Wang, Y. Wang, and F. Wang, “Application of microimpinging stream reactor coupled with ultrasound in Cu/CeZrOx solid solution catalyst preparation for CO_2 hydrogenation to methanol,” *Renew. Energy*, vol. 202, no. November 2022, pp. 834–843, 2023, doi: 10.1016/j.renene.2022.11.075.
[80] L. Angelo, M. Girleanu, O. Ersen, C. Serra, K. Parkhomenko, and A. C. Roger, “Catalyst synthesis by continuous coprecipitation under micro-fluidic conditions: Application to the preparation of catalysts for methanol synthesis from CO_2/H_2,” *Catal. Today*, vol. 270, pp. 59–67, 2016, doi: 10.1016/j.cattod.2015.09.028.
[81] S. Natesakhawat, P. R. Ohodnicki, B. H. Howard, J. W. Lekse, J. P. Baltrus, and C. Matranga, “Adsorption and deactivation characteristics of Cu/ZnO-based catalysts for methanol synthesis from carbon dioxide,” *Top. Catal.*, vol. 56, no. 18–20, pp. 1752–1763, 2013, doi: 10.1007/s11244-013-0111-5.
[82] S. Kattel, P. J. Ramírez, J. G. Chen, J. A. Rodriguez, and P. Liu, “Active sites for CO_2 hydrogenation to methanol on Cu/ZnO catalysts,” *Science (80-.).*, vol. Science 35, pp. 1296–1299, 2017.
[83] J. M. Thomas, *Principles and practice of heterogeneous catalysis*. Wiley-VCH, 2015.

[84] J. Xiao, D. Mao, X. Guo, and J. Yu, “Effect of TiO_2 , ZrO_2 , and TiO_2 -ZrO_2 on the performance of CuO-ZnO catalyst for CO_2 hydrogenation to methanol,” *Appl. Surf. Sci.*, vol. 338, pp. 146–153, 2015, doi: 10.1016/j.apsusc.2015.02.122.

[85] T. Phongamwong, U. Chantaprasertporn, T. Witoon, T. Numpilai, Y. Poo-arporn, W. Limphirat, W. Donphai, P. Dittanet, M. Chareonpanich, and J. Limtrakul, “CO_2 hydrogenation to methanol over CuO–ZnO–ZrO_2–SiO_2 catalysts: Effects of SiO_2 contents,” *Chem. Eng. J.*, vol. 316, pp. 692–703, 2017, doi: 10.1016/j.cej.2017.02.010.

[86] Y. Liang, D. Mao, X. Guo, J. Yu, G. Wu, and Z. Ma, “Solvothermal preparation of CuO-ZnO-ZrO_2 catalysts for methanol synthesis via CO_2 hydrogenation,” *J. Taiwan Inst. Chem. Eng.*, vol. 121, pp. 81–91, 2021, doi: 10.1016/j.jtice.2021.03.049.

[87] J. Niu, H. Liu, Y. Jin, B. Fan, W. Qi, and J. Ran, “Comprehensive review of Cu-based CO_2 hydrogenation to CH_3OH: Insights from experimental work and theoretical analysis,” *Int. J. Hydrogen Energy*, vol. 47, no. 15, pp. 9183–9200, 2022, doi: 10.1016/j.ijhydene.2022.01.021.

[88] N. J. Azhari, D. Erika, S. Mardiana, T. Ilmi, M. L. Gunawan, I. G. B. N. Makertihartha, and G. T. M. Kadja, “Methanol synthesis from CO_2: A mechanistic overview,” *Results Eng.*, vol. 16, no. October, p. 100711, 2022, doi: 10.1016/j.rineng.2022.100711.

[89] F. Arena, G. Italiano, K. Barbera, S. Bordiga, G. Bonura, L. Spadaro, and F. Frusteri, “Solid-state interactions, adsorption sites and functionality of Cu-ZnO/ZrO_2 catalysts in the CO_2 hydrogenation to CH_3OH,” *Appl. Catal. A Gen.*, vol. 350, no. 1, pp. 16–23, 2008, doi: 10.1016/j.apcata.2008.07.028.

[90] H. Ahouari, A. Soualah, A. Le Valant, L. Pinard, P. Magnoux, and Y. Pouilloux, “Methanol synthesis from CO_2 hydrogenation over copper based catalysts,” *React. Kinet. Mech. Catal.*, vol. 110, no. 1, pp. 131–145, 2013, doi: 10.1007/s11144-013-0587-9.

[91] S. Poto, D. Vico van Berkel, F. Gallucci, and M. Fernanda Neira d’Angelo, “Kinetic modelling of the methanol synthesis from CO_2 and H_2 over a CuO/CeO_2/ZrO_2 catalyst: The role of CO_2 and CO hydrogenation,” *Chem. Eng. J.*, vol. 435, no. P2, p. 134946, 2022, doi: 10.1016/j.cej.2022.134946.

[92] J. Wang, G. Zhang, J. Zhu, X. Zhang, F. Ding, A. Zhang, X. Guo, and C. Song, “CO_2 Hydrogenation to Methanol over In_2O_3-Based Catalysts: From Mechanism to Catalyst Development,” *ACS Catal.*, vol. 11, no. 3, pp. 1406–1423, 2021, doi: 10.1021/acscatal.0c03665.

[93] B. Bems, M. Schur, A. Dassenoy, H. Junkes, D. Herein, and R. Schlögl, “Relations between synthesis and microstructural properties of copper/zinc hydroxycarbonates,” *Chem. - A Eur. J.*, vol. 9, no. 9, pp. 2039–2052, 2003, doi: 10.1002/chem.200204122.

[94] N. Mota, R. Guil-Lopez, B. G. Pawelec, J. L. G. Fierro, and R. M. Navarro, “Highly active Cu/ZnO-Al catalyst for methanol synthesis: Effect of aging on its structure and activity,” *RSC Adv.*, vol. 8, no. 37, pp. 20619–20629, 2018, doi: 10.1039/c8ra03291b.

[95] R. Raudaskoski, M. V. Niemelä, and R. L. Keiski, “The effect of ageing time on co-precipitated Cu/ZnO/ZrO_2 catalysts used in methanol synthesis from CO_2 and H_2,” *Top. Catal.*, vol. 45, no. 1–4, pp. 57–60, 2007, doi: 10.1007/s11244-007-0240-9.

[96] L. Zwiener, F. Girgsdies, D. Brennecke, D. Teschner, A. G. F. Machoke, R. Schlögl, and E. Frei, “Evolution of zincian malachite synthesis by low

temperature co-precipitation and its catalytic impact on the methanol synthesis," *Appl. Catal. B Environ.*, vol. 249, no. November 2018, pp. 218–226, 2019, doi: 10.1016/j.apcatb.2019.02.023.
[97] T. Witoon, N. Kachaban, W. Donphai, P. Kidkhunthod, K. Faungnawakij, M. Chareonpanich, and J. Limtrakul, "Tuning of catalytic CO_2 hydrogenation by changing composition of CuO-ZnO-ZrO_2 catalysts," *Energy Convers. Manag.*, vol. 118, pp. 21–31, 2016, doi: 10.1016/j.enconman.2016.03.075.
[98] K. Chang, T. Wang, and J. G. Chen, "Methanol Synthesis from CO_2 Hydrogenation over CuZnCeTi Mixed Oxide Catalysts," *Ind. Eng. Chem. Res.*, vol. 58, no. 19, pp. 7922–7928, 2019, doi: 10.1021/acs.iecr.9b00554.
[99] C. Huang, S. Chen, X. Fei, D. Liu, and Y. Zhang, "Catalytic hydrogenation of CO_2 to methanol: Study of synergistic effect on adsorption properties of CO_2 and H_2 in CuO/ZnO/ZrO_2 system," *Catalysts*, vol. 5, no. 4, pp. 1846–1861, 2015, doi: 10.3390/catal5041846.
[100] W. Wang, Z. Qu, L. Song, and Q. Fu, "Effect of the nature of copper species on methanol synthesis from CO_2 hydrogenation reaction over CuO/$Ce_{0.4}Zr_{0.6}O_2$ catalyst," *Mol. Catal.*, vol. 493, no. June, p. 111105, 2020, doi: 10.1016/j.mcat.2020.111105.
[101] S. Li, L. Guo, and T. Ishihara, "Hydrogenation of CO_2 to methanol over Cu/AlCeO catalyst," *Catal. Today*, vol. 339, no. July 2018, pp. 352–361, 2020, doi: 10.1016/j.cattod.2019.01.015.
[102] B. Ouyang, W. Tan, and B. Liu, "Morphology effect of nanostructure ceria on the Cu/CeO_2 catalysts for synthesis of methanol from CO_2 hydrogenation," *Catal. Commun.*, vol. 95, pp. 36–39, 2017, doi: 10.1016/j.catcom.2017.03.005.
[103] L. Lin, S. Yao, Z. Liu, F. Zhang, N. Li, D. Vovchok, A. Martínez-Arias, R. Castañeda, J. Lin, S. D. Senanayake, D. Su, D. Ma, and J. A. Rodriguez, "In Situ Characterization of Cu/CeO_2 Nanocatalysts for CO_2 Hydrogenation: Morphological Effects of Nanostructured Ceria on the Catalytic Activity," *J. Phys. Chem. C*, vol. 122, no. 24, pp. 12934–12943, Jun. 2018, doi: 10.1021/acs.jpcc.8b03596.
[104] B. Yang, W. Deng, L. Guo, and T. Ishihara, "Copper-ceria solid solution with improved catalytic activity for hydrogenation of CO_2 to CH_3OH," *Chinese J. Catal.*, vol. 41, no. 9, pp. 1348–1359, 2020, doi: 10.1016/S1872-2067(20)63605-1.
[105] Q. Tan, Z. Shi, and D. Wu, "CO_2 hydrogenation over differently morphological CeO_2-supported Cu-Ni catalysts," *Int. J. Energy Res.*, vol. 43, no. 10, pp. 5392–5404, 2019, doi: 10.1002/er.4636.
[106] G. Bonura, F. Arena, G. Mezzatesta, C. Cannilla, L. Spadaro, and F. Frusteri, "Role of the ceria promoter and carrier on the functionality of Cu-based catalysts in the CO_2-to-methanol hydrogenation reaction," *Catal. Today*, vol. 171, no. 1, pp. 251–256, 2011, doi: 10.1016/j.cattod.2011.04.038.
[107] Z. Shi, Q. Tan, C. Tian, Y. Pan, X. Sun, J. Zhang, and D. Wu, "CO_2 hydrogenation to methanol over Cu-In intermetallic catalysts: Effect of reduction temperature," *J. Catal.*, vol. 379, pp. 78–89, 2019, doi: 10.1016/j.jcat.2019.09.024.
[108] F. Salomone, E. Sartoretti, S. Ballauri, M. Castellino, C. Novara, F. Giorgis, R. Pirone, and S. Bensaid, "CO_2 hydrogenation to methanol over Zr- and Ce-doped indium oxide," *Catal. Today*, vol. 423, no. January, p. 114023, 2023, doi: 10.1016/j.cattod.2023.01.030.
[109] S. K. Sharma, B. Paul, R. S. Pal, P. Bhanja, A. Banerjee, C. Samanta, and R.

Bal, “Influence of Indium as a Promoter on the Stability and Selectivity of the Nanocrystalline Cu/CeO_2 Catalyst for CO_2 Hydrogenation to Methanol,” *ACS Appl. Mater. Interfaces*, vol. 13, no. 24, pp. 28201–28213, 2021, doi: 10.1021/acsami.1c05586.

[110] J. Wang, K. Sun, X. Jia, and C. jun Liu, “CO_2 hydrogenation to methanol over Rh/In_2O_3 catalyst,” *Catal. Today*, vol. 365, no. February 2020, pp. 341–347, 2021, doi: 10.1016/j.cattod.2020.05.020.

[111] K. Sun, Z. Fan, J. Ye, J. Yan, Q. Ge, Y. Li, W. He, W. Yang, and C. J. Liu, “Hydrogenation of CO_2 to methanol over In_2O_3 catalyst,” *J. CO2 Util.*, vol. 12, pp. 1–6, 2015, doi: 10.1016/j.jcou.2015.09.002.

[112] M. S. Frei, C. Mondelli, A. Cesarini, F. Krumeich, R. Hauert, J. A. Stewart, D. Curulla Ferré, and J. Pérez-Ramírez, “Role of Zirconia in Indium Oxide-Catalyzed CO_2 Hydrogenation to Methanol,” *ACS Catal.*, vol. 10, no. 2, pp. 1133–1145, Jan. 2020, doi: 10.1021/acscatal.9b03305.

Chapter 2 Materials and methods

2.1 Reagents and chemicals

Copper nitrate (II) hemi(pentahydrate) $Cu(NO_3)_2 \cdot 2.5H_2O$, zinc nitrate hexahydrate $Zn(NO_3)_2 \cdot 6H_2O$, hydrated zirconium oxynitrate (IV) $ZrO(NO_3)_2 \cdot 6.2H_2O$, cerium nitrate (III) hexahydrate $Ce(NO_3)_3 \cdot 6H_2O$, and Indium (III) nitrate hydrate $In(NO_3)_3 \cdot 4.6H_2O$, all from Alfa Aesar, were used as the metal precursors of the solid catalysts without further purification. Sodium carbonate from Sigma Aldrich with >99% purity was used as precipitating agent. Deionized water was procured from a water purification system available on site in the laboratory.

For the determination of the response factors of the gas chromatograph and for the determination of the methanol concentration of the liquid product collected in the trap after the catalytic tests, methanol and 1-Propanol from Sigma Aldrich with a purity >99.9% were used.

For the catalytic tests, two different high pressure gas bottles from Linde were employed. One containing pure hydrogen (>99.9%) and the other one containing a gas mixture of 63.5 mole% of H_2, 31.5 mole% of CO_2 and 5 mole% N_2 used as an internal standard.

2.2 Catalysts synthesis methods and summary of all the catalysts prepared in this work

All the catalysts were prepared by a continuous coprecipitation method using a microfluidic device, with the exception of one catalyst prepared by the batch method. The processing steps used to obtain the final calcined catalysts are shown in Figure 2.1.

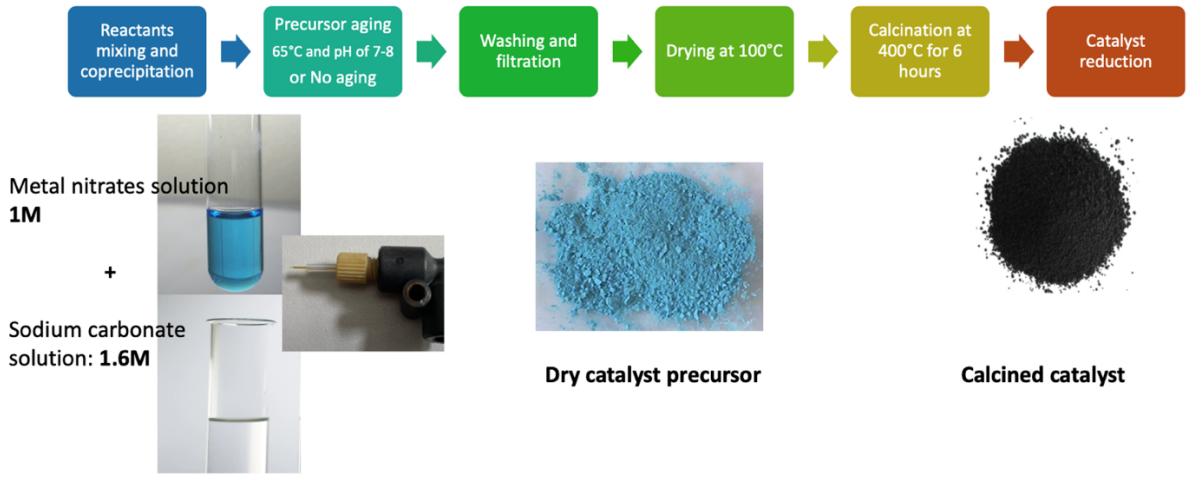

Figure 2.1 Processing steps to produce the final calcined catalysts.

Some modifications of the microfluidic synthesis process were made in order to investigate some parameters that affect the final properties of the catalysts. All the catalyst synthesis methods employed in this work are presented next.

2.2.1. Microfluidic continuous coprecipitation

A 1M metal precursors solution was prepared with the desired metals composition by using the metal nitrates presented before. A 1.6M solution of sodium carbonate was prepared separately using deionized water as a solvent. The solutions were then mixed at ambient temperature using a capillary micromixer with flowrates of 0.030 ml min^{-1} for each solution. Two Gilson 307 pumps were used to dose the aforementioned reactants' solutions. A HNP Mikrosysteme pump was used to pump 1.20 ml min^{-1} of deionized water used as a carrier fluid to transport the precipitate formed at the tip of the concentric capillaries to a stirred beaker heated to a temperature of 65ºC. This process was done continuously for approximately 7 hours, to obtain a mass of precipitate of approximately 1.2 g, depending on the composition of the catalyst. More details about this method can be found in the works of Angelo *et al*. [1] and l'hospital *et al*. [2].

After 7 hours of the synthesis time, the samples were collected and washed several times with warm deionized water, then filtered and dried in an oven at 100ºC for 15 hours. After obtaining the dried **precursor** material, the samples were ground and then calcined to obtain the unreduced powdered **catalyst**. The calcination was done with a heating ramp of 2ºC min^{-1} from ambient temperature to 400ºC. The 400ºC calcination temperature was held for 6 hours. After calcination, the samples were left to cool down slowly to ambient temperature. Lastly, before the catalytic tests, the calcined catalysts were reduced overnight, from ambient temperature to 280ºC at a heating rate of 1ºC min^{-1}, with a H_2 volume flowrate of 14 ml min^{-1} at a pressure of 50 bar. The only exception to this procedure was the catalysts containing In_2O_3, which were reduced at a temperature of 350ºC at a pressure of 5 bar, to avoid damages to the system caused by high temperatures and high pressures. Figure 2.2 shows the schematic of this catalyst's synthesis technique.

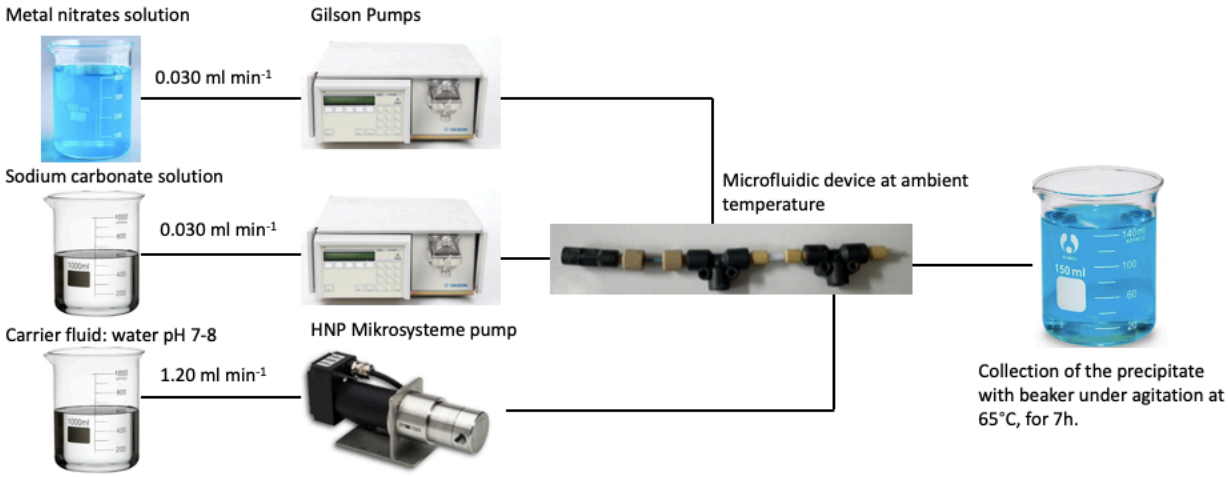

Figure 2.2 Schematic of the microfluidic continuous coprecipitation process.

2.2.2. Microfluidic synthesis with immediate filtration

This catalyst synthesis process was the same as the one above, except that the precipitate produced at the tip of the micromixer was not sent to a beaker for aging (Figure 2.3), but rather it was sent to a filter to collect it for the whole time of the synthesis (i.e. approximately 7 hours). After the end of the coprecipitation process, the collected precipitate was washed, filtered, dried and calcined with no aging, or it was aged for 17 hours, then washed, filtered dried and calcined. The washing, filtration, drying and calcination steps were identical for all the catalysts, as presented in the synthesis method explained above. This method was used to be able to control the aging time of the catalyst precursors.

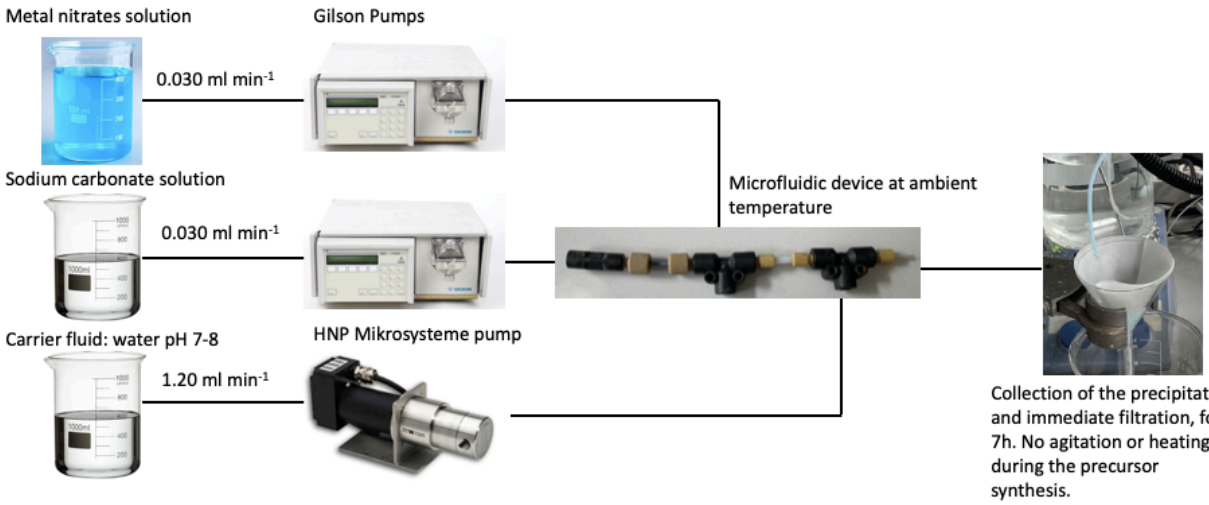

Figure 2.3 Schematic of the microfluidic synthesis with immediate filtration process.

2.2.3. Microfluidic synthesis with immediate filtration with heating of precipitation zone to 65ºC

This catalyst preparation procedure was the same as the one presented just above, but in this case, the microfluidic device was immersed in a hot water bath. In this way, the temperature of the microfluidic device and the reactants was adjusted to approximately 65ºC. Figure 2.4 shows the schematic of this synthesis approach.

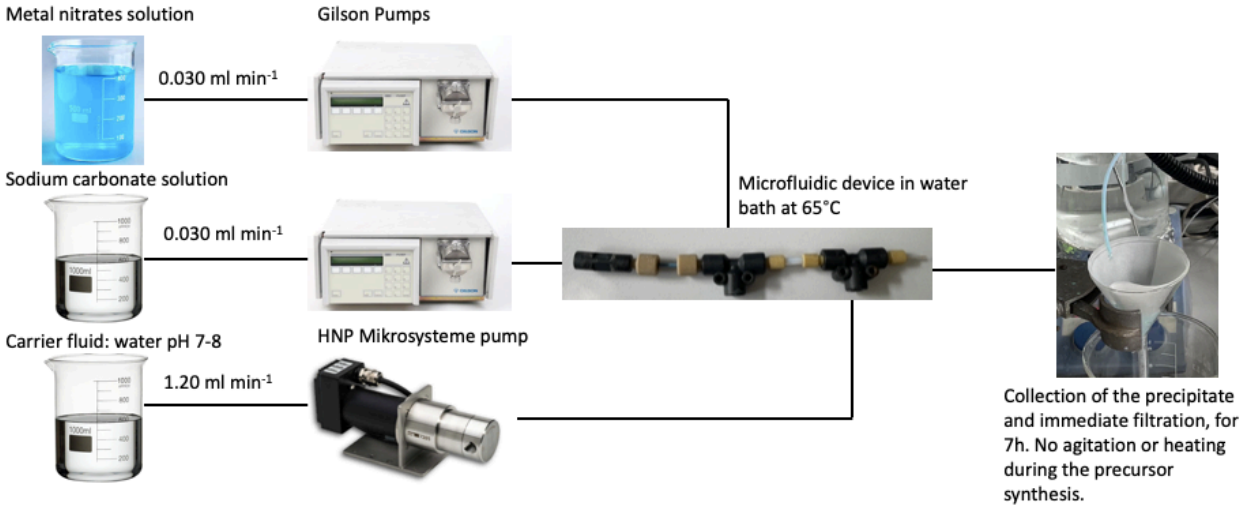

Figure 2.4 Schematic of the microfluidic synthesis with immediate filtration + heating of the precipitation zone to 65ºC.

2.2.4. Batch method synthesis

During this process, 20 ml of a metal nitrates solution (Cu, Zn and Zr nitrates) of 1M concentration and 20 ml of sodium carbonate of 1.6M concentration were added at a rate of 2 ml min^{-1} each to a stirred beaker containing 300 ml of distilled water at a temperature of 65ºC with a pH of 7. After the addition of the reactants which took 10 minutes, the precipitate was aged for 1 hour in the beaker at 65ºC, and then washed several times with warm distilled water, filtered and dried at 100ºC for 15 hours. The calcination step was performed under the same conditions used for the other catalysts.

2.2.5. Catalysts synthesized in this thesis and their composition

The names, compositions and corresponding chapters of all the catalysts synthesized in this thesis are presented in Table 2.1. The employed ZnO/ZrO_2 ratio for the catalysts containing Cu, Zn and Zr was 1.95. This value was selected from the work of L'hospital *et al*. [3] who determined it was the optimum ZnO/ZrO_2 ratio giving a Cu-ZnO-ZrO_2 catalyst with the optimum catalytic performance.

Table 2.1 Catalysts of each chapter and their mass % composition.

Catalyst name	Catalyst composition, wt%	Chapter
Microfluidic	33% CuO, 33% ZnO, 33% ZrO_2	3
Batch	33% CuO, 33% ZnO, 33% ZrO_2	3
CuO 33-0h	33% CuO, 33% ZnO, 33% ZrO_2	4
CuO 33-17h	33% CuO, 33% ZnO, 33% ZrO_2	4
CuO 50-0h	50% CuO, 33% ZnO, 17% ZrO_2	4
CuO 50-0h-65	50% CuO, 33% ZnO, 17% ZrO_2	4
40% CuO	40% CuO, 39.6% ZnO, 20.4% ZrO_2	5
50% CuO	50% CuO, 33% ZnO, 17% ZrO_2	5
60% CuO	60% CuO, 26.4% ZnO, 13.6% ZrO_2	5
CuO 50 CeO_2 10-0h	50% CuO, 33% ZnO, 10.2% CeO_2 6.8% ZrO_2	5
CuO 50 CeO_2 10-0h-65	50% CuO, 33% ZnO, 10.2% CeO_2 6.8% ZrO_2	5
ZnZrIn	60% ZnO, 30% ZrO_2 and 10% In_2O_3	5
CuZnZrIn	40% CuO, 33.3% ZnO, 16.6% ZrO_2 and 10% In_2O_3	5

2.3. Catalyst characterization techniques

2.3.1. X-ray diffraction (XRD) analysis

X-Ray diffraction analysis provides important information regarding the crystalline structure of materials, and it allows identifying the presence of different phases based on standards of other substances available in databases. Both qualitative and quantitative information of a sample can be obtained by the use of this technique [4]. X-Ray diffractograms can tell the user if the material is crystalline, amorphous or semi crystalline. Also, they can give an estimate of the size of the nanocrystallites of the material, as well as the spacing between planes and unit cell dimensions, which can give information about the unit cell of the material [5]. In general, the presence of broad diffractogram peaks occur due to the presence of small and defect-rich crystallites, as well as anisotropic crystallites, whereas isotropic crystallite shapes produce narrow XRD diffractograms [6]. Solid catalyst materials often consist of nanocrystalline and defect-rich phases [6]. The following equations can give important information about the crystallinity of a determined material:

Equation 2.1 Scherrer equation.

$$FWHM = \frac{K\,\lambda\,\times\,57.3}{D\,\cos\Theta}$$

Equation 2.2 Wilson equation.

$$FWHM = 4\,\varepsilon\,\tan\Theta$$

Equation 2.3 Bragg's Law.

$$\lambda = 2d_{hkl} \sin\Theta$$

Where FWHM is in ºθ, K is the crystallite shape form factor, λ is the X-ray wavelength, D is the crystallite size, Θ is the Bragg angle corresponding to the maximum of the diffraction peak (in θ) and ε is the micro-strain, d_{hkl} is the distance between parallel planes of atoms in the family (hkl) [6].

The XRD technique also allows to calculate the degree of crystallinity of a material expressed as a percentage, by taking into account the area corresponding to crystalline material and the area corresponding to amorphous material. The EVA XRD software allows determining this property. An example is presented in Figure 2.5, in which it can be seen that the gray area of the diffractogram corresponds to the amorphous fraction of the material and the rest of the area corresponds to the fraction of crystalline material.

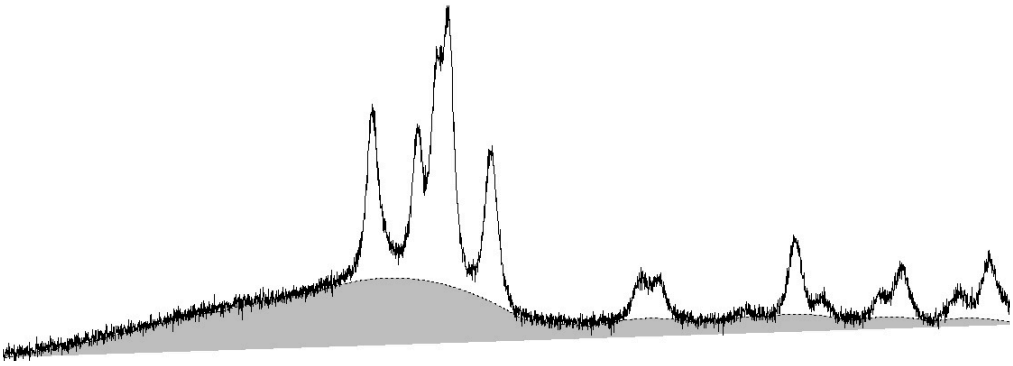

Figure 2.5 Example of the determination of the crystallinity % of the 40% CuO catalyst by calculating the areas of crystalline and amorphous material. Image taken from EVA XRD software.

Analysis procedure

The crystalline structure of the catalyst precursors and calcined catalysts was determined by the X-Ray diffraction technique, with a Bruker D8 Advance apparatus, equipped with a LYNXEYE detector and a nickel filter to remove the Kα emissions of copper. The measurements were performed from a 2θ value of 10º to 70º with a step of 0.016º every 0.5 seconds. The identification of the phases was done with the aid of Powder Diffraction Files, from data available in the literature and with the EVA XRD software. The crystallite sizes were calculated with the Debye-Scherrer equation (eq. 2.1).

2.3.2. Thermogravimetric analysis (TGA)

TGA is a destructive technique that allows investigating the mass changes of a material while increasing the temperature at a controlled rate using high purity air or an inert gas atmosphere. The mass changes that occur are due to chemical (e.g. oxidation, decomposition) and/or physical (e.g. evaporation) transformations. These changes are detected by a high precision scale that monitors all the mass changes of the sample. The main results of this analysis are a mass vs. temperature graph and also the derivative of the same curve, which allows identifying the temperatures at which important mass changes occur. This technique can also be used to study the composition of the sample by comparing its decomposition profile to the decomposition profile of a known material. This technique also allows studying the thermal stability of a material.

Analysis procedure

Thermogravimetric analysis of the catalyst precursors was performed using a TGA Q5000 TA Instruments apparatus. A mass of non-calcined precursor of 1 to 5 mg is placed in a small platinum basket and then the samples are heated and decomposed from ambient temperature to 700ºC, using a heating rate of 10 ºC min^{-1} under an air atmosphere supplied at a rate of 25 ml min^{-1}. After the analysis, a mass % decomposition curve as a function of temperature was obtained as well as a derivative curve.

2.3.3. N_2-physisorption analysis

The surface area determination of porous solid materials by employing the BET theory is still the most widely utilized method [7]. For the determination of the surface area, first it is necessary to transform a physisorption isotherm into a “BET plot” and then derive a value of the BET monolayer capacity n_m. Then, the BET area is calculated from the value of specific monolayer capacity n_m, by taking an appropriate value of the molecular cross-sectional area σ_m of the adsorbate [7]. The BET equation in the linear form is the following:

Equation 2.4 Linearized BET equation.

$$\frac{P/P^o}{n(1-P/P^o)} = \frac{1}{n_m C} + \frac{C-1}{n_m C}\left(P/P^o\right)$$

Where n is the specific amount adsorbed at the relative pressure P/P^o, C is the BET C-value and n_m is the specific monolayer capacity. The BET surface area is calculated by using equation 2.5:

Equation 2.5 BET surface area equation.

$$S_{BET} = \frac{n_m \, L \, \sigma_m}{V_o \, m}$$

Where L is the Avogadro constant, σ_m the molecular cross-sectional area of the adsorbate (i.e. 0.162 nm^2 for nitrogen), V_o the molar gas volume of the adsorbate at STP and m is the sample mass. The amount of gas being adsorbed as a function of the relative pressure is what defines the adsorption isotherms. Their shape is related to the texture of the solid [8]. Hysteresis is observed in porous material and it is a difference in paths between the adsorption and desorption processes caused by the shape of the pores [8].

The shape of the adsorption-desorption isotherms and the hysteresis loops give an indication of the adsorption and pores filling mechanisms [9]. The classification of the isotherms and the hysteresis loops is done according to the IUPAC standards. There are 6 different types of adsorption isotherms, which relate to six different surface textures of material. It is important to keep in mind that the obtained results of surface area and porosity depend on the experimental methods used, and that in the case of highly porous materials, absolute values of these properties may not be obtained [9].

Analysis procedure

The textural properties of the calcined catalysts were analyzed by the adsorption-desorption of nitrogen at -196ºC, using the BET method in a Micromeritics ASAP 2420 device. The isotherms were built in accordance with the BET theory for surface area calculation, and the Barrett-Joyner-Halenda (BJH) method was used to determine the pore size distribution (PSD) of the materials. Approximately 200 mg of powdered catalysts were degassed under vacuum to eliminate impurities and moisture adsorbed to the surface. After degassing, the adsorption and desorption isotherms were measured at -196°C. The surface area values were calculated by applying the BET equation to the N_2 adsorption isotherm within the relative pressures $0.05 < P/P^o < 0.30$. On the other hand, desorption data were used to determine the pore size distribution by applying the Barrett–Joyner–Halenda (BJH) method, assuming a cylindrical pore model [10].

2.3.4. Scanning electron microscopy (SEM) and energy dispersive X-ray spectroscopy (EDS)

Scanning electron microscopy (SEM) is a technique employed to study the morphology and the surface of a material [11]. In SEM, the image is produced by scanning a focused probe beam across the surface of the sample under vacuum and by detecting the backscattered and secondary electrons generated, with the secondary electrons being the most used [11], [12].

The energy dispersive X-ray spectroscopy (EDS or EDX) is used to determine the elemental composition of the samples. A detector of the length of the characteristic X-rays allows the identification and quantification of the elements present in the sample, giving as a result a spectrum that is used for the quantification of the elements [11].

Analysis procedure

The morphology of the materials was studied with the use of a scanning electron microscope ZEISS GEMINI SEM 500 with a resolution of 1.2nm at 500V and 1.1nm at 1kV, equipped with an Inlens detector and simultaneous analysis EDS.

2.3.5. Fourier transform infrared spectroscopy (FT-IR)

FT-IR is one of the most common spectroscopic techniques used today, thanks to its many advantages, such as its use as a qualitative and also quantitative technique, its rapidness, sensitivity and ease of use [13]. In this analytical technique, infrared radiation is passed through the sample. Some of this radiation is absorbed by it while the rest passes through it or is transmitted [14]. As the name implies, infrared radiation is used, which goes from 4000 to 400cm^{-1} wave number. After recording the emitted, transmitted and scattered radiation, a spectrum is created, which serves as a fingerprint of the sample, by giving information about the frequencies of vibrations between the bonds of the atoms that make up the material analyzed [14].

For the interpretation of the resulting spectra, information of the IR absorption peaks can be taken from the literature. For example, hydrocarbons present absorption peaks between 600 and 3300 cm^{-1} due to C-H stretching vibrations, benzene rings give absorptions at about 680-900 cm^{-1}, CN triple bonds absorption occurs between 2200-2300 cm^{-1}, alcohols and amines present OH or NH stretching absorption at 3000-3700 cm^{-1}, ethers have a C-O stretch in the region of 1050-1260 cm^{-1}, carbonyl compounds C=O stretch can be found at 1640-1820 cm^{-1}, and carboxylic acids present a distinctive OH band around 3300cm^{-1} [14].

Analysis procedure

The FT-IR analysis was done with the use of a FT-IR Nicolet iS10 spectrometer from Thermo Scientific. Before analyzing the catalyst samples, a calibration was done to remove the signals corresponding to the CO_2 present in the environment. Afterwards, the sample was placed in the corresponding place, and then the FT-IR spectrum was generated and collected. Each analysis involved 16 scans with a resolution of 6.

2.3.6. Composition determination by X-ray fluorescence (XRF)

X-ray Fluorescence is a spectroscopic technique that is used to determine the elemental composition of materials, and it can determine almost all the elements present in a sample [15]. The principle of functioning of this technique is based on the emission of fluorescent or secondary X-rays from a sample that is excited by primary X-rays. When an atom in the sample is hit with an X-ray of sufficient energy from a controlled X-ray tube, an electron of the atom's inner orbital shell is dislodged [16]. The atom then becomes stable by filling the vacancy left in the inner orbital shell with an electron from one of the atom's higher energy orbital shells. The electron then drops to the lower energy state by releasing a fluorescent X-ray [16]. The energy of the produced X-ray is equal to the difference in energy between the two quantum states of the electron and this energy difference is what is measured during the XRF analysis [16]. The execution of this analysis by Mrs. Véronique Delval and by Mr. Jeremy Brandel from École Européene d'ingénieurs de chimie, polymères et matériaux (ECPM) of Strasbourg, is greatly appreciated.

Analysis procedure

A Shimadzu EDX-7000 instrument was employed to analyze the catalysts by XRF. The solid samples were deposited in capsules specific to the analysis of XRF. A first method was created allowing the analysis of elements from sodium to uranium with a collimator diameter set at 5 mm in order to verify the feasibility of the analysis and a focus on the alpha lines of the elements. On the spectrum of Figure 2.6, a superposition of the alpha line of zinc with the beta line of copper was observed. Therefore, it was decided to follow the beta line of Zinc by creating a second method.

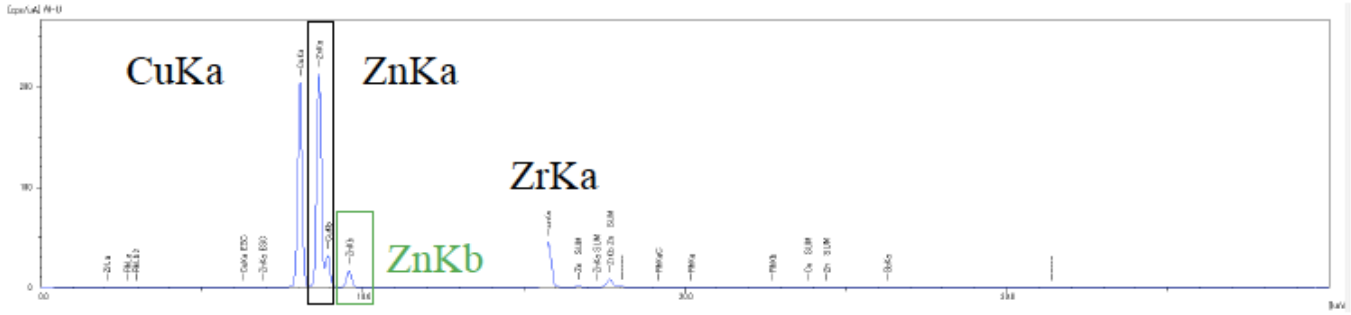

Figure 2.6 XRF spectrum for the quantification of Cu, Zn and Zr.

2.3.7. CO_2-temperature programmed desorption (CO_2-TPD)

The CO_2-TPD analysis is used to characterize the surface basicity of a catalyst and to determine the presence and quantity of weak, moderate strength and strong basic sites. The strength of the basic sites is related to the desorption temperatures during the analysis, where weak desorption peaks occur at temperatures below than 300ºC, moderate strength desorption peaks occur at temperatures between 300 and 500ºC

and strong basic sites occur at temperatures above 500ºC [17]. The technique is based on the ability of CO_2, an acid molecule, to react with the basic sites of the catalyst, which may be attributed to surface hydroxyl groups in the case of weak basic sites, metal-oxygen pairs to moderate strength basic sites or low coordination oxygen atoms in the case of strong basic sites [18]. This analysis shares many similarities with other temperature programmed techniques [19], as the procedure consists of the following steps: catalyst reduction and pretreatment with an inert gas, gas adsorption or saturation with a probe molecule (e.g. CO_2 in this case), purge of excess gas, temperature increase and gas desorption and quantification.

Analysis procedure

The surface basicity of the catalysts was studied with the use of a Micromeritics Autochem II 2920 apparatus equipped with a thermal conductivity detector (TCD) and a mass spectrometer Pfeiffer. For the analysis, 200 mg of the powdered catalyst were placed in a quartz U-shaped reactor between two quartz wool plugs. The catalyst was then reduced under a flow 50 ml min^{-1} of 10% H_2/Ar until 300ºC with a heating rate of 3ºC min^{-1}. The catalyst was then cooled to 50ºC under pure Ar flow 50 ml min^{-1} and then it was saturated using a stream of 20 ml min^{-1} of pure CO_2 during 20 minutes. The excess and weakly adsorbed CO_2 was purged [19] from the catalyst with the use of a 50 ml min^{-1} flow of helium until the TCD baseline became stable. Finally, the sample was heated from 50ºC to 900ºC with a temperature ramp of 20 ºC min^{-1} under a helium flow of 20 ml min^{-1}. When achieving a temperature of 900ºC, it was held at 900ºC for 1 hour. The CO_2 desorbed during the final temperature ramp was monitored with the use of a TCD and also with a mass spectrometer.

2.3.8. H_2-temperature programmed reduction (H_2-TPR)

H_2-TPR analysis is used to determine the number of reducible species present in the catalyst. It can also determine the temperature at which the reduction reaction occurs, as well as the amount of reducible metal present in the sample [20]. Equation 2.6, shows a general reduction reaction of a metal oxide.

Equation 2.6 General metal oxide reduction reaction.

$$M_xO_y + yH_2 \rightarrow xM + yH_2O$$

During this process, a stream of hydrogen diluted with an inert gas (i.e. nitrogen or argon) is passed over the sample in a controlled manner following a specified temperature ramp, which gradually reduces the metal species. The products of this reaction are the reduced metal and water, which is normally removed from the product gas by using a cold trap. As the analysis goes on, the hydrogen is consumed in the reduction reaction, which decreases the thermal conductivity of the flowing gas. This change in thermal conductivity is measured by the TCD, and transformed to a signal

that contains the results of the hydrogen consumption during the analysis. This technique can also give important information, useful to evaluate the reproducibility of the catalyst surface, the interactions between promoters and metal-support [21], as well as the redox behavior of the catalyst [22]. The features of the H_2-TPR profiles providing information about the catalyst are the peak positions, areas, and peak widths [23]. Generally, it is beneficial when the reduction starts at low temperature to minimize particle growth [23].

Analysis procedure

The reducibility of the calcined catalysts was determined using a Micromeritics Autochem II 2920 apparatus equipped with a thermal conductivity detector (TCD), using a flow of 50 ml min^{-1} of reducing gas (10 mole% of hydrogen in argon) with a heating ramp of 10ºC min^{-1} up to 900ºC, or in some cases up to 280ºC. A final reduction temperature of 280ºC was selected when the sample was going to be subjected to N_2O surface reaction analysis after the reduction step. For the analysis, 50 mg of the powdered catalyst were placed in a quartz reactor between two quartz wool plugs. Prior to the analysis, the sample was kept under a flow of 50 ml min^{-1} of 10 mol% H_2 diluted in argon at ambient temperature until a stable baseline was obtained. The effluent gases generated during the reduction reaction passed through a cold trap to condense the water formed during the test. The hydrogen consumed during the process was measured with the help of a thermal conductivity detector (TCD).

2.3.9. Nitrous oxide (N_2O) surface reaction

The study of the surface characteristics of the active metal phases in solid catalysts is important to understand different properties of these materials, as well as reaction mechanisms and pathways during chemical reactions. Properties such as active metallic surface area, metal dispersion, particle size and productivity per unit of surface metal can be determined using nitrous oxide surface reaction [24].

During this analysis, a bed of catalyst is reduced at mild conditions in order to obtain a material with the reduced metal available for reaction. The metal studied in this case is copper. After the preliminary reduction process, a diluted flow of nitrous oxide in argon or helium (e.g. 2%) is sent through the bed of catalyst, where the nitrous oxide molecules adsorb on the active copper surface and decompose into nitrogen gas and oxygen [25]. The oxygen remains bound to the surface copper, which is only oxidized from its Cu^0 state to the Cu^{+1} state, if the conditions of the analysis are appropriate [26]. During this mild oxidation process, only the most superficial copper is oxidized, leaving the bulk copper in its original state. This allows the characterization of the copper surface area available for reaction. Equation 2.7 shows the chemical reaction that occurs during the analysis [25]

Equation 2.7 Surface Cu oxidation with N_2O for the determination of Cu surface area, dispersion and particle size

$$N_2O_{(g)} + 2Cu_{(s)} \rightarrow N_{2(g)} + (Cu - O - Cu)_s$$

During the entire process, the effluent from the reactor is analyzed, typically by using a thermal conductivity detector (TCD) to measure the evolved N_2 [27]. The process finishes when the N_2O stops reacting and being converted into N_2. The metal surface area is a property that can be used to characterize the catalyst, by quantifying the metal area that's exposed and available for reaction. After finding the metal surface area, other properties such as metal dispersion, metal particle size and the degree of reduction of the metal can be calculated. Equation 2.8 can be used to calculate the copper particle size d_{Cu} by using the copper dispersion D_{Cu} [28]**.** The rest of the calculations for this analysis can be found in the thesis of Jiang [29].

Equation 2.8 Calculation of Cu particles size

$$\mathrm{d_{Cu}(nm)} = \frac{104}{\mathrm{D_{Cu}}}\ (\%)$$

Analysis procedure

The determination of the metallic copper surface area, copper dispersion and particle size was done using a Micromeritics AutoChem II 2920 equipped with a quartz reactor and a cold trap used to condense the water that is produced during the reduction step. During this analysis, the catalyst is pre-reduced under a 50 ml min^{-1} flow of reducing gas (i.e. 10% of hydrogen in argon) with a ramp of 1ºC min^{-1} until 280ºC. This temperature is maintained for 12h and then the sample is cooled under a flow 50 ml min^{-1} of argon. Once the catalyst is cooled to 50ºC, a flow of 50 ml min^{-1} of oxidizing gas (i.e. 2% N_2O/Ar) is turned on and left to react with the superficial copper of the catalyst during 20 minutes. The N_2 formation during the oxidation of the superficial Cu by N_2O was followed by a thermal conductivity detector.

2.4. Reaction setup and catalytic tests

2.4.1. Description of the reaction setup

The activity of the catalysts was determined using a high pressure reactor setup equipped with different elements, including 1/8" stainless steel pipelines, high pressure gas bottles, a gas mixer, different valves to regulate the gas flows, a stainless steel high pressure reactor equipped with a heating coil, a removable trap used to condense the water and the methanol produced during the reaction, among others. The producer of the pipes, valves and the high pressure reactor used in this work was

Swagelok. The system also included the appropriate instrumentation to guarantee the desired temperature, flowrates, pressure and composition of the feed gases. The reactor setup was built to resist pressures higher than 50 bar. It was also equipped with a bypass used to deviate the gas flow to the reactor, and it allowed to calibrate the gas flowmeters. A simplified process flow diagram of the reaction setup is presented in Figure 2.7.

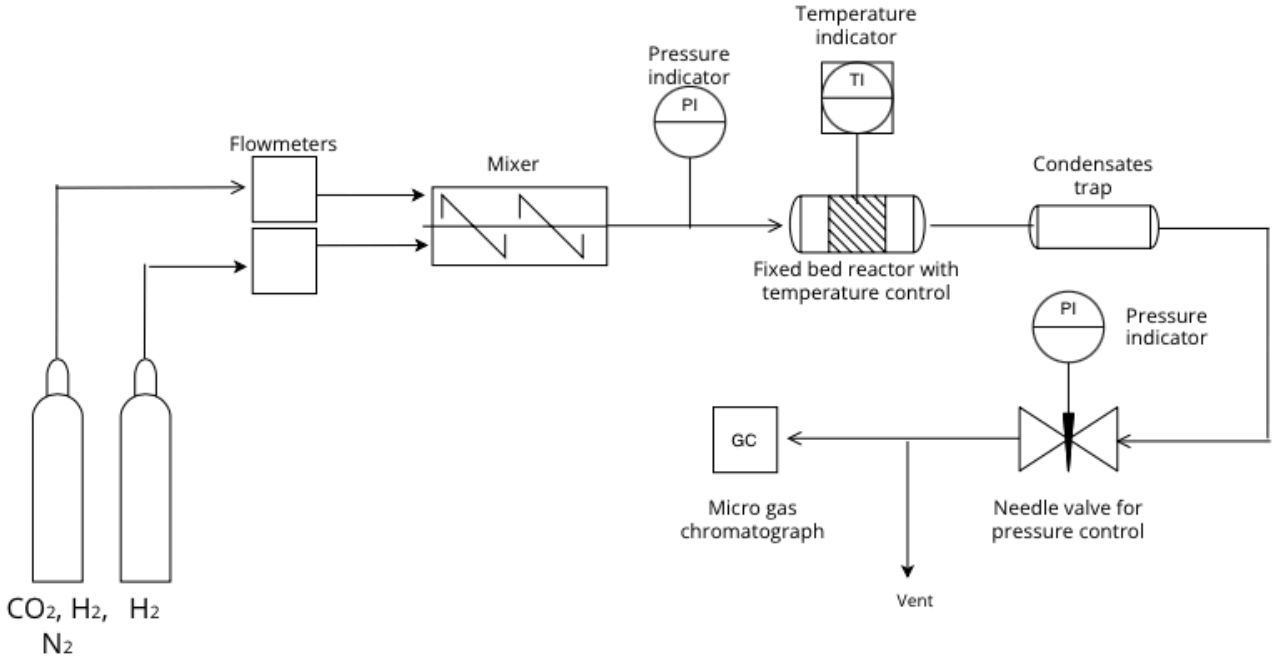

Figure 2.7 Simplified process flow diagram of the reaction setup employed for the catalytic tests.

Two different high pressure gas bottles from Linde were used for the catalytic tests. One containing pure hydrogen (>99.9%) and the other one containing a gas mixture of 63.5 mole% of H_2, 31.5 mole% of CO_2 and 5 mole% N_2 used as an internal standard. The adjustment of the flowrates was done with the use of Brooks Smart Mass Flow flowmeters controlled with a Brooks 0254 electronic control unit. The adjustment of the flowrates from each one of the two bottles allowed obtaining a feed gas with a molar ratio of 3.9 H_2/CO_2 and a total volumetric flowrate of 40 Nml min^{-1} used for all the catalytic tests.

After leaving the flowmeters, the gases passed through a mixer filled with small glass balls to ensure the proper mixing of the feed gases. Before entering the reactor, the line was equipped with a Keller Léo 2 pressure indicator and a bypass consisting of 3 valves used to calibrate the flowmeters connected to the 2 high pressure gas bottles.

The reactor had a length of 27 cm and internal and external diameters of 6.0 mm and 9.5 mm respectively, which gives a wall reactor thickness of 1.8 mm. The airtightness of the reactor was ensured by the use of Swagelok metal gaskets at the upper and lower connectors of the reactor, avoiding gas leakages during the catalytic tests. The reactor was heated with a 11Ω. Thermocoax heating resistance coiled around it and

insulated with a thick layer of quartz wool. A thermocouple connected to a Minicor 42 temperature regulator was placed around the reactor at the catalyst bed level to maintain the temperature of the reactor as close to the nominal value as possible.

After going through the reactor, the gas flowed to a removable metal trap where the condensable compounds were recovered (i.e. methanol and water) and then encountered another manometer. Finally, the gas flowed through a Brooks 5866 pressure controller connected to a Brooks 0254 electronic control unit, which controlled and maintained the pressure of the whole system. After the above step, the gas was at ambient pressure and flowed to the micro-chromatography system that allowed to determine its composition.

2.4.2. Catalytic tests methodology

For each catalytic test, 100 mg of catalyst in the form of a powder were packed between two beds of inert quartz wool in the middle of the reactor. Before loading the catalyst into the reactor, the material was crushed thoroughly with a mortar and pestle, which allowed obtaining a very fine powder, avoiding the need of sieving the catalyst to a determined particle size range. After closing the reactor properly, the pressure was increased from ambient to 50 bar by using H_2 gas only. The catalyst was then reduced under a stream of 14 ml min^{-1} of H_2 for a minimum of 12 hours, heated with a temperature ramp of 1 ºC min^{-1} from ambient temperature to 280 ºC. After the reduction process, the reactor was left to cool down to a temperature of 100 ºC and purged with the reactant gases (i.e. pure hydrogen and CO_2-H_2-N_2 gas mixture). Blank measurements were taken during this step in order to determine the real composition of the inlet gas stream used during the catalytic test. After the stabilization of the flows and the measurement of the blanks, the reactor was heated up to the first reaction temperature of 240 ºC with a heating ramp of 1 ºC min^{-1} at a pressure of 50 bar. The micro-chromatograph gas injections were done every 30 minutes for more than 36 hours for each reaction temperature. The process was repeated for the remaining temperatures (i.e. 260, 280 and 300 ºC). More details about the catalytic tests methodology are discussed next.

2.4.3. Gas and liquid products analysis

The analysis of the gas product of the reactor was done with an INFICON 3000 micro gas chromatograph equipped with two TCD detectors and 2 columns for the separation of gases. A Molsieve column (10m x 320µm x 30µm) for the separation of hydrogen, nitrogen, methane and carbon monoxide, with argon as vector gas at 100ºC and at 33psi was used, as well as a PPQ module with backflush, a Poraplot Q precolumn (1m x 320µm x 10µm) and a Poraplot Q column (8m x 320µm x 10µm) at 60ºC for the separation of light gases (N_2, O_2, CO, CH_4, Ar), CO_2 and also methanol,

with helium as vector gas. The GC calculations were performed with the aid of response factors and internal standards as explained by Rome *et al.* [30].

Equation 2.9 Calculation of response factors.

$$Response\ factor\ A = \frac{Peak\ area\ A}{Concentration\ A}$$

The response factor of each compound participating in the reaction was calculated by using a calibration gas bottle containing approximately 20 mole% of each of the following compounds: H_2, N_2, CH_4, CO and CO_2.

Equation 2.10 Calculation of relative response factors.

$$Relative\ response\ factor\ RRF = \frac{Response\ factor\ A}{Response\ factor\ B}$$

Compound B corresponded to the internal standard N_2 whose concentration is known before and after the dilution of the reactant gases.

Finally, the concentration of the compounds and their molar flowrate can be calculated with Equation 2.11.

Equation 2.11 Calculation of the concentration of species A from the response factors and the concentration of the known species B.

$$Concentration\ A = \frac{Peak\ area\ A}{Peak\ area\ B}\ x\ \frac{1}{RRF}\ x\ Concentration\ B$$

Moreover, the analysis of the liquid phase recovered from the trap after each catalytic test temperature was done with an Agilent Technologies 6890N chromatograph, equipped with a heated injector and a Solgelwax column from SGE analyticals (60m x 320µm x 0.25µm), using He as a carrier gas and equipped with a flame ionization detector (FID). For the analysis, a known amount of the sample was mixed with 1-propanol used as an external standard. The resulting mixture was diluted with distilled water, and then 2 µl volume was injected into the GC.

2.4.4. Catalytic tests calculations by considering the gas phase or the gas phase + the liquid phase

At this point, it should be explained that the catalytic tests calculations were carried out by two different methods. The first method consisted in using only the components peak areas obtained with the micro-gas chromatograph and calculating the effluent gas H_2, CO and CO_2 concentrations. Knowing the quantities of these gases in the effluent gas, it is possible to calculate the H_2 and CO_2 conversions, as well as the methanol selectivity and productivity by using the quantities of these components at

the inlet. The calculation of the methanol produced during the catalytic tests was done by subtracting the CO and CO_2 molar amounts in the effluent gas from the CO_2 at the inlet. It is safe to assume that the only carbon containing species in this system are CO, CO_2 and CH_3OH, as CH_4 or any other carbon containing species were not detected in this work. This method also allowed the reduction of the catalytic tests time, reducing it to less than 10 hours per catalytic test temperature.

The second method consisted in the collection of the liquid formed (i.e. water + methanol) during each reaction temperature of the catalytic test with the use of the metal trap located downstream of the reactor. Each liquid product obtained was analyzed separately by gas chromatography to determine its methanol concentration and to carry out the corresponding material balances. By determining the mass and the methanol fraction of this liquid, it is possible to calculate the H_2 and CO_2 conversions as well as the methanol selectivity and the methanol productivity. This method required more work as after each catalytic test temperature, the pressure of the system had to be lowered and the trap had to be uninstalled and weighed and then reinstalled again, and the pressure had to be increased again up to the working pressure of 50 bar.

Both methods were used for many of the catalysts studied in this work. However, due to practical reasons, the first method was applied to some catalysts at the end of this work to accelerate the catalytic tests, by avoiding the pressure reduction and pressure increase steps and the act of removing, weighing and reinstalling the trap after each catalytic test temperature. It is important to mention that the two methods allowed obtaining very similar results, validating the use of only the gas phase data for the calculations. A sample of the calculations by both methodologies is shown in Table 2.2.

Table 2.2 Catalytic tests results of catalyst CuO 50-0h obtained by the gas phase and the gas+ liquid phase method.

Temperature ºC	H_2 conversion %	CO_2 conversion %	Methanol selectivity %	Methanol productivity (gMeOH / kg cat . h)
Gas phase method				
240ºC	8.2	11.8	67.8	509
260ºC	10.6	17.6	57.1	640
280ºC	12.7	23.0	51.4	754
300ºC	13.8	26.5	46.1	779
Gas + liquid phase method				
240ºC	6.8	11.8	67.8	509
260ºC	9.0	18.0	57.9	662
280ºC	10.9	22.6	50.6	728
300ºC	12.4	26.9	46.9	803

As observed above, the resulting values of hydrogen and carbon dioxide conversions as well as methanol selectivity and productivities were very similar for both gas phase and gas + liquid phase calculation methods.

2.4.5. Catalysts performance calculations

The H_2 and CO_2 conversions as well as methanol and carbon monoxide selectivity % and the methanol productivity % are some of the most important parameters that describe the catalyst performance. The calculations of these parameters were done as indicated in the following equations.

2.4.5.1. Gas hourly space velocity (GHSV)

The gas hourly space velocity (i.e. GHSV) is calculated with the volumetric flowrate of the reactants fed to the reactor and the catalyst volume which is calculated with its apparent density.

Equation 2.12 Calculation of GHSV.

$$GHSV\ h^{-1} = \frac{volumetric\ rate\ of\ feed}{volume\ of\ catalyst}$$

Or it can be calculated as the volumetric rate of feed per mass of catalyst.

$$GHSV\ {}^{ml}/_{g\ x\ h} = \frac{volumetric\ rate\ of\ feed}{mass\ of\ catalyst}$$

2.4.5.2. Reactants conversion

The reactants conversion is calculated by dividing the moles of reactant consumed during the reaction by the moles of the reactant fed into the reactor. The conversion equations are shown next.

Equation 2.13 Calculation of CO_2 conversion %.

$$x_{CO2} = \frac{Moles\ CO_{2\ in} - \ Moes\ CO_{2\ out}}{Moles\ CO_{2\ in}}\ x\ 100$$

Equation 2.14 Calculation of H_2 conversion %.

$$x_{H2} = \frac{Moles\ H_{2\ in} - \ Moles\ H_{2\ out}}{Moles\ H_{2\ in}}\ x\ 100$$

2.4.5.3. Methanol and carbon monoxide selectivity

The selectivity % is calculated by taking into account the products of interest of the reaction and the undesirable byproducts. In this case, methanol was the product of interest and carbon monoxide was the undesirable byproduct. Methanol and carbon monoxide were the only carbon containing products in this process.

Equation 2.15 Calculation of the methanol selectivity %.

$$S_{CH3OH} = \frac{Moles\ CH_3OH_{out}}{Moles\ CH_3OH_{out} + Moles\ CO_{out}}\ x\ 100$$

Equation 2.16 Calculation of the CO selectivity %.

$$S_{CO} = \frac{Moles\ CO_{out}}{Moles\ CH_3OH_{out} + Moles\ CO_{out}}\ x\ 100$$

2.4.5.4. Methanol productivity

The productivity of methanol is calculated by using its mass flowrate and dividing it by the total mass of catalyst used for the catalytic test, as presented in Equation 2.17.

Equation 2.17 Calculation of the methanol productivity.

$$Productivity_{CH3OH} = \frac{Mass\ flowrate\ of\ methanol\ produced}{Mass\ of\ catalyst} = \frac{g_{CH3OH}}{kg\ cat\ x\ h}$$

2.5. Catalysts densities, gas-hourly space velocities (GHSV) and catalyst synthesis yields after the coprecipitation reaction

This section presents the densities of the catalysts, the calculated GHSVs and the catalyst yields obtained during the coprecipitation step.

The densities were measured by using a glass tube of a known internal diameter and mass and filling this tube with catalyst at different heights, to obtain different volumes measurements. The mass of each volume of catalyst was determined and the densities were calculated. The densities are shown in Table 2.3. The GHSVs of all the catalysts are shown in Table 2.3. They were calculated by dividing the volume flowrate of reactants which was 40 Nml min^{-1} by the volume of catalyst, calculated with the density and the mass. As mentioned before, the mass of catalyst employed for all the catalytic tests was 100 mg, in order to determine the catalytic performance per unit mass of catalyst.

Table 2.3 Catalysts densities, GHSVs and synthesis yields.

Catalyst	Density, g/cm^3	GHSVs, h^{-1}	Catalyst synthesis yields, %
Microfluidic	0.52	12 375	81.4
Batch	1.16	27 938	-
CuO 33-0h	0.69	16 479	83.0
CuO 33-17h	0.72	17 239	83.5
CuO 50-0h	0.58	13 943	92.2
CuO 50-0h-65	0.57	13 626	76.6
40% CuO	0.42	10 073	81.4
50% CuO	0.39	9 253	81.4
60% CuO	0.59	14 222	81.9
CuO 50 CeO_2 10-0h	0.81	19 351	82.2
CuO 50 CeO_2 10-0h-65	0.85	20 330	84.8
CuZnZrIn	0.73	17 552	96.2
ZnZrIn	1.08	25 823	84.7

Finally, the catalyst yields of each catalyst during the coprecipitation step are presented in Table 2.3. These values correspond to the ratio of the mass of catalyst obtained to the theoretical mass that should be obtained after the duration of the catalyst synthesis, which was approximately 7 hours. The values are lower than 100% due to the loss of catalyst during the different processing steps of the catalyst, such as washing, filtration, drying and calcination.

2.6. Bibliography of chapter 2

[1] L. Angelo, M. Girleanu, O. Ersen, C. Serra, K. Parkhomenko, and A. C. Roger, "Catalyst synthesis by continuous coprecipitation under micro-fluidic conditions: Application to the preparation of catalysts for methanol synthesis from CO_2/H_2," *Catal. Today*, vol. 270, pp. 59–67, 2016, doi: 10.1016/j.cattod.2015.09.028.

[2] V. L'hospital, S. Heyte, S. Paul, K. Parkhomenko, and A.-C. Roger, "Optimization of the continuous coprecipitation in a microfluidic reactor: Cu-based catalysts for CO_2 hydrogenation into methanol," *Fuel*, vol. 319, no. February, p. 123689, Jul. 2022, doi: 10.1016/j.fuel.2022.123689.

[3] V. L'hospital, L. Angelo, Y. Zimmermann, K. Parkhomenko, and A. C. Roger, "Influence of the Zn/Zr ratio in the support of a copper-based catalyst for the synthesis of methanol from CO_2," *Catal. Today*, vol. 369, no. April 2020, pp. 95–104, 2021, doi: 10.1016/j.cattod.2020.05.018.

[4] R. Schlögl, "Chapter 5 X-ray Diffraction. A Basic Tool for Characterization of Solid Catalysts in the Working State," *Adv. Catal.*, vol. 52, no. C, pp. 273–338, 2009, doi: 10.1016/S0360-0564(08)00005-9.

[5] J. M. Thomas, *Principles and practice of heterogeneous catalysis*. Wiley-VCH, 2015.

[6] D. Herein, "X-Ray Powder Diffraction," in *Handbook of Heterogeneous Catalysis*, 2008, pp. 765–774. doi: https://doi.org/10.1002/9783527610044.hetcat0039.

[7] M. Thommes, K. Kaneko, A. V. Neimark, J. P. Olivier, F. Rodriguez-Reinoso, J. Rouquerol, and K. S. W. Sing, "Physisorption of gases, with special reference to the evaluation of surface area and pore size distribution (IUPAC Technical Report)," *Pure Appl. Chem.*, vol. 87, no. 9–10, pp. 1051–1069, 2015, doi: 10.1515/pac-2014-1117.

[8] Micromeritics, "Micromeritics webinars on physical adsorption and surface phenomena." Accessed: Aug. 20, 2021. [Online]. Available: https://www.micromeritics.com/resources/videos/

[9] J. B. Hansen and P. E. Højlund Nielsen, "Methanol Synthesis," in *Handbook of Heterogeneous Catalysis*, 2008, pp. 2920–2949. doi: https://doi.org/10.1002/9783527610044.hetcat0148.

[10] N. Mota, R. Guil-Lopez, B. G. Pawelec, J. L. G. Fierro, and R. M. Navarro, "Highly active Cu/ZnO-Al catalyst for methanol synthesis: Effect of aging on its structure and activity," *RSC Adv.*, vol. 8, no. 37, pp. 20619–20629, 2018, doi: 10.1039/c8ra03291b.

[11] B. J. Inkson, *Scanning Electron Microscopy (SEM) and Transmission Electron Microscopy (TEM) for Materials Characterization*. Elsevier Ltd, 2016. doi: 10.1016/B978-0-08-100040-3.00002-X.

[12] H. K. K. Deutschmann, Olaf; Knözinger, "Heterogeneous Catalysis and Solid Catalysts," in *Ullmann's Encyclopedia of Industrial Chemistry*, Wiley-VCH Verlag GmbH & Co. KGaA, Weinheim, 2011, pp. 457–481.

[13] M. Hof, "Basics of Optical Spectroscopy," in *Handbook of Spectroscopy*, G. Gauglitz, Ed., Weinheim, Germany: Wiley-VCH, 2003, pp. 39–66.

[14] A. Dutta, "Fourier Transform Infrared Spectroscopy," in *Spectroscopic Methods for Nanomaterials Characterization*, S. Thomas, Ed., Elsevier, 2017, pp. 73–93.

[15] K. Janssens, "X-Ray Fluorescence Analysis," in *Handbook of Spectroscopy*, G. Gauglitz, Ed., Weinheim, Germany: Wiley-VCH, 2003, pp. 365–419.

[16] Thermofisher, "Thermofisher Scientific," What is XRF (X-ray Fluorescence) and

How Does it Work. Accessed: Aug. 08, 2023. [Online]. Available: https://www.thermofisher.com/blog/ask-a-scientist/what-is-xrf-x-ray-fluorescence-and-how-does-it-work/
[17] Z. Shi, Q. Tan, C. Tian, Y. Pan, X. Sun, J. Zhang, and D. Wu, "CO_2 hydrogenation to methanol over Cu-In intermetallic catalysts: Effect of reduction temperature," *J. Catal.*, vol. 379, pp. 78–89, 2019, doi: 10.1016/j.jcat.2019.09.024.
[18] T. Witoon, N. Kachaban, W. Donphai, P. Kidkhunthod, K. Faungnawakij, M. Chareonpanich, and J. Limtrakul, "Tuning of catalytic CO_2 hydrogenation by changing composition of CuO-ZnO-ZrO_2 catalysts," *Energy Convers. Manag.*, vol. 118, pp. 21–31, 2016, doi: 10.1016/j.enconman.2016.03.075.
[19] J. A. Schwarz, "Temperature-Programmed Desorption and Reaction: Applications to Supported Catalysts," *Catal. Rev.*, vol. 25, no. 2, pp. 141–227, 1983, doi: 10.1080/01614948308079666.
[20] Micromeritics, *AutoChem 2920 Automated Catalyst Characterization System Operator's Manual*, no. July. Micromeritics, 2009. [Online]. Available: https://www.micromeritics.com/Repository/Files/AutoChem_II_2920_Operator_Manual_V4.00.pdf
[21] Micromeritics, "Application note 120: TPR using the Autochem," 2021. [Online]. Available: https://www.micromeritics.com/Repository/Files/appnote120.pdf
[22] A. Pintar, J. Batista, and S. Hoevar, "TPR, TPO and TPD Examination of $Cu_{0.15}Ce_{0.85}O_{2-y}$ Mixed Oxide Catalyst Prepared by Co-precipitation Synthesis," *Micromeritics*, vol. 2, pp. 1–4, 2011.
[23] Schimpf and Muhler, "Synthesis of Solid Catalysts," in *Synthesis of Solid Catalysts*, K. P. de Jong, Ed., Wiley-VCH, 2009, pp. 1–401. doi: 10.1002/9783527626854.
[24] X. Jiang, X. Nie, X. Guo, C. Song, and J. G. Chen, "Recent Advances in Carbon Dioxide Hydrogenation to Methanol via Heterogeneous Catalysis," *Chem. Rev.*, vol. 120, no. 15, pp. 7984–8034, 2020, doi: 10.1021/acs.chemrev.9b00723.
[25] G. C. Chinchen, C. M. Hay, H. D. Vandervell, and K. C. Waugh, "The measurement of copper surface areas by reactive frontal chromatography," *J. Catal.*, vol. 103, no. 1, pp. 79–86, 1987, doi: 10.1016/0021-9517(87)90094-7.
[26] O. Hinrichsen, T. Genger, and M. Muhler, "Chemisorption of N_2O and H_2 for the surface determination of copper catalysts," *Chem. Eng. Technol.*, vol. 23, no. 11, pp. 956–959, 2000, doi: 10.1002/1521-4125(200011)23:11<956::AID-CEAT956>3.0.CO;2-L.
[27] M. Behrens and R. Schlögl, "How to prepare a good Cu/ZnO catalyst or the role of solid state chemistry for the synthesis of nanostructured catalysts," *Zeitschrift fur Anorg. und Allg. Chemie*, vol. 639, no. 15, pp. 2683–2695, 2013, doi: 10.1002/zaac.201300356.
[28] G. Bonura, M. Cordaro, C. Cannilla, F. Arena, and F. Frusteri, "The changing nature of the active site of Cu-Zn-Zr catalysts for the CO_2 hydrogenation reaction to methanol," *Appl. Catal. B Environ.*, vol. 152–153, pp. 152–161, 2014, doi: 10.1016/j.apcatb.2014.01.035.
[29] Q. Jiang, "Synthèse directe de diméthyl éther à partir de CO_2/H_2," Université de Strasbourg, 2017.
[30] K. Rome and A. Mcintyre, "Intelligent use of relative response factors in gas chromatography-flame ionisation detection," *Chromatogr. Today*, no. June, pp. 52–56, 2012.

Chapter 3 Effect of the synthesis method on the properties of CuO-ZnO-ZrO_2 catalysts for the hydrogenation of carbon dioxide to methanol

3.1. Introduction

The catalysts based on Cu-ZnO-ZrO_2 for the hydrogenation of CO_2 to methanol have gained increasing attention due to their interesting properties and catalytic performance under CO_2 rich feedstock. Different synthesis techniques have been investigated for the production of these catalysts, with the synthesis by batch method being one of the simplest and easiest way to carry out the coprecipitation reactions. However, the batch synthesis coprecipitation technique presents disadvantages such as the occurrence of pH, temperature and concentration gradients [1], which can affect the repeatability of the synthesis, resulting in non-uniform properties in the catalysts. These problems can be mitigated with the application of the microfluidic coprecipitation technique, which is known for its beneficial effects on the Cu crystallite sizes, Cu surface area and dispersion, and on the specific surface area of the catalysts [2]–[4].

In this chapter, two Cu-ZnO-ZrO_2 catalysts with the same compositions (i.e. 33.3wt% CuO, 33.3wt% ZnO, 33.3wt% ZrO_2) were prepared by the microfluidic and by the batch methods with the aim of determining the main differences in their properties and their final catalytic performance for the hydrogenation of CO_2 to methanol. The catalyst composition given above was chosen due to the possibility of studying the promoting effects of ZnO and ZrO_2 allowing to obtain catalysts with high activity and selectivity for the CO_2 hydrogenation to methanol.

Different analysis techniques were used for the characterization of the catalysts and they are presented in the following sections along with the discussion of the results and the results of the catalytic tests.

3.2. Catalysts characterization results and discussion

Two catalysts were investigated in this chapter, the Microfluidic and Batch catalysts, which were prepared by the Microfluidic continuous coprecipitation and by the Batch method, respectively. The description of the batch and microfluidic continuous coprecipitation synthesis methods employed in this chapter can be found in Chapter 2, section 2.2.

For more clarity, the catalyst precursors correspond to the materials obtained by coprecipitation (i.e. hydroxycarbonates) after drying and before calcination, and the calcined catalysts correspond to the catalyst precursors after calcination.

The X-ray diffractograms of the precursors and the calcined catalysts prepared by the Batch and Microfluidic methods are presented in Figures 3.1a and 3.1b. As seen in Figure 3.1a, the phases aurichalcite $Zn_3Cu_2(OH)_6(CO_3)_2$ (PDF number: 82-1253) and hydrozincite $Zn_5(CO_3)_2(OH)_6$ (PDF number: 72-1100) were identified in both precursors. As mentioned before, aurichalcite is a hydroxycarbonate that contains

both Cu and Zn in its crystalline structure, which is desirable given the close contact and interaction of these two metal species [5]–[7]. No Zr-containing crystalline phase was observed in the precursors due to the presence of this species in an amorphous state [8]–[11].

The crystallite sizes of the aurichalcite and hydrozincite phases in the precursors were calculated with Scherrer's equation and are shown in Table 3.1. The 2Theta values used to calculate the crystallite sizes were 13º for both aurichalcite and hydrozincite (hkl: 200 for both phases). The results show that the aurichalcite and hydrozincite phases in the precursor prepared by the batch method presented smaller crystallite sizes (i.e. 8 nm) compared to the phases developed in the precursor synthesized by the microfluidic method (i.e. 13 nm). This size difference may be due to the different aging time of both catalysts, which was longer for the precursor synthesized by the microfluidic method, thus developing bigger crystallites. The longer aging time of the microfluidic method in this case was due to the inherent slow coprecipitation process, as the metal nitrates solution and the precipitating agent sodium carbonate are pumped at a flowrate of 0.030 ml min^{-1} each for several hours, while during the batch synthesis all of the reactants are pumped in only a few minutes.

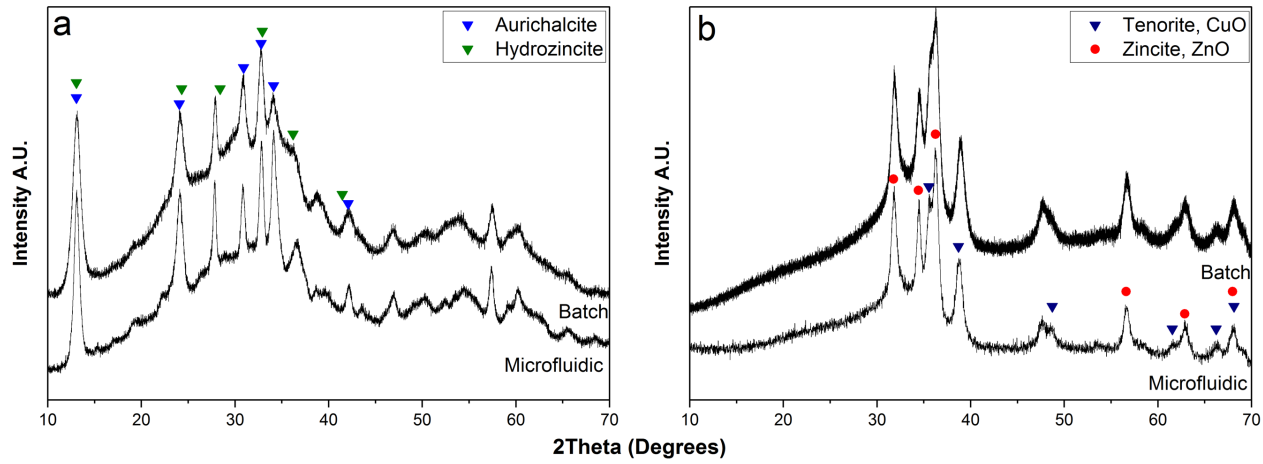

Figure 3.1 X-ray diffractograms of the catalyst precursors (a) and the calcined catalysts (b) synthesized by the batch and microfluidic methods.

Table 3.1 Crystallite sizes (nm) of the phases present in the catalyst precursors and in the catalysts after calcination calculated by Scherrer's equation.

	Catalyst precursor		Calcined catalyst		
Sample	**Aurichalcite**	**Hydrozincite**	**Tenorite, CuO**	**Zincite, ZnO**	**Crystallinity %**
Microfluidic	13	13	12	12	43.5
Batch	8.4	8.4	10	11	40.2

Regarding the calcined catalysts, the X-ray diffractograms in Figure 3.1b show the presence of tenorite (CuO) (PDF number: 72-0629) and zincite (ZnO) (PDF number:

75-1526) phases in both catalysts. The crystallite sizes of CuO and ZnO of the catalysts after calcination were calculated with Scherrer's equation and are shown in Table 3.1. The 2Theta values used to calculate the crystallite sizes were 38.7º (hkl: 111) for CuO and 32º (hkl: 100) for ZnO. No zirconium compounds were identified in the diffractograms of the calcined catalysts, which is in agreement with the literature which suggests that zirconia is present in an amorphous state [12]–[14]. No tetragonal or monoclinic zirconia (PDF numbers: 50-1089 and 37-1484 respectively) with the main reflections at the 2Theta values of 30.2º and 28.1º respectively, were detected in the diffractograms. From the results of different research works [6], [15], [16], it can be inferred that the formation of crystalline forms of zirconia such as tetragonal and monoclinic zirconia is favored at temperatures above 400ºC, which is the calcination temperature of all the catalysts in this thesis. Despite being present as an amorphous compound, the presence of zirconia is important as a component of Cu-ZnO catalysts for the hydrogenation of CO_2 to methanol, given its less hydrophilic character compared to Al_2O_3 [17], which favors the desorption of the water formed during the methanol synthesis reaction and also during the RWGS reaction. Zirconia can also increase the copper dispersion and the surface basicity of the catalyst, which have a positive effect on the CO_2 adsorption properties and the methanol selectivity [18]–[22].

As can be seen in Table 3.1, the crystallite sizes of CuO and ZnO were between 10 nm and 12 nm for both calcined catalysts. The reason of the slightly smaller crystallite sizes of CuO and ZnO of the catalyst synthesized by the batch method (CuO: 10 nm and ZnO: 11 nm) may be because of the smaller crystallite sizes of the aurichalcite and hydrozincite phases obtained after the coprecipitation step. As observed from the results presented above, both catalysts presented only small differences in their crystalline structure.

In their work, Bonura *et al*. [23] synthesized 3 different Cu-ZnO-ZrO_2 catalysts each by a different synthesis method (i.e. coprecipitation, complexation by citric acid and gel oxalate coprecipitation) and found that the 3 catalysts presented the same crystalline structures (same diffractograms), suggesting that the synthesis methods didn't affect considerably the final crystallinity of the catalysts. In fact, they used the same drying and calcination procedures for each of the three catalysts (i.e. drying at 110ºC for 16 hours and calcination at 350ºC for 4 hours), which suggests that possibly the calcination temperature and duration influenced considerably the development of the metal oxides crystalline phases. The occurrence of this behavior can be extrapolated to the catalysts produced in the present work, which presented similar X-ray diffractograms and similar CuO and ZnO crystallite sizes even when synthesizing the catalysts by different methods. To help in the discussion about why the crystallite sizes of CuO and ZnO are similar in the two catalysts synthesized in the present work, it is worth mentioning that the coprecipitation temperature employed for the synthesis of the catalyst precursors was 65ºC for both catalysts, which is an optimal temperature suggested in the literature [24][25]. In addition, the work of Li *et al*. [26] showed that increasing the calcination temperature of the precursors causes a growth in the size

of the CuO, ZnO and even ZrO_2 particles as determined by XRD. The results of the work of Guo *et al*. [16] also indicated that the crystallite size of CuO increased with increasing calcination temperatures. Therefore, it can be said that the coprecipitation temperature and the calcination conditions play an important role in the formation of the crystalline phases of CuO and ZnO, determining the final crystallite sizes of these materials. The aging time can also have an effect on the final crystallite sizes of the catalysts after calcination [2].

Moreover, from the XRD results shown in Figure 3.1, it is evident that the two precursors and the two calcined catalysts are composed not only of a crystalline fraction which corresponds to the area of the peaks, but also of an amorphous fraction, which corresponds to the background of the diffractograms (i.e. the area of the diffractograms that doesn't correspond to the peaks, see Chapter 2.3.1). Due to their lack of periodicity the amorphous materials can be identified by the presence of a diffractogram that shows one or two very broad maxima [27]. The presence of background in the diffractograms of the precursors indicates that there's an amorphous fraction of material in the sample, which may correspond to other components besides the amorphous ZrO_2 [28]. In fact, the amorphous hydroxycarbonate georgeite, with the formula $Cu_2(OH)_2CO_3 \cdot 6H_2O$, is known to exist in this type of precursors [7], [25]. Georgeite is formed as a precipitate that converts into malachite after aging [29] and it can also be modified with Zn to form Cu-Zn georgeite, which presents interesting catalytic properties [30]. In addition, the background present in the calcined catalysts must correspond to the presence of the amorphous zirconia and possibly a fraction of amorphous Cu and Zn compounds. The residual carbonates that might be present after the calcination step could also contribute to the background obtained in the diffractograms of the calcined catalysts [7].

Table 3.1 also shows the crystallinity degree % calculated for both the Batch and Microfluidic catalysts, with values of 40.2% and 43.5%, respectively. These percentages confirm the presence of amorphous Cu and Zn species together with the amorphous zirconia, because the content of ZrO_2 of both catalysts was 33.3 wt%. Moreover, the longer aging time of the catalyst Microfluidic, as discussed before, explains its higher crystallinity (i.e. 43.5%) compared to that of the Batch catalyst (i.e. 40.2%).

Thermogravimetric analysis (TGA) was done to the two catalyst precursors prepared by the batch and microfluidic methods to study the decomposition of these materials under temperature controlled conditions. This technique also allowed to study more in

depth the decomposition of the materials and the interactions between different species. The results are presented in Figure 3.2.

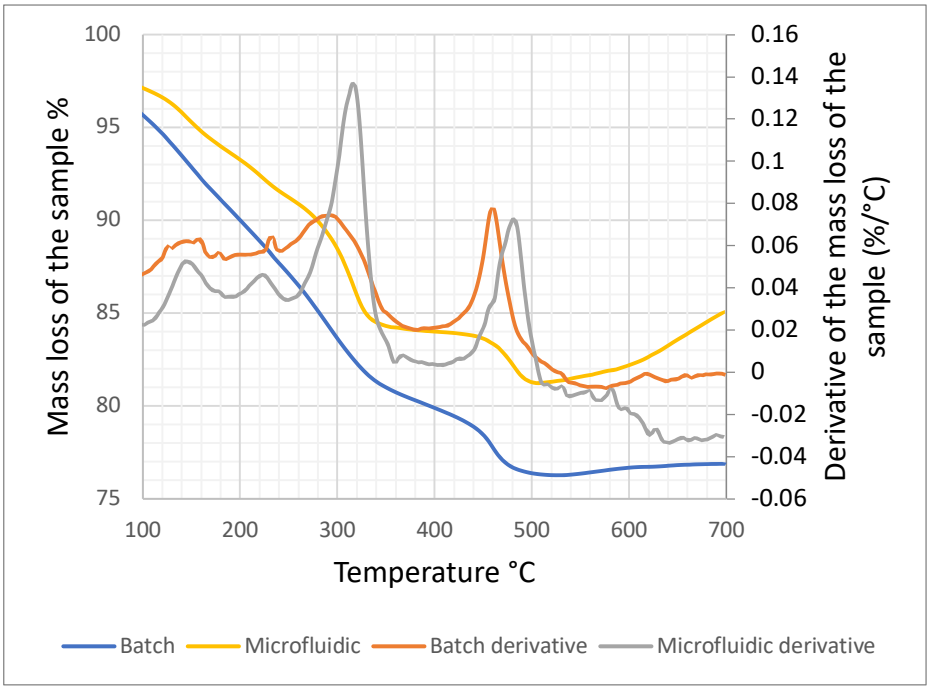

Figure 3.2 TGA results of the precursors prepared by the Batch and Microfluidic methods.

The decomposition of the two catalyst precursors led to a mass loss of 18.7% and 23.0% at approximately 500ºC for the catalysts synthesized by the microfluidic and batch methods, respectively. Despite the above, the mass loss % of the catalyst synthesized by the microfluidic method changed to a value of approximately 15% at a temperature of 700ºC. This phenomenon can be explained by other reactions occurring during the temperature increase process under an air atmosphere, such as the oxidation of Cu, Zn and Zr metal species.

As can be seen from the derivatives of the mass loss % of both materials, there were two main decomposition zones occurring around 320ºC and 480ºC for the two precursors. In general, according to the work of Schumann *et al*. [31], the hydroxycarbonates typically decompose in two main steps, which include first a decomposition with the formation of H_2O and CO_2 as products and then a decomposition at higher temperatures which involves the formation of CO_2 only.

According to the work of Phongamwong *et al*. [32], the aurichalcite phase decomposes at temperatures between 100ºC and 350ºC which causes the loss of water and carbon dioxide. This is in agreement with the decomposition zone around 320ºC evidenced in the derivatives of the mass loss % of the two precursors under study. The work of Vágvölgyi *et al*. [33] indicates that during thermal decomposition, aurichalcite can first lose some adsorbed water at a temperature of 66ºC and then it can suffer a further

decomposition at 285ºC, giving CuO and ZnO as the main decomposition products. The chemical equation of this thermal decomposition is shown in Equation 3.1 [33].

Equation 3.1 Thermal decomposition of aurichalcite.

$$Zn_{4.5}Cu_{0.5}(OH)_6(CO_3)_2 \rightarrow 0.5CuO + 4.5ZnO + 2CO_2 + 3H_2O$$

In the case of hydrozincite, Vágvölgyi *et al*. [34] showed that the thermal decomposition of this component starts around 155ºC and finishes at 340ºC, which is in agreement with the peaks identified in the TGA profiles of both precursors. The chemical equation of the thermal decomposition of hydrozincite is shown in Equation 3.2 [34].

Equation 3.2 Thermal decomposition of hydrozincite.

$$Zn_5(CO_3)_2(OH)_6 \rightarrow 5ZnO + 2CO_2 + 3H_2O$$

Regarding Zr, the work of L'hospital [35] showed that a Zr-based precursor prepared by coprecipitation of Zr nitrate salts with sodium carbonate decomposes around 150ºC. Such peak is present in the TGA profiles of the two precursors studied in this work, indicating the decomposition of a Zr component. In addition, at temperatures between 400 and 600ºC, the decomposition of a mixture of carbonates and oxides [7] explains the decomposition peaks occurring between these two temperatures. Another work [29] also indicates that a high temperature carbonate phase (HT-CO_3) decomposes at higher temperatures.

The nitrogen adsorption and desorption isotherms of the two calcined catalysts are presented in Figure 3.3. The isotherms are of type IV which indicate a mesoporous structure with cylindrical shaped pores. The isotherms also presented a hysteresis loop of type 3, which is characteristic of layered solids with narrow pore networks [13], [36].

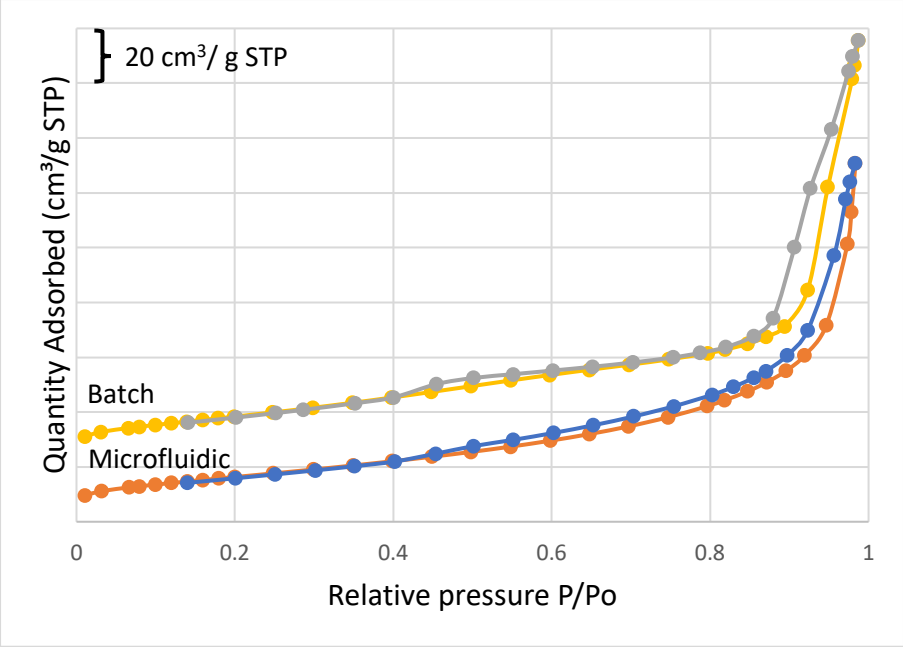

Figure 3.3 Adsorption and desorption isotherms of the catalysts synthesized by the batch and microfluidic methods.

Table 3.2 shows the results of the textural properties, including the specific surface area, the pore volume and the pore size of the catalysts. The specific surface area of the catalyst synthesized by the batch method was slightly superior to that of the catalyst synthesized by the microfluidic method (i.e. 67 to 60 m^2/g, respectively). On the other hand, both materials presented similar pore volumes and pore sizes. Angelo *et al*. [37] prepared a Cu-ZnO-ZrO_2 catalyst by the microfluidic method and compared it with a catalyst with the same composition synthesized by the classical batch method. In their study, the catalyst synthesized by the microfluidic method presented a lower specific surface area (40 m^2/g) than the catalyst synthesized by the batch method (79 m^2/g). Their two catalysts also presented similar pore volume (microfluidic: 0.37 and batch: 0.38 cm^3/g) and pore sizes (microfluidic: 20 nm and batch: 17 nm).

Yang *et al.* [22] also synthesized a Cu-ZnO-ZrO_2 catalyst with a composition of 33.1, 32.2 and 13.5 wt. % of elemental Cu, Zn and Zr respectively, by a successive precipitation method, and obtained a material with a specific surface area of 62 m^2/g, a pore volume of 0.16 cm^3/g and a pore size of 10 nm. However, their catalyst composition was different from the composition investigated in this work.

Table 3.2 Specific surface areas, pore volumes and pore sizes of the Microfluidic and Batch catalysts.

Sample	BET surface area (m^2/g)	Pore volume (cm^3/g)	Pore size (nm)
Microfluidic	60	0.15	12
Batch	67	0.21	13

The CO_2 adsorption properties of Cu-ZnO-ZrO_2 based catalysts are an important parameter that influences the catalytic performance [14], [38]. These properties were studied by CO_2-TPD after a reduction step. Figure 3.4 shows the CO_2-TPD results of the catalysts synthesized by the batch and microfluidic methods. As observed in the CO_2-TPD profiles, three main desorption peaks occurred around temperatures of 140ºC, 430ºC and 630ºC. These three peaks correspond to the presence on the catalysts' surface of weak, moderate strength and strong basic sites, respectively [39].

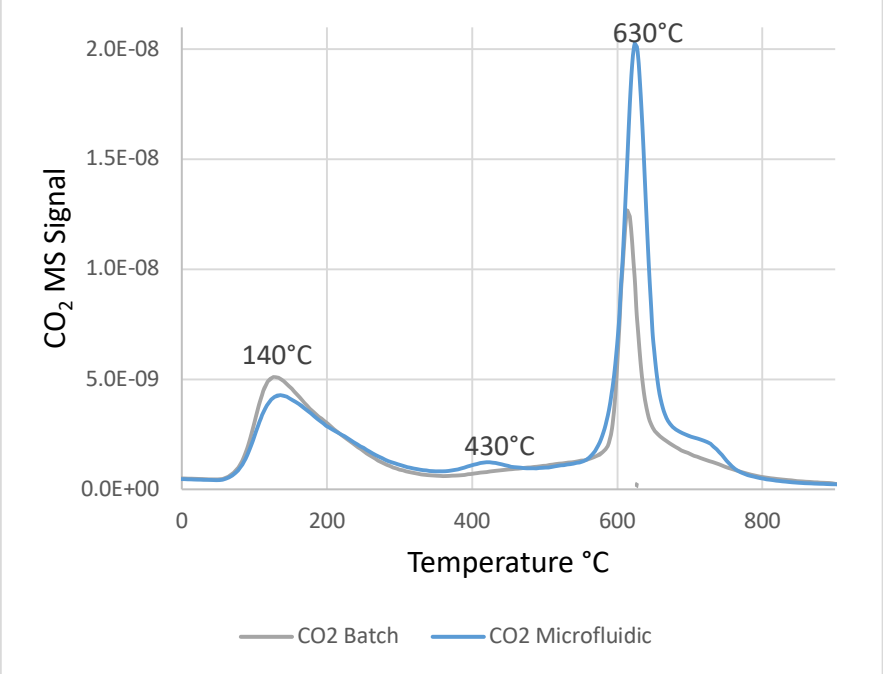

Figure 3.4 CO_2-TPD profiles of the catalysts prepared by the batch and microfluidic methods.

The weak basic sites are typically associated with surface hydroxyl groups and considered a Brönsted base, the moderately basic sites correspond to metal-oxygen pairs and the strong basic sites are associated with low coordination oxygen atoms [11], [13], [40], [41]. The quantitative results of the CO_2-TPD analysis obtained by integration of the peak areas of the MS signals are shown in Table 3.3.

Table 3.3 Quantity of weak, moderate strength and strong basic sites of the catalysts prepared by the batch and microfluidic methods.

Sample	Weak basic sites (μmol/g)	Moderate strength basic sites (μmol/g)	Strong basic sites (μmol/g)	Total basic sites (μmol/g)	Basic sites per unit surface area (μmol/m^2)
Microfluidic	78.0	16.0	140.0	234.0	3.90
Batch	91.0	-	100.0	191.0	2.85

As seen in Table 3.3, both catalysts presented different amounts of weak and strong basic sites while only a small amount of moderate strength basic sites was present in the catalyst synthesized by the microfluidic method. The total basicity of the catalysts prepared by the microfluidic and batch methods were 234.0 and 191.0 μmol/g, respectively, which is a difference of 22% in the concentration of total basic sites. According to Zhan *et al*. [42], it is the moderate strength basic sites the ones that have a strong influence on the catalytic performance, while the strong basic sites don't play an important role in the catalysis. As mentioned above, the catalyst that presented moderate strength basic sites is the catalyst synthesized by the microfluidic method. This difference in surface basicity may be responsible for the different catalytic performances of the two catalysts investigated in this work, as will be shown in the corresponding section. As for the amount of strong basic sites on the catalysts surface, it was the catalyst produced by the microfluidic method the one that presented a higher amount of them (140.0 μmol/g). A higher basicity in the surface of a catalyst improves the adsorption of acidic CO_2, which in turn has a positive effect on the activity of the catalyst [14]. In contrast with the previous idea about the inactivity of the strong basic sites during the methanol production reaction, Xaba *et al*. [43] found that the catalyst with the highest basicity including strong basic sites presented the best catalytic results, indicating that the catalyst with the highest basicity presented the highest CO_2 adsorption capacity. However, their catalyst was composed of Cu-ZnO-Al_2O_3-ZrO_2, which differs from the catalyst compositions studied in this work. From the above analysis it is clear that there is not a consensus regarding the relationship between surface basicity and catalytic activity. In the present work the microfluidic catalyst presents higher amount of both moderate and strong basic sites, so the positive effect on catalytic activity is expected following the two theories (Xaba and Zhan). The results in Table 3.3 also showed that the Microfluidic catalyst presented a 36% higher amount of basic sites per unit surface area (μmol/m^2) than the Batch catalyst, suggesting an improved CO_2 adsorption on the surface of the catalyst synthesized by the microfluidic method.

The reducibility of the calcined catalysts was studied by H_2-TPR. This technique is typically used to study the reduction behavior of copper in Cu-ZnO-ZrO_2 catalysts for the hydrogenation of CO_2 to methanol. The H_2-TPR profiles of the catalysts synthesized by the batch and microfluidic methods are presented in Figure 3.5.

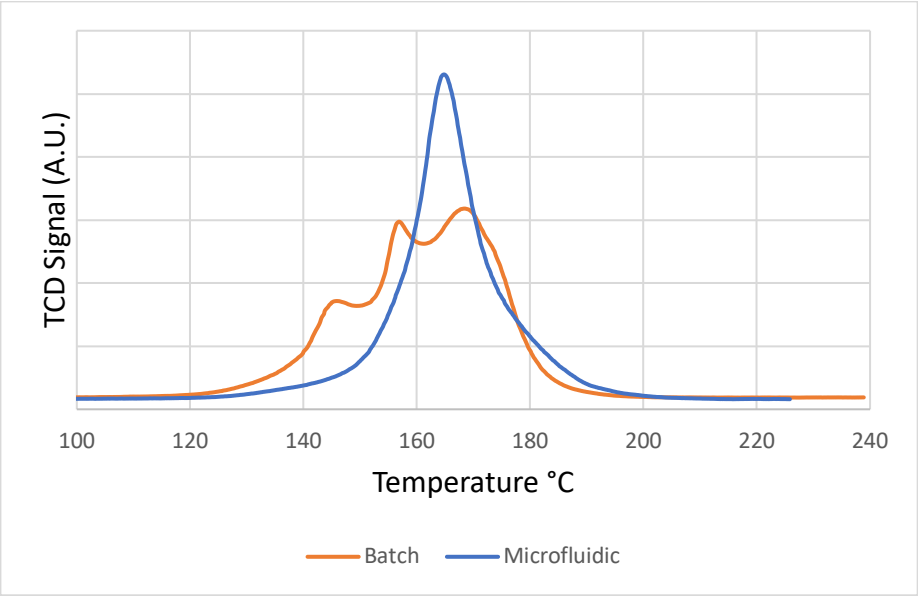

Figure 3.5 H_2-TPR profiles of the catalysts prepared by the batch and by the microfluidic methods.

Since ZnO and ZrO_2 cannot be reduced at temperatures below 300ºC, the peaks obtained with the H_2-TPR technique must correspond to the reduction of CuO particles of different sizes and/or morphologies as well as different interactions of CuO with the other metals present in the catalysts [13]. Typically, low reduction temperatures are associated with highly dispersed copper species, while higher reduction temperatures are associated to the reduction of bulk CuO species [14], [22], [44], [45].

As can be observed, the catalyst synthesized by the batch method presented 3 different reduction peaks at 147, 156 and 170ºC, while the catalyst synthesized by the microfluidic method presented only one symmetric peak at a temperature of 165ºC. The three reduction peaks of the batch catalyst indicate the presence of a CuO particle size distribution and a heterogeneous distribution of CuO crystallites over the surface of the catalyst [3][45]. The research work of Zhang *et al*. [3] indicates that the catalytic activity is associated with the reducibility of the catalysts. Therefore, in this case, the catalyst synthesized by the microfluidic method which presents a narrower CuO size distribution and easier reducibility is expected to have a better catalytic performance.

According to Liu *et al*. [40], the reduction behavior of CuO is mainly affected by the crystallite size of this species and by its interaction with the other components present in the material. The reduction temperature is also associated with the CuO crystallite sizes, where the smaller crystallites are reduced at lower temperatures and higher crystallites are reduced at higher temperatures [40][46]. Lower reduction temperatures can also be an indication of better copper dispersion [3][13], which can facilitate the reduction of the CuO particles. It has been demonstrated that the addition of ZnO and ZrO_2 to CuO based catalysts can facilitate the reducibility of the material, which can be seen in the shift of the reduction temperatures to lower values [45].

The quantitative results of the H_2-TPR analysis are presented in Table 3.4. As can be seen, the calculated CuO content of the catalysts by using the H_2 consumption during the H_2-TPR analysis was close to the nominal value of 33.3% for the two catalysts investigated in this work, which confirms an adequate loading of copper in the catalysts during the catalyst synthesis. Also, the lower reduction percentage of the catalyst prepared by the microfluidic method may also be an indication of stronger metal-support interactions comparing to the batch sample.

Table 3.4 H_2-TPR quantitative results of the catalysts prepared by the batch and microfluidic methods.

Sample	H_2 consumption, mmol/g	Catalyst theoretical Cu content, mmol Cu/g	H_2/Cu ratio	Calculated CuO % of the catalyst
Microfluidic	3.8	4.19	0.92	30.7
Batch	4.0	4.19	0.95	31.8

The results of the N_2O surface reaction (i.e. copper surface area, copper dispersion % and particle size) of the catalysts under study are presented in Table 3.5. As observed, the catalyst synthesized by the microfluidic method presented an 11% higher metallic copper surface area, as well as better dispersion and lower particle size than the catalyst synthesized by the batch method. This is in agreement with the results of the work of Tofighi *et al*. 2022 [2], who prepared a Cu-ZnO-Al_2O_3 catalyst by the microfluidic method and obtained a catalyst with higher metallic copper surface area of 17 $m^2\ g^{-1}$, smaller copper particle size and higher copper dispersion compared to a catalyst prepared by the batch method, with a copper surface area of 9.5 $m^2\ g^{-1}$. Obviously, their catalyst composition was different from the one used in the present work, but their results point out that the microfluidic coprecipitation technique helps tuning the metallic copper surface area and copper particle size of the catalyst. Angelo *et al*. [37] synthesized two catalysts by the microfluidic and batch methods and obtained metallic Cu surface area values of 14.5 and 10.5 $m^2\ g^{-1}$ respectively [37]. Their findings suggest that the properties measured by the N_2-physisorption technique are not directly correlated to the catalytic performance of the catalyst. It is in fact the metallic Cu surface area the property that seems to have a more important correlation to the catalytic activity [37]. Zhang *et al*. [3], also prepared a Cu-ZnO-Al_2O_3 catalyst and showed that the microfluidic coprecipitation method allowed to obtain a Cu surface area of 22.4 $m^2\ g^{-1}$ which contrasts the Cu surface area of 13.4 $m^2\ g^{-1}$ of a catalyst prepared by the batch method.

Furthermore, according to the work of Sloczynski *et al*. [47], the Cu particle sizes obtained via the calculation of the surface Cu properties with N_2O surface reaction tend to be 1.5 to 2.5 times larger than the Cu crystallite sizes obtained by XRD. This indicates that the Cu particles are formed by an agglomeration of Cu crystallites, which leads to the formation of larger grains [47]. These calculations were done to the

catalysts investigated in this work, by using the Cu particle sizes obtained by N_2O surface reaction and the CuO crystallite sizes obtained by XRD. These calculations are presented in Table 3.5 under the column N_2O/XRD ratio**.** The results show that the Cu particles in the catalysts synthesized by the microfluidic and batch methods originate from an agglomeration of approximately 2.1 and 2.9 CuO crystallites, respectively. This confirms a strong metal-support interaction in the catalyst prepared by the microfluidic method and a more effective dispersion and stabilization of the Cu crystallites on the surface of the Microfluidic catalyst.

Table 3.5 N_2O surface reaction results of the catalysts synthesized by the batch and microfluidic methods.

Sample	Copper surface area m^2/g	Copper dispersion %	Copper particle size nm	N_2O/XRD ratio[1]
Microfluidic	7.0	4.1	25.4	2.1 (12 nm)
Batch	6.3	3.6	28.7	2.9 (10 nm)

[1] Ratio of the Cu particle size obtained by N_2O surface reaction analysis to the CuO crystallite size obtained by XRD. The values in parentheses are the CuO crystallite sizes obtained by XRD.

3.3. Catalytic tests results

Figure 3.6 and Table 3.6 show the results of the H_2 and CO_2 conversions, the methanol selectivity plotted against the CO_2 conversion and the methanol productivity of the catalysts synthesized by the batch and microfluidic methods.

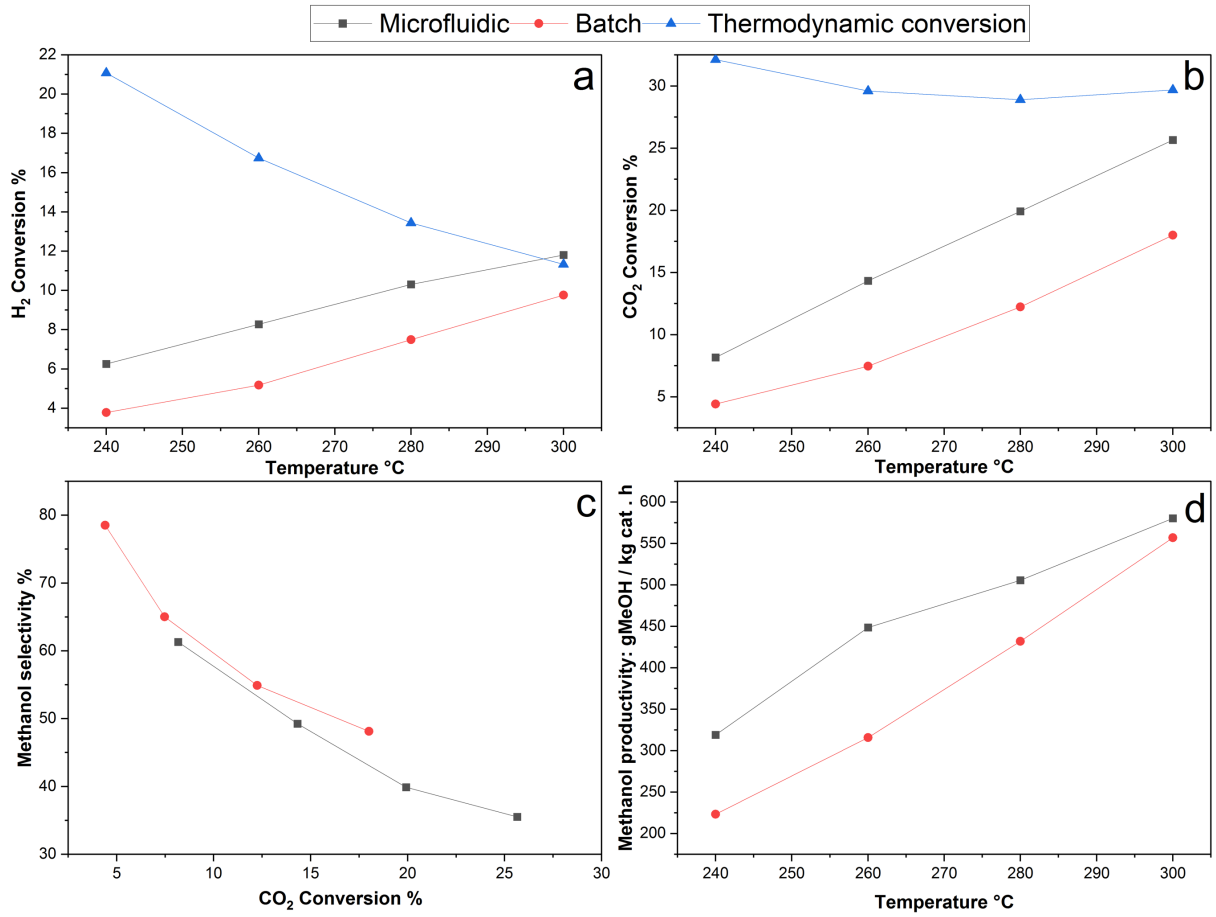

Figure 3.6 Catalytic performance of the catalysts under study. (a) H_2 conversion, (b) CO_2 conversion, (c) methanol selectivity against CO_2 conversion and (d) methanol productivity. P: 50bar, GHSV: 24000Nml h^{-1} g^{-1}, molar ratio H_2/CO_2: 3.9.

Figures 3.6a and 3.6b show that the conversions of H_2 and CO_2 in comparison to the thermodynamic limitations (Chapter 1.2) increase with increasing reaction temperature for both catalysts. The reason behind the increasing H_2 and CO_2 conversions during the methanol synthesis is the simultaneous occurrence of the methanol production reactions with the reverse water-gas shift (RWGS) reaction which consumes both H_2 and CO_2 to produce CO and H_2O [48]. The RWGS reaction is an endothermic reaction with a reaction enthalpy of $\Delta Hr_{298K} = 41.19\ kJ/mol$ which means that this reaction is favored at higher temperatures [48]. On the other hand, the methanol formation reactions are exothermic, which means that their equilibrium conversion % will decrease with increasing temperature. These reactions are also thermodynamically favored at higher pressures, which is the reason why the catalytic tests are carried out at 50 bar.

The catalyst prepared by the microfluidic method showed higher conversions of CO_2 and H_2 at all the tested temperatures. According to the characterization results obtained and presented in the preceding sections, the reason for the superior conversion values of this catalyst can be attributed to the higher Cu surface area, its narrower copper particle size distribution and also by the higher surface basicity of this material. The presence of moderate strength basic sites may also be a contributor to the better catalytic performance of this catalyst.

Some research works [40][49] indicate that the role of copper in the hydrogenation of CO_2 to methanol is to dissociate H_2 into atomic hydrogen and providing it to the copper-support interface or to the support by spillover. Atomic hydrogen then participates in the reaction with the C containing intermediates adsorbed on the Cu-support interface and on the support to produce methanol. The availability of Cu surface area is then beneficial for the methanol production reaction and is directly correlated to the catalytic activity as suggested in other works [26], [37], [39] which indicate that the yield of methanol increases with the increase in the Cu surface area, but not in a linear way.

Table 3.6 Results of the catalytic tests of the catalysts under study. P: 50bar, GHSV: 24000Nml h^{-1} g^{-1}, molar ratio H_2/CO_2: 3.9.

Catalyst	Temperature ºC	H_2 Conversion %	CO_2 Conversion %	Methanol selectivity %	Methanol productivity g CH_3OH/(kg of catalyst x hour)
Microfluidic	240	6.3	8.2	61.3	319
	260	8.3	14.3	49.3	449
	280	10.3	19.9	39.9	505
	300	11.8	25.6	35.5	580
Batch	240	3.8	4.4	78.5	223
	260	5.2	7.4	65.0	316
	280	7.5	12.2	54.9	432
	300	9.8	18.0	48.1	557

Even though the methanol selectivity has been associated to the surface basicity of the catalysts, there's no agreement in the literature in this regard [40]. Despite the above, an increasing amount of basic sites has been associated with an increase in the chemisorption of CO_2, which causes a promotion of the CO_2 hydrogenation reactions [46]. A higher surface basicity can improve the adsorption and activation of the CO_2 molecule, which increases the kinetics of the transformation and hydrogenation reactions of CO_2 into different intermediates, such as the formate (HCO_2^-) and the methoxy (H_3CO) intermediates [50]. For such reasons, the adsorption of CO_2 is considered one of the most important steps in CO_2 hydrogenation to methanol [41].

As mentioned above, at higher temperatures, the other competing reaction that occurs on this type of catalysts is the RWGS reaction, which is favored with increasing temperatures [38]. The thermodynamics of the methanol production reactions which are exothermic and of the RWGS reaction which is endothermic [48], explain why the selectivity of the methanol production reactions decreases with increasing temperature, while the RWGS reaction is favored. As indicated in other works [39], methanol and CO are the only carbon-containing products under the present reaction conditions.

In addition, the methanol productivity over the catalyst prepared by the microfluidic method was superior to the methanol productivity of the catalyst prepared by the batch method. This is due to the higher reactants conversions of the catalyst synthesized by the microfluidic method, as explained above. Moreover, the larger amount of basic sites per unit surface area of the catalyst prepared by the microfluidic method suggests a larger surface density of active sites for the activation of CO_2. A higher number of active sites per unit surface area would mean a smaller distance between the active sites for the activation of CO_2 and the active sites responsible for the dissociation of H_2, causing an increase in the rate of reaction. This can also explain the higher methanol productivity of this catalyst.

The results of the catalytic performance of the two catalysts investigated in this work are in agreement with other research works [39], which indicate that the conversion of CO_2 increased with the increase in the reaction temperature due to both the methanol production reaction and also due to the occurrence of the RWGS reaction, accompanied also by a decrease in methanol selectivity, over the temperature range of 240–300 ºC.

3.4. Apparent activation energy of the CO_2 hydrogenation to methanol reaction

To study more in-depth the catalytic properties of each of the two catalysts investigated in this work, the apparent activation energies of the CO_2 hydrogenation to methanol reaction were calculated for both of them. A first order reaction kinetics with respect to the concentration of CO_2 was assumed and a rate constant k as a function of a pre-exponential factor and the reaction temperature. Despite the complexity of the reaction mechanism which may include adsorption, chemisorption and desorption steps of the reactants and product species, a first order reaction with respect to CO_2 was assumed due to the simplicity of the calculations. The equations 3.3-3.5 were used for the determination of the activation energy and pre-exponential factor.

Equation 3.3: rate of formation of methanol.

$$r_{CH3OH} = k \cdot C_i$$

Equation 3.4: Arrhenius equation - rate constant dependent on the reaction temperature.

$$k = A\, e^{-Ea/RT}$$

Equation 3.5: linearization of the Arrhenius equation for the calculation of the activation energy and pre-exponential factor.

$$\ln(k) = \frac{-Ea}{R}\frac{1}{T} + \ln(A)$$

Where r_A is the rate of reaction, k is the rate constant, C_i is the concentration of the reactant i, A is the pre-exponential factor, Ea is the apparent activation energy, R is the gas constant and T is the reaction temperature.

Figure 3.7 shows the linearization of the Arrhenius equation as presented in Equation 3.5. It shows the results of the natural log of the rate constant plotted against the inverse of the reaction temperature in Kelvin. After the corresponding mathematical treatment, it was found that the apparent activation energy of the methanol production reaction on the catalysts synthesized by the batch and microfluidic methods were 41.89 kJ mol^{-1} and 28.07 kJ mol^{-1}, respectively. Other values of activation energies reported in the literature range from 43-44 kJ mol^{-1} for a Cu-ZnO-Al_2O_3 in the work of Bukhtiyarova *et al*. [51], 58-62 kJ mol^{-1} for a Cu/SiO_2 + ZnO/SiO_2 catalyst in the work of Choi *et al*. [52], 105-117 kJ mol^{-1} for a Cu-ZnO-Al_2O_3 in the work of Fichtl *et al*. [53] and 31 kJ mol^{-1} for a Cu-ZnO-ZrO_2 catalyst promoted with Ga in the work of Ladera *et al*. [54]. These results indicate that indeed, the energy barrier for the occurrence of the methanol production reaction is lower for the catalyst synthesized by the microfluidic method, which highlights the better performance of this catalyst and its higher ability to catalyze this reaction.

In a previous research work [55], a kinetic model based on the use of power-law models was created for a Cu-ZnO-ZrO_2 catalyst. This model was based on the production of methanol from CO_2 only and on the production of CO from the RWGS reaction. The catalysts of their study were prepared by a classical batch method. Their results showed that the CO_2 hydrogenation reaction was more selective on a Cu-ZnO-ZrO_2 catalyst than on a Cu-ZnO-Al_2O_3 catalyst, mainly due to differences in the turnover frequency of the RWGS reaction, which was lower in the catalyst prepared with the ZrO_2 support.

The work of Poto *et al*. [56] offered a study of the kinetics and the reaction mechanism of the methanol synthesis on a CuO-CeO_2-ZrO_2 catalyst based on different reaction pathways, concluding that the dual site model of Graaf *et al*. [57] had the best fit to their kinetics data. Their work allowed concluding that metallic Cu acts as a

dissociative surface for H_2, while the oxygen vacancies of the CeO_2-ZrO_2 solid solution allowed the adsorption of one of the oxygens of the CO_2 molecules.

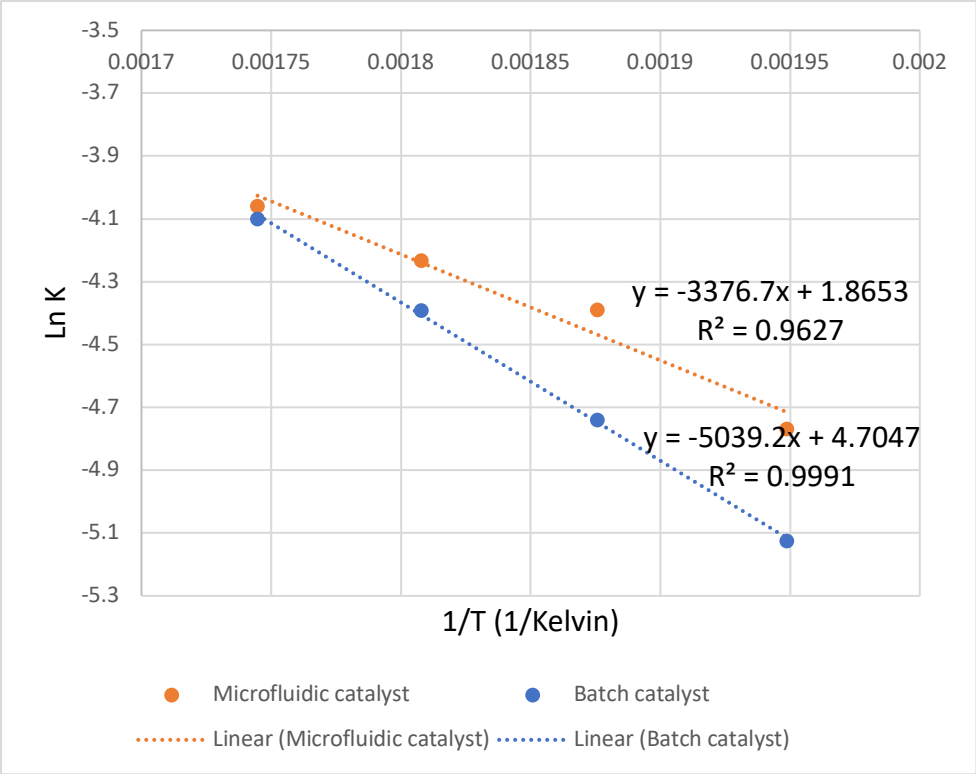

Figure 3.7 Mathematical treatment of the kinetics data for the determination of the apparent activation energy of the methanol production reaction.

From the above analysis, it is clear that a deeper study of the kinetics and reaction mechanisms of the CO_2 hydrogenation to methanol on Cu-ZnO-ZrO_2 catalysts prepared by the microfluidic method would be useful and interesting to understand more the advantages of this catalyst synthesis approach.

3.5. Conclusions

Two Cu-ZnO-ZrO_2 catalysts of the same composition were synthesized by the microfluidic and by the batch methods. The two materials were characterized and their catalytic performance was determined.

It was shown that the catalyst synthesized by the microfluidic method presented the best catalytic performance due to the improved adsorption and activation of CO_2 on the surface of the catalyst due to its higher surface basicity and possibly by the presence of moderate strength basic sites. The higher surface basicity of the catalyst prepared by the microfluidic method suggests the occurrence of a higher surface density of active sites for the activation of CO_2 and consequently lower distances between the active sites responsible for CO_2 activation and the active sites responsible for the dissociation of H_2, causing an increase in the rate of reaction of the methanol

production. This indicates that the microfluidic technique can decrease the distance between active sites, due to better interactions between the metal species.

The Microfluidic catalyst also presented a more uniform size distribution of copper species and a higher copper surface area. A high copper surface area can increase the rate of H_2 dissociation that occurs on the metallic copper. All of these properties have an effect on the reaction kinetics, increasing the conversion of the reactants and the methanol productivity. The above makes the Cu-ZnO-ZrO_2 catalysts prepared by the microfluidic method interesting for the production of methanol from the hydrogenation of carbon dioxide due to their higher reactants conversions and methanol productivity. This highlights the positive effects of the synthesis of catalysts by coprecipitation using a microfluidic device.

The next chapter provides an exploration of the microfluidic synthesis conditions by studying the effect of the aging time of the precursors and the coprecipitation temperature on the properties of the catalysts and their catalytic performance. The effects of these two parameters haven't been studied before on Cu-ZnO-ZrO_2 catalysts synthesized by the microfluidic method and they are important because they affect the formation of crystalline phases, the morphology and the surface properties of the catalysts. The study of the aging time and the coprecipitation temperature will offer valuable information about this catalyst synthesis technique and will allow to find optimal synthesis conditions for the production of Cu-ZnO-ZrO_2 catalysts by this technique.

3.6. Bibliography of chapter 3

[1] S. G. Robles Macias L, Curulla-Ferre D, Ferreira C, Santiago Redondo M, “Process for manufacturing a methanol synthesis catalyst,” WO2013/120711 Al, 2013 [Online].Available:https://patentimages.storage.googleapis.com/94/2c/3b/d73feaab0591c1/WO2013120711A1.pdf

[2] G. Tofighi, H. Lichtenberg, A. Gaur, W. Wang, S. Wild, K. Herrera Delgado, S. Pitter, R. Dittmeyer, J.-D. Grunwaldt, and D. E. Doronkin, “ Continuous synthesis of $Cu/ZnO/Al_2O_3$ nanoparticles in a co-precipitation reaction using a silicon based microfluidic reactor ,” *React. Chem. Eng.*, 2022, doi: 10.1039/d1re00499a.

[3] Q. C. Zhang, K. P. Cheng, L. X. Wen, K. Guo, and J. F. Chen, “A study on the precipitating and aging processes of $CuO/ZnO/Al_2O_3$ catalysts synthesized in micro-impinging stream reactors,” *RSC Adv.*, vol. 6, no. 40, pp. 33611–33621, 2016, doi: 10.1039/c6ra02512a.

[4] V. L’hospital, S. Heyte, S. Paul, K. Parkhomenko, and A.-C. Roger, “Optimization of the continuous coprecipitation in a microfluidic reactor: Cu-based catalysts for CO_2 hydrogenation into methanol,” *Fuel*, vol. 319, no. February, p. 123689, Jul. 2022, doi: 10.1016/j.fuel.2022.123689.

[5] S. I. Fujita, Y. Kanamori, A. M. Satriyo, and N. Takezawa, “Methanol synthesis from CO_2 over Cu/ZnO catalysts prepared from various coprecipitated precursors,” *Catal. Today*, vol. 45, no. 1–4, pp. 241–244, 1998, doi: 10.1016/S0920-5861(98)00222-3.

[6] E. Frei, A. Schaadt, T. Ludwig, H. Hillebrecht, and I. Krossing, “The influence of the precipitation/ageing temperature on a $Cu/ZnO/ZrO_2$ catalyst for methanol synthesis from H_2 and CO_2,” *ChemCatChem*, vol. 6, no. 6, pp. 1721–1730, 2014, doi: 10.1002/cctc.201300665.

[7] N. Mota, R. Guil-Lopez, B. G. Pawelec, J. L. G. Fierro, and R. M. Navarro, “Highly active Cu/ZnO-Al catalyst for methanol synthesis: Effect of aging on its structure and activity,” *RSC Adv.*, vol. 8, no. 37, pp. 20619–20629, 2018, doi: 10.1039/c8ra03291b.

[8] Y. Ma, Q. Sun, D. Wu, W. H. Fan, Y. L. Zhang, and J. F. Deng, “A practical approach for the preparation of high activity $Cu/ZnO/ZrO_2$ catalyst for methanol synthesis from CO_2 hydrogenation,” *Appl. Catal. A Gen.*, vol. 171, no. 1, pp. 45–55, 1998, doi: 10.1016/S0926-860X(98)00079-9.

[9] R. Raudaskoski, M. V. Niemelä, and R. L. Keiski, “The effect of ageing time on co-precipitated $Cu/ZnO/ZrO_2$ catalysts used in methanol synthesis from CO_2 and H_2,” *Top. Catal.*, vol. 45, no. 1–4, pp. 57–60, 2007, doi: 10.1007/s11244-007-0240-9.

[10] C. Huang, S. Chen, X. Fei, D. Liu, and Y. Zhang, “Catalytic hydrogenation of CO_2 to methanol: Study of synergistic effect on adsorption properties of CO_2 and H_2 in $CuO/ZnO/ZrO_2$ system,” *Catalysts*, vol. 5, no. 4, pp. 1846–1861, 2015, doi: 10.3390/catal5041846.

[11] T. Witoon, N. Kachaban, W. Donphai, P. Kidkhunthod, K. Faungnawakij, M. Chareonpanich, and J. Limtrakul, “Tuning of catalytic CO_2 hydrogenation by changing composition of $CuO-ZnO-ZrO_2$ catalysts,” *Energy Convers. Manag.*, vol. 118, pp. 21–31, 2016, doi: 10.1016/j.enconman.2016.03.075.

[12] P. Gao, F. Li, H. Zhan, N. Zhao, F. Xiao, W. Wei, L. Zhong, H. Wang, and Y. Sun, “Influence of Zr on the performance of Cu/Zn/Al/Zr catalysts via

hydrotalcite-like precursors for CO_2 hydrogenation to methanol," *J. Catal.*, vol. 298, pp. 51–60, 2013, doi: 10.1016/j.jcat.2012.10.030.
[13] Y. Liang, D. Mao, X. Guo, J. Yu, G. Wu, and Z. Ma, "Solvothermal preparation of CuO-ZnO-ZrO_2 catalysts for methanol synthesis via CO_2 hydrogenation," *J. Taiwan Inst. Chem. Eng.*, vol. 121, pp. 81–91, 2021, doi: 10.1016/j.jtice.2021.03.049.
[14] C. Huang, D. Mao, X. Guo, and J. Yu, "Microwave-Assisted Hydrothermal Synthesis of CuO–ZnO–ZrO_2 as Catalyst for Direct Synthesis of Methanol by Carbon Dioxide Hydrogenation," *Energy Technol.*, vol. 5, no. 11, pp. 2100–2107, 2017, doi: 10.1002/ente.201700190.
[15] L. Lin, G. Wang, and F. Zhao, "CO_2 Hydrogenation to Methanol on ZnO/ZrO_2 Catalysts: Effects of Zirconia Phase," *ChemistrySelect*, vol. 6, no. 9, pp. 2119–2125, 2021, doi: 10.1002/slct.202002108.
[16] X. Guo, D. Mao, G. Lu, S. Wang, and G. Wu, "CO_2 hydrogenation to methanol over Cu/ZnO/ZrO_2 catalysts prepared via a route of solid-state reaction," *Catal. Commun.*, vol. 12, no. 12, pp. 1095–1098, 2011, doi: 10.1016/j.catcom.2011.03.033.
[17] K. Li and J. G. Chen, "CO_2 Hydrogenation to Methanol over ZrO_2-Containing Catalysts: Insights into ZrO_2 Induced Synergy," *ACS Catal.*, vol. 9, no. 9, pp. 7840–7861, 2019, doi: 10.1021/acscatal.9b01943.
[18] Y. Nitta, O. Suwata, Y. Ikeda, Y. Okamoto, and T. Imanaka, "Copper-zirconia catalysts for methanol synthesis from carbon dioxide: Effect of ZnO addition to Cu-ZrO_2 catalysts," *Catal. Letters*, vol. 26, no. 3–4, pp. 345–354, 1994, doi: 10.1007/BF00810608.
[19] F. Arena, G. Italiano, K. Barbera, G. Bonura, L. Spadaro, and F. Frusteri, "Basic evidences for methanol-synthesis catalyst design," *Catal. Today*, vol. 143, no. 1–2, pp. 80–85, 2009, doi: 10.1016/j.cattod.2008.11.022.
[20] X. Dong, F. Li, N. Zhao, F. Xiao, J. Wang, and Y. Tan, "CO_2 hydrogenation to methanol over Cu/ZnO/ZrO_2 catalysts prepared by precipitation-reduction method," *Appl. Catal. B Environ.*, vol. 191, pp. 8–17, 2016, doi: 10.1016/j.apcatb.2016.03.014.
[21] Y. Wang, S. Kattel, W. Gao, K. Li, P. Liu, J. G. Chen, and H. Wang, "Exploring the ternary interactions in Cu–ZnO–ZrO_2 catalysts for efficient CO_2 hydrogenation to methanol," *Nat. Commun.*, vol. 10, no. 1, 2019, doi: 10.1038/s41467-019-09072-6.
[22] C. Yang, Z. Ma, N. Zhao, W. Wei, T. Hu, and Y. Sun, "Methanol synthesis from CO_2-rich syngas over a ZrO_2 doped CuZnO catalyst," *Catal. Today*, vol. 115, no. 1–4, pp. 222–227, 2006, doi: 10.1016/j.cattod.2006.02.077.
[23] G. Bonura, M. Cordaro, C. Cannilla, F. Arena, and F. Frusteri, "The changing nature of the active site of Cu-Zn-Zr catalysts for the CO_2 hydrogenation reaction to methanol," *Appl. Catal. B Environ.*, vol. 152–153, pp. 152–161, 2014, doi: 10.1016/j.apcatb.2014.01.035.
[24] K. Y. Y. Yamagishi, "Process for manufacturing methanol and process for manufacturing catalyst for methanol synthesis," 1996 [Online]. Available: https://patents.google.com/patent/US5767039A/en?oq=5767039
[25] M. Behrens, D. Brennecke, F. Girgsdies, S. Kißner, A. Trunschke, N. Nasrudin, S. Zakaria, N. F. Idris, S. B. A. Hamid, B. Kniep, R. Fischer, W. Busser, M. Muhler, and R. Schlögl, "Understanding the complexity of a catalyst synthesis: Co-precipitation of mixed Cu,Zn,Al hydroxycarbonate precursors for Cu/ZnO/Al_2O_3 catalysts investigated by titration experiments," *Appl. Catal. A*

Gen., vol. 392, no. 1–2, pp. 93–102, 2011, doi: 10.1016/j.apcata.2010.10.031.
[26] L. Li, D. Mao, J. Yu, and X. Guo, "Highly selective hydrogenation of CO_2 to methanol over CuO-ZnO-ZrO_2 catalysts prepared by a surfactant-assisted co-precipitation method," vol. 279, pp. 394–404, 2015, doi: 10.1016/j.jpowsour.2014.12.142.
[27] B. Cullity, *Elements of X-RAY DIFFRACTION*. Massachusetts: Addison-Wesley Publishing Company, 1978.
[28] Schimpf and Muhler, "Synthesis of Solid Catalysts," in *Synthesis of Solid Catalysts*, K. P. de Jong, Ed., Wiley-VCH, 2009, pp. 1–401. doi: 10.1002/9783527626854.
[29] P. J. Smith, S. A. Kondrat, P. A. Chater, B. R. Yeo, G. M. Shaw, L. Lu, J. K. Bartley, S. H. Taylor, M. S. Spencer, C. J. Kiely, G. J. Kelly, C. W. Park, and G. J. Hutchings, "A new class of Cu/ZnO catalysts derived from zincian georgeite precursors prepared by co-precipitation," *Chem. Sci.*, vol. 8, no. 3, pp. 2436–2447, 2017, doi: 10.1039/c6sc04130b.
[30] S. Dang, H. Yang, P. Gao, H. Wang, X. Li, W. Wei, and Y. Sun, "A review of research progress on heterogeneous catalysts for methanol synthesis from carbon dioxide hydrogenation," *Catal. Today*, vol. 330, no. March 2018, pp. 61–75, 2019, doi: 10.1016/j.cattod.2018.04.021.
[31] J. Schumann, A. Tarasov, N. Thomas, R. Schlögl, and M. Behrens, "Cu,Zn-based catalysts for methanol synthesis: On the effect of calcination conditions and the part of residual carbonates," *Appl. Catal. A Gen.*, vol. 516, pp. 117–126, 2016, doi: 10.1016/j.apcata.2016.01.037.
[32] T. Phongamwong, U. Chantaprasertporn, T. Witoon, T. Numpilai, Y. Poo-arporn, W. Limphirat, W. Donphai, P. Dittanet, M. Chareonpanich, and J. Limtrakul, "CO_2 hydrogenation to methanol over CuO–ZnO–ZrO_2–SiO_2 catalysts: Effects of SiO_2 contents," *Chem. Eng. J.*, vol. 316, pp. 692–703, 2017, doi: 10.1016/j.cej.2017.02.010.
[33] V. Vágvölgyi, A. Locke, M. Hales, J. Kristóf, R. L. Frost, E. Horváth, and W. N. Martens, "Mechanism for decomposition of aurichalcite-A controlled rate thermal analysis study," *Thermochim. Acta*, vol. 468, no. 1–2, pp. 81–86, 2008, doi: 10.1016/j.tca.2007.11.024.
[34] V. Vágvölgyi, M. Hales, W. Martens, J. Kristóf, E. Horváth, and R. L. Frost, "Dynamic and controlled rate thermal analysis of hydrozincite and smithsonite," *J. Therm. Anal. Calorim.*, vol. 92, no. 3, pp. 911–916, 2008, doi: 10.1007/s10973-007-8846-5.
[35] V. L'Hospital, "Développement et optimisation de catalyseurs à base de cuivre pour la synthèse de méthanol et de diméthyléther à partir de CO2," University of Strasbourg, 2018.
[36] E. S. Borovinskaya, S. Trebbin, F. Alscher, and C. Breitkopf, "Synthesis, Modification, and Characterization of CuO/ZnO/ZrO_2 Mixed Metal Oxide Catalysts for CO_2/H_2 Conversion," *Catalysts*, vol. 9, no. 12, p. 1037, Dec. 2019, doi: 10.3390/catal9121037.
[37] L. Angelo, M. Girleanu, O. Ersen, C. Serra, K. Parkhomenko, and A. C. Roger, "Catalyst synthesis by continuous coprecipitation under micro-fluidic conditions: Application to the preparation of catalysts for methanol synthesis from CO_2/H_2," *Catal. Today*, vol. 270, pp. 59–67, 2016, doi: 10.1016/j.cattod.2015.09.028.
[38] Z. Shi, Q. Tan, C. Tian, Y. Pan, X. Sun, J. Zhang, and D. Wu, "CO_2 hydrogenation to methanol over Cu-In intermetallic catalysts: Effect of reduction temperature," *J. Catal.*, vol. 379, pp. 78–89, 2019, doi:

10.1016/j.jcat.2019.09.024.
[39] J. Xiao, D. Mao, X. Guo, and J. Yu, “Effect of TiO_2 , ZrO_2 , and TiO_2-ZrO_2 on the performance of CuO-ZnO catalyst for CO_2 hydrogenation to methanol,” *Appl. Surf. Sci.*, vol. 338, pp. 146–153, 2015, doi: 10.1016/j.apsusc.2015.02.122.
[40] C. Liu, X. Guo, Q. Guo, D. Mao, J. Yu, and G. Lu, “Methanol synthesis from CO_2 hydrogenation over copper catalysts supported on MgO-modified TiO_2,” *J. Mol. Catal. A Chem.*, vol. 425, pp. 86–93, 2016, doi: 10.1016/j.molcata.2016.09.032.
[41] W. Wang, Z. Qu, L. Song, and Q. Fu, “CO_2 hydrogenation to methanol over Cu/CeO_2 and Cu/ZrO_2 catalysts: Tuning methanol selectivity via metal-support interaction,” *J. Energy Chem.*, vol. 40, no. xxxx, pp. 22–30, 2020, doi: 10.1016/j.jechem.2019.03.001.
[42] H. Zhan, X. Shi, B. Tang, G. Wang, B. Ma, and W. Liu, “The performance of Cu/Zn/Zr catalysts of different Zr/(Cu+Zn) ratio for CO_2 hydrogenation to methanol,” *Catal. Commun.*, vol. 149, no. December 2020, p. 106264, 2021, doi: 10.1016/j.catcom.2020.106264.
[43] B. S. Xaba, A. S. Mahomed, and H. B. Friedrich, “The effect of CO_2 and H_2 adsorption strength and capacity on the performance of Ga and Zr modified Cu-Zn catalysts for CO_2 hydrogenation to methanol,” *J. Environ. Chem. Eng.*, vol. 9, no. 1, p. 104834, 2021, doi: 10.1016/j.jece.2020.104834.
[44] X. Guo, D. Mao, S. Wang, G. Wu, and G. Lu, “Combustion synthesis of CuO-ZnO-ZrO_2 catalysts for the hydrogenation of carbon dioxide to methanol,” *Catal. Commun.*, vol. 10, no. 13, pp. 1661–1664, 2009, doi: 10.1016/j.catcom.2009.05.004.
[45] S. Natesakhawat, J. W. Lekse, J. P. Baltrus, P. R. Ohodnicki, B. H. Howard, X. Deng, and C. Matranga, “Active sites and structure-activity relationships of copper-based catalysts for carbon dioxide hydrogenation to methanol,” *ACS Catal.*, vol. 2, no. 8, pp. 1667–1676, 2012, doi: 10.1021/cs300008g.
[46] S. Li, L. Guo, and T. Ishihara, “Hydrogenation of CO_2 to methanol over Cu/AlCeO catalyst,” *Catal. Today*, vol. 339, no. July 2018, pp. 352–361, 2020, doi: 10.1016/j.cattod.2019.01.015.
[47] J. Słoczyński, R. Grabowski, A. Kozłowska, P. Olszewski, M. Lachowska, J. Skrzypek, and J. Stoch, “Effect of Mg and Mn oxide additions on structural and adsorptive properties of $Cu/ZnO/ZrO_2$ catalysts for the methanol synthesis from CO_2,” *Appl. Catal. A Gen.*, vol. 249, no. 1, pp. 129–138, 2003, doi: 10.1016/S0926-860X(03)00191-1.
[48] J. Skrzypek, M. Lachowska, M. Grzesik, J. Słoczyński, and P. Nowak, “Thermodynamics and kinetics of low pressure methanol synthesis,” *Chem. Eng. J. Biochem. Eng. J.*, vol. 58, no. 2, pp. 101–108, 1995, doi: 10.1016/0923-0467(94)02955-5.
[49] J. Zhong, X. Yang, Z. Wu, B. Liang, Y. Huang, and T. Zhang, “State of the art and perspectives in heterogeneous catalysis of CO_2 hydrogenation to methanol,” *Chem. Soc. Rev.*, vol. 49, no. 5, pp. 1385–1413, 2020, doi: 10.1039/c9cs00614a.
[50] N. J. Azhari, D. Erika, S. Mardiana, T. Ilmi, M. L. Gunawan, I. G. B. N. Makertihartha, and G. T. M. Kadja, “Methanol synthesis from CO_2: A mechanistic overview,” *Results Eng.*, vol. 16, no. October, p. 100711, 2022, doi: 10.1016/j.rineng.2022.100711.
[51] M. Bukhtiyarova, T. Lunkenbein, K. Kähler, and R. Schlögl, “Methanol Synthesis from Industrial CO_2 Sources: A Contribution to Chemical Energy Conversion,” *Catal. Letters*, vol. 147, no. 2, pp. 416–427, 2017, doi: 10.1007/s10562-016-

1960-x.
[52] Y. Choi, K. Futagami, T. Fujitani, and J. Nakamura, “Role of ZnO in Cu/ZnO methanol synthesis catalysts - morphology effect or active site model?,” *Appl. Catal. A Gen.*, vol. 208, no. 1–2, pp. 163–167, 2001, doi: 10.1016/S0926-860X(00)00712-2.
[53] M. B. Fichtl, D. Schlereth, N. Jacobsen, I. Kasatkin, J. Schumann, M. Behrens, R. Schlögl, and O. Hinrichsen, “Kinetics of deactivation on $Cu/ZnO/Al_2O_3$ methanol synthesis catalysts,” *Appl. Catal. A Gen.*, vol. 502, pp. 262–270, 2015, doi: 10.1016/j.apcata.2015.06.014.
[54] R. Ladera, F. J. Pérez-Alonso, J. M. González-Carballo, M. Ojeda, S. Rojas, and J. L. G. Fierro, “Catalytic valorization of CO_2 via methanol synthesis with Ga-promoted $Cu-ZnO-ZrO_2$ catalysts,” *Appl. Catal. B Environ.*, vol. 142–143, pp. 241–248, 2013, doi: 10.1016/j.apcatb.2013.05.019.
[55] K. Kobl, S. Thomas, Y. Zimmermann, K. Parkhomenko, and A. C. Roger, “Power-law kinetics of methanol synthesis from carbon dioxide and hydrogen on copper-zinc oxide catalysts with alumina or zirconia supports,” *Catal. Today*, vol. 270, pp. 31–42, 2016, doi: 10.1016/j.cattod.2015.11.020.
[56] S. Poto, D. Vico van Berkel, F. Gallucci, and M. Fernanda Neira d’Angelo, “Kinetic modelling of the methanol synthesis from CO_2 and H_2 over a $CuO/CeO_2/ZrO_2$ catalyst: The role of CO_2 and CO hydrogenation,” *Chem. Eng. J.*, vol. 435, no. P2, p. 134946, 2022, doi: 10.1016/j.cej.2022.134946.
[57] G. H. Graaf, E. J. Stamhuis, and A. A. C. M. Beenackers, “Kinetics of low-pressure methanol synthesis,” *Chem. Eng. Sci.*, vol. 43, no. 12, pp. 3185–3195, 1988, doi: 10.1016/0009-2509(88)85127-3.

Chapter 4 Effect of the aging time and the coprecipitation temperature on Cu-ZnO-ZrO_2 catalysts synthesized by the microfluidic method

4.1. Introduction

The coprecipitation method is preferred over other catalyst synthesis methods because it allows a good contact and a high homogeneity between the metallic species in the solid if the conditions are controlled adequately. This is desirable for producing a good solid catalyst. Nevertheless, the coprecipitation process is characterized by the complexity and the effects of different variables on the final catalyst, such as the coprecipitation temperature, the aging time, the pH, the reactants concentrations, among others. All of the variables involved during the coprecipitation will have an important effect on the final properties of the catalysts, including the crystallites and particle sizes, the specific and the Cu surface areas as well as surface properties and morphology due to the known “chemical memory effect” [1][2]. This effect means that the final properties and the activity of the catalysts depend on the conditions applied to the precursors during the catalyst synthesis step [3].

This chapter presents the effects of the aging time and the effects of the coprecipitation temperature on the properties and catalytic performance of Cu-ZnO-ZrO_2 catalysts prepared by coprecipitation using the microfluidic method. This chapter is constructed in two sub-chapters. The first one addresses the effect of the aging time on the catalyst properties and activity and the second one the effects of the coprecipitation temperature.

In the first sub-chapter, three Cu-ZnO-ZrO_2 catalysts were prepared by coprecipitation using a microfluidic device and the effects of the aging time on the properties of the catalysts and their catalytic activity were studied. The three catalysts were named CuO 33-0h, CuO 50-0h and CuO 33-17h, where the number 33 or 50 corresponds to the mass % of CuO in the catalyst while the term 0h or 17h corresponds to an aging time of 0h (i.e. no aging) or 17h, respectively. The technique employed to study the aging time by using a microfluidic device corresponds to the method named microfluidic synthesis with immediate filtration which can be found in Chapter 2 section 2.2. This method consisted in collecting the precipitate produced with the microfluidic device with the help of a filter during the whole time of the catalyst synthesis. After the end of the synthesis, the obtained precipitate was washed, filtered and dried in the case of precursors with no aging, or aged at 65ºC, washed, filtered and dried in the case of the catalyst aged for 17 hours.

In the second sub-chapter, another catalyst was prepared to study the effect of heating the precipitation zone and the reactants to 65ºC during the coprecipitation step. Such catalyst was named CuO 50-0h-65, where 0h indicates a zero aging time and the number 65 corresponds to the coprecipitation temperature in ºC. The characterization and the catalytic performance results of the CuO 50-0h-65 catalyst were compared to those of the CuO 50-0h catalyst, which was prepared in the same way but at ambient temperature.

For more clarity, the term “aging temperature” corresponds to the temperature of the contents of the stirred beaker which is used for the aging of the precursor (i.e. the only precursor that was aged in this chapter was the CuO 33-17h precursor), while the term “coprecipitation temperature” corresponds to the temperature of the precipitation zone and the temperature of the reactants during the catalyst synthesis.

Table 4.1 shows the names and some synthesis conditions of the catalysts investigated in this chapter.

Table 4.1 Names and synthesis conditions of the catalysts studied in this chapter.

Catalyst	Catalyst composition, mass %	Aging time, hours	Aging and coprecipitation temperatures ºC
CuO 33-0h	33.3% CuO, 33.3% ZnO, 33.3% ZrO_2	0	No aging / Ambient
CuO 50-0h	50% CuO, 33% ZnO, 17% ZrO_2	0	No aging / Ambient
CuO 33-17h	33.3% CuO, 33.3% ZnO, 33.3% ZrO_2	17	65ºC / Ambient
CuO 50-0h-65	50% CuO, 33% ZnO, 17% ZrO_2	0	No aging / 65ºC

Lastly, a review of different catalysts for the production of methanol available in the literature is presented at the end of this chapter and used to compare with the catalysts synthesized in this work.

4.2. Effect of the aging time on the properties and catalytic performance of Cu-ZnO-ZrO_2 catalysts

The aging time during the coprecipitation can affect the crystallite sizes and the formation of different phases in the precursors, which can have an effect on the final properties of the catalysts [4]. Currently there are no available studies addressing the effects of the aging time on Cu-ZnO-ZrO_2 catalysts synthesized by coprecipitation using the microfluidic method. For such reason, studying the effects of the aging time on Cu-ZnO-ZrO_2 catalysts prepared by the microfluidic technique would allow to improve the understanding of this catalyst synthesis method and help fill a gap present in the literature. In addition, the investigation of the aging time may lead to the production of catalysts with better properties and catalytic performance. The catalysts characterization results and discussion are presented next.

4.2.1. Catalysts characterization results and discussion

The X-ray diffractograms of the precursors after drying and before calcination step are presented on the left side of Figure 4.1 and the diffractograms of the calcined materials are presented on the right side. The X-ray diffractograms of the precursors show that the lack of aging of the samples CuO 33-0h and CuO 50-0h resulted in amorphous materials. Conversely, when an aging time of 17h was employed, the formation of two phases could be observed. These two phases corresponded to aurichalcite $Zn_3Cu_2(OH)_6(CO_3)_2$ (PDF number: 82-1253) and hydrozincite $Zn_5(CO_3)_2(OH)_6$ (PDF number: 72-1100). This shows that the aging time plays an important role in the formation of crystalline phases in the catalyst precursors. These results are in agreement with other works [5]–[7] which indicate that during the coprecipitation step the catalyst precursors are first amorphous and then develop a crystalline structure during the aging process. No Zr species were detected in any of the precursors due to its amorphous state.

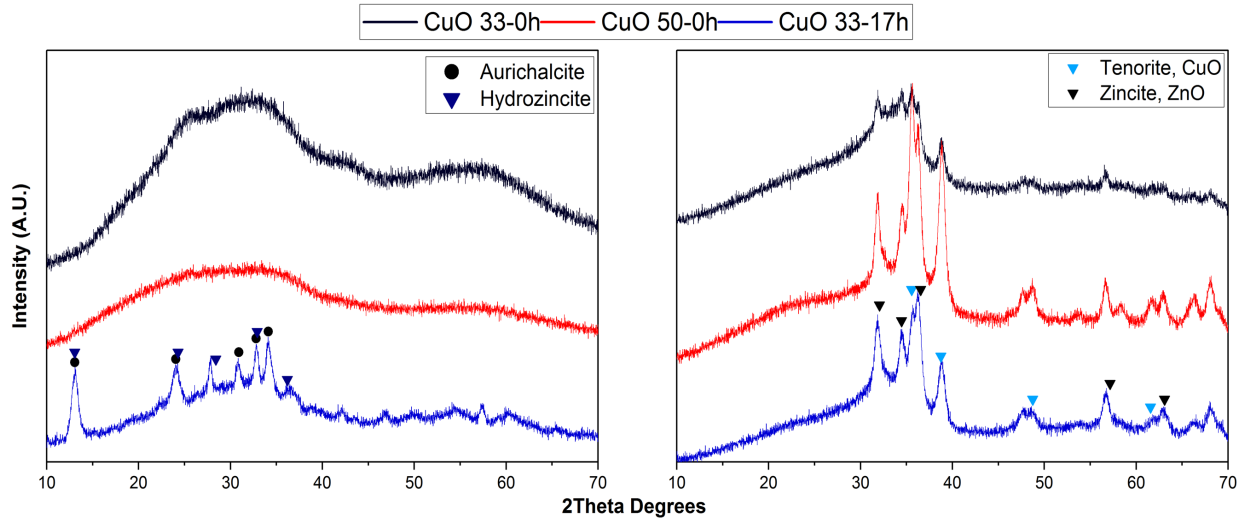

Figure 4.1 X-ray diffractograms of the precursors on the left side and their respective calcined catalysts on the right side.

Using Scherrer's equation, the crystallite sizes of the identified phases were calculated and are shown in Table 4.2. The 2Theta values used for these calculations were 13° for both aurichalcite and for hydrozincite (hkl: 200 for both phases). Only the crystallite sizes of the precursor CuO 33-17h were calculated because the diffractograms of the other two catalyst precursors indicated that they are amorphous.

Table 4.2 Crystallite sizes (nm) of the formed crystalline phases calculated with Scherrer's equation and crystallinity % computed from the diffractograms.

	Catalyst precursor		Calcined catalyst		
Sample	**Aurichalcite**	**Hydrozincite**	**Tenorite, CuO**	**Zincite, ZnO**	**Crystallinity %**
CuO 33-0h	-	-	NC	NC	22.7
CuO 50-0h	-	-	12	12	36.7
CuO 33-17h	10	10	11	11	35.4

- : Amorphous
NC : Not calculated

The diffractograms of the calcined catalysts are shown on the right side of Figure 4.1. As can be evidenced, all the catalysts developed crystalline phases corresponding to CuO (PDF number: 72-0629) and ZnO (PDF number: 75-1526). No phases containing ZrO_2 were detected either due to its amorphous nature, as indicated in previous research works [8]–[11].

The catalyst CuO 33-0h presented broad peaks of CuO and ZnO indicating lower crystallinity compared to the other catalysts. In fact, the crystallite sizes of the catalyst CuO 33-0h were not calculated due to the low crystallization of the sample, which caused the peaks to have very low resolution. The crystallite sizes of CuO and ZnO

calculated by Scherrer's equation are also presented in Table 4.2. The 2Theta values used to calculate crystallite sizes were 38.7º for CuO (hkl: 111) and 32º for ZnO (hkl: 100). The CuO and ZnO phases of the catalysts CuO 50-0h and CuO 33-17h presented crystallite sizes between 11 and 12nm, very close to the crystallite sizes of the catalysts studied in the previous chapter. The results of the X-ray diffractograms of the calcined catalysts CuO 33-0h and CuO 33-17h show that longer aging times favor the crystallization process of the CuO and ZnO phases in the calcined catalysts. Also, when comparing the diffractograms of the calcined catalysts CuO 33-0h and CuO 50-0h it can be concluded that the increase of the CuO content from 33.3 wt% to 50 wt% favored the development of crystalline phases, which may be due to the lower relative content of amorphous ZrO_2 in the CuO 50-0h catalyst.

The crystallinity of the catalysts was determined by taking into account the area of the X-ray diffractograms that corresponded to the crystalline phases (i.e. the peaks), and the area corresponding to the amorphous fraction of the catalyst, and then dividing the crystalline phase area by the crystalline phase + amorphous phase area. This was calculated with the EVA software for XRD analysis. The crystallinity results are reported in % and are presented in Table 4.2. These results show that the catalyst prepared without aging CuO 33-0h presented a crystallinity of 22.7% while the catalyst CuO 33-17h presented a crystallinity of 35.4%, indicating that the longer aging time caused an increase in the content of crystalline phases in the material, in this case more crystalline CuO and ZnO. In the case of the catalyst CuO 50-0h, it presented a higher crystallinity than the CuO 33-0h which may be due to the higher content of the CuO phase and the consequent lower content of amorphous ZrO_2, as mentioned above. Given that the increase in the crystallinity of the catalyst CuO 50-0h is not entirely proportional to the decrease in ZrO_2 content with respect to catalyst CuO 33-0h, other factors must also have an effect on the crystallinity of the catalyst, such as the interaction between components containing Cu and the presence of amorphous georgeite.

TGA was employed to study the thermal decomposition of the catalyst precursors after drying and before the calcination step. The results of the TGA analysis of the three catalyst precursors are presented in Figure 4.2. The total mass loss after heating the precursors to 700ºC were 22, 21 and 22% for the CuO 33-0h, CuO 50-0h and CuO 33-17h catalysts, respectively. Particularly, the total mass loss % of the samples CuO 33-0h and CuO 33-17h presented a high similarity because they were prepared from the same solution and have therefore the same bulk concentrations of Cu, Zn and Zr. Despite the similarity in total mass loss %, the TGA decomposition profiles presented in Figure 4.2 indicate some differences in the decomposition process. As can be seen, the derivatives of the mass loss of the catalyst precursors presented differences in peak intensities and the temperatures where the peaks occurred.

The peaks of the derivative of the mass loss of the catalyst precursors CuO 33-0h and CuO 50-0h occurred around the temperatures of 150ºC and 480ºC, while in the case

of the catalyst precursor CuO 33-17h the peaks occurred around the temperatures 150ºC, 300ºC and 480ºC. The work of L'hospital [12] showed that a Zr-based precursor decomposes around 150ºC, which explains the presence of the peak at 150ºC in the three catalyst precursors. The peak occurring around 300ºC in the decomposition profile of the catalyst precursor CuO 33-17h can be associated to the decomposition of the aurichalcite phase [13][14]. In fact, the catalyst precursor CuO 33-17h was the only one that developed this crystalline phase according to the XRD results and the only sample with a decomposition peak occurring at 300ºC. According to the work of L'hospital [12], the Cu-Zn species (i.e. aurichalcite) also presents a decomposition temperature around 466ºC, which could contribute to the peak occurring around this temperature. The higher crystallization degree of aurichalcite in the catalyst CuO 33-17h compared to catalyst CuO 33-0h may be responsible of the larger peak obtained between 450ºC and 500ºC.

Moreover, as discussed in the works of Yurieva *et al*. [15] and Mota *et al*. [7], the thermal decomposition of hydroxycarbonates occurs in two steps. The first one occurs at temperatures around 300ºC and involves the formation of anion-modified oxides (i.e. oxides in which some oxygen ions are substituted by OH^- and CO_3^{2-} groups) from the hydroxycarbonates. The second stage occurs at temperatures above 500ºC and consists in the decomposition of the anion modified oxides into true oxides. The two steps of the decomposition of the hydroxycarbonates explain the presence of decomposition peaks occurring at temperatures around 300ºC and between 400-600ºC.

In the thesis of L'hospital [12], a CuO-ZnO-ZrO_2 catalyst was prepared by coprecipitation of metal nitrates with sodium carbonate using the microfluidic method and it was found that this material presented different thermal decomposition peaks around 161ºC, 316°C, 368°C, 409°C and 492°C. This indicates that the presence of a ternary component containing Cu, Zn and Zr may be at the origin of the decomposition peaks occurring around 160ºC, 300ºC and between 400ºC and 500ºC.

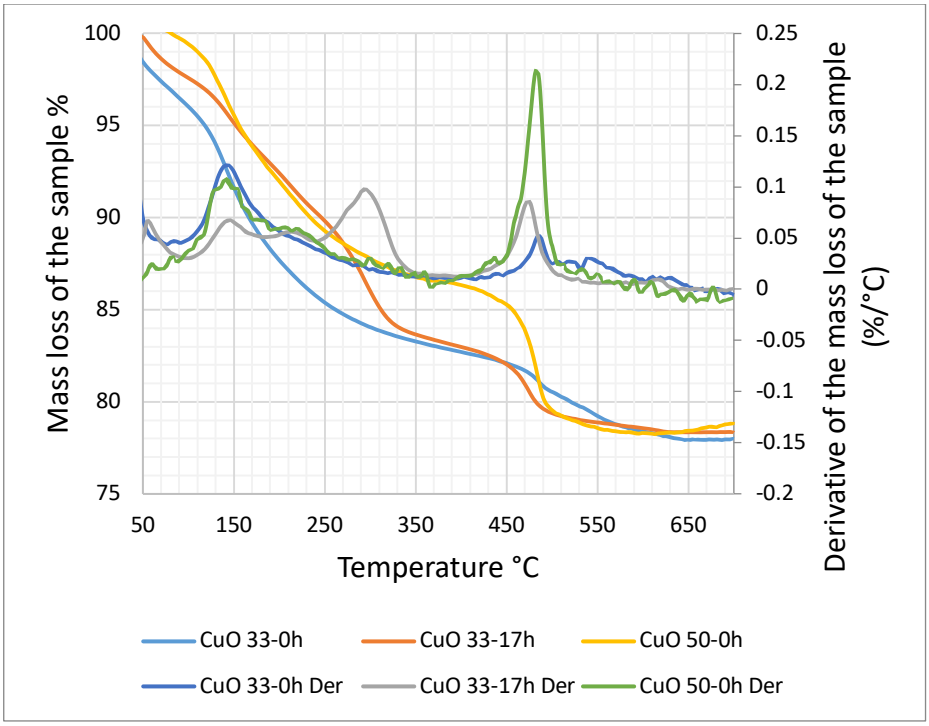

Figure 4.2 Mass loss % and Mass loss % derivatives of the catalyst precursors. Der: Derivative.

The FT-IR spectroscopy technique was used to study more in depth the nature and the functional groups that are present in the materials before and after the calcination step. The results of the FT-IR study of the catalyst precursors and the calcined catalysts are presented in Figures 4.3a and 4.3b, respectively. The spectra of the catalyst precursors show the presence of peaks around 800cm^{-1}, between 1200 and 1600cm^{-1} and around 3300cm^{-1}. These peaks correspond to the presence of NO_3^-, CO_3^{2-} and NO_3^-, and -OH functional groups, respectively. Colored bands in Figures 4.3a and b are used to identify the presence of these functional groups, where the green bands correspond to hydroxyl groups, the gray bands correspond to carbonate and nitrate groups and the light blue bands correspond to nitrate groups. The signals obtained at 1470, 1394 and 832 cm^{-1} shown as vertical dashed lines in Figure 4.3a are also an indication of the presence of the hydroxycarbonate zincian georgeite $(Cu,Zn)_7(OH)_4(CO_3)_5$ [7], which is present as an amorphous compound, so it's not detected by XRD. Furthermore, the FT-IR characteristic peaks of aurichalcite (i.e. 1556, 1201 and 971 cm^{-1} [16]) and malachite (i.e. 1510, 1408 and 1368 cm^{-1} [17]) were not detected in the CuO 33-0h and CuO 50-0h catalysts, which is in agreement with the XRD results which showed that these two catalysts were completely amorphous.

After the calcination step, the 3 catalysts presented similar FT-IR spectra, with a significant decrease of the peaks between 1200 and 1600cm^{-1}, indicating an important reduction in the concentration of the carbonate groups. However, these peaks didn't disappear completely, which indicates that a residual carbonate fraction was present in the calcined catalysts. This may indicate the presence of the typically referred as high temperature carbonate phase (HT-CO_3) [6], [18], [19]. The carbonate retention of

the catalysts after calcination can have important effects on the segregation and crystallization of CuO and ZnO [7]. In addition, the peaks around 3300cm^{-1} didn't disappear completely either after calcination, indicating the presence of -OH functional groups in the calcined catalysts. The weak signals close to 800cm^{-1} also indicate that the nitrate groups were decomposed after the calcination step.

Lastly, the noise appreciable around 2200 cm^{-1} wavenumber corresponds to the ambient CO_2, which gives peaks around 600, 2200 and 3600 cm^{-1} according to the NIST database [20]. Before each analysis the device was calibrated to remove this interference from the FT-IR spectra.

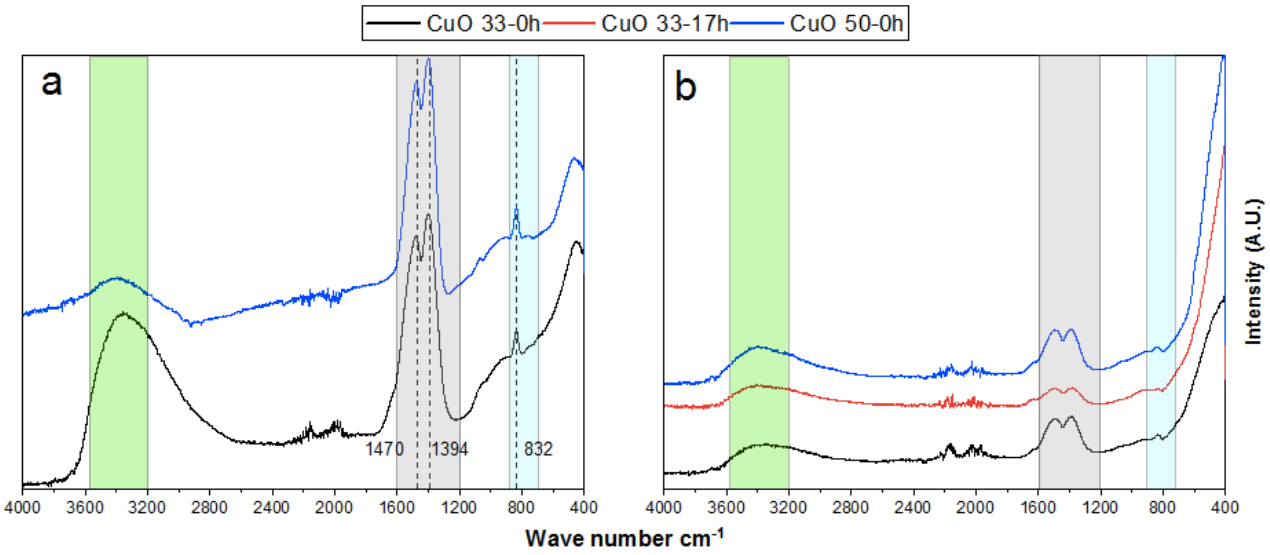

Figure 4.3 FT-IR spectra of the catalyst precursors (a) and the calcined catalysts (b).

The specific surface areas and pore sizes of the catalysts were investigated by N_2-physisorption. The adsorption-desorption isotherms of the catalysts are presented in Figure 4.4. As can be observed, all of the catalysts presented type IV isotherms, which are characteristic of mesoporous materials with cylindrical shaped pores [21][22].

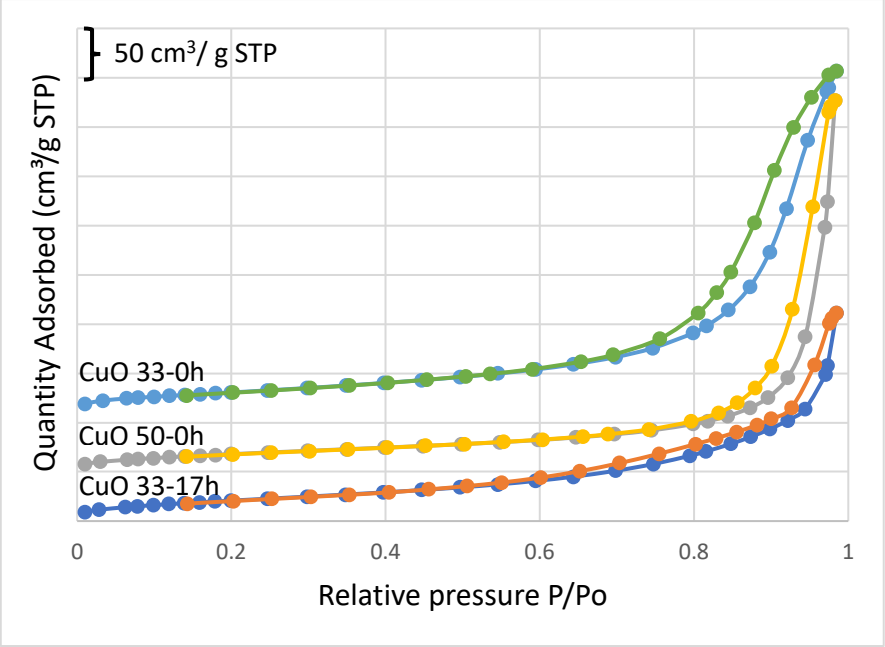

Figure 4.4 N_2-Physisorption isotherms of the CuO 33-0h, CuO 33-17h and CuO 50-0h calcined catalysts.

Table 4.3 shows the results of the specific surface area and the pore size of the calcined catalysts. When comparing the results of the textural properties of the samples CuO 33-0h and CuO 33-17h, it is clear that longer aging times cause an important decrease in the specific surface area (i.e. from 109 to 81 m^2/g) and in the pore size (i.e. 16 to 6 nm). From these results and under the conditions of this study, it is clear that the unaged catalyst presented a higher specific surface area. Moreover, when comparing the textural properties of the catalysts CuO 33-0h and CuO 50-0h it is evident that the increase in the copper oxide content of the catalysts with the consequent decrease in ZnO and ZrO_2 relative contents (i.e. a ZnO/CuO mass ratio change from 1 to a ratio of 0.66 and a ZrO_2/CuO ratio change from 1 to a ratio of 0.34), causes a decrease in the specific surface area (i.e. from a value of 109 to 70 m^2/g) and an increase in the pore size (i.e. from 16nm to 28nm). The decrease in the specific surface area after the increase in the relative content of copper may be due to the loss of the promoting effects of ZnO and ZrO_2 which are known to act as stabilizers and promoters of the specific surface area of Cu-ZnO-ZrO_2 catalysts [23]–[25].

Table 4.3 N_2-Physisorption surface area and pore size of the CuO 33-0h, CuO 33-17h and CuO 50-0h catalysts.

Sample	BET surface area (m^2/g)	Pore size (nm)
CuO 33-0h	109	16
CuO 33-17h	81	6.0
CuO 50-0h	70	28

The work of Raudaskoski *et al*. [8] dealing with the study of the effects of aging time on the properties of Cu-ZnO-ZrO_2 catalysts, showed that the specific surface areas obtained by N_2-physisorption increased with increasing aging time. However, the catalyst synthesis method that they investigated was a coprecipitation of metal nitrates with sodium carbonate in a batch stirred beaker with an aging temperature of 80ºC, which is different from the microfluidic method employed in this work, with no aging time in the case of the catalysts CuO 33-0h and CuO 50-0h, and with an aging temperature of 65ºC in the case of catalyst CuO 33-17h. Moreover, the catalyst compositions that they investigated were 33wt% Cu, 30wt% Zn and 6wt% Zr, which differed from those of this work too. Such results about the specific surface area contradict the results of this work, which showed that the increasing aging times cause a decrease in the specific surface area of the catalysts. It is worth noting that the catalyst synthesis conditions they used differed importantly from those employed in the present work, as mentioned above.

Figure 4.5 shows SEM images of the catalysts CuO 33-0h (a and b) and CuO 33-17h (c and d). In the case of the catalyst CuO 33-0h, it can be appreciated that this catalyst presented a grainy morphology consisting of agglomerations of particles, which according to SEM images reported in the literature [26]–[28] correspond to crystalline CuO. In contrast, the catalyst CuO 33-17h developed plate-like or flower-like structures corresponding to crystalline ZnO [29] along with agglomeration of CuO particles. These results indicate that the aging time is important for the development of crystalline phases, which is in agreement with the XRD results. The porosity appreciated in the SEM images of catalyst CuO 33-17h also confirms the N_2-physisorption characterization results, which indicated that the material is mesoporous.

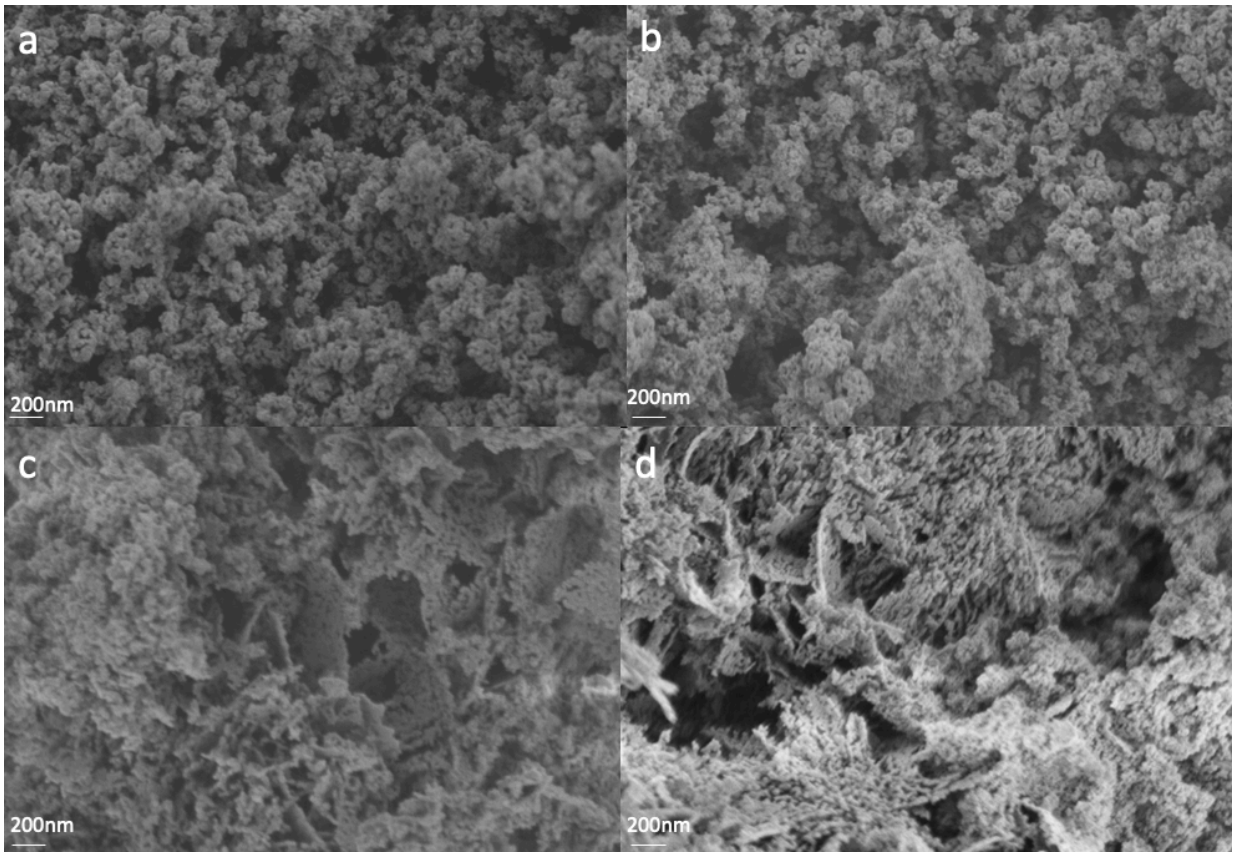

Figure 4.5 SEM images of the catalysts CuO 33-0h (a and b) and CuO 33-17h (c and d).

Using SEM, Raudaskoski *et al*. [8] investigated the effect of the aging time on the morphology of a Cu-ZnO-ZrO_2 catalyst prepared by coprecipitation in a stirred beaker and found morphology differences between a catalyst aged for 0.5 h, for 12 h and for 24 h. These morphology differences may be due to the increasing crystallinity of the catalysts with increasing aging time. The experimental conditions of their work were discussed just above in the N_2-physisorption results section.

Table 4.4 shows the compositions obtained by EDS of the CuO 33-0h and CuO 33-17h catalysts. These results can give an idea about the homogeneity in the composition of the materials. The EDS results of the catalyst CuO 33-17h indicate that the composition of this catalyst was more uniform, approaching more the theoretical composition than the catalyst CuO 33-0h. In fact, the CuO/ZnO ratio of the catalyst CuO 33-17h was closer to unity (i.e. 1.1) than that of the catalyst CuO 33-0h (i.e. 1.6). This may indicate that the catalyst CuO 33-17h presented a higher homogeneity than the catalyst CuO 33-0h. The cause of the higher homogeneity of the CuO 33-17h catalyst might be related to the development of the crystalline aurichalcite and hydrozincite phases, previously identified by XRD analysis. As shown before, the aurichalcite phase is composed of Cu and Zn, which could contribute to a better intermixing between these two metal species in the solid material.

Table 4.4 EDS composition analysis results of the CuO 33-0h and the CuO 33-17h catalysts.

Catalyst	CuO Content wt%	ZnO Content wt%	ZrO_2 Content wt%
CuO 33-0h	38.0	24.1	37.8
CuO 33-17h	35.9	32.1	31.9
Theoretical	33.3	33.3	33.3

The surface basicity of the three catalysts was investigated with the use of CO_2-TPD analysis technique. As shown in Figure 4.6, the three catalysts analyzed presented two main CO_2 desorption peaks around 200ºC and 600ºC, corresponding to weak and strong basic sites, respectively. The CO_2 desorption peaks indicating the presence of moderate strength basic sites around 430ºC were very small compared to the weak and strong basic sites, but were still present in the catalysts CuO 33-17h and CuO 50-0h. As discussed before, weak, moderate strength and strong basic sites are related to the presence of surface hydroxyl groups, metal-oxygen pairs and low coordination oxygen atoms, respectively [30]. The presence of hydroxyl groups was detected in the three calcined catalysts by employing FT-IR analysis, as discussed before, and it was found that the signal corresponding to the hydroxyl groups of the catalyst CuO 33-0h was larger than that of catalyst CuO 50-0h. This fact correlates well with the larger amount of weak basic sites calculated for the catalyst CuO 33-0h.

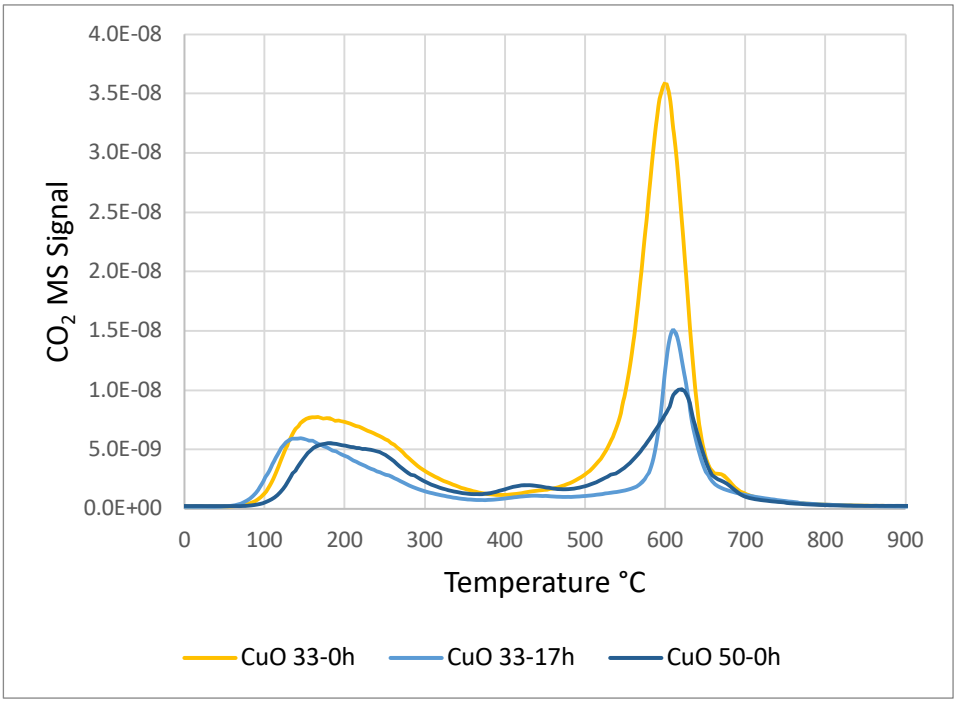

Figure 4.6 CO_2-TPD profiles of the CuO 33-0h, CuO 33-17h and CuO 50-0h catalysts.

Table 4.5 shows the quantitative results of the CO_2-TPD analysis. The catalysts CuO 33-17h and CuO 50-0h presented a similar quantity of weak basic sites (i.e. 100.0

μmol g^{-1} for both catalysts) while the catalyst CuO 33-0h presented a higher quantity (i.e. 160.0 μmol g^{-1}). The quantity of moderate strength basic sites in catalysts CuO 33-17h and CuO 50-0h was very small, with values of 13.0 and 21.0 μmol g^{-1}, respectively. Regarding the amount of strong basic sites, the catalyst CuO 33-0h presented a higher quantity corresponding to 330.0 μmol g^{-1} compared to the other two catalysts CuO 33-17h and CuO 50-0h, which presented a quantity of strong basic sites of 100.0 and 110.0 μmol g^{-1}, respectively.

Table 4.5 Quantity of weak, moderate strength and strong basic sites and basic sites per unit surface area of the CuO 33-0h, CuO 33-17h and CuO 50-0h catalysts after calcination.

Sample	Weak basic sites (μmol/g)	Moderate strength basic sites (μmol/g)	Strong basic sites (μmol/g)	Total basic sites (μmol/g)	Basic sites per unit surface area (μmol/m^2)
CuO 33-0h	160.0	-	330.0	490.0	4.49
CuO 33-17h	100.0	13.0	100.0	213.0	2.59
CuO 50-0h	100.0	21.0	110.0	231.0	3.28

Therefore, the total amount of basic sites was the highest for the catalyst CuO 33-0h with a value of 490.0 μmol g^{-1}, compared to the other two catalysts CuO 33-17h and CuO 50-0h, which presented a total amount of basic sites of 213.0 and 231.0 μmol g^{-1}, respectively. The differences in the amount and strength of basic sites can be explained in part by the much higher specific surface area of the CuO 33-0h catalyst compared to the other ones, which allows the adsorption of a larger quantity of CO_2 per unit mass of catalyst. The surface chemistry also has an effect on the affinity for CO_2 of the catalyst. The three catalysts under study presented residual hydroxyl groups after calcination, as evidenced in the FT-IR spectra discussed before. The hydroxyl groups are responsible of the adsorption of CO_2 below temperatures of 300ºC, which correspond to weak basic sites. Due to the weak character of hydroxyl basic sites, the mechanism of adsorption on these sites may correspond to physical adsorption only. In addition, the presence of carbonate groups remaining after the calcination of the catalysts, as found by FT-IR analysis, may also be a contributor to the surface basicity of the catalysts.

Moreover, when comparing the CuO 33-0h and the CuO 50-0h catalysts, it is clear that the amount of surface basic sites decreases with increasing CuO content in the catalyst. This can be explained by the lower relative content of ZnO and ZrO_2 in the CuO 50-0h catalyst (i.e. CuO/ZrO_2 ratio of 1 and 3 in the CuO 33-0h and CuO 50-0h catalysts, respectively). ZrO_2 can activate the CO_2 molecule and has a higher chemisorption capacity towards CO_2 compared to other oxide supports, such as the oxides of Al, Ti, Mg and Si [31]. ZnO and ZrO_2 also possess an alkaline character that increases the affinity of CO_2 of the catalysts [32]. In fact, the EDS analysis results

showed that the catalyst CuO 33-0h presented a higher content of ZrO_2 than the catalyst CuO 33-17h, which also explains the higher surface basicity of the catalyst CuO 33-0h.

Lastly, the total basic sites per unit surface area presented in Table 4.5 indicate that the catalyst CuO 33-0h presented the largest amount of basic sites per unit surface area, followed by the CuO 50-0h and CuO 33-17h catalysts. This means that the catalyst CuO 33-0h possesses a higher surface density of basic sites which can adsorb and activate CO_2.

The H_2-TPR profiles of the catalysts are presented in Figure 4.7. In line with previous research works [8], the Cu-ZnO-ZrO_2 catalysts presented reduction peaks between 150-200ºC, indicating the reduction of copper oxide to metallic copper, given that the reduction of ZnO and ZrO_2 does not occur below temperatures of 300ºC [8][10].

The quantification of the H_2 consumed during the H_2-TPR analysis for the reduction of CuO to Cu was used to determine the CuO content of the catalysts, assuming that no other reduction process occurs. These results are presented in Table 4.6. As shown in the table, the three catalysts presented a CuO content very close to the theoretical CuO content of the catalysts, which means that the CuO loading during the catalyst synthesis was correct.

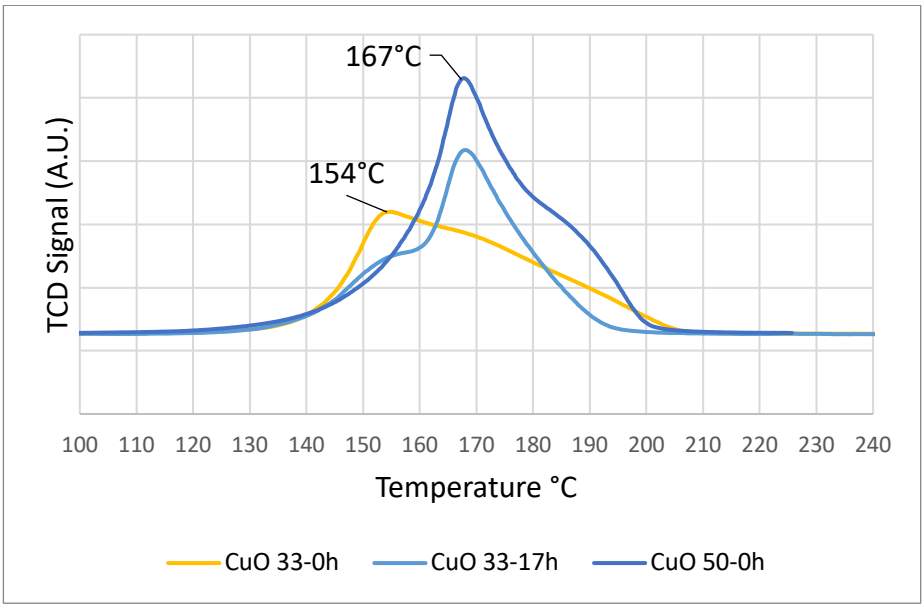

Figure 4.7 H_2-TPR profiles of the CuO 33-0h, CuO 33-17h and CuO 50-0h catalysts.

From the analysis of different sources [33]–[36], a low temperature reduction peak may correspond to the reduction of surface dispersed CuO or small CuO particles while a high temperature reduction peak may correspond to the reduction of bulk CuO or to the reduction of bigger CuO particles. The presence of different peak shapes or differences in the reduction profiles obtained can indicate the presence of different size distribution of reducible CuO species.

Table 4.6 H_2-TPR quantitative results of the CuO 33-0h, CuO 33-17h and CuO 50-0h catalysts.

Sample	H_2 consumption, mmol/g	Catalyst theoretical Cu content, mmol Cu/g	H_2/Cu ratio	Calculated CuO % of the catalyst
CuO 33-0h	4.35	4.19	1.04	34.6
CuO 33-17h	4.16	4.19	0.99	33.1
CuO 50-0h	6.21	6.29	0.99	49.4

The catalysts CuO 33-0h and CuO 33-17h presented different reduction profiles despite having very similar Cu content. The reduction profiles of the two catalysts presented different shapes and reduction peaks, which indicate the reduction of copper oxide particles of different sizes and possibly surface dispersed as well as bulk copper oxide. The catalyst CuO 33-0h presented a maximum peak temperature of 154ºC while the catalyst CuO 33-17h presented a peak shoulder at 154ºC and a peak maximum at 167ºC. Therefore, the catalyst CuO 33-0h presented an easier reducibility, indicating the presence of smaller CuO particles that facilitate the reduction process of the CuO species. On the contrary, the higher reduction temperatures of the CuO 33-17h catalyst may indicate a higher relative amount of bigger CuO particles compared to the catalyst CuO 33-0h. Different metal-support interactions can also explain the different reducibilities of these two catalysts, indicating that the Cu-support interactions in CuO 33-0h catalyst are more favorable, causing a decrease in the reduction temperature of this catalyst. These interactions may be due to the better promotion caused by ZnO and ZrO_2, due to more intimate contact of the support with the Cu nanoparticles.

Regarding the reduction profile of the catalyst CuO 50-0h, it presented a larger area, which indicates a higher H_2 consumption per mass of catalyst during the analysis. This result is consistent given that the Cu content of this catalyst is higher than that of the other two catalysts which have CuO content of 33.3wt%. The reduction temperatures of this catalyst also presented a shift to higher temperatures, which indicates the presence of bigger CuO particles than catalyst CuO 33-0h. This can be explained by the decreased contents of ZnO and ZrO_2 in this catalyst compared to the other two catalysts. As discussed before, ZnO and ZrO_2 can improve the Cu dispersion and stabilize the Cu crystallite sizes.

To analyze more in depth the resulting H_2-TPR profiles, a deconvolution was done to the reduction profiles of the 3 catalysts assuming two different peaks identified as α and β, corresponding to the fitted low and high temperature peaks present in each catalyst. Figure 4.8 shows the deconvolution results of the three catalysts and Table

4.7 shows the areas and the % of the 2 assumed reduction peaks. The deconvolutions were done by curve fitting with a Gaussian function.

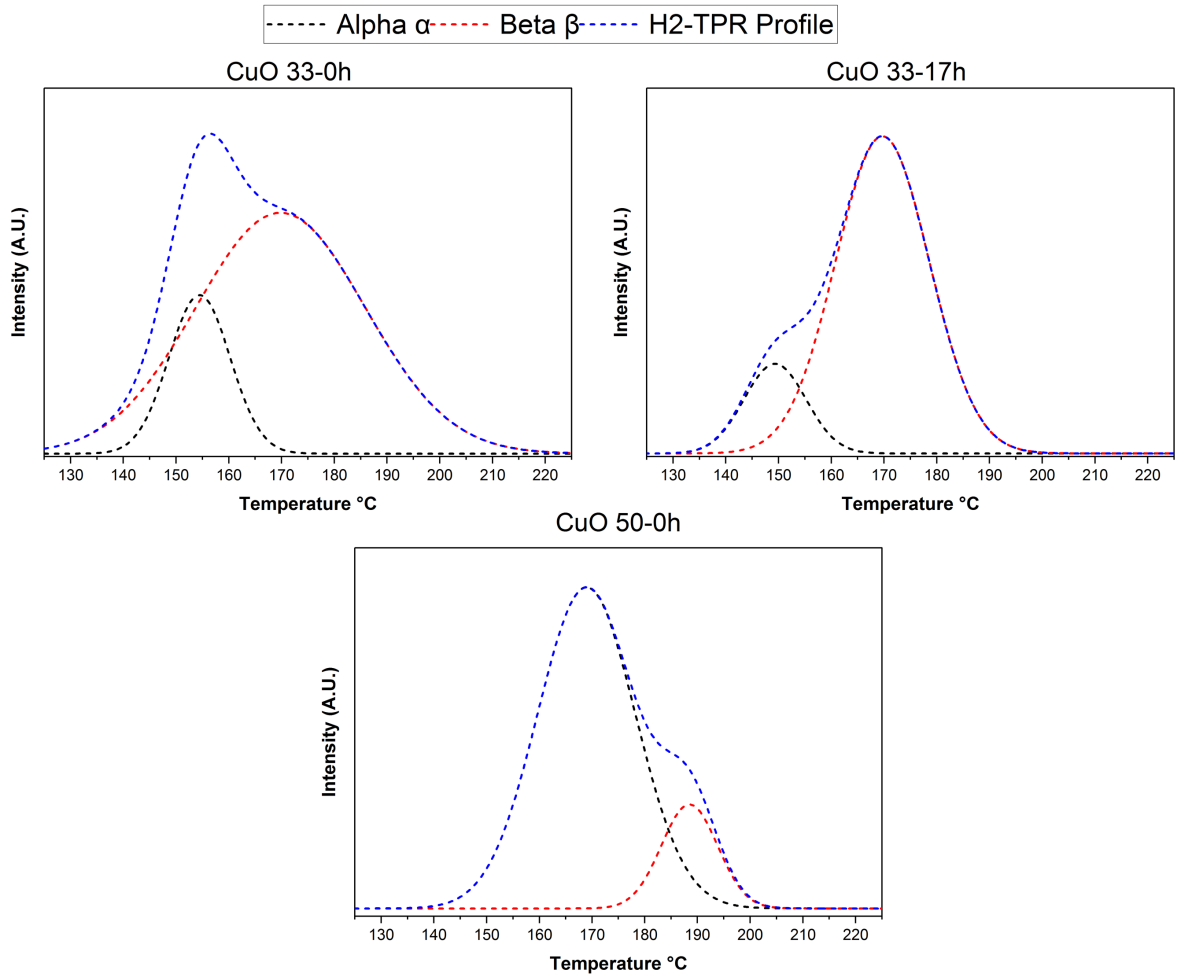

Figure 4.8 H_2-TPR profiles deconvolution of CuO 33-0h, CuO 33-17h and CuO 50-0h catalysts.

In the case of the catalyst CuO 33-0h the main reduction peak α occurred at 154ºC and the β shoulder at approximately 170ºC. In the case of the catalyst CuO 33-17h, it presented an α shoulder at 154ºC and the main reduction peak β at 167ºC, while the catalyst CuO 50-0h presented a main reduction peak α at 170ºC and a β shoulder at approximately 185ºC.

When comparing the quantitative results of the deconvolution of the H_2-TPR profiles of catalysts CuO 33-0h and CuO 33-17h it can be seen that a longer aging time caused a decrease in the amount of smaller CuO particles (i.e. at 154ºC) and the increase in the amount of bigger CuO particles (i.e. around 170ºC), which makes the reduction process of CuO more difficult. This indicates that longer aging times favor the formation of bigger CuO particles, which can result in the loss of copper surface area. These estimations were done by taking into account the area percentages calculated and presented in Table 4.7

In the case of the catalyst CuO 50-0h, there was a shift in the reduction temperatures to higher values (i.e. 170ºC and 185ºC for the α and β peaks, respectively), which indicates that the CuO particle size distribution of this catalyst moved to bigger particle sizes.

To summarize, the deconvolutions of the H_2-TPR profiles of the three catalysts show that each catalyst has a CuO particle size distribution which shifts to bigger CuO particle sizes with the increase of the CuO content of the catalyst. This means that the "small particles" of the catalyst CuO 33-0h do not have the same size of the "small particles" present in the catalyst CuO 50-0h. In other words, this occurs due to the displacement of the α and β peaks to higher temperatures when the content of CuO is increased.

Table 4.7 Deconvolution quantitative results of the H_2-TPR profiles of the CuO 33-0h, CuO 33-17h and CuO 50-0h catalysts.

CuO 33-0h			
Peak	Temperature ºC	Area	Percentage
α	154	28.2	19
β	170	118.6	81
Total		146.8	100
CuO 33-17h			
Peak	**Temperature ºC**	**Area**	**Percentage**
α	154	21.5	16
β	167	114.9	84
Total		136.4	100
CuO 50-0h			
Peak	**Temperature ºC**	**Area**	**Percentage**
α	170	162.3	84
β	185	30.1	16
Total		192.4	100

The above results indicate that in the case of Cu-ZnO-ZrO_2 catalysts with equal contents of CuO, ZnO and ZrO_2, a zero aging time allows obtaining catalysts with smaller CuO particles, which translates into lower reduction temperatures and an easier reduction process. Also, a longer aging time of 17 hours or a 50% CuO content cause the formation of bigger CuO particles which are reduced at higher temperatures, making the reduction process more difficult.

The copper surface area, copper dispersion and copper particle sizes investigated with the use of N_2O surface reaction analysis are presented in Table 4.8. The analysis results show that the catalyst CuO 33-0h presented a higher copper surface area than the catalyst CuO 33-17h. This difference in copper surface area can be explained by

the higher specific surface areas obtained when using shorter aging times (i.e. catalyst CuO 33-0h presented a specific surface area of 109 m^2/g while catalyst CuO 33-17h presented a specific surface area of 81 m^2/g). This indicates that zero aging time favor the formation of Cu-ZnO-ZrO_2 catalysts with higher specific surface areas which in turn increases the Cu surface area because the Cu particles can be dispersed on a larger surface. When comparing the results of the CuO 33-0h and CuO 33-17h catalysts it can be appreciated that the catalyst CuO 33-0h presents smaller copper particle size (i.e. 11nm against 18nm) and higher copper dispersion (i.e. 9.4% against 5.9%), which are desirable properties for Cu-ZnO-ZrO_2 catalysts. Moreover, the smaller copper particle size of the catalyst CuO 33-0h can explain the lower reduction temperature of this catalyst, compared to the CuO 33-17h and CuO 50-0h catalysts.

Table 4.8 N_2O surface reaction analysis results of the CuO 33-0h, CuO 33-17h and CuO 50-0h catalysts.

Sample	Copper surface area m^2/g	Copper dispersion %	Copper particle size nm	N_2O/XRD ratio[1]
CuO 33-0h	16.2	9.4	11	(-)
CuO 33-17h	10.2	5.9	18	1.6 (11 nm)
CuO 50-0h	17.0	6.5	16	1.5 (11 nm)

[1] Ratio of the Cu particle size obtained by N_2O surface reaction analysis to the CuO crystallite size obtained by XRD. The values in parentheses are the CuO crystallite sizes obtained by XRD.

In the case of the catalyst CuO 50-0h, the copper surface area was a little higher than that of catalyst CuO 33-0h. This may be due to the larger amount of Cu available for dispersion over all the surface of the material. Despite the above, the copper dispersion of the catalyst CuO 50-0h was lower and its particle size higher than those of catalyst CuO 33-0h, which may be due to the lower relative contents of Zn and Zr in the catalyst CuO 50-0h. Both of these metals are known promoters of the Cu species in this type of catalysts improving the copper surface area and dispersion, as well as stabilizing the copper species [31].

Table 4.8 also shows the ratio of the Cu particle sizes obtained by N_2O surface reaction to the crystallite sizes of CuO obtained by XRD. The results show that the Cu particles are composed by approximately 1.6 and 1.5 CuO crystallites in the case of the CuO 33-17h and CuO 50-0h catalysts, respectively. This ratio wasn't calculated for catalyst CuO 33-0h because the low crystallization of the sample didn't allow to calculate the crystallite size from the X-ray diffractogram.

4.2.2. Catalytic tests results

The results of the catalytic tests are presented in Figure 4.9 and Table 4.9. The H_2 conversions obtained for the catalysts CuO 33-0h and CuO 33-17h presented an increasing tendency which attained a maximum value and then decreased slightly. The maximum H_2 conversion values occurred at 260ºC (i.e. 13.9%) and at 280ºC (i.e. 14.3%) for the catalysts CuO 33-0h and CuO 33-17h, respectively. The H_2 conversion of the CuO 50-0h catalyst presented an increasing trend with increasing temperature and didn't show a decrease in the temperature range of the catalytic tests.

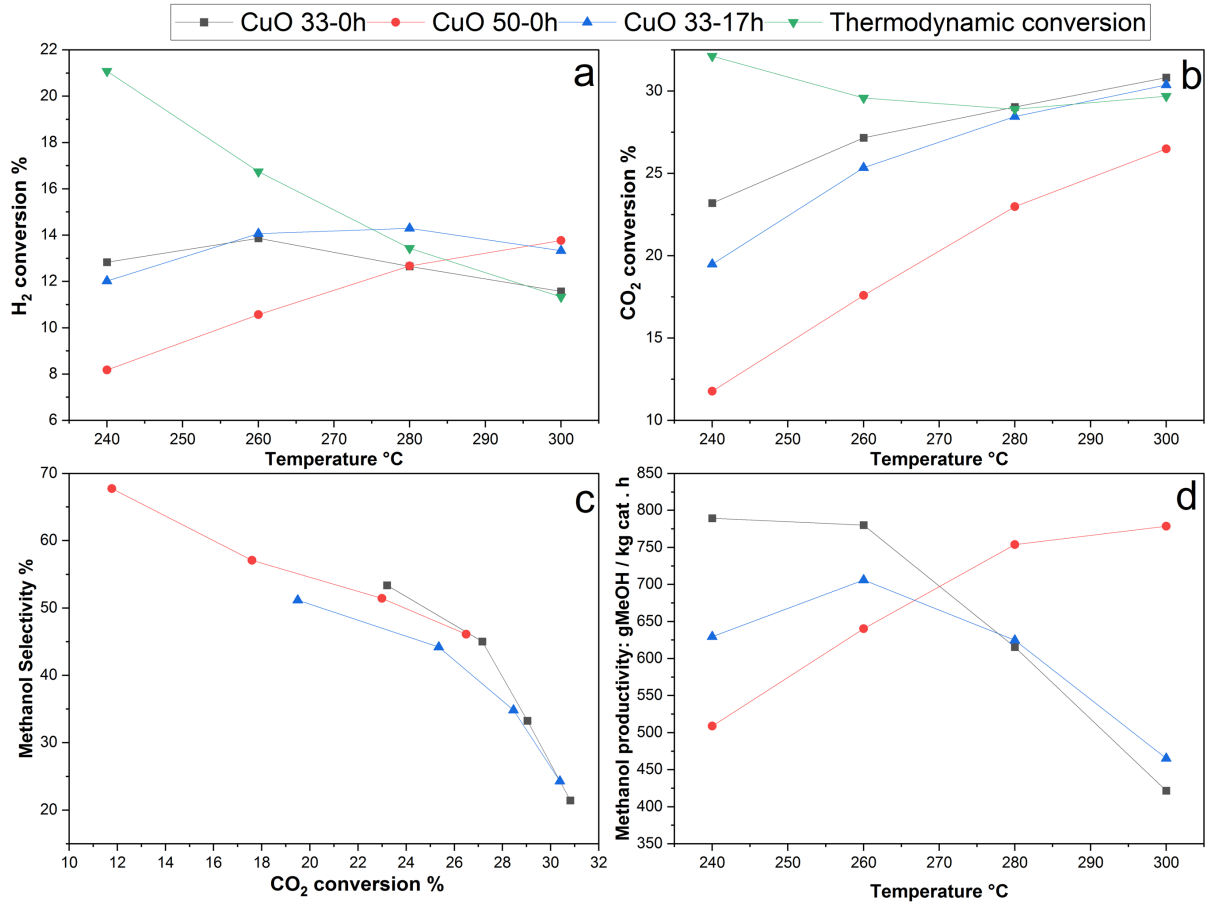

Figure 4.9 Catalytic performance of the catalysts under study. (a) H_2 conversion, (b) CO_2 conversion, (c) methanol selectivity and (d) methanol productivity. P: 50 bar, GHSV: 24000Nml h^{-1} g^{-1}, molar ratio H_2/CO_2: 3.9.

The fact that the H_2 and CO_2 conversions exceed the thermodynamic limits shown in Figures 4.9a and 4.9b can be explained by the occurrence of temperature differences between the catalytic bed and the heating system of the reactor due to a normal heat transfer process. Also, the thermodynamic limits calculations, which were done by minimization of the Gibbs free energy may also give values that deviate to some extent from the real ones. This applies to the catalytic tests results presented in all the sections of this thesis.

Regarding the CO_2 conversions, they showed an increasing tendency with increasing temperature for all the catalysts under study. This can be explained by the increasing

production of carbon monoxide via the RWGS reaction, which is endothermic and therefore favored at higher temperatures [8], as explained before.

In the case of the catalyst CuO 50-0h, the lower CO_2 conversion can be explained in part by the lower relative contents of ZnO and ZrO_2 of this catalyst compared to the other ones. ZnO has an important effect on the stability and the catalytic activity of this type of catalysts, by helping stabilize copper particles and acting as an active site for the adsorption and activation of CO and CO_2 [37][38]. Moreover, it is known that the addition of ZrO_2 can improve both the catalytic activity and the methanol selectivity [8]. Therefore, lowering the relative contents of both ZnO and ZrO_2 can have a negative effect on the catalytic performance. The catalyst CuO 50-0h also presented a lower surface basicity compared to that of catalyst CuO 33-0h, which may also be another factor contributing to the lower CO_2 conversion of this catalyst.

Another factor related to the catalytic activity of Cu-ZnO-ZrO_2 catalysts is the crystallinity of ZrO_2. Many works suggest that compounds with different crystallinity can have different properties and catalytic activity. More specifically, the work of Tada *et al.* [39] suggests that the interfacial sites in Cu supported on amorphous ZrO_2 give a better methanol yield compared to Cu supported on monoclinic or tetragonal ZrO_2. As shown previously in this work, ZrO_2 was present as an amorphous compound.

Table 4.9 Results of the catalytic tests of the CuO 33-0h, CuO 33-17h and CuO 50-0h catalysts. P: 50bar, GHSV: 24000Nml h^{-1} g^{-1}, molar ratio H_2/CO_2: 3.9.

Catalyst	Temperature ºC	H_2 Conversion %	CO_2 Conversion %	Methanol selectivity %	Methanol productivity g CH_3OH/(kg of catalyst x hour)
CuO 33-0h	240	12.8	23.2	53.3	789
	260	13.9	27.2	45.0	780
	280	12.6	29.0	33.2	616
	300	11.6	30.8	21.4	421
CuO 33-17h	240	12.0	19.5	51.2	629
	260	14.1	25.3	44.2	706
	280	14.3	28.4	34.8	624
	300	13.3	30.4	24.3	465
CuO 50-0h	240	8.2	11.8	67.7	508
	260	10.6	17.6	57.0	640
	280	12.7	23.0	51.4	753
	300	13.8	26.5	46.1	778

The results of Figure 4.9c show the methanol selectivity of the catalysts plotted against the CO_2 conversion. As can be seen, the methanol selectivity of the 3 catalysts decreased with increasing CO_2 conversion which is caused by the increasing conversion of the RWGS reaction at higher temperatures and consequently at higher

CO_2 conversions [8].

Regarding the methanol productivity, the catalysts CuO 33-0h and CuO 33-17h presented an increasing behavior until 260ºC, after which the productivity presented a sharp decrease. This behavior occurs due to the decreasing methanol selectivity of the catalysts with increasing temperature. In the case of the methanol productivity of the catalyst CuO 50-0h, it presented an increase until 300ºC, where it seems to reach a thermodynamic equilibrium value. This catalyst presented a higher methanol productivity at 280-300ºC compared to the other two catalysts, which can also be correlated to the higher selectivity of this catalyst in this temperature range. However, a decrease in the methanol productivity of the catalyst CuO 50-0h at temperatures above 300ºC is expected as the CO_2 conversion reaches the thermodynamic limit.

In addition, the catalyst CuO 33-0h presented a high methanol productivity of 789 g_{CH3OH} kg^{-1} h^{-1} at 240ºC. This high methanol productivity is interesting given the relatively low temperature at which it was achieved. In comparison, the highest methanol productivity of catalyst CuO 50-0h occurred at 300ºC with a value of 778 g_{CH3OH} kg^{-1} h^{-1}. The use of lower reaction temperatures is always preferred due to process, economic and energy efficiency reasons. Moreover, the exposure of the solid catalyst to lower reaction temperatures may increase its lifetime.

As shown above, the aging time and the CuO content had an effect on different catalyst properties such as the specific surface area, the Cu surface area, the copper particle size, the surface basicity and reducibility. In turn, these properties had an effect on the performance of the catalysts, including the reactants conversions, the methanol selectivity and the methanol productivity. For instance, the N_2-physisorption analysis results showed that a zero aging time allowed the synthesis of a catalyst with a high specific surface area of 109 m^2/g, which is favorable for the Cu dispersion and can also have a positive effect on other surface properties. In addition, the higher CO_2 conversion that the CuO 33-0h catalyst presented can be correlated to the higher Cu surface area obtained and to the smaller Cu particles size of 11 nm compared to those of the other catalysts. As discussed previously, the Cu surface area has an important effect on the catalytic activity given the role of Cu as an active site for H_2 dissociation during the CO_2 hydrogenation.

Also, the CO_2 adsorption properties of Cu-ZnO-ZrO_2 based catalysts have an important effect on the catalytic performance for the hydrogenation of CO_2 to methanol [11][40]. In fact, the catalyst CuO 33-0h presented the highest surface basicity as found by CO_2-TPD analysis and this catalyst showed a high CO_2 conversion in the temperature range investigated, along with high methanol productivity at 240 and 260ºC. The results obtained with the FT-IR analysis also supported the presence of hydroxyl weak basic sites which can participate in the reaction and contribute to the total basicity of the catalysts.

Another reason that can explain why the microfluidic synthesis without aging time gives better CuO-ZnO-ZrO_2 catalysts, is the occurrence of more interactions between the Cu, Zn and Zr species during the microfluidic synthesis, increasing the promoting effects of the support. Also, the zero aging time of this type of precursors may cause a different configuration of the metal species on the surface of the catalyst, by favoring the proximity of the sites where the H_2 and CO_2 chemisorption occurs. In the case of CO_2, this idea is supported by the results of the CO_2-TPD technique, which indicated that the CuO 33-0h catalyst presented a higher density of basic sites per unit surface area of the material. In the case of the adsorption of H_2, the use of the H_2-TPD analysis in future works, would allow understanding better the adsorption of H_2 on the surface of the catalyst just as in CO_2-TPD, by indicating the density of sites per surface area of material that can adsorb hydrogen, and also the strength of the adsorption sites of this compound by determining the temperatures at which the H_2 desorption occurs.

4.2.3. Catalysts stability tests

The stability of the catalysts was analyzed by monitoring the value of the CO_2 conversion with respect to time for the duration of the catalytic tests. Some of the deactivation mechanisms that can affect this type of catalysts include poisoning due to impurities, sintering of the copper particles, coke deposition, among others [41]. A linear fit of each of the group of data corresponding to each reaction temperature was done to obtain the trendline indicating if there's an increasing or a decreasing tendency of the CO_2 conversion.

As can be seen in Figures 4.10a, b and c, the catalysts presented a mild decrease during the approximately 200 hours of reaction at temperatures between 240 and 300ºC and at a pressure of 50 bar. This degradation of the catalysts can be explained by the loss of Cu surface area due to sintering and also by the increase of the Cu crystallite size and the agglomeration of Cu particles. Other deactivation mechanisms concerning this type of catalysts include the aggregation of ZnO species and the oxidation of Cu, both caused by the presence of water [41]–[43].

Most of the trendlines presented a decreasing behavior, indicating the deactivation of the catalyst with the time of reaction. The lines showing an increasing tendency occurring mostly at 300ºC indicate the decrease in the methanol selectivity and the increase of the production of CO, which explains the increase of the CO_2 conversions. The obtained results indicate that the degradation of the catalytic activity occurs faster at higher reaction temperatures. The work of Li *et al*. [44] showed that a catalyst made up of Cu-ZnO-ZrO_2-Al_2O_3 presented a stability of more than 100 hours, compared to a catalyst composed of Cu-ZnO-Al_2O_3, which presented a stability of less than 100 hours. In addition, in the work of Bonura *et al*. [45], a catalyst composed of Cu, Zn and Zr that was synthesized by gel oxalate coprecipitation presented a catalyst stability of more than 200 hours. The work of Ren *et al*. [46] showed that a catalyst based on Cu-Zn-Zr-Al presented a mild decrease in the CO_2 conversion, methanol selectivity and

yield after 300 hours of catalytic tests. These results found in the literature indicate that there's indeed a deactivation of the catalysts during the catalytic tests, around reaction times of 100 hours. This can vary with the compositions, the reaction conditions and the resistance of each catalyst to deactivation.

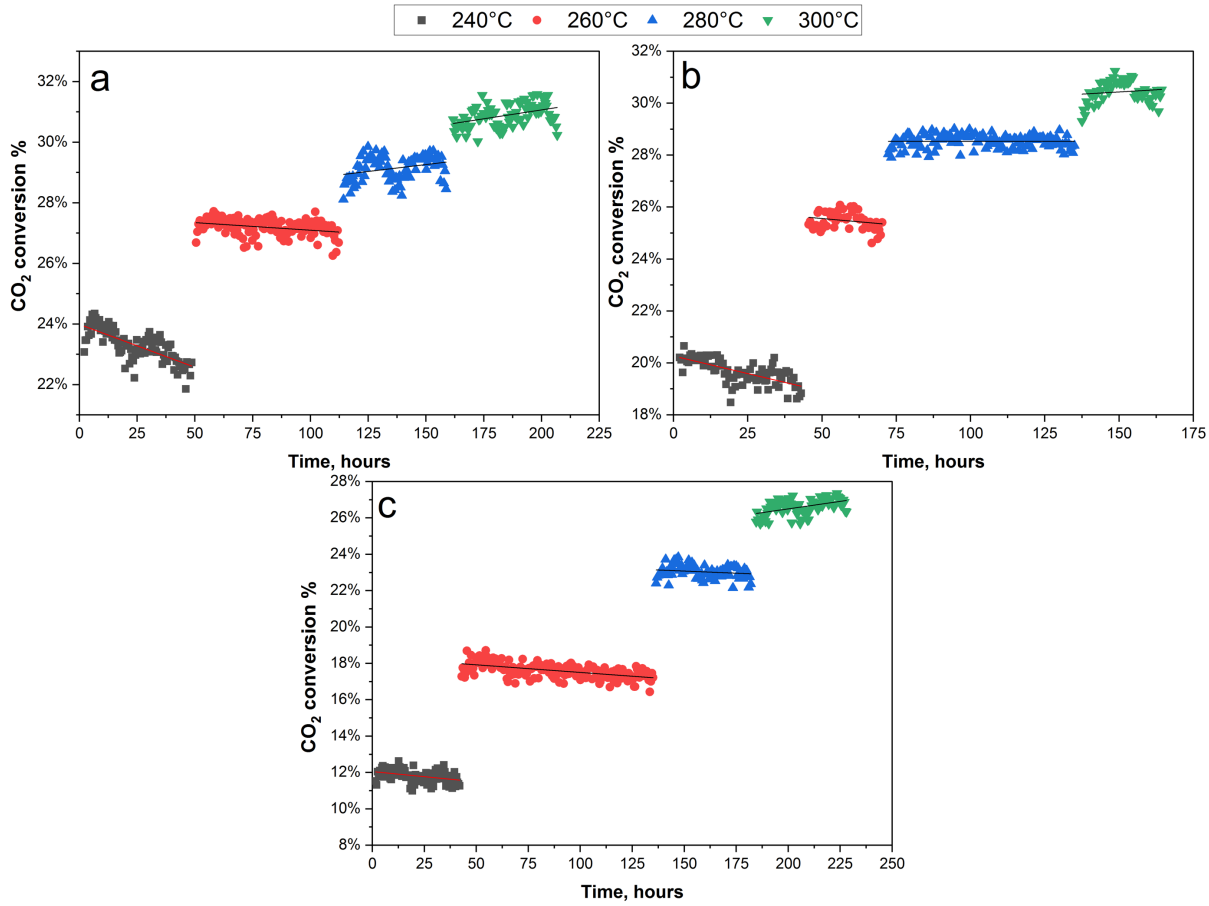

Figure 4.10 CO_2 conversion versus time on stream of the catalysts (a) CuO 33-0h, (b) CuO 33-17h, (c) CuO 50-0h. P: 50bar, GHSV: 24000Nml h^{-1} g^{-1}, molar ratio H_2/CO_2: 3.9.

4.2.4. Conclusions

The effects of the aging time on the properties and catalytic performance of Cu-ZnO-ZrO_2 catalysts prepared by the microfluidic method were investigated in this work.

The results showed that the lack of aging of the catalyst precursor CuO 33-0h produced a material with a considerably higher specific surface area, higher surface basicity, higher Cu surface area and smaller Cu particle size. This catalyst also presented a lower reduction temperature compared to the other two catalysts, indicating the presence of smaller Cu particles that are reduced at lower temperatures. All of these properties had a positive effect on the catalytic activity of this material. The CuO 33-0h catalyst presented high H_2 and CO_2 conversions as well as high methanol productivity per mass of catalyst. Another reason explaining the high performance of the catalyst CuO 33-0h is the smaller distance between the sites where the

chemisorption of CO_2 occurs. This may be due to stronger interactions between the Cu, Zn and Zr during the catalyst synthesis, causing a higher proximity between active sites. As explained before, the CO_2-TPD results support the idea of a higher density of active sites per unit surface area. These results show that the synthesis of Cu-ZnO-ZrO_2 catalysts by coprecipitation with a microfluidic device and without an aging step can give catalysts with desirable properties and high catalytic performance.

Regarding the stability of the catalysts, it was found that they presented a mild deactivation during the catalytic tests, which can be explained by the sintering and oxidation of Cu particles, and the aggregation of ZnO due to continuous exposure to water at high temperatures. For future works, the study of the deactivation of the catalysts by employing different analysis techniques such as X-ray photoelectron spectroscopy (XPS) and transmission electron microscopy (TEM) would be interesting to study the effects of the reaction conditions on the surface composition of the catalysts, on the degree of oxidation of Cu and on the crystalline structure at a nanometer scale.

Due to the favorable results obtained with the lack of an aging step on the properties and the catalytic activity of the catalysts synthesized by the microfluidic method, this technique was employed to synthesize different catalysts in the following sections of this thesis.

4.3. Effect of the coprecipitation temperature on the properties and catalytic performance of Cu-ZnO-ZrO_2 catalysts

The temperature during the coprecipitation process is one of the most important variables that influence the final properties and performance of the Cu based catalysts for the production of methanol [47][48]. The temperature can affect the rates of precipitation and nucleation, which have an effect on the crystals growth, the formation of phases, the morphology and textural properties, among others [4][49][50]. In this work, the precipitation zone was heated to 65ºC in order to explore potential process conditions that may allow the synthesis of catalysts with better properties and performance. The properties of the catalyst CuO 50-0h-65 were compared to those of the catalyst CuO 50-0h in order to determine the effect of the coprecipitation done at 65ºC. The catalysts characterization results and discussion of this sub-chapter are presented in the following section.

4.3.1. Catalysts characterization results and discussion

Figure 4.11 shows the diffractograms of the two catalysts investigated in this section. These results correspond only to the catalysts after calcination because the diffractograms of the precursors showed that both were completely amorphous.

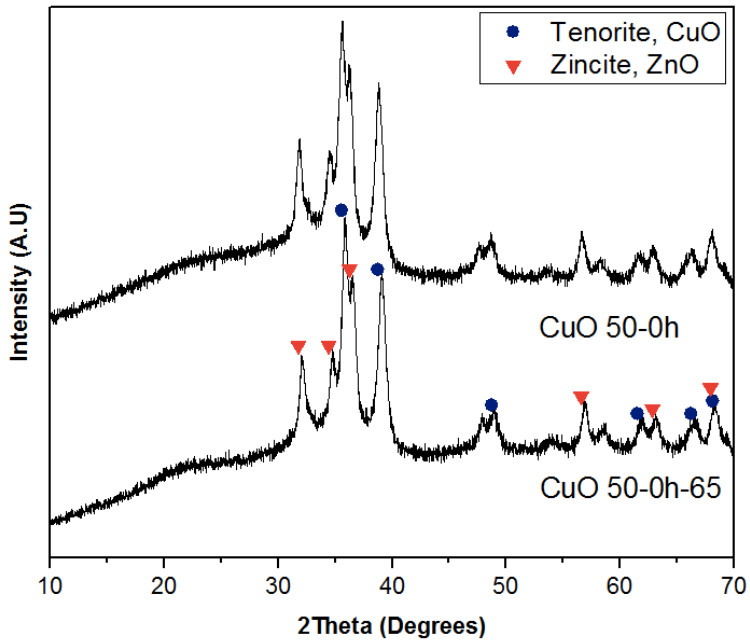

Figure 4.11 X-ray diffractograms of the CuO 50-0h-65 and the CuO 50-0h catalysts.

The phases identified in the calcined catalysts corresponded to CuO (PDF number: 72-0629) and ZnO (PDF number: 75-1526). The calculations of the crystallite sizes were done by using Scherrer's equation and they are shown in Table 4.10. The results

indicate that both phases presented similar crystallite sizes and they indicate that the use of a coprecipitation temperature of 65ºC doesn't have an important effect on the crystalline structure of the catalysts, which presented similar diffractograms and crystallite sizes. This is also probably due to the short duration of the heating that occurs when using this catalyst synthesis technique, compared to other techniques where the precursors are aged at 65ºC and agitated for longer periods of time. Despite the above, according to Schuth *et al*. [4] the nucleation rates are very sensitive to temperature variations which can affect the properties of the precipitates such as crystallite sizes, surface area and the phases that are formed. Therefore, the differences in the temperature of coprecipitation can explain the small differences presented in the crystallinity of the catalysts. As has already been discussed in previous sections, no ZrO_2 peaks were detected in the diffractograms of the calcined catalysts, which indicates that it is present in an amorphous state.

Table 4.10 Crystallite sizes (nm) of tenorite and zincite in the CuO 50-0h-65 and CuO 50-0h calcined catalysts.

Crystallite sizes	**Calcined catalyst**	
Catalyst	**Tenorite, CuO**	**Zincite, ZnO**
CuO 50-0h-65	12	13
CuO 50-0h	12	12

The TGA profiles of the two precursors investigated are presented in Figure 4.12. As can be observed, the two catalysts presented a mass loss of approximately 22% and very similar decomposition profiles. In fact, as evidenced by the derivatives of the mass loss of the two catalysts, it is clear that the decomposition of the two catalyst precursors presented two main decomposition peaks around 150 and 480ºC. These results indicate that the two materials didn't present large differences in their composition, as they have the same bulk composition of 50% CuO, 33% ZnO and 17% ZrO_2. As already discussed in previous sections, the peak of the derivative of the mass loss % of the precursors occurring around 150ºC indicates the decomposition of Zr-based precursor [12] and the peak between 400 and 600ºC can be attributed to the final decomposition step of the amorphous hydroxycarbonates that may be present in the precursors [15]. Also, according to the work of L'hospital [12], the derivative of the mass loss of a Cu-Zn hydroxycarbonate precipitate presents a decomposition peak at 466ºC, which can explain the peak formed around this temperature.

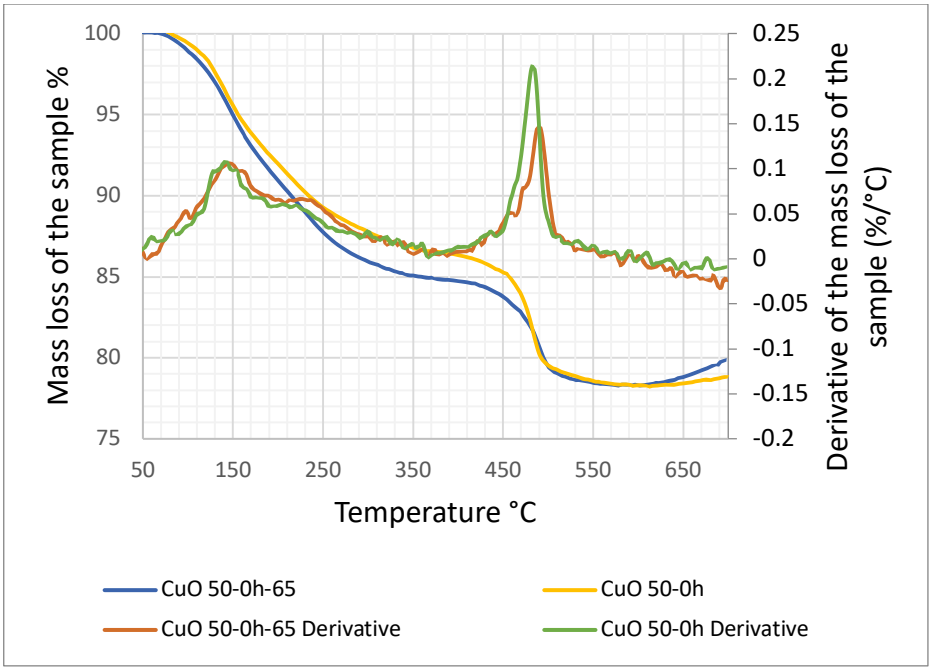

Figure 4.12 TGA results of the CuO 50-0h-65 and CuO 50-0h catalyst precursors.

The results of the N_2-physisorption analysis presented in Figure 4.13 indicate that the isotherms are of type IV and that the material is mesoporous. No significant differences are appreciable in the adsorption-desorption isotherms of these two catalysts, suggesting that the textural properties of these catalysts are very similar.

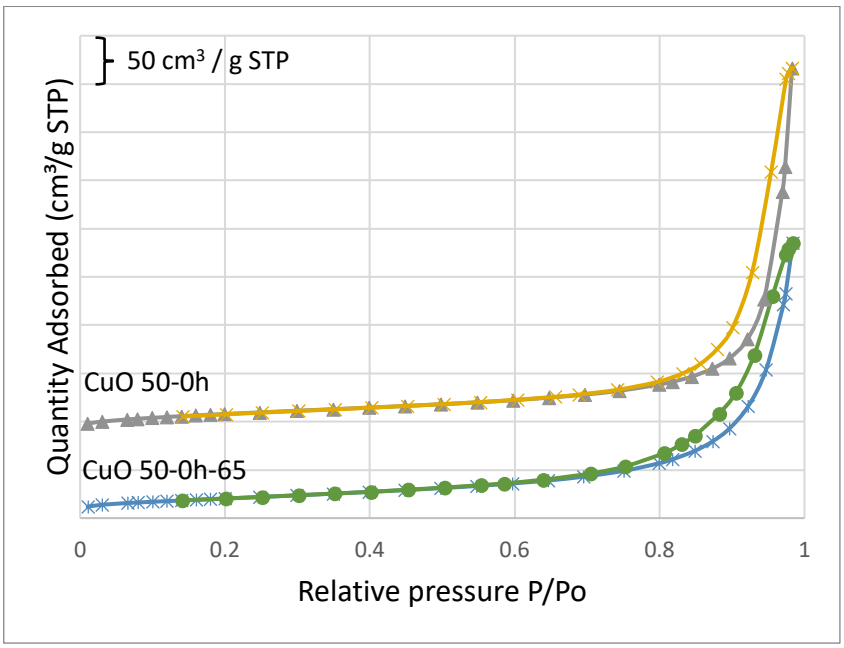

Figure 4.13 N_2-physisorption isotherms of the CuO 50-0h-65 and CuO 50-0h catalysts.

The quantitative results of the N_2-physisorption analysis are presented in Table 4.11. These results show that the specific surface area of the catalyst CuO 50-0h-65 presented a small increase, while its pore volume and pore sizes decreased slightly with respect to the CuO 50-0h catalyst. These findings also demonstrate that the

heating of the precipitation zone and the reactants to 65ºC during the coprecipitation process doesn't have an important effect on the textural properties of the catalysts.

Table 4.11 N_2-Physisorption specific surface area, pore volume and pore size of the CuO 50-0h-65 and CuO 50-0h catalysts.

Sample	BET surface area (m^2/g)	Pore volume (cm^3/g)	Pore size (nm)
CuO 50-0h-65	74	0.34	20
CuO 50-0h	70	0.38	28

The results of the H_2-TPR analysis show that there were some slight differences in the reducibility of copper oxide species of the two catalysts under study. As can be seen in Figure 4.14, the reduction profiles are similar in terms of the reduction temperatures. Both catalysts presented a peak reduction temperature close to 170ºC, while the CuO 50-0h catalyst presented a small shoulder at a temperature of 180ºC. The presence of this shoulder may be due to a higher relative amount of bigger CuO particles in the catalyst. The quantitative results of this analysis presented in Table 4.12 showed that the sample CuO 50-0h-65 had a deviation from the intended CuO content. This can be due to the reduction of hydroxycarbonate species remaining after calcination [24]. Nevertheless, the value remained close to the theoretical value of 50% CuO. These results indicate that the reducibility of both catalysts was very similar, suggesting that the CuO particle size distribution was also similar.

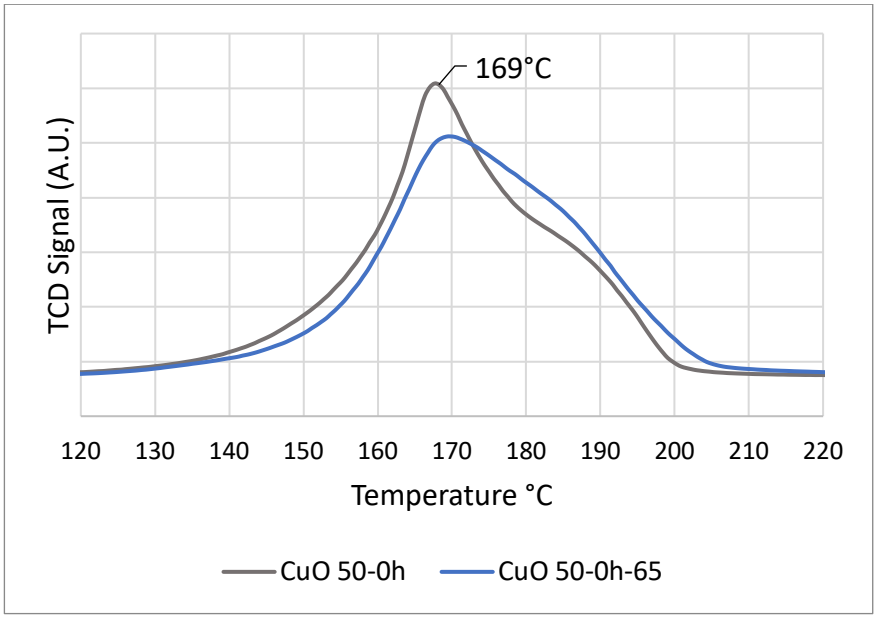

Figure 4.14 H_2-TPR profiles of the CuO 50-0h-65 and CuO 50-0h catalysts.

Table 4.12 H_2-TPR quantitative results of the CuO 50-0h-65 and CuO 50-0h catalysts.

Sample	H_2 consumption, mmol/g	Catalyst theoretical Cu content, mmol Cu/g	H_2/Cu ratio	Calculated CuO % of the catalyst
CuO 50-0h-65	6.8	6.29	1.08	53.9
CuO 50-0h	6.2	6.29	0.99	49.3

The results of the N_2O surface reaction analysis are presented in Table 4.13. These results indicate that the values of the copper surface area and copper dispersion decreased for the catalyst CuO 50-0h-65 while its copper particle size increased. The differences in these properties indicate that the coprecipitation temperature has an effect on the Cu surface area, dispersion and Cu particles size. This can be explained by higher nucleation rates during the synthesis process of the catalyst CuO 50-0h-65 due to the higher coprecipitation temperature, causing an increase in the size of the Cu particles, as evidenced in the Cu particle size results presented in Table 4.13.

Table 4.13 N_2O surface reaction results of the CuO 50-0h-65 and CuO 50-0h catalysts.

Sample	Copper surface area m^2/g	Copper dispersion %	Copper particle size nm	N_2O/XRD ratio[2]
CuO 50-0h-65	14.2	5.5	19.0	1.6 (12 nm)
CuO 50-0h	17.0	6.5	16.0	1.3 (12 nm)

[2]Ratio of the Cu particle size obtained by N_2O surface reaction analysis to the CuO crystallite size obtained by XRD. The values in parentheses are the CuO crystallite sizes obtained by XRD.

The ratio of the Cu particle sizes obtained by N_2O surface reaction to the crystallite sizes obtained by XRD for the two catalysts investigated are presented in Table 4.13. The results show that the Cu particles are composed by approximately 1.6 and 1.3 CuO crystallites in the case of the CuO 50-0h-65 and the CuO 50-0h catalysts, respectively. This is due to the higher nucleation rates occurring during the synthesis of the catalyst CuO 50-0h-65, which favor the formation of larger Cu particles, given that the CuO crystallite sizes determined by XRD of both catalysts were the same.

4.3.2. Catalytic tests results

Figure 4.15 and Table 4.14 show the results of the catalytic tests of the CuO 50-0h-65 and the CuO 50-0h catalysts. As observed, the catalyst CuO 50-0h-65 presented better H_2 and CO_2 conversions compared to the CuO 50-0h catalyst. The reason behind the increase in the reactants conversion of the CuO 50-0h-65 catalyst may be the increase in the precipitation and nucleation kinetics during the catalyst synthesis step, despite the fact that the characterization results didn't show any important

differences in the properties of the two catalysts, except for the decrease of Cu surface area, dispersion and increase of the Cu particle size.

The results of the methanol productivity show that the catalyst CuO 50-0h-65 presented a maximum at 260ºC with a productivity of 780 g of CH_3OH kg^{-1} h^{-1}, while the CuO 50-0h catalyst presented a productivity of 778 g of CH_3OH kg^{-1} h^{-1} at a temperature of 300ºC. These results show that the catalyst CuO 50-0h-65 is better in terms of methanol productivity due to the higher production of methanol at a considerably lower temperature. Also, the methanol productivity of the catalyst CuO 50-0h-65 presented a decrease above 260ºC which may be due to this catalyst approaching the thermodynamic limitations.

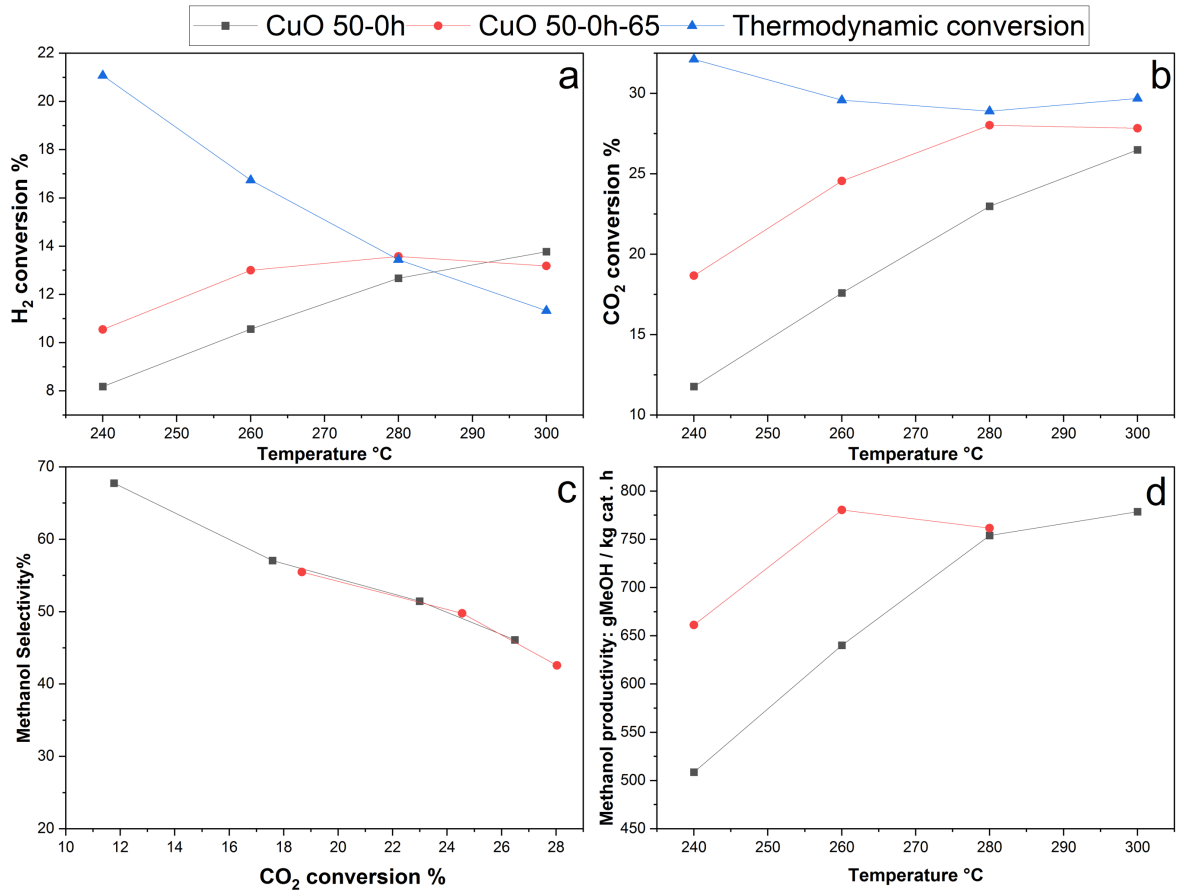

Figure 4.15 Catalytic performance of the CuO 50-0h-65 and CuO 50-0h catalysts. (a) H_2 conversion, (b) CO_2 conversion, (c) methanol selectivity and (d) methanol productivity. P: 50bar, GHSV: 24000Nml h^{-1} g^{-1}, molar ratio H_2/CO_2: 3.9.

The methanol productivity per unit of Cu surface area of the two investigated catalysts is presented in Figure 4.16. According to these results, the higher productivity of the catalyst CuO 50-0h-65 can be explained by the higher intrinsic activity of the Cu sites of this catalyst which may be due to the increased promotion effects of ZnO and ZrO_2 on the Cu nanoparticles, due to the higher precipitation and nucleation kinetics of the Cu, Zn and Zr metal species during the synthesis of this catalyst. This suggests the occurrence of stronger interactions between the 3 metal species of this catalyst during

the coprecipitation reaction at 65ºC, causing an increase of the promoting effects of the support.

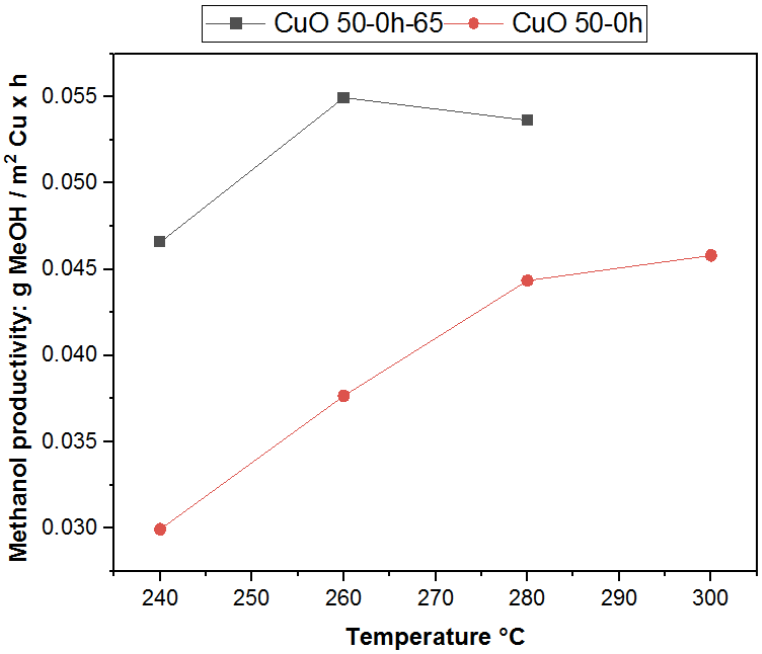

Figure 4.16 Methanol productivity in grams per m^2 of Cu surface area per hour, of the catalysts CuO 50-0h-65 and CuO 50-0h.

Table 4.14 Results of the catalytic tests of the CuO 50-0h-65 and CuO 50-0h catalysts. P: 50bar, GHSV: 24000Nml h^{-1} g^{-1}, molar ratio H_2/CO_2: 3.9.

Catalyst	Temperature ºC	H_2 Conversion %	CO_2 Conversion %	Methanol selectivity %	Methanol productivity g CH_3OH/(kg of catalyst x hour)
CuO 50-0h-65	240	10.5	18.6	55.4	661
	260	13.0	24.5	49.8	780
	280	13.6	28.0	42.5	762
	300	13.2	27.8	27.0	479
CuO 50-0h	240	8.2	11.8	67.7	509
	260	10.6	17.6	57.0	640
	280	12.7	23.0	51.4	754
	300	13.8	26.5	46.1	779

4.3.3. Catalytic performance of different catalysts available in the literature

The catalytic tests results of different catalysts reported in the literature are presented in Table 4.15 along with some of the catalysts synthesized in this work. This served as a comparison of the catalysts of this work with other catalysts available in the literature.

Table 4.15 Catalytic performance of different catalysts for the production of methanol available in the literature.

Cu-ZnO-Al_2O_3 catalysts								
Catalyst composition	**Synthesis method**	**H_2:CO_2 mole ratio**	**Pressure, bar**	**CO_2 Conversion %**	**Methanol selectivity %**	**Methanol productivity**	**GHSV**	**Ref.**
35% CuO 34.3% ZnO 30.7% Al_2O_3 wt%	Coprecipitation – Commercial catalyst.	3:1	30	220°C – 10.1% 240°C – 16.9% 260°C – 20.8%	220°C – 57.9% 240°C – 43.4% 260°C – 34.3%	220°C – 170 240°C – 210 260°C – 205 g MeOH kg_{cat}^{-1} h^{-1}	8800 cm^3 g_{cat}^{-1} h^{-1}	[51]
37.5% CuO 38.4% ZnO 24.1% Al_2O_3 wt%	Coprecipitation – hydrotalcite derived catalyst.	3:1	30	220°C – 9.1% 240°C – 13.1% 260°C – 18.7%	220°C – 70.7% 240°C – 51.7% 260°C – 37.6%	220°C – 185 240°C – 195 260°C – 205 g MeOH kg_{cat}^{-1} h^{-1}	8800 cm^3 g_{cat}^{-1} h^{-1}	[51]
Cu-ZnO-ZrO_2 catalysts								
Catalyst composition	**Synthesis method**	**H_2:CO_2 mole ratio**	**Pressure, bar**	**CO_2 Conversion %**	**Methanol selectivity %**	**Methanol productivity**	**GHSV**	**Ref.**
36.4% Cu 27.2% Zn 36.3% Zr wt%	Coprecipitation.	3:1	20	200°C – 3% 220°C – 7% 240°C – 13% 260°C – 18% 280°C – 24%	200°C – 72% 220°C – 53% 240°C – 32% 260°C – 15%	200°C – 115 220°C – 170 240°C – 190 260°C – 120 280°C – 60 g MeOH kg_{cat}^{-1} h^{-1}	15600 cm^3 g_{cat}^{-1} h^{-1}	[52]
35% Cu 26.8% Zn 36.7% Zr 1.4% GO wt%	Coprecipitation + addition of graphene oxide.	3:1	20	200°C – 4.5% 220°C – 8.5% 240°C – 15% 260°C – 21% 280°C – 23%	200°C – 76% 220°C – 57% 240°C – 35% 260°C – 23% 280°C – 8%	200°C – 170 220°C – 260 240°C – 270 260°C – 240 280°C – 100 g MeOH kg_{cat}^{-1} h^{-1}	15600 cm^3 g_{cat}^{-1} h^{-1}	[52]
Catalysts Synthesized with a microfluidic device								
Catalyst composition	**Synthesis method**	**H_2:CO_2 mole ratio**	**Pressure, bar**	**CO_2 Conversion %**	**Methanol selectivity %**	**Methanol productivity**	**GHSV**	**Ref.**
35% CuO 34.3% ZnO 30.7% Al_2O_3 wt%	Coprecipitation with a micro-impinging stream reactor.	H_2:CO mole ratio 2:1	50	CO conversion % 250°C – 33.7%	250°C – 99.3%	-	4000 cm^3 g_{cat}^{-1} h^{-1}	[53]
59.2% Cu 4.5% Zn 5.2% Al wt%	Coprecipitation in a microfluidic reactor.	H_2/N_2/CO/CO_2/Ar 34 : 15 : 15 : 0 : 36 and 34 : 15 : 14 : 1 : 36	50	-	250°C – 98.1%	250°C – 701.6 g MeOH kg_{cat}^{-1} h^{-1}	24000 cm^3 g_{cat}^{-1} h^{-1}	[54]

ZnO ZrO_2 Molar ratio Zn/Zr: 0.14	Coprecipitation in a microfluidic reactor.	3:1	30	320°C – 9.2%	320°C – 93.1%	320°C – 350 g MeOH kg_{cat}^{-1} h^{-1}	12000 cm^3 g_{cat}^{-1} h^{-1}	[55]
12.1% Cu Ce Zr wt%	Coprecipitation with oxalic acid in a microfluidic reactor.	3:1	30	240°C – 4.67%	240°C – 55.6%	240°C – 222.4 g MeOH kg_{cat}^{-1} h^{-1}	30000 cm^3 g_{cat}^{-1} h^{-1}	[56]
Catalysts of this work								
Catalyst composition	**Synthesis method**	**H_2:CO_2 mole ratio**	**Pressure, bar**	**CO_2 Conversion %**	**Methanol selectivity %**	**Methanol productivity**	**GHSV**	**Ref.**
CuO 33.3% ZnO 33.3% ZrO_2 33.3% wt% Catalyst: Microfluidic.	Coprecipitation with a microfluidic reactor.	3.9:1	50	240°C – 8.2 260°C – 14.3 280°C – 19.9 300ºC – 25.6	240°C – 61.3 260°C – 49.3 280°C – 39.9 300ºC – 35.5	240°C – 319 260°C – 448 280°C – 505 300ºC – 580 g MeOH kg_{cat}^{-1} h^{-1}	12375 h^{-1} 24000 Ncm^3 g_{cat}^{-1} h^{-1}	This work.
CuO 33.3% ZnO 33.3% ZrO_2 33.3% wt% Catalyst: CuO 33-0h.	Coprecipitation with a microfluidic reactor. No aging.	3.9:1	50	240°C – 23.2 260°C – 27.2 280°C – 29.0 300ºC – 30.8	240°C – 53.3 260°C – 45.0 280°C – 33.2 300ºC – 21.4	240°C – 789 260°C – 780 280°C – 616 300ºC – 421 g MeOH kg_{cat}^{-1} h^{-1}	16479 h^{-1} 24000 Ncm^3 g_{cat}^{-1} h^{-1}	This work.
CuO 33.3% ZnO 33.3% ZrO_2 33.3% wt% Catalyst: CuO 33-17h.	Coprecipitation with a microfluidic reactor.	3.9:1	50	240°C – 19.5 260°C – 25.3 280°C – 28.4 300ºC – 30.4	240°C – 51.2 260°C – 44.2 280°C – 34.8 300ºC – 24.3	240°C – 629 260°C – 706 280°C – 624 300ºC – 465 g MeOH kg_{cat}^{-1} h^{-1}	17239 h^{-1} 24000 Ncm^3 g_{cat}^{-1} h^{-1}	This work.
CuO 50% ZnO 33% ZrO_2 17% wt% Catalyst: CuO 50-0h.	Coprecipitation with a microfluidic reactor. No aging.	3.9:1	50	240°C – 11.8 260°C – 17.6 280°C – 23.0 300ºC – 26.5	240°C – 67.7 260°C – 57.0 280°C – 51.4 300ºC – 46.1	240°C – 508 260°C – 640 280°C – 753 300ºC – 778 g MeOH kg_{cat}^{-1} h^{-1}	13943 h^{-1} 24000 Ncm^3 g_{cat}^{-1} h^{-1}	This work.

Frusteri *et al*. [51] prepared a Cu-ZnO-Al_2O_3 catalyst and tested its catalytic performance along with a commercial catalyst and obtained a methanol productivity of 205 g MeOH kg_{cat}^{-1} h^{-1} at 260ºC with both catalysts. These productivity values are below the methanol productivity values obtained with the catalysts of the present work, which points out the necessity of replacing Al_2O_3 by other supports, such as ZrO_2 when using a CO_2 rich feedstock for the hydrogenation of CO_2 to methanol. Moreover, it's important to mention that the conditions of their catalytic tests differed from those of this work, which can have an important effect on the catalytic performance.

Tofighi *et al*. [54] synthesized a Cu-ZnO-Al_2O_3 catalyst by the microfluidic method for the production of methanol from synthesis gas and obtained a methanol productivity of 701.6 g MeOH kg_{cat}^{-1} h^{-1} at 250ºC. The GHSV they employed (i.e. 24000 cm^3 g_{cat}^{-1} h^{-1}) was the same as those of the catalysts of this work along with the reaction pressure (i.e. 50 bar). The only different parameters were the composition of the catalyst and the composition of the feed gas. Despite the above, the methanol productivity that they obtained was close to the productivity of some of the catalysts prepared in this work, which supports the higher catalytic activity of catalysts synthesized by the microfluidic method.

Witoon *et al*. [52] synthesized a catalyst composed of Cu-ZnO-ZrO_2 and obtained a methanol productivity of 190 g MeOH kg_{cat}^{-1} h^{-1} at 240ºC. This methanol productivity was lower than the methanol productivities obtained in the present work. However, the H_2:CO_2 ratio and the reaction pressure that they employed were much lower than those of this work, which can explain the lower catalytic performance of their catalyst. The synthesis of the catalysts by batch reverse coprecipitation may also be a reason explaining the lower methanol productivity of the catalysts that they synthesized.

The works of X. Wang and Y. Wang *et al*. [55], [56] dealt with the synthesis of a ZnO-ZrO_2 and a Cu-CeO_2-ZrO_2 catalysts, respectively, by coprecipitation using a microfluidic device. The results of the catalytic tests of the ZnO-ZrO_2 catalyst showed a methanol productivity of 350 g MeOH kg_{cat}^{-1} h^{-1}, which is close to the productivity results of the catalyst "Microfluidic" of this work. These results are interesting because this catalyst didn't present Cu in its composition. On the other hand, the Cu-CeO_2-ZrO_2 catalyst presented a productivity of 222.4 g MeOH kg_{cat}^{-1} h^{-1}, which is lower than that of the catalysts of this work.

Lastly, the methanol productivity at 240ºC of the CuO 33-0h catalyst of this work was 789 g MeOH kg_{cat}^{-1} h^{-1}, which is higher than the productivity of all of the reviewed catalysts including the catalyst of Tofighi *et al*., [54] which presented a comparable methanol productivity with a value of 701.6 g MeOH kg_{cat}^{-1} h^{-1} at 250ºC. The use of the microfluidic method for the synthesis of the catalysts is a contributing factor explaining the better catalytic performance obtained in this work, compared to other catalysts prepared by other methods. However, as explained before the higher methanol productivities can also be explained by the use of a higher H_2:CO_2 ratio, a higher reaction pressure and a different GHSV. Figure 4.17 shows the methanol productivities plotted as a function of the CO_2 conversion at 240ºC for the catalysts investigated in the literature and some of the catalysts of this work. From this figure it is clear that most of the catalysts synthesized in this work present higher methanol productivity values at higher CO_2 conversions.

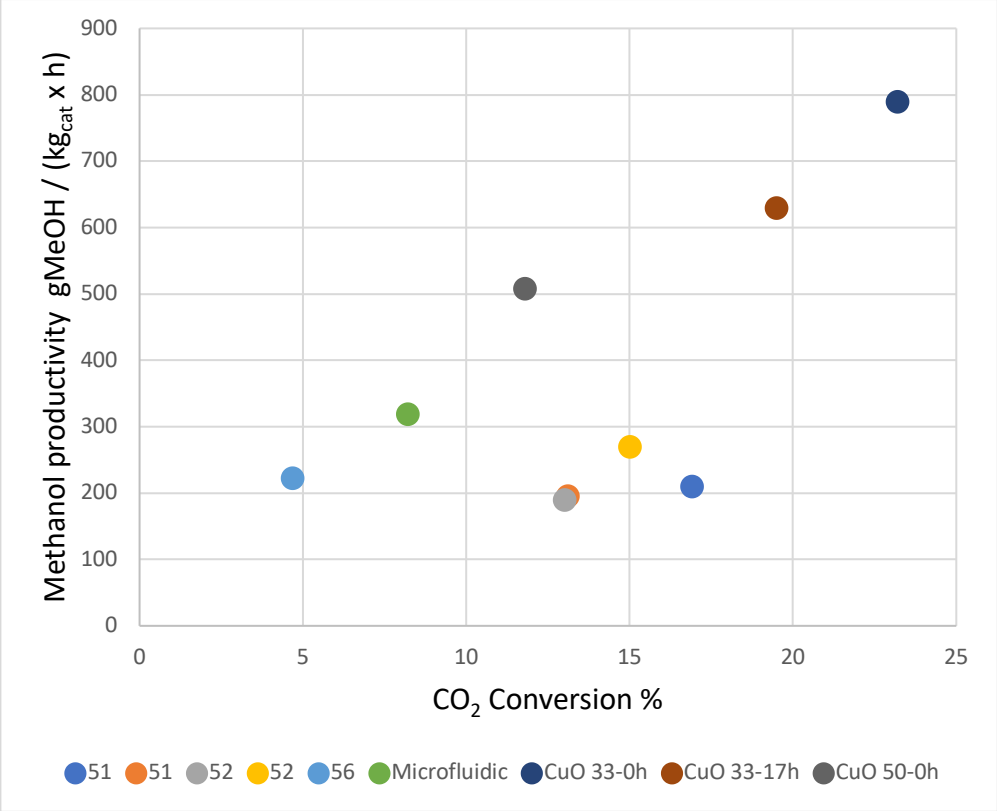

Figure 4.17 Methanol productivity vs. CO_2 conversion % at 240ºC for some of the catalysts included in Table 4.15. Each number corresponds to the reference of the work.

It can be concluded that the catalysts synthesized in this work present conversions and methanol productivities similar or above some of the catalysts available in the literature. This could be explained by the use of the microfluidic technique, which produced catalysts with higher catalytic activity. Also, the employed conditions of the catalytic tests can have an effect on the catalytic performance.

4.3.4. Conclusions

The effects of the coprecipitation temperature on the properties and catalytic activity of Cu-ZnO-ZrO_2 catalysts prepared by the microfluidic method were investigated in this section.

The results showed that the use of higher coprecipitation temperatures (i.e. 65ºC) during the catalyst synthesis didn't have considerable effects on the crystalline structure, the thermal decomposition, the textural properties and the reducibility of the catalysts. However, the CuO 50-0h-65 catalyst presented a decrease in the Cu surface area and the Cu dispersion, and an increase in the Cu particle size. This behavior may be due to the increased nucleation rates of the coprecipitation carried out at 65ºC, causing a growth of the size of the Cu-containing species in the precursors and consequently in a growth of the Cu particles in the calcined catalysts. Despite the above, the CuO 50-0h-65 catalyst presented higher H_2 and CO_2 conversions, as well as higher methanol productivity, which can be explained by a higher intrinsic activity

of the Cu nanoparticles occurring due to stronger interactions between the metal species. For future works, the study of coprecipitation temperatures higher than 65ºC could be interesting to see if it can produce catalysts with higher intrinsic activity.

In the next chapter, the effects of the catalyst's composition, including different CuO contents, the promotion with CeO_2 and the use of In_2O_3 as a promoter and as active metal will be investigated. Some of these catalysts were synthesized with a coprecipitation temperature of 65ºC and without aging, in order to explore the effects of these synthesis conditions on catalysts with different compositions.

4.4. Bibliography of chapter 4

[1] C. Jeong and Y. W. Suh, “Role of ZrO_2 in Cu/ZnO/ZrO_2 catalysts prepared from the precipitated Cu/Zn/Zr precursors,” *Catal. Today*, vol. 265, pp. 254–263, 2016, doi: 10.1016/j.cattod.2015.07.053.

[2] S. Polierer, D. Guse, S. Wild, K. H. Delgado, T. N. Otto, T. A. Zevaco, M. Kind, J. Sauer, F. Studt, and S. Pitter, “Enhanced direct dimethyl ether synthesis from CO_2-rich syngas with Cu/ZnO/ZrO_2 catalysts prepared by continuous co-precipitation,” *Catalysts*, vol. 10, no. 8, pp. 1–18, 2020, doi: 10.3390/catal10080816.

[3] S. I. Fujita, Y. Kanamori, A. M. Satriyo, and N. Takezawa, “Methanol synthesis from CO_2 over Cu/ZnO catalysts prepared from various coprecipitated precursors,” *Catal. Today*, vol. 45, no. 1–4, pp. 241–244, 1998, doi: 10.1016/S0920-5861(98)00222-3.

[4] F. Schuth, M. Hesse, and K. K. Unger, “Precipitation and Coprecipitation,” in *Handbook of Heterogeneous Catalysis*, John Wiley & Sons, Ltd, 2008, pp. 100–119. doi: 10.1002/9783527610044.HETCAT0008.

[5] Schimpf and Muhler, “Synthesis of Solid Catalysts,” in *Synthesis of Solid Catalysts*, K. P. de Jong, Ed., Wiley-VCH, 2009, pp. 1–401. doi: 10.1002/9783527626854.

[6] P. J. Smith, S. A. Kondrat, P. A. Chater, B. R. Yeo, G. M. Shaw, L. Lu, J. K. Bartley, S. H. Taylor, M. S. Spencer, C. J. Kiely, G. J. Kelly, C. W. Park, and G. J. Hutchings, “A new class of Cu/ZnO catalysts derived from zincian georgeite precursors prepared by co-precipitation,” *Chem. Sci.*, vol. 8, no. 3, pp. 2436–2447, 2017, doi: 10.1039/c6sc04130b.

[7] N. Mota, R. Guil-Lopez, B. G. Pawelec, J. L. G. Fierro, and R. M. Navarro, “Highly active Cu/ZnO-Al catalyst for methanol synthesis: Effect of aging on its structure and activity,” *RSC Adv.*, vol. 8, no. 37, pp. 20619–20629, 2018, doi: 10.1039/c8ra03291b.

[8] R. Raudaskoski, M. V. Niemelä, and R. L. Keiski, “The effect of ageing time on co-precipitated Cu/ZnO/ZrO_2 catalysts used in methanol synthesis from CO_2 and H_2,” *Top. Catal.*, vol. 45, no. 1–4, pp. 57–60, 2007, doi: 10.1007/s11244-007-0240-9.

[9] P. Gao, F. Li, H. Zhan, N. Zhao, F. Xiao, W. Wei, L. Zhong, H. Wang, and Y. Sun, “Influence of Zr on the performance of Cu/Zn/Al/Zr catalysts via hydrotalcite-like precursors for CO_2 hydrogenation to methanol,” *J. Catal.*, vol. 298, pp. 51–60, 2013, doi: 10.1016/j.jcat.2012.10.030.

[10] Y. Liang, D. Mao, X. Guo, J. Yu, G. Wu, and Z. Ma, “Solvothermal preparation of CuO-ZnO-ZrO_2 catalysts for methanol synthesis via CO_2 hydrogenation,” *J. Taiwan Inst. Chem. Eng.*, vol. 121, pp. 81–91, 2021, doi: 10.1016/j.jtice.2021.03.049.

[11] C. Huang, D. Mao, X. Guo, and J. Yu, “Microwave-Assisted Hydrothermal Synthesis of CuO–ZnO–ZrO_2 as Catalyst for Direct Synthesis of Methanol by Carbon Dioxide Hydrogenation,” *Energy Technol.*, vol. 5, no. 11, pp. 2100–2107, 2017, doi: 10.1002/ente.201700190.

[12] V. L’Hospital, “Développement et optimisation de catalyseurs à base de cuivre pour la synthèse de méthanol et de diméthyléther à partir de CO_2,” University of Strasbourg, 2018.

[13] V. Vágvölgyi, A. Locke, M. Hales, J. Kristóf, R. L. Frost, E. Horváth, and W. N. Martens, “Mechanism for decomposition of aurichalcite-A controlled rate thermal

analysis study," *Thermochim. Acta*, vol. 468, no. 1–2, pp. 81–86, 2008, doi: 10.1016/j.tca.2007.11.024.
[14] T. Phongamwong, U. Chantaprasertporn, T. Witoon, T. Numpilai, Y. Poo-arporn, W. Limphirat, W. Donphai, P. Dittanet, M. Chareonpanich, and J. Limtrakul, "CO_2 hydrogenation to methanol over CuO–ZnO–ZrO_2–SiO_2 catalysts: Effects of SiO_2 contents," *Chem. Eng. J.*, vol. 316, pp. 692–703, 2017, doi: 10.1016/j.cej.2017.02.010.
[15] T. M. Yurieva, "Catalyst for methanol synthesis: Preparation and activation," *React. Kinet. Catal. Lett.*, vol. 55, no. 2, pp. 513–521, 1995, doi: 10.1007/BF02073088.
[16] D. Waller, D. Stirling, F. S. Stone, and M. S. Spencer, "Copper-zinc oxide catalysts: Activity in relation to precursor structure and morphology," *Faraday Discuss. Chem. Soc.*, vol. 87, pp. 107–120, 1989, doi: 10.1039/DC9898700107.
[17] G. J. Millar, I. H. Holm, P. J. R. Uwins, and J. Drennan, "Characterization of precursors to methanol synthesis catalysts Cu/ZnO system," *J. Chem. Soc. - Faraday Trans.*, vol. 94, no. 4, pp. 593–600, 1998, doi: 10.1039/a703954i.
[18] J. Schumann, A. Tarasov, N. Thomas, R. Schlögl, and M. Behrens, "Cu,Zn-based catalysts for methanol synthesis: On the effect of calcination conditions and the part of residual carbonates," *Appl. Catal. A Gen.*, vol. 516, pp. 117–126, 2016, doi: 10.1016/j.apcata.2016.01.037.
[19] R. Guil-López, N. Mota, J. Llorente, E. Millan, B. G. Pawelec, J. L. G. Fierro, and R. M. Navarro, "Unravelling the structural modification (Meso-nano-) of Cu/ZnO-Al_2O_3 catalysts for methanol synthesis by the residual $NaNO_3$ in hydroxycarbonate precursors," *Catalysts*, vol. 10, no. 11, pp. 1–17, 2020, doi: 10.3390/catal10111346.
[20] Coblentz Society, "CO_2 Infrared spectrum.," NIST Webbook. Accessed: Dec. 13, 2023. [Online]. Available: https://webbook.nist.gov/cgi/cbook.cgi?ID=C124389&Type=IR-SPEC&Index=1#IR-SPEC
[21] M. Thommes, K. Kaneko, A. V. Neimark, J. P. Olivier, F. Rodriguez-Reinoso, J. Rouquerol, and K. S. W. Sing, "Physisorption of gases, with special reference to the evaluation of surface area and pore size distribution (IUPAC Technical Report)," *Pure Appl. Chem.*, vol. 87, no. 9–10, pp. 1051–1069, 2015, doi: 10.1515/pac-2014-1117.
[22] E. S. Borovinskaya, S. Trebbin, F. Alscher, and C. Breitkopf, "Synthesis, Modification, and Characterization of CuO/ZnO/ZrO_2 Mixed Metal Oxide Catalysts for CO_2/H_2 Conversion," *Catalysts*, vol. 9, no. 12, p. 1037, Dec. 2019, doi: 10.3390/catal9121037.
[23] V. L'hospital, S. Heyte, S. Paul, K. Parkhomenko, and A.-C. Roger, "Optimization of the continuous coprecipitation in a microfluidic reactor: Cu-based catalysts for CO_2 hydrogenation into methanol," *Fuel*, vol. 319, no. February, p. 123689, Jul. 2022, doi: 10.1016/j.fuel.2022.123689.
[24] S. Natesakhawat, J. W. Lekse, J. P. Baltrus, P. R. Ohodnicki, B. H. Howard, X. Deng, and C. Matranga, "Active sites and structure-activity relationships of copper-based catalysts for carbon dioxide hydrogenation to methanol," *ACS Catal.*, vol. 2, no. 8, pp. 1667–1676, 2012, doi: 10.1021/cs300008g.
[25] J. Zhong, X. Yang, Z. Wu, B. Liang, Y. Huang, and T. Zhang, "State of the art and perspectives in heterogeneous catalysis of CO_2 hydrogenation to methanol," *Chem. Soc. Rev.*, vol. 49, no. 5, pp. 1385–1413, 2020, doi: 10.1039/c9cs00614a.

[26] M. Ahamed, H. A. Alhadlaq, M. A. M. Khan, P. Karuppiah, and N. A. Al-Dhabi, “Synthesis, Characterization, and Antimicrobial Activity of Copper Oxide Nanoparticles,” *J. Nanomater.*, vol. 2014, p. 637858, 2014, doi: 10.1155/2014/637858.

[27] I. Z. Luna, L. N. Hilary, A. M. S. Chowdhury, M. A. Gafur, N. Khan, and R. A. Khan, “Preparation and Characterization of Copper Oxide Nanoparticles Synthesized via Chemical Precipitation Method,” *OALib*, vol. 02, no. 03, pp. 1–8, 2015, doi: 10.4236/oalib.1101409.

[28] S. Jadhav, S. Gaikwad, M. Nimse, and A. Rajbhoj, “Copper Oxide Nanoparticles: Synthesis, Characterization and Their Antibacterial Activity,” *J. Clust. Sci.*, vol. 22, no. 2, pp. 121–129, 2011, doi: 10.1007/s10876-011-0349-7.

[29] T. Witoon, T. Permsirivanich, W. Donphai, A. Jaree, and M. Chareonpanich, “CO_2 hydrogenation to methanol over Cu/ZnO nanocatalysts prepared via a chitosan-assisted co-precipitation method,” *Fuel Process. Technol.*, vol. 116, pp. 72–78, 2013, doi: 10.1016/j.fuproc.2013.04.024.

[30] T. Witoon, N. Kachaban, W. Donphai, P. Kidkhunthod, K. Faungnawakij, M. Chareonpanich, and J. Limtrakul, “Tuning of catalytic CO_2 hydrogenation by changing composition of CuO-ZnO-ZrO_2 catalysts,” *Energy Convers. Manag.*, vol. 118, pp. 21–31, 2016, doi: 10.1016/j.enconman.2016.03.075.

[31] Y. Nitta, O. Suwata, Y. Ikeda, Y. Okamoto, and T. Imanaka, “Copper-zirconia catalysts for methanol synthesis from carbon dioxide: Effect of ZnO addition to Cu-ZrO_2 catalysts,” *Catal. Letters*, vol. 26, no. 3–4, pp. 345–354, 1994, doi: 10.1007/BF00810608.

[32] F. Arena, G. Italiano, K. Barbera, G. Bonura, L. Spadaro, and F. Frusteri, “Basic evidences for methanol-synthesis catalyst design,” *Catal. Today*, vol. 143, no. 1–2, pp. 80–85, 2009, doi: 10.1016/j.cattod.2008.11.022.

[33] L. Li, D. Mao, J. Yu, and X. Guo, “Highly selective hydrogenation of CO_2 to methanol over CuO-ZnO-ZrO_2 catalysts prepared by a surfactant-assisted co-precipitation method,” vol. 279, pp. 394–404, 2015, doi: 10.1016/j.jpowsour.2014.12.142.

[34] P. Gao, F. Li, F. Xiao, N. Zhao, W. Wei, L. Zhong, and Y. Sun, “Effect of hydrotalcite-containing precursors on the performance of Cu/Zn/Al/Zr catalysts for CO_2 hydrogenation: Introduction of Cu^{2+} at different formation stages of precursors,” *Catal. Today*, vol. 194, no. 1, pp. 9–15, 2012, doi: 10.1016/j.cattod.2012.06.012.

[35] Z. Shi, Q. Tan, and D. Wu, “Ternary copper-cerium-zirconium mixed metal oxide catalyst for direct CO_2 hydrogenation to methanol,” *Mater. Chem. Phys.*, vol. 219, no. July, pp. 263–272, 2018, doi: 10.1016/j.matchemphys.2018.08.038.

[36] F. C. F. Marcos, L. Lin, L. E. Betancourt, S. D. Senanayake, J. A. Rodriguez, J. M. Assaf, R. Giudici, and E. M. Assaf, “Insights into the methanol synthesis mechanism via CO_2 hydrogenation over Cu-ZnO-ZrO_2 catalysts: Effects of surfactant/Cu-Zn-Zr molar ratio,” *J. CO_2 Util.*, vol. 41, no. May, 2020, doi: 10.1016/j.jcou.2020.101215.

[37] H. Y. Chen, S. P. Lau, L. Chen, J. Lin, C. H. A. Huan, K. L. Tan, and J. S. Pan, “Synergism between Cu and Zn sites in Cu/Zn catalysts for methanol synthesis,” *Appl. Surf. Sci.*, vol. 152, no. 3, pp. 193–199, 1999, doi: 10.1016/S0169-4332(99)00317-7.

[38] S. Natesakhawat, P. R. Ohodnicki, B. H. Howard, J. W. Lekse, J. P. Baltrus, and C. Matranga, “Adsorption and deactivation characteristics of Cu/ZnO-based catalysts for methanol synthesis from carbon dioxide,” *Top. Catal.*, vol. 56, no.

18–20, pp. 1752–1763, 2013, doi: 10.1007/s11244-013-0111-5.
[39] S. Tada, S. Kayamori, T. Honma, H. Kamei, A. Nariyuki, K. Kon, T. Toyao, K. I. Shimizu, and S. Satokawa, “Design of Interfacial Sites between Cu and Amorphous ZrO_2 Dedicated to CO_2-to-Methanol Hydrogenation,” *ACS Catal.*, vol. 8, no. 9, pp. 7809–7819, 2018, doi: 10.1021/acscatal.8b01396.
[40] Z. Shi, Q. Tan, C. Tian, Y. Pan, X. Sun, J. Zhang, and D. Wu, “CO_2 hydrogenation to methanol over Cu-In intermetallic catalysts: Effect of reduction temperature,” *J. Catal.*, vol. 379, pp. 78–89, 2019, doi: 10.1016/j.jcat.2019.09.024.
[41] B. Liang, J. Ma, X. Su, C. Yang, H. Duan, H. Zhou, S. Deng, L. Li, and Y. Huang, “Investigation on Deactivation of $Cu/ZnO/Al_2O_3$ Catalyst for CO_2 Hydrogenation to Methanol,” *Ind. Eng. Chem. Res.*, vol. 58, no. 21, pp. 9030–9037, 2019, doi: 10.1021/acs.iecr.9b01546.
[42] S. Dang, H. Yang, P. Gao, H. Wang, X. Li, W. Wei, and Y. Sun, “A review of research progress on heterogeneous catalysts for methanol synthesis from carbon dioxide hydrogenation,” *Catal. Today*, vol. 330, no. March 2018, pp. 61–75, 2019, doi: 10.1016/j.cattod.2018.04.021.
[43] K. Chang, T. Wang, and J. G. Chen, “Methanol Synthesis from CO_2 Hydrogenation over CuZnCeTi Mixed Oxide Catalysts,” *Ind. Eng. Chem. Res.*, vol. 58, no. 19, pp. 7922–7928, 2019, doi: 10.1021/acs.iecr.9b00554.
[44] C. Li, X. Yuan, and K. Fujimoto, “Development of highly stable catalyst for methanol synthesis from carbon dioxide,” *Appl. Catal. A Gen.*, vol. 469, pp. 306–311, 2014, doi: 10.1016/j.apcata.2013.10.010.
[45] G. Bonura, M. Cordaro, C. Cannilla, F. Arena, and F. Frusteri, “The changing nature of the active site of Cu-Zn-Zr catalysts for the CO_2 hydrogenation reaction to methanol,” *Appl. Catal. B Environ.*, vol. 152–153, pp. 152–161, 2014, doi: 10.1016/j.apcatb.2014.01.035.
[46] S. Ren, X. Fan, Z. Shang, W. R. Shoemaker, L. Ma, T. Wu, S. Li, N. B. Klinghoffer, M. Yu, and X. Liang, “Enhanced catalytic performance of Zr modified $CuO/ZnO/Al_2O_3$ catalyst for methanol and DME synthesis via CO_2 hydrogenation,” *J. CO_2 Util.*, vol. 36, no. November 2019, pp. 82–95, 2020, doi: 10.1016/j.jcou.2019.11.013.
[47] M. Behrens, D. Brennecke, F. Girgsdies, S. Kißner, A. Trunschke, N. Nasrudin, S. Zakaria, N. F. Idris, S. B. A. Hamid, B. Kniep, R. Fischer, W. Busser, M. Muhler, and R. Schlögl, “Understanding the complexity of a catalyst synthesis: Co-precipitation of mixed Cu,Zn,Al hydroxycarbonate precursors for $Cu/ZnO/Al_2O_3$ catalysts investigated by titration experiments,” *Appl. Catal. A Gen.*, vol. 392, no. 1–2, pp. 93–102, 2011, doi: 10.1016/j.apcata.2010.10.031.
[48] M. Behrens and R. Schlögl, “How to prepare a good Cu/ZnO catalyst or the role of solid state chemistry for the synthesis of nanostructured catalysts,” *Zeitschrift fur Anorg. und Allg. Chemie*, vol. 639, no. 15, pp. 2683–2695, 2013, doi: 10.1002/zaac.201300356.
[49] M. Lok, “Coprecipitation,” in *Synthesis of Solid Catalysts*, K. P. de Jong, Ed., Wiley-VCH, 2009. [Online]. Available: https://onlinelibrary.wiley.com/doi/book/10.1002/9783527626854
[50] P. Munnik, P. E. De Jongh, and K. P. De Jong, “Recent Developments in the Synthesis of Supported Catalysts,” *Chem. Rev.*, vol. 115, no. 14, pp. 6687–6718, 2015, doi: 10.1021/cr500486u.
[51] L. Frusteri, C. Cannilla, S. Todaro, F. Frusteri, and G. Bonura, “Tailoring of hydrotalcite-derived Cu-based catalysts for CO_2 hydrogenation to methanol,”

Catalysts, vol. 9, no. 12, 2019, doi: 10.3390/catal9121058.
[52] T. Witoon, T. Numpilai, T. Phongamwong, W. Donphai, C. Boonyuen, C. Warakulwit, M. Chareonpanich, and J. Limtrakul, “Enhanced activity, selectivity and stability of a CuO-ZnO-ZrO_2 catalyst by adding graphene oxide for CO_2 hydrogenation to methanol,” *Chem. Eng. J.*, vol. 334, pp. 1781–1791, 2018, doi: 10.1016/j.cej.2017.11.117.
[53] Q. C. Zhang, K. P. Cheng, L. X. Wen, K. Guo, and J. F. Chen, “A study on the precipitating and aging processes of CuO/ZnO/Al_2O_3 catalysts synthesized in micro-impinging stream reactors,” *RSC Adv.*, vol. 6, no. 40, pp. 33611–33621, 2016, doi: 10.1039/c6ra02512a.
[54] G. Tofighi, H. Lichtenberg, A. Gaur, W. Wang, S. Wild, K. Herrera Delgado, S. Pitter, R. Dittmeyer, J.-D. Grunwaldt, and D. E. Doronkin, “ Continuous synthesis of Cu/ZnO/Al_2O_3 nanoparticles in a co-precipitation reaction using a silicon based microfluidic reactor ,” *React. Chem. Eng.*, 2022, doi: 10.1039/d1re00499a.
[55] X. Wang, Y. Wang, C. Yang, Y. Yi, X. Wang, F. Liu, J. Cao, and H. Pan, “A novel microreaction strategy to fabricate superior hybrid zirconium and zinc oxides for methanol synthesis from CO_2,” *Appl. Catal. A Gen.*, vol. 595, no. March, p. 117507, 2020, doi: 10.1016/j.apcata.2020.117507.
[56] Y. Wang, H. Yu, Q. Hu, Y. Huang, X. Wang, Y. Wang, and F. Wang, “Application of microimpinging stream reactor coupled with ultrasound in Cu/$CeZrO_x$ solid solution catalyst preparation for CO_2 hydrogenation to methanol,” *Renew. Energy*, vol. 202, no. November 2022, pp. 834–843, 2023, doi: 10.1016/j.renene.2022.11.075.

Chapter 5 Study of the composition of Cu based catalysts synthesized by the microfluidic method

5.1. Introduction

In this chapter, the effect of different catalyst compositions was investigated by varying the CuO content and by adding CeO_2 or In_2O_3 to the CuO-ZnO-ZrO_2 catalysts. A catalyst without copper with the composition In_2O_3-ZnO-ZrO_2 was also investigated for comparison. The chapter is constructed in several sub-chapters in order to evaluate three different effects:

- Effect of the CuO content on CuO-ZnO-ZrO_2 catalysts prepared by the microfluidic method

Three catalysts named 40% CuO (theoretical mass composition 40wt% CuO, 39.6wt% ZnO and 20.4wt% ZrO_2,) 50% CuO (theoretical mass composition 50wt% CuO, 33wt% ZnO and 17wt% ZrO_2) and 60% CuO (theoretical mass composition 60wt% CuO, 26.4wt% ZnO and 13.6wt% ZrO_2) with different mass compositions as their name indicates and with different ZnO/CuO and ZrO_2/CuO ratios were synthesized by the microfluidic continuous coprecipitation method as presented in Chapter 2, section 2.2, and characterized by a number of analysis techniques. The catalytic activity of the catalysts in the CO_2 hydrogenation to methanol was evaluated.

- Effect of the addition of CeO_2 to CuO-ZnO-ZrO_2 catalysts prepared by the microfluidic method

Two CuO-ZnO-ZrO_2 catalysts containing CeO_2 as a promoter were prepared, characterized and their catalytic performance was determined. The composition of these two catalysts was the same, and the catalyst synthesis method used was the microfluidic synthesis with immediate filtration. For one of these two catalysts, the precipitation zone was heated to 65ºC to investigate the effect of a higher precipitation temperature on the properties and performance of the catalyst. The mass compositions of the two CeO_2 containing catalysts were 50% CuO, 33% ZnO, 6.8% ZrO_2 and 10.2% CeO_2. These catalysts were named CuO 50 CeO_2 10-0h and CuO 50 CeO_2 10-0h-65, where the first one was prepared without heating of the precipitation zone to 65ºC and the second one was prepared with it. The 50 and 10 numbers indicate the mass CuO % and the CeO_2 % of the catalysts, respectively. The characterization results were compared to those of a catalyst synthesized by the microfluidic synthesis with immediate filtration composed only of Cu-ZnO-ZrO_2 in order to study the effects of the addition of CeO_2.

The catalysts of this section were synthesized by the microfluidic synthesis with immediate filtration, one with heating of the precipitation zone and another one without it as presented in Chapter 2, section 2.2.

- Effect of the addition of In_2O_3 to Cu-ZnO-ZrO_2 catalysts prepared by the microfluidic method

This work presents the investigation of two catalysts containing In_2O_3 with different compositions applied to the production of methanol from the hydrogenation of CO_2. The two indium containing catalysts investigated in this work were named CuZnZrIn and ZnZrIn and their nominal mass compositions were 40% CuO, 33.3% ZnO, 16.6% ZrO_2 and 10% In_2O_3 for the CuZnZrIn catalyst and 60% ZnO, 30% ZrO_2 and 10% In_2O_3 for the ZnZrIn catalyst. These compositions were selected to study the use of In_2O_3 as a promoter in the copper containing catalyst CuZnZrIn and to study its use as the main active metal in the ZnZrIn catalyst.

The catalysts of this section were synthesized by the microfluidic synthesis with immediate filtration and with heating of the precipitation zone to 65ºC, as presented in Chapter 2, section 2.2.

At the end of this subchapter, a review of the catalytic activity of different catalysts containing In_2O_3 available in the literature was done in order to compare their catalytic performance with that of the catalysts of this work.

5.2. Effect of the CuO content on Cu-ZnO-ZrO_2 catalysts prepared by the microfluidic method

The CuO-ZnO-ZrO_2 catalysts have attracted increasing attention since decades ago due to their suitability for the CO_2 hydrogenation to methanol reaction. Since then, catalysts prepared by different methods and with different compositions have been studied [1]. Different works [1]–[3], indicate that the composition of CuO-ZnO-ZrO_2 catalysts has an important effect on different properties of the catalyst, such as the specific and the copper surface areas, the surface basicity, the reducibility of the catalysts and also on the catalytic performance.

The synthesis of CuO-ZnO-ZrO_2 catalysts with different CuO contents and with different ZnO/CuO and ZrO_2/CuO ratios by the microfluidic method hasn't been explored before. Therefore, a study addressing the effect of the composition of Cu-ZnO-ZrO_2 catalysts on the properties and performance of catalysts synthesized by this technique would help optimize this catalyst synthesis approach for the production of better catalysts for the hydrogenation of CO_2 to methanol.

5.2.1. Catalysts characterization results and discussion

The XRD results of the precursors after the drying step and before the calcination step are presented on the left side of Figure 5.1 and the XRD diffractograms of the calcined catalysts are presented on the right side of the same Figure. It can be noticed that all the precursors developed a crystalline fraction with different phases identified as aurichalcite $Zn_3Cu_2(OH)_6(CO_3)_2$ (PDF number: 82-1253), hydrozincite $Zn_5(CO_3)_2(OH)_6$ (PDF number: 72-1100) and malachite $Cu_2(OH)_2CO_3$ (PDF number: 41-1390). However, the precursor 40% CuO was the only one that didn't develop the malachite phase, which suggests that malachite could be formed preferentially at higher CuO concentrations in the CuZnZr material, in this case, for the catalysts with 50% CuO and 60% CuO. On the diffractograms of the mentioned precursors there were no Zr containing species identified, which indicates that Zr was present in an amorphous state, as indicated in the previous sections of this work. The crystallite sizes of the detected phases calculated using Scherrer's equation are presented in Table 5.1. As can be observed, the crystallite sizes were similar for all the catalyst precursors, with crystallite sizes between 8 and 9 nm for both aurichalcite and hydrozincite in the three investigated catalysts and crystallite sizes between 16 and 17 nm for malachite in the 50% CuO and 60% CuO catalysts, respectively. The 2Theta values used to calculate crystallite sizes were 13º for both aurichalcite and hydrozincite (hkl: 200 for both phases) and 24.3º for malachite (hkl: 220).

As discussed before, the occurrence of the background in the diffractograms of the precursors is an indication of the presence of amorphous compounds. In this case, it

can be associated with the presence of hydroxycarbonates that didn't crystallize such as georgeite, which is the amorphous form of malachite [4] and also the Zr-containing amorphous species.

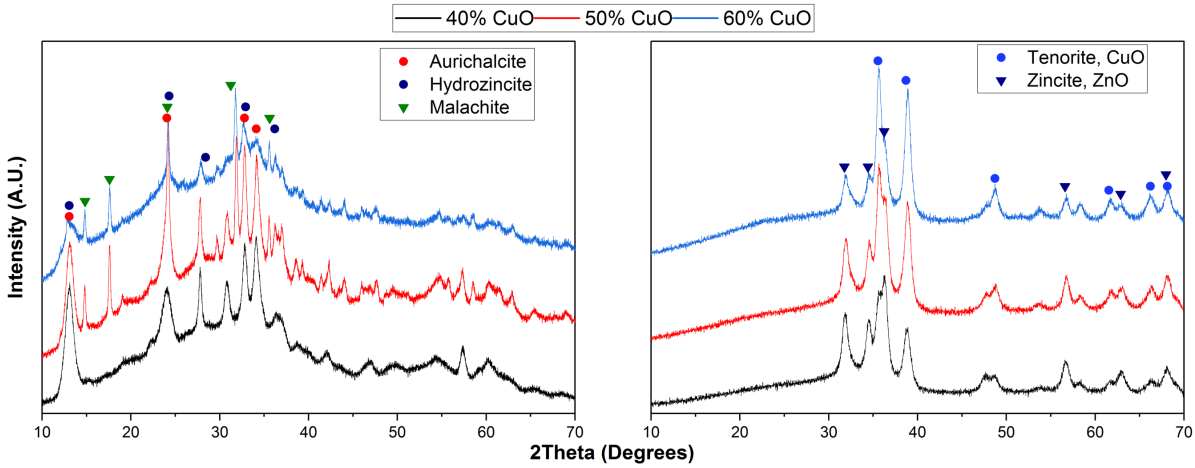

Figure 5.1 X-ray diffractograms of catalyst precursors on the left side and their respective calcined catalysts on the right side.

Table 5.1 Crystallite sizes (nm) of the phases present in the catalyst precursors and in the catalysts after calcination calculated with Scherrer's equation.

	Catalyst precursor			Calcined catalyst		
Sample	**Aurichalcite**	**Malachite**	**Hydrozincite**	**Tenorite, CuO**	**Zincite, ZnO**	**Crystallinity %**
40% CuO	8	-	8	11	11	49.7
50% CuO	9	16	9	11	11	50.5
60% CuO	8	17	8	12	11	36.4

After calcination, the three samples developed CuO (PDF number: 72-0629) and ZnO (PDF number: 75-1526) crystalline phases, as shown in the X-ray diffractograms presented on the right side of Figure 5.1. As expected, Zr species were not detected due to its amorphous state [1], [5]–[7].

A good intergrowth of the CuO and ZnO phases was observed close to the 2 Theta value of 35º [8], where CuO and ZnO present important XRD peaks. This intergrowth of the two metal oxides loses intensity as the CuO content of the catalyst increases, which is logical because an increase in the content of CuO of the catalyst is accompanied by a reduction in the relative contents of ZnO causing a reduction in the interactions between these two metallic elements of the catalysts. For example, it can be seen that the ZnO peak at a 2Theta value of 32º loses intensity as the CuO % is increased. The crystallite sizes calculated by Scherrer's equation show similar results for CuO and ZnO in all the samples (Table 5.1). The 2Theta values used to calculate

the crystallite sizes were 38.7º for CuO (hkl: 111) and 32º for ZnO (hkl: 100). The CuO and ZnO crystallite sizes of the three catalysts of this work didn't present large differences. The only meaningful differences were seen in the precursors, where the presence of malachite was observed in only two of the three precursors. In addition, Table 5.1 shows that the catalysts 40% CuO and 50% CuO presented crystallinities of 49.7% and 50.5%, respectively, while the crystallinity of the catalyst 60% CuO decreased importantly to a value of 36.4% (Table 5.1). The lower content of ZnO of the 60% CuO catalyst may contribute to a decrease in the crystallinity degree, given that typically the ZnO phase develops a crystalline structure. It is also possible that the high concentration of CuO in the 60% CuO catalyst inhibited the crystallization of ZnO, causing a lower crystallinity degree of this catalyst.

TGA was employed to study the thermal decomposition of the catalyst precursors to help identify compounds or species present in a material with the help of data available in the literature. The total mass losses of the samples 40, 50 and 60% CuO were 22%, 23% and 22% respectively. The TGA results also indicate that a complete decomposition of the precursors takes place approximately above 500ºC, after which no significant mass loss can be seen in the decomposition profiles. Despite the similarity in mass loss % of the three precursors, the samples presented different decomposition profiles as evidenced by the derivative peaks shown in Figure 5.2, indicating the presence of different species in the precursors.

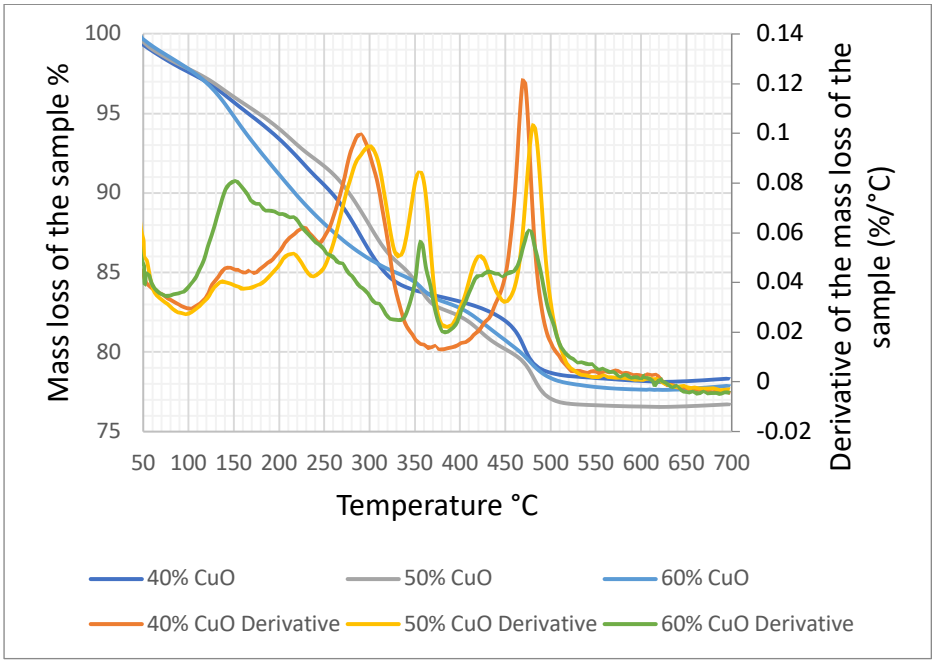

Figure 5.2 TGA profiles of the catalyst precursors with 40, 50 and 60 mass % CuO content.

In the work of L'hospital [9], the main decomposition temperatures of the single, binary and ternary Cu, Zn and Zr metal precursors were determined by TGA and they can be used as a reference to identify the phases or species that decompose during this analysis. This information is presented in Table 5.2 and it provides a reference of the

decomposition temperatures obtained by using TGA on the different metal precursors of Cu, Zn and Zr.

Table 5.2 TGA decomposition temperatures of different species determined by L'hospital [9].

Precursor	Main decomposition temperatures
Single metal precursors	
Cu	Between 324 and 332ºC
Zn	Around 237ºC
Zr	Around 148ºC
Binary metal precursors	
Cu-Zn	Between 280-300°C and around 466°C
Cu-Zr	Between 147-159°C and 320-340°C
Zn-Zr	Around 157°C and 237°C
Ternary metal precursor	
Cu-Zn-Zr	Around 161°C, 316°C, 368°C, 409°C and 492°C

The precursor 40% CuO presented four different peaks around 148, 231, 290 and 472 ºC on the TGA derivative profile (Figure 5.2). The peak found at 148°C can be associated to the decomposition of the Zr single precursor, which could correspond to Zr carbonate, Zr hydroxide or zirconium hydroxycarbonate. The peak at 231°C can be associated to the single Zn precursor decomposition or hydrozincite as identified by XRD [10]. The hydrozincite phase decomposes between 155ºC and 340ºC [10]. As shown in Table 5.2, the binary Cu-Zn precursor presents 2 main decomposition temperatures around 290°C and around 466°C, which matches 2 of the peaks present in this sample. This is in agreement with the presence of aurichalcite detected by XRD, which contains both Cu and Zn [11][12].

Regarding the precursor 50% CuO, its TGA derivative profile presented many different peaks indicating the decomposition of different species at 143, 220, 300, 360, 420 and 480ºC. Some agreement can be seen between the peaks of this precursor and the decomposition temperatures presented in the work of L'hospital [9] and in other references [10][11]. As mentioned before, the decomposition of the Zr precursor can be attributed to the peak at 143 °C present in the sample. According to the data above, the decomposition of the single Zn precursor occurs around 237°C. This is in agreement with the presence of the hydrozincite phase and the decomposition peaks identified around this temperature. Moreover, the decomposition of the Cu-Zn binary precursor aurichalcite occurs between 280 and 300°C and at 460°C, which matches some of the peaks present in this precursor. The peaks present at 250 and 350ºC can also be linked to the thermal decomposition of malachite [13].

Lastly, different peaks were identified around 155, 358, 437 and 478 °C in the precursors' 60% CuO TGA derivative profile. Again, the peak at 155ºC can be associated to the decomposition of the Zr single precursor as well as with the binary

Cu-Zr and Zn-Zr metal precursors. The peak at 358ºC can be associated to the decomposition of malachite [13] and the peaks occurring above 400ºC can be associated to the decomposition of the Cu-Zn precursor (i.e. aurichalcite) [9]. The decomposition of the anion-modified oxides can also explain the decomposition occurring around 500ºC as stated before in Chapter 4 citing the work of Yurieva *et al*. [14]. Also, the peak present between 450ºC and 500ºC was weaker in the catalyst 60% CuO, which could be an indication of the lower crystallization of this species, as found in the XRD characterization results.

Furthermore, other research works [10]–[12], [15], [16] provide a reference about the decomposition process of this type of catalysts. Below 200ºC it is reasonable to say that water that makes part of the components as well as moisture and adsorbed water are removed from the catalysts [12], [16]. In the research works [10]–[12], [15] it is indicated that aurichalcite decomposes at temperatures between 100ºC and 350ºC, releasing carbon dioxide and water in the process, while the decomposition temperature of hydrozincite occurs around 245ºC. In addition, malachite decomposes at temperatures between 327ºC and 380ºC which causes the production of carbon dioxide and water [15][17]. Such process can be represented by the following chemical equation [15]:

Equation 5.1 Thermal decomposition of malachite.

$$Cu_2(CO_3)(OH)_2 \rightarrow 2CuO + CO_2 + H_2O$$

As can be seen in the TGA profiles, increasing CuO contents caused the formation of decomposition peaks around 350ºC. This peak is associated to the presence of malachite and was only present in the catalysts 50% CuO and 60% CuO, which is in agreement with the phase identification done by XRD. The TGA analysis allowed the identification of the crystalline phases aurichalcite, hydrozincite and malachite in the catalysts, confirming the results obtained with the XRD analysis. It can be seen that between 450ºC and 500ºC there's a reduction in the intensity of the peaks with increasing CuO content, indicating a decrease in the interactions between Cu and Zn that occur in the aurichalcite phase. From the above results it is clear that the increase of the CuO content has an effect on the formation of phases, the interactions between components and on the composition of the precursors, affecting their thermal decomposition profiles.

Figures 5.3a, b and c show the results of the FT-IR analysis of the catalyst precursors, of the calcined catalysts and the identification of functional groups characteristic of different crystalline phases in the precursors, respectively.

According to the literature [18]–[20], the presence of peaks between 3550-3200 cm^{-1} are characteristic of O-H stretching, which indicates the presence of hydroxy functional groups which are present in the hydroxycarbonates produced during the coprecipitation step. The three analyzed precursors presented noticeable peaks between 3550-3200 cm^{-1} while the calcined catalysts presented much weaker peaks

between the same interval, which indicates the decomposition of the majority of the hydroxycarbonates and hydroxy groups after calcination. Other references [8], [19], [20] indicate that the characteristic peaks of carbonates appear around 1515, 1428 and 1390 cm^{-1} which are due to asymmetric C–O stretching, and also an out of plane OCO bending mode at 820 cm^{-1}, and an asymmetric OCO bending mode at 742 cm^{-1}. In addition, the presence of peaks at 1380 and 833 cm^{-1} are characteristic of NO_3^- vibrations [8]. NO_3^- groups are present during the coprecipitation step as the metal precursors used for the synthesis are nitrates, as explained before. Also, in the literature review it was shown that some compounds present during the coprecipitation reactions can have NO_3^- groups in their composition. Similarly to what happened to the hydroxy functional groups, the peaks between 1600-1200 cm^{-1} and around 800 cm^{-1} presented an important reduction after calcination, which indicates the decomposition of the carbonate and nitrate functional groups. The colored bands in Figure 5.3 a and b correspond to the different functional groups detected, where green bands correspond to hydroxyl groups, the gray bands correspond to carbonate and nitrate groups and the light blue bands correspond to the presence of nitrate groups.

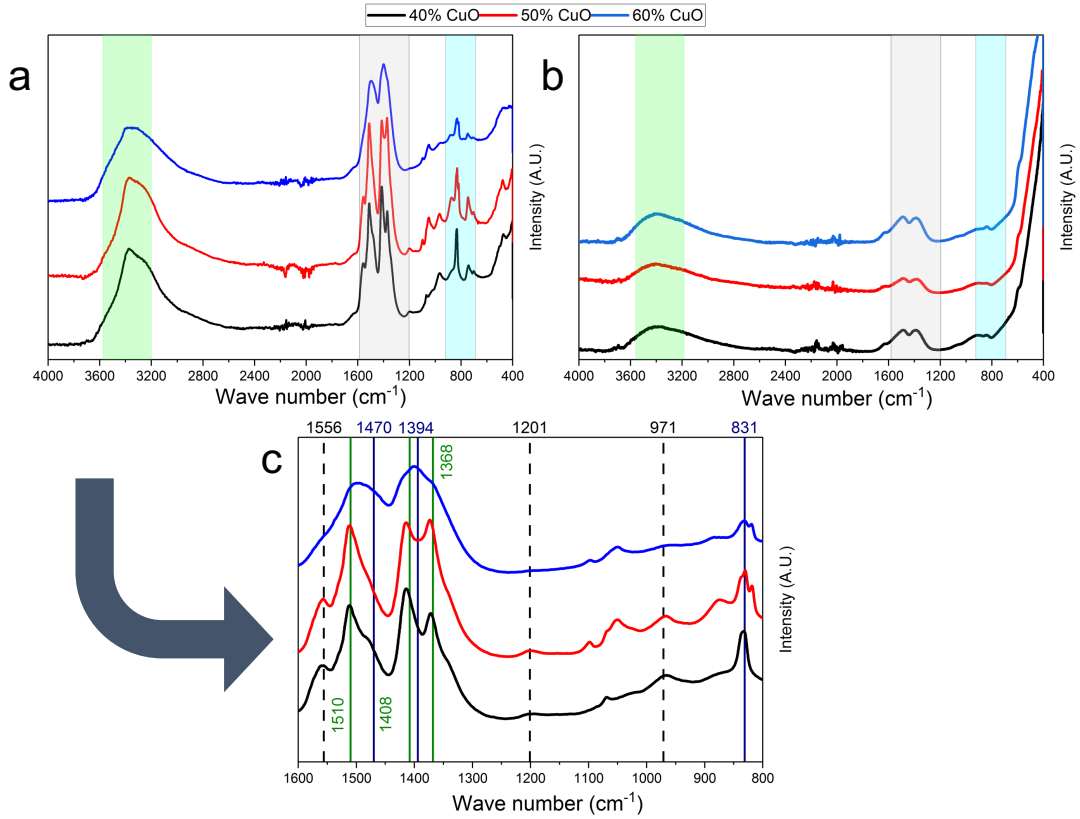

Figure 5.3 FT-IR spectra of the 40% CuO, 50% CuO and 60% CuO catalyst precursors (a), the calcined catalysts (b) and identification of different crystalline phases in the catalyst precursors (c).

Besides the identification of functional groups, FT-IR technique could also help to describe the possible crystalline phases present in this type of material. The aurichalcite phase representative bands are positioned in the 1556, 1201 and 971 cm^{-1} wavenumbers [21] shown as vertical dashed lines, while bands at 1510, 1408

and 1368 cm^{-1} shown as vertical green lines can indicate the presence of malachite [15]. In the case of the sample 40% CuO the possible presence of malachite phase could be supposed due to FT-IR results but was not detected on XRD diffractogram. This could be due to the very tiny crystallite size of this phase which is under the detection limit of XRD analysis (less than 5 nm). These results allow supposing that malachite phase will be present in all three samples but in form of particles (crystallite) of different sizes, more copper is present in the sample bigger will be the crystallite size of developed malachite (below 5nm, 16 nm and 17 nm for 40% CuO, 50% CuO and 60% CuO respectively).

The presence of the malachite and aurichalcite phases in the 60% CuO precursor was confirmed by the XRD analysis but not by FT-IR. In fact, the scan of the 60% CuO catalyst differed from those of the two other catalysts, which may be due to the lower crystallinity of this catalyst, which may affect the detection of these two phases by FT-IR.

Furthermore, bands at 1470, 1394 and 831 cm^{-1} shown as vertical dark blue lines in Figure 5.3c are an indication of carbonate vibrations characteristic of the amorphous georgeite phase $Cu_2(OH)_2CO_3 \cdot 6H_2O$ [8]. However, none of the FT-IR spectra matched the bands characteristic of this phase, which indicates that it may be present in very low concentrations or that it was converted completely into malachite in the catalysts 50% CuO and 60% CuO. These findings show the most prevalent functional groups and crystalline phases present in the precursors and in the calcined catalysts.

Finally, the noise detected around 2200 cm^{-1} corresponds to carbon dioxide present in the environment, and the corresponding peak was eliminated by a background adjustment before each analysis [22].

To summarize the results up to this point, the XRD, TGA and FT-IR characterization results evidenced that the materials present complexities caused by the different contents and proportions of CuO, ZnO and ZrO_2, which cause different interactions between the formed phases and the metal species of the catalysts. The XRD results showed that the catalysts are composed of an amorphous and a crystalline part, where the amorphous part includes ZrO_2, but may also include a fraction of CuO and ZnO or other Cu or Zn species that remained in an amorphous state. The TGA also showed that the thermal decomposition of the three catalyst precursors were different, indicating composition and morphological differences which can have an effect on other properties of these catalysts, such as the textural properties, the reducibility and also on the catalytic activity.

The elemental composition of the three catalysts of this study was analyzed by the help of X-ray fluorescence. The results are given in Table 5.3.

Table 5.3 Catalysts mass composition determined by XRF analysis.

Catalyst	CuO wt% content			ZnO wt% content			ZrO_2 wt% content		
	XRF	Theory	%	XRF	Theory	%	XRF	Theory	%
40% CuO	41.1	40.0	2.7	40.8	39.6	3.0	18.1	20.4	-11.3
50% CuO	51.2	50.0	2.4	34.2	33.0	3.6	14.6	17.0	-14.1
60% CuO	62.4	60.0	4.0	24.9	26.4	-5.1	12.7	13.6	-6.6

As shown above, the CuO, ZnO and ZrO_2 compositions of the three catalysts presented deviations from the theoretical values, specially the ZrO_2 content of the catalyst 50% CuO. These deviations may be caused by the different kinetics of coprecipitation of the metal species, which can be affected by conditions such as the pH and the aging temperature. The results show that the precipitation of ZrO_2 presented the highest deviations from the theoretical values, which could indicate that the precipitation of this species was the most difficult. The Cu and Zn species presented lower deviations, indicating good precipitation and more adequate loading in the catalysts.

The SEM images of the catalysts 40% CuO, 50% CuO and 60% CuO are presented in Figures 5.4a, b and c, respectively. These images show that the morphologies of the three catalysts are different and this is caused by the different compositions and also by differences in the crystallinity % of the catalysts. The SEM images evidence the presence of crystalline structures, which is in agreement with the XRD results presented before. The visible crystalline phases correspond to CuO and ZnO which according to the work of Witoon *et al*. [23] are present as an agglomeration of particles [24] and plate-like structures, respectively. Other previous works also confirm the grainy or irregular particles morphology characteristic of crystalline CuO [25]–[27]. Moreover, some particles with irregular shapes present in some areas of the images may correspond to the amorphous zirconia, as shown in the work of Lin *et al*. [28]. As can be observed in the SEM image of the 60% CuO catalyst (Figure 5.4c), the presence of particles with irregular sizes corresponding to CuO [24][25] is more evident, while the presence of the so called plate-like structures is significantly decreased, which can be associated to the lower ZnO content of this catalyst. The lower crystallinity degree of the catalyst 60% CuO as calculated with the X-ray diffractograms may also be responsible of the different morphology appreciated in this material.

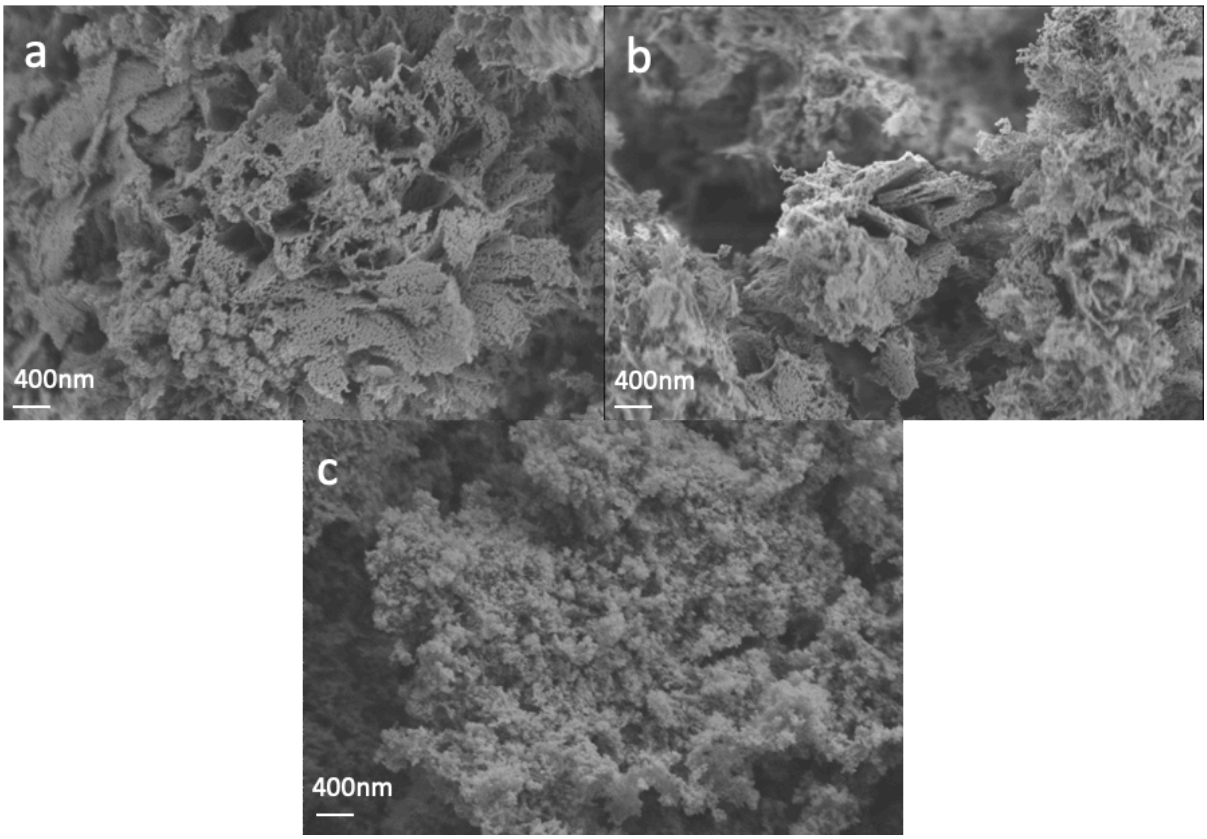

Figure 5.4 SEM images of the catalysts 40% CuO (a), 50% CuO (b) and 60% CuO (c).

Lastly, the presence of plate-like or flower-like morphologies of the catalysts 40% CuO and 50% CuO can be explained by the higher content of ZnO [23] of these two catalysts as discussed in Chapter 4, and also by their higher degree of crystallization. Each of the “petals” that make up the ZnO morphology is composed of an agglomeration of particles with a size comparable to the size of the ZnO crystallites.

The surface and the textural properties of the catalysts were investigated by N_2-physisorption. Figure 5.5 shows the N_2 adsorption and desorption isotherms of the three catalysts under study. All the catalysts presented isotherms of type IV, which indicates that the materials are mesoporous and have cylindrical shaped pores [29]. Also, the catalysts presented a H3 hysteresis loop, which can be present in layered solids with narrow pore networks [29], [30].

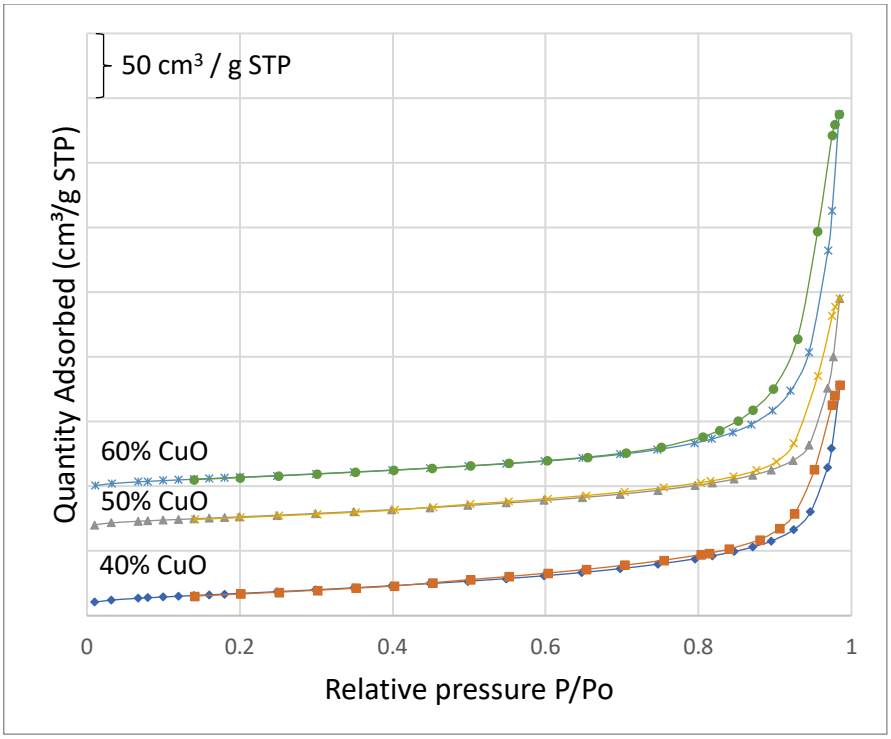

Figure 5.5 N_2-physisorption isotherms of the 40, 50 and 60% CuO catalysts.

The specific surface areas and the pore size distribution graphs of the three catalysts are presented in Table 5.4 and in Figure 5.6, respectively. The N_2-physisorption analysis showed that the specific surface areas of the three catalysts were similar, with a mean value of 60 m^2/g. On the pore size distribution graphs (BJH desorption branch) of Figure 5.6, it could be seen that the catalysts 40% and 50 % CuO are quite similar and have very close pore distribution – 3 nm characteristic mesopores visible from the N_2 adsorption-desorption isotherms and 30 nm large mesopores – could be attributed to the specific morphology in petals and the N_2 adsorption in the intraparticle spaces. For the 60% CuO catalyst the contribution of the 3 nm mesoporosity is very small compared to the large 30 nm mesopores, that supposedly come from the different morphology of the 60% CuO sample. This can be due to different crystallinity of the catalysts and also different phase composition as well as different thermal decomposition patterns obtained from TGA, which indicate different interactions between the metal species of the catalysts. In fact, the catalyst 60% CuO presented a lower degree of crystallization compared to the catalysts 40% CuO and 50% CuO. This may be the cause of the differences in morphology and the textural properties of this catalyst, causing an increase in the pore size of this catalyst. As explained before, the catalyst 60% CuO presented a morphology composed mainly of irregular particles of different sizes, which corresponds mostly to the presence of crystalline CuO.

Table 5.4 Specific surface area and porosity results of the three catalysts under study obtained with N_2-physisorption.

Sample	BET surface area (m^2/g)	Pore size (nm)
40% CuO	62	3 and 30 nm
50% CuO	59	3 and 30 nm
60% CuO	58	30 nm

Figure 5.6 BJH pore size distribution of the 40% CuO, 50% CuO and 60% CuO catalysts.

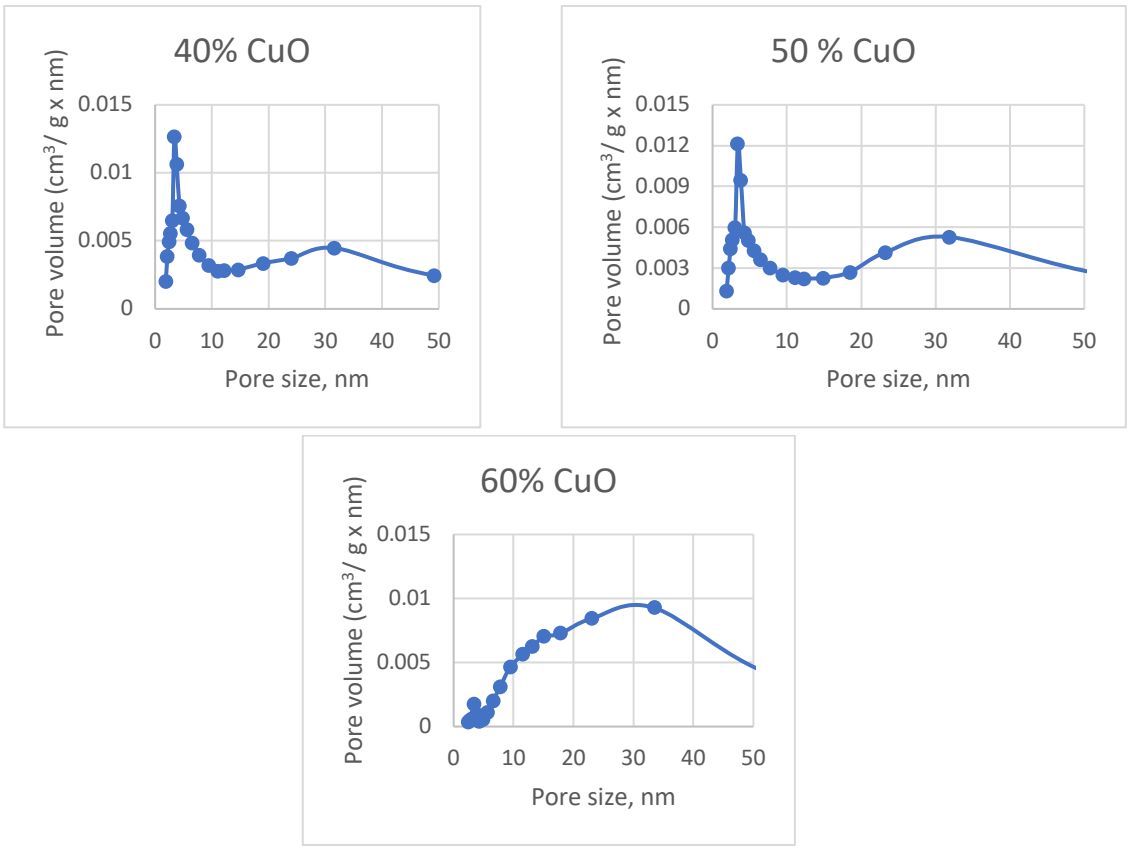

According to the work of Borovinskaya *et al*. [30], the CuO-ZnO-ZrO_2 catalysts present very similar textural and pore properties regardless of the synthesis method. In their work they investigated three different synthesis methods, which were batch coprecipitation, one pot synthesis and wet impregnation methods. However, the compositions of their catalysts were different from those employed in this work (60 wt% CuO, 30 wt% ZnO and 10 wt% ZrO_2).

From the obtained results it can be concluded that the content of CuO in the catalysts has an important effect on the textural properties of the materials, by increasing the pore size distribution with increasing CuO contents. This is in agreement with the SEM

results where the morphology of 60% CuO catalyst differs from the 40% CuO and 50% CuO catalysts.

Figure 5.7 shows the H_2-TPR profiles of the 40% CuO, 50% CuO and 60% CuO catalysts. Previous works [1], [3], [16] have shown that the single metal oxides ZnO and ZrO_2 are not reduced under the conditions applied during the H_2-TPR analysis. The reduction of ZnO is known to take place above 300ºC [31]. Therefore, it is expected that all the peaks present in these results correspond only to copper species with different sizes and also species with different reducibility that can be attributed to highly dispersed CuO interacting with ZnO and ZrO_2 at lower reduction temperatures or bulk copper at more elevated temperatures [1]. Different reduction peaks also indicate different CuO particle sizes or CuO nanoparticles in contact with ZnO [7][8]. According to previous works [31][32], the consumption of H_2 between 170–290 °C is characteristic of the reduction of Cu^{2+} to Cu^0, and smaller particles are reduced at lower temperatures while the largest particles are reduced at higher temperatures. Furthermore, other references [12], [15], [33] indicate that the increase of the reduction temperature of copper oxide is due to the formation of larger particles but can also be because of a strong interaction of copper oxide with the other metals.

As it can be seen the presented reduction profiles are not similar. The catalyst with 40% CuO presented a reduction peak at 162°C and a more symmetrical shape than the other profiles. The lower reduction temperature is an indication of a more uniform Cu particles size distribution. The catalyst with 50% CuO content exhibited a profile with a first reduction peak at 162ºC and a wide shoulder peak positioned to the higher temperatures around 170°C. The catalyst 60% CuO presented a reduction peak at temperature of 170°C with a small shoulder at 187ºC, which may be due to larger copper oxide particles that could be reduced at higher temperatures [34]. The presence of shoulders can also indicate the existence of different CuO species. As it can be observed, the reduction temperature of the catalysts increased with increasing CuO content. Easier reducibility of CuO at low temperature in the 40% CuO and 50% CuO can be explained by a higher promotion effect due to the higher relative contents of Zn and Zr. Switch of the reduction temperature to the higher values in 60% CuO indicates the presence of different CuO species or different interactions between CuO species and the support.

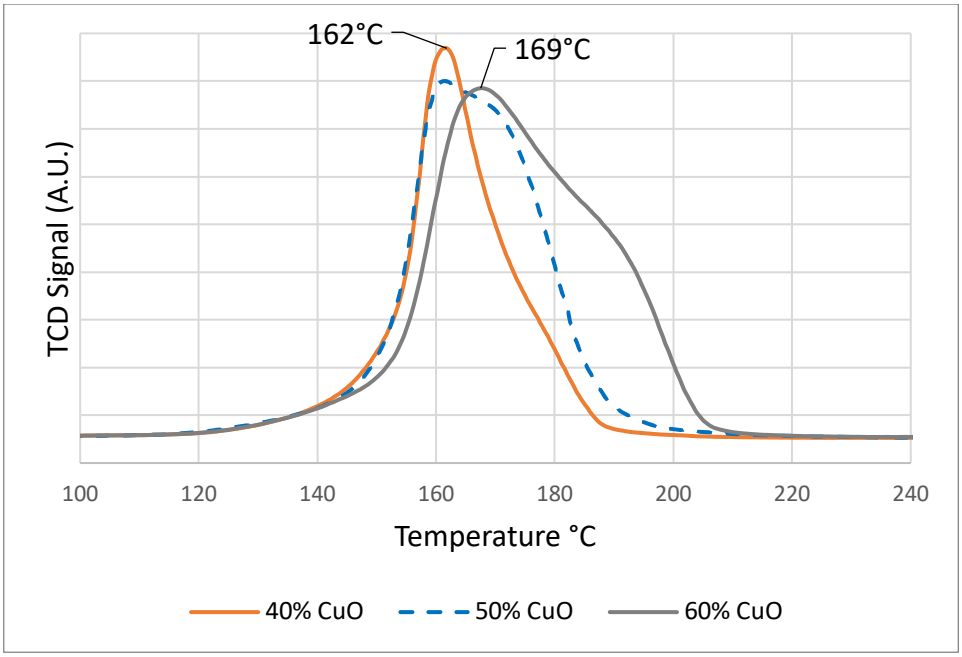

Figure 5.7 H_2-TPR of the 40, 50 and 60% CuO catalysts.

Table 5.5. shows the hydrogen consumption during the reduction of each sample in mmol of H_2 per gram of catalyst and the theoretical copper content of each catalyst in mmol of copper per gram of catalyst. The calculated CuO % of the catalysts by this approach were lower than the theoretical values. This indicates that Cu was not totally reduced and that the unreduced Cu participates in the metal-support interactions.

Table 5.5 H_2-TPR quantitative results of the catalysts 40% CuO, 50% CuO and 60% CuO.

Sample	H_2 consumption, mmol/g	Catalyst theoretical Cu content, mmol Cu/g	H_2/Cu ratio	Calculated CuO wt% of the catalyst
40% CuO	4.7	5.0	0.94	37.6
50% CuO	6.0	6.3	0.96	48.2
60% CuO	7.3	7.5	0.98	58.6

Given the asymmetric reduction profiles of the catalysts 50% CuO and 60% CuO, the TPR reduction profiles of such catalysts were deconvoluted into two different reduction peaks (Figure 5.8). The deconvolutions were done by curve fitting with a Gaussian function and it allowed the determination of the relative contents of Cu species with lower and higher reduction temperatures. These two reduction peaks in the two catalysts were named α and β. The results of the peaks deconvolution are presented in Figure 5.8 and the quantitative results in Table 5.6. This procedure allowed the calculation of the relative contents of the different copper species or different particles' size present in these two catalysts. The results indicate that the catalyst 50% CuO

presented a lower temperature reduction peak at 162ºC, corresponding to a peak area of 61% of the total area and a higher temperature reduction peak at approximately 175ºC corresponding to the remaining 39% of the total area. In the case of the catalyst 60% CuO, it presented a lower temperature reduction peak at 169ºC with an area of 70% of the total area and a higher temperature reduction peak at approximately 190ºC with the remaining 30% of the total area. These results suggest that the increasing CuO content of the catalysts causes a shift of the reduction temperatures to higher values, changing also the Cu particle size distribution. The results of the area calculations suggest that with increasing CuO content, there's a shift of the reduction temperatures to higher values, which indicates an increase in the relative amount of bigger Cu particles. This may indicate stronger metal interactions with increasing CuO content. Also, the lower relative content of supports in the 60% CuO catalyst causes a decrease in the Cu dispersion and an increase in the Cu particles size.

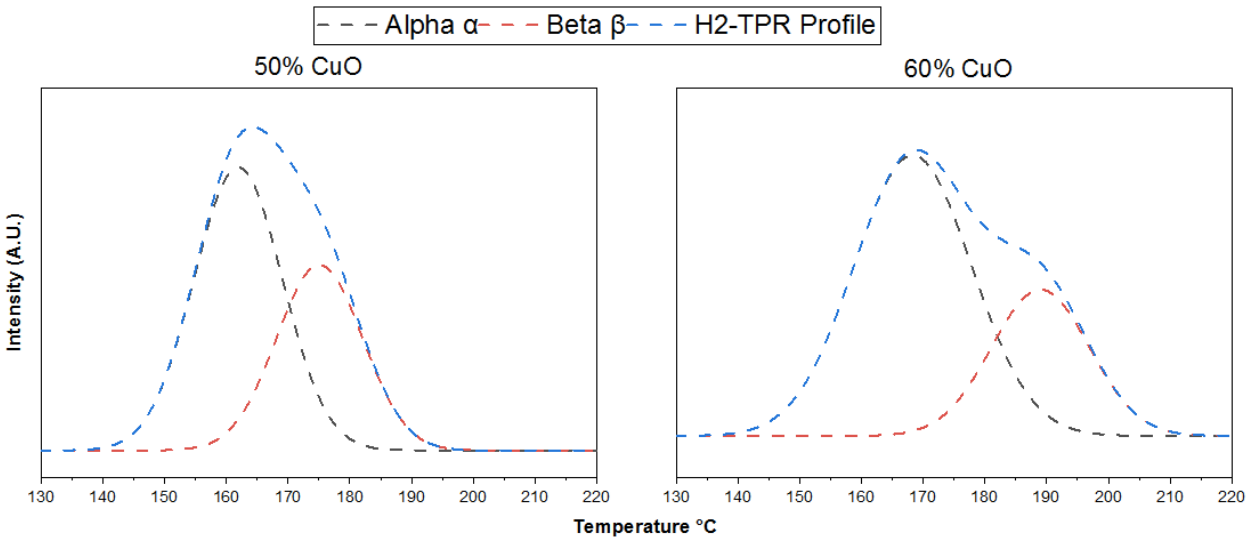

Figure 5.8 H_2-TPR peaks deconvolution of the 50% and 60% CuO catalysts

Table 5.6 Deconvolution peaks areas of the catalyst 50% CuO and 60% CuO.

50% CuO			
Peak	**Temperature ºC**	**Area**	**Percentage**
α	162	117.6	61
β	175	74.9	39
	Total	192.5	100
60% CuO			
Peak	**Temperature ºC**	**Area**	**Percentage**
α	169	172.2	70
β	190	74.7	30
	Total	246.8	100

The results of the N_2O surface reaction analysis are presented in Table 5.7. The catalysts 40% CuO and 50% CuO presented similar metallic copper surface areas (i.e.

9.6 and 9.3 m^2/g respectively), while the catalyst 60% CuO presented the highest metallic copper surface area (i.e. 12.5 m^2/g) of the three catalysts. The higher concentration of CuO present in the 60% CuO catalyst and the presence of malachite and aurichalcite in the precursor explain the higher Cu surface area of this catalyst. The higher CuO content of the catalyst 60% CuO is responsible for the higher amount of Cu available to be dispersed on the surface of the catalyst. The comparison of the Cu^0 particle sizes obtained by N_2O surface reaction analysis and the crystallite sizes obtained by XRD is shown in Table 5.7. These results show that the Cu particles of the 40% CuO, 50% CuO and 60% CuO catalysts are composed of an agglomeration of several CuO crystallites, approximately 2, 2.6 and 2.1 CuO crystallites, respectively. These results indicate stronger metal-support interactions of the catalysts 40% CuO and 60% CuO.

Table 5.7. N_2O surface reaction results of the catalysts with different CuO contents.

Sample	Copper surface area m^2/g	Copper dispersion	Copper particle size nm	N_2O/XRD ratio[1]
40% CuO	9.6	4.6	22.3	2.0 (11 nm)
50% CuO	9.3	3.6	28.8	2.6 (11 nm)
60% CuO	12.5	4.0	25.7	2.1 (12 nm)

[1] Ratio of the Cu particle size obtained by N_2O surface reaction analysis to the CuO crystallite size obtained by XRD. The values in parentheses are the CuO crystallite sizes obtained by XRD.

5.2.2. Catalytic tests results

The H_2 and CO_2 conversions as well as the methanol selectivity and the methanol productivity obtained over the 40% CuO, 50% CuO and 60% CuO catalysts are presented in Figure 5.9 and Table 5.8. It was discovered that between 240ºC and 300ºC, the H_2 conversion (Figure 5.9a) is higher for the 60% CuO catalyst, followed by the 40% CuO and the 50% CuO catalysts. At temperatures higher than 300°C the H_2 conversion values decrease for all the samples due to the thermodynamic limitations reached. Regarding the CO_2 conversions (Figure 5.9b), it was shown that the 3 catalysts present an increasing tendency with respect to the reaction temperature. The reason of this behavior can be explained by the increasing production of methanol but also an increasing production of carbon monoxide at higher temperatures due to the RWGS reaction, which produces CO and H_2O from CO_2 and H_2. Such results are in agreement with other works in the literature [6]. The CO_2 conversion values are the highest for the 60% CuO catalyst followed by the 40% CuO and 50% CuO catalysts which follows the same trend as found for the H_2 conversion. This can be explained by different properties of the catalyst 60% CuO, including its higher Cu surface area and the presence of aurichalcite and malachite, which can originate stronger Cu-Zn interactions and consequently higher catalytic activity. The higher Cu surface area of the catalyst 60% CuO gives it more active sites for the

adsorption of H_2 and for its dissociation [35] which causes a promotion of the catalytic activity. Also, the higher content of CuO in the 60% CuO catalyst can cause an increase in the formation of Cu-support interface, which can improve the catalytic activity due to the higher amount of active sites available for the splitting of H_2 and for the adsorption of CO_2. Moreover, the lower degree of crystallinity (i.e. 36.4%) of this catalyst may be a contributing factor to the improved catalytic activity, as demonstrated in Chapter 4. Previously it was explained that the presence of amorphous ZrO_2 has a promoting effect on the catalytic activity of the methanol production reaction, compared to other crystalline forms, such as monoclinic or tetragonal ZrO_2 [36], which were not formed under the conditions employed in the microfluidic synthesis.

In contrast, the catalyst 50% CuO, presented the highest Cu particle size corresponding to 28.8 nm and the lowest Cu surface area as calculated by the N_2O surface reaction analysis which can explain the lower reactant conversions of this catalyst.

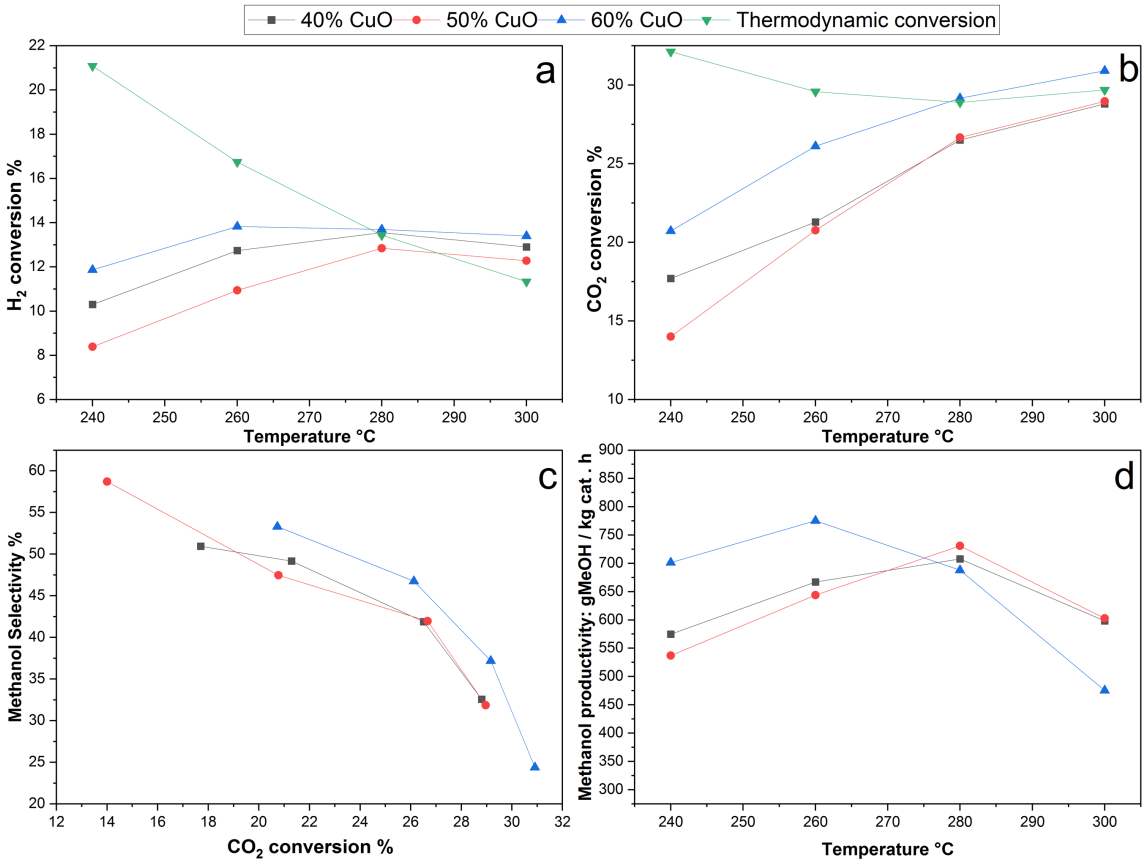

Figure 5.9 Catalytic performance of the catalysts 40% CuO, 50% CuO and 60% CuO. (a) H_2 conversion, (b) CO_2 conversion, (c) methanol selectivity against CO_2 conversion % and (d) methanol productivity. P: 50bar, GHSV: 24000Nml h^{-1} g^{-1}, molar ratio H_2/CO_2: 3.9.

Regarding the methanol selectivity, all the catalysts presented the expected decrease of methanol selectivity with increasing temperatures due to the occurrence of the RWGS reaction [6][37].

The methanol productivity of the catalysts is shown in Figure 5.9d. At the lowest studied temperature 240ºC, the methanol productivity was the highest for the 60% CuO catalyst, followed by 40% CuO and 50% CuO catalysts. At 260ºC the catalyst 60% CuO presented a maximum productivity value of 775 g CH_3OH kg_{cat}^{-1} h^{-1}, which makes it the catalyst with the highest methanol productivity of the three catalysts under study. At higher temperatures it seems that the thermodynamic limitations were reached and the productivity of the 60% CuO presented a noticeable decrease while the increasing trend in productivity of the 40% CuO and 50%CuO catalysts was maintained until a temperature of 280ºC, where the catalysts with the highest productivity became 50% CuO and 40% CuO. The gap in productivities was more noticeable at 300ºC, where the 40% CuO and 50% CuO catalysts presented a small decrease, while the productivity of the 60% CuO sample presented a considerable drop in productivity. This drop can be explained by the CO_2 conversion reaching the thermodynamic limitation and by the drop in the methanol selectivity at 300ºC. At this temperature, the catalyst 60% CuO presented the highest CO_2 conversion and the lowest methanol selectivity, indicating that CO was produced along with water from the RWGS reaction. The presence of water can increase the sintering of the active sites of the catalyst, which can lead to the loss of catalytic activity [37]. So, it is possible that at this temperature the catalyst suffered a degradation due to the conditions explained above.

Table 5.8 Catalytic tests results of the 40, 50 and 60% CuO catalysts. P: 50bar, GHSV: 24000Nml h^{-1} g^{-1}, molar ratio H_2/CO_2: 3.9.

Catalyst	Temperature ºC	H_2 Conversion %	CO_2 Conversion %	Methanol selectivity %	Methanol productivity g CH_3OH/(kg of catalyst x hour)
40% CuO	240	10.3	17.7	50.9	575
	260	12.7	21.3	49.1	667
	280	13.5	26.5	41.8	708
	300	12.9	28.8	32.5	598
50% CuO	240	8.4	14.0	58.7	537
	260	10.9	20.7	47.4	644
	280	12.8	26.6	41.9	731
	300	12.3	28.9	31.8	603
60% CuO	240	11.9	20.7	53.3	701
	260	13.8	26.1	46.7	775
	280	13.7	29.1	37.2	688
	300	13.4	30.9	24.4	476

To summarize, the catalyst 60% CuO presented the highest H_2 and CO_2 conversions along with high methanol productivity at lower temperatures, which can be attributed to the higher Cu surface area of this catalyst and also to the presence of both malachite and aurichalcite in the precursor. The presence of these two phases has been linked

to stronger Cu-Zn and Cu-support interactions, increasing the activity of the catalysts and improving catalyst properties such as the Cu surface area and the Cu dispersion. The microfluidic technique allowed the production of catalysts with improved properties compared to catalysts prepared by other synthesis methods such as batch, as was presented in Chapter 3.

5.2.3. Catalyst stability tests

The catalysts stability was investigated by comparing the crystalline structure of the samples before and after the catalytic tests, as shown in Figure 5.10 and Table 5.9, and by analyzing the CO_2 conversion for the duration of the catalytic tests, as shown in Figure 5.11.

The 40% CuO and 50% CuO catalysts developed a crystalline Cu phase as a consequence of the reduction treatment applied to the catalysts before the catalytic tests. After the catalytic tests, the catalyst 40% CuO presented small peaks corresponding to the presence of a crystalline phase of CuO, which can be explained by the oxidation of the catalyst when recovering it from the reactor. This catalyst also presented a diffraction peak indicating the presence of metallic Cu formed during the reduction of the catalyst. In the case of the catalyst 50% CuO an important peak of Cu was detected, indicating a bigger crystallite size compared to the 40% CuO catalyst. No CuO crystalline phase was detected in the catalyst 50% CuO after the catalytic tests.

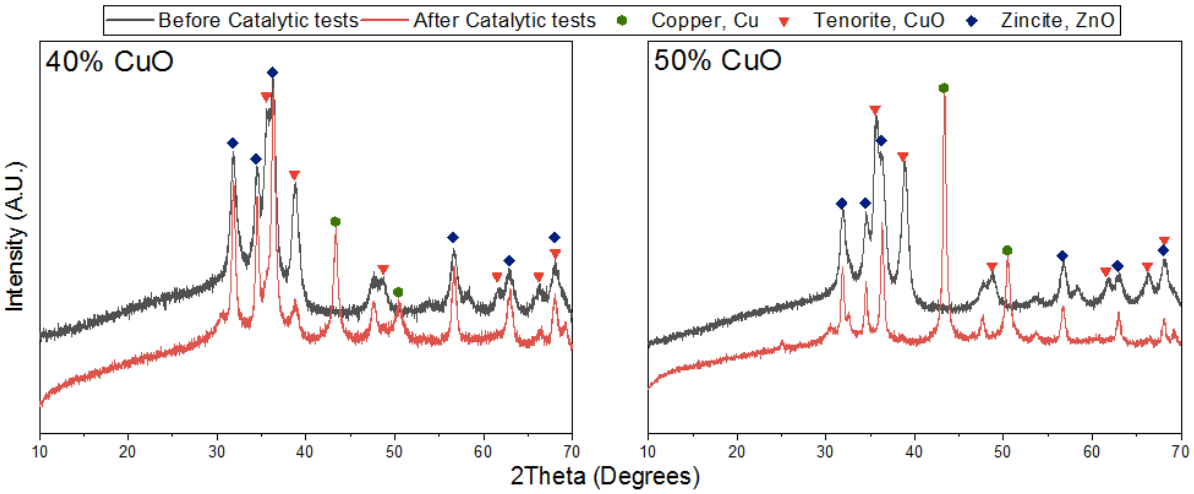

Figure 5.10 X-ray diffractograms of the catalysts 40% CuO and 50% CuO before and after the catalytic tests.

The crystallite sizes calculated by Scherrer's equation are presented in Table 5.9. The 2Theta values used for the calculation of the Cu (PDF number: 04-0836) crystallite sizes was 43.3º (hkl: 111). As can be observed, the Cu crystallite sizes after reduction and before the catalytic tests were 8.3 and 12nm for the catalysts 40% CuO and 50% CuO, respectively, indicating that the increasing CuO content of the catalysts causes an increase in the size of the reduced Cu crystallites. Moreover, the size of the Cu

crystallites after the catalytic tests increased with increasing CuO content of the catalyst, going from a value of 13 nm for the 40% CuO catalyst to 17 nm for the 50% CuO catalyst. This suggests that the Cu crystallites suffer more from sintering in catalysts with higher Cu contents and consequently with lower Zn and Zr relative contents, indicating that the stabilization effect of the support decreased due to the lower content of support in the 50% CuO catalyst.

Table 5.9 Crystallite sizes (nm) of the Cu, CuO and ZnO phases before and after catalytic tests.

Sample	Copper, Cu		Tenorite, CuO		Zincite, ZnO	
	Before	After	Before	After	Before	After
40% CuO	8.3	13	11	14	11	18
50% CuO	12	17	11	-	11	17

The crystallite sizes of the CuO and ZnO phases of the 40% CuO and 50% CuO catalysts also presented an increase after the catalytic tests. The cause of this increase in crystallite sizes may be due to the reduction and the exposition of the catalysts to high temperatures for long reaction times, as well as the exposure to water, which may cause sintering of the CuO and ZnO crystallites [2], [37], [38], as explained in Chapter 4.

The stability of the catalysts was also assessed by analyzing the CO_2 conversions of the catalysts with respect to time, as presented in Figure 5.11. A linear regression was done to each of the reaction temperature points to determine if the slope of the trendline was negative or positive. Most of these curves indicate that there was a decrease in the CO_2 conversions at low temperatures with increasing time, which can be attributed to the deactivation of the catalysts. The occurrence of positive trendlines at high temperatures indicate an increase of the CO_2 conversion due to the increased production of CO by the RWGS reaction, causing a decrease in the methanol selectivity. As discussed before, the presence of water at high temperatures and high conversions can cause the sintering and agglomeration of Cu and ZnO, causing a loss in the Cu surface area and possibly blocking the access of the reactants to the active sites. These results show that the CO_2 conversions presented a decrease during the time of reaction and that the degradation of the catalysts was more noticeable at higher temperatures, as evidenced by the increase in the CO_2 conversion, which indicates an increasing production of CO. As suggested in Chapter 4, the use of analysis techniques such as XPS, TEM, and elemental mapping by TEM-EDS or SEM-EDS before and after the catalytic tests would complement the studies about the deactivation of the catalysts, and offer more information about the exact mechanisms that cause the loss of catalytic activity.

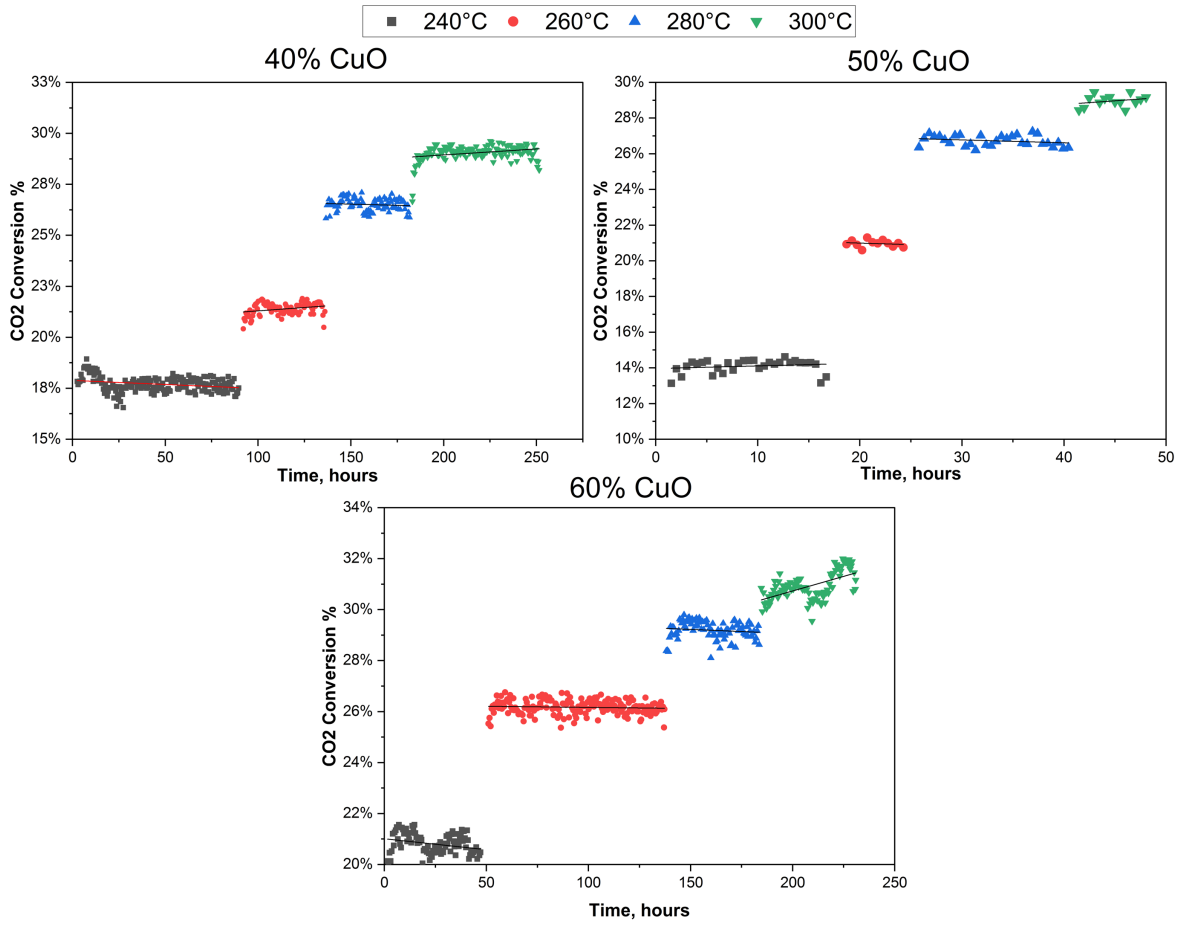

Figure 5.11 CO_2 conversion versus time on stream of the 40, 50 and 60% CuO catalysts. P: 50bar, GHSV: 24000Nml h^{-1} g^{-1}, molar ratio H_2/CO_2: 3.9.

5.2.4. Conclusions

Three catalysts with different CuO contents were synthesized with a microfluidic device and analyzed by different characterization techniques. Their catalytic performance in methanol synthesis from CO_2 was investigated in temperature range of 240 to 300ºC at a reaction pressure of 50 bar.

The characterization of the catalysts showed that the CuO content of the catalysts influenced the formation of crystalline phases in the precursors but didn't have significant effects on the crystallite sizes of the CuO and ZnO phases after calcination. Moreover, the increasing content of CuO didn't cause changes in the specific surface area of the catalysts, but caused differences in the pore size distribution and on the morphology of the catalysts as evidenced in the N_2-physisorption and SEM analysis results. There were also differences in the Cu surface area and the reducibility of the catalysts, indicating that the increasing CuO content caused an increase in the Cu surface area, given the higher content of Cu available for dispersion on the surface of the catalyst. The catalyst 60% CuO presented the highest CO_2 conversions and methanol productivity, which was associated with its higher Cu surface area and due

to the formation of malachite and aurichalcite phases during the catalyst synthesis step, which allows a close contact between the metal species of the catalyst and consequently stronger metal-support interactions.

5.3. Effect of the addition of CeO_2 to Cu-ZnO-ZrO_2 catalysts prepared by the microfluidic method

The use of CeO_2 as a promoter of Cu-ZnO-ZrO_2 catalysts for the hydrogenation of CO_2 to methanol seems like a good alternative to develop a catalyst with improved properties and better catalytic performance, given the positive effects of CeO_2 reported in the literature [39]–[45]. Furthermore, no Cu based catalysts containing CeO_2 prepared by the microfluidic method have been reported before. The aim of this work is to investigate the effect of the addition of CeO_2 to Cu-ZnO-ZrO_2 catalysts synthesized by the microfluidic method on the properties and performance of the catalysts.

Two CeO_2 containing catalysts named CuO 50 CeO_2 10-0h and CuO 50 CeO_2 10-0h-65 were prepared and their properties and catalytic performance were compared to those of the catalyst CuO 50-0h containing no CeO_2. The catalyst CuO 50 CeO_2 10-0h was prepared with a coprecipitation step at ambient temperature, while the coprecipitation temperature of the catalyst CuO 50 CeO_2 10-0h-65 was 65ºC. The following section presents the characterization results and discussion.

5.3.1. Catalysts characterization results and discussion

The X-ray diffractograms of the three catalyst precursors of this work were not presented because the results showed that they were all amorphous. This can be attributed to the zero aging time of these materials, as previously it was shown that increasing the aging time improves the crystallinity of the materials. Despite the above, after the calcination step, the three catalysts developed a crystalline structure consisting mainly of CuO (PDF number: 72-0629) and ZnO (PDF number: 75-1526). The X-ray diffractograms of the catalysts after the calcination are presented in Figure 5.12. No peaks associated with the presence ZrO_2 or CeO_2 (PDF number: 34-0394) were detected, indicating that these phases were present in an amorphous state or under the detection limits.

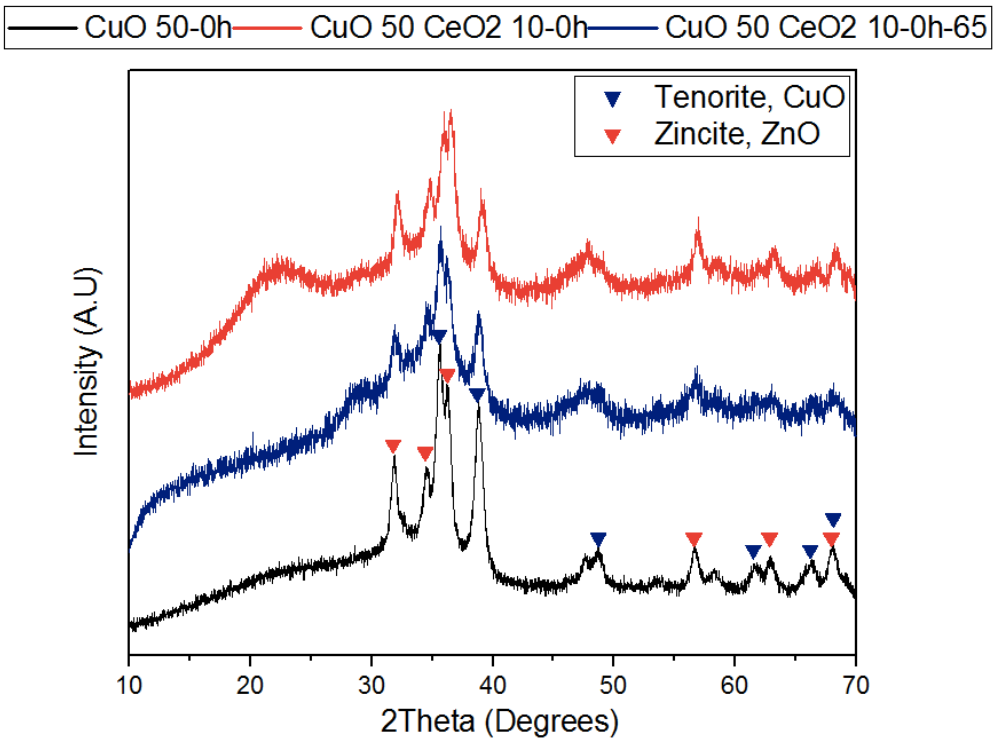

Figure 5.12 X-ray diffractograms of the ceria containing catalysts and the CuO 50-0h catalyst.

Using Scherrer's equation, the crystallite sizes of the identified phases were calculated and are shown in Table 5.10. As can be seen, the crystallite sizes of the CuO and ZnO didn't present considerable differences, with an average crystallite size of 12nm for the three catalysts. These results indicate that the replacement of some ZrO_2 by CeO_2 didn't affect the crystallinity of the catalysts and also that a higher coprecipitation temperature didn't have an important on the crystalline structure of the catalyst CuO 50 CeO_2 10-0h-65.

Table 5.10 Crystallite sizes (nm) of the phases present in the ceria containing and the CuO 50-0h calcined catalysts.

Catalyst	Tenorite, CuO	Zincite, ZnO	Ceria, CeO_2
CuO 50-0h	12	12	-
CuO 50 CeO_2 10-0h	13	12	ND
CuO 50 CeO_2 10-0h-65	12	14	ND

ND: Not detected

Figure 5.13 shows the mass loss and the mass loss derivatives of the three catalyst precursors of this study. The results show that the mass loss % curves and their respective derivatives were rather similar, indicating a similar thermal decomposition profile and consequently a good and homogeneous CeO_2 incorporation in the material. The final mass loss % was 25, 21 and 20 % for the catalysts CuO 50 CeO_2 10-0h, CuO 50-0h and CuO 50 CeO_2 10-0h-65, respectively. As already discussed, the XRD

results showed that the three precursors didn't develop crystalline phases such as aurichalcite, hydrozincite, malachite etc., which explains the absence of certain decomposition peaks in the results of the TGA. However, the derivatives of the mass loss % of the three precursors showed peaks around 150ºC and 500ºC. As discussed previously, the peak present around 150ºC might correspond to the decomposition of a Zr-based species and to the decomposition of the Cu-Zn precursor present in an amorphous state [9]. The conversion of the hydroxycarbonates to oxides explain the peaks obtained around 500ºC as explained before in the work of Yurieva *et al*. [14]. Also, as previously discussed, the work of L'hospital [9] indicated that a Cu-Zn precursor presents a decomposition peak at 466ºC, while a Cu-Zn-Zr precursor also presents a decomposition peak at 492ºC, which explains the peak close to 500ºC. In addition, Heidari *et al*. [46] investigated the thermal decomposition of cerium (III) carbonate prepared by the precipitation of cerium nitrate hexahydrate with sodium carbonate, as it was done in the present work. The results of the TGA analysis done to their material showed that it presented a moderate thermal decomposition between 50ºC and 250ºC with a mass loss of approximately 5% and a more important thermal decomposition between 250ºC and 300ºC of approximately 23%. These temperature peaks in the derivative curves are not evident, probably due to the low content of CeO_2 in the catalysts investigated.

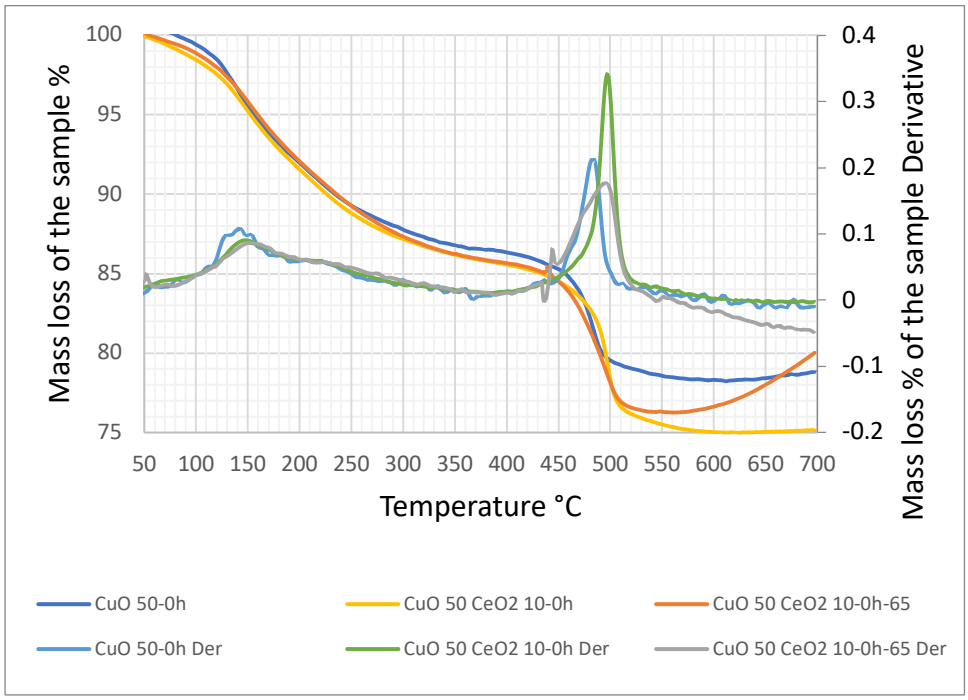

Figure 5.13 TGA results of the precursors under study. Der: Derivative.

The N_2 adsorption and desorption isotherms of the three catalysts are presented in Figure 5.14. As in the case of previously analyzed catalysts in this work, the isotherms were of type IV indicating a mesoporous structure with cylindrical shaped pores with a hysteresis loop of type 3, which is characteristic of layered solids of plate like particles with narrow pore networks with slit shapes [30], [47].

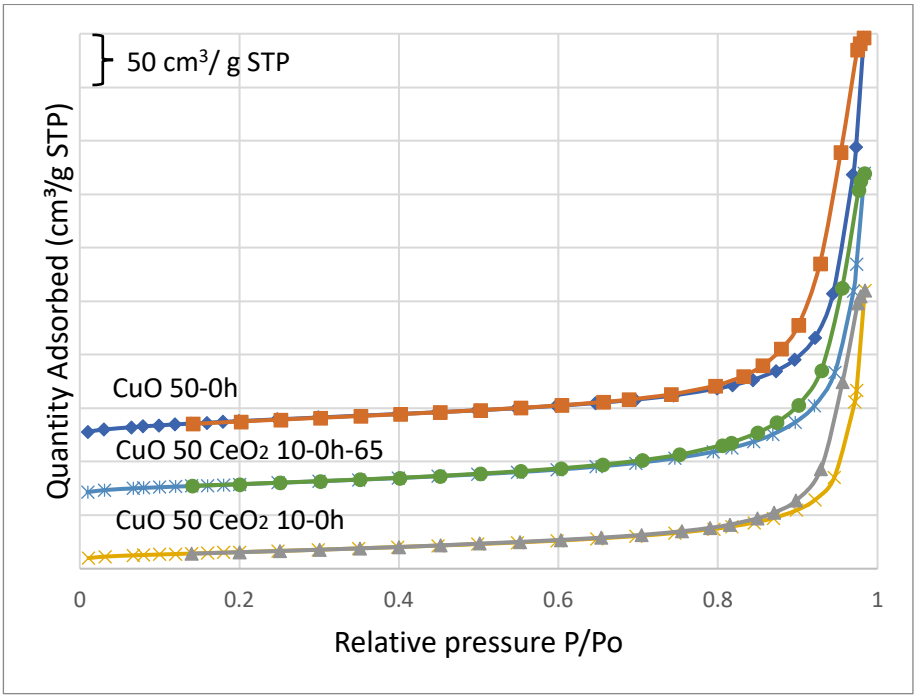

Figure 5.14 N_2-physisorption isotherms of the CeO_2 containing catalysts and the CuO 50-0h catalyst.

Table 5.11 shows the results of the surface area, pore volume and pore size of the three catalysts investigated in this work. As can be appreciated, the replacement of some zirconia by ceria observed in the catalysts CuO 50-0h and CuO 50 CeO_2 10-0h caused an important reduction in the specific surface area and in the pore volume of the catalysts (from 70 m^2/g to 55 m^2/g and from 0.38 cm^3/g to 0.24 cm^3/g). The reduction in the surface area can cause a decrease in the catalytic activity of the material due to the consequent reduction in the active metal surface area and possibly on the amount of basic sites available for the CO_2 chemisorption. These findings are in agreement with the work of Bonura *et al*. [48], who synthesized Cu based catalysts using CeO_2 as a promoter and obtained a decrease in the specific and Cu surface areas of the catalyst. The N_2-physisorption characterization results in the work of Hu *et al*. [49] also showed that a catalyst made up of 50% Cu and 50% Zn presented a higher specific surface area (i.e. 79 m^2/g) than a catalyst composed of 50% Cu and 50% Ce (i.e. 39 m^2/g). Their catalysts were synthesized by coprecipitation of metal nitrates with sodium carbonate, as in the case of this work. The results of this work and some of the reviewed references [48][49] clearly show that CeO_2 addition causes a reduction in the specific surface area and the Cu surface area of Cu-based catalysts. This may be due to the morphology of the CeO_2, which was amorphous in this work. The work of Khobragade *et al*. [50] showed that the morphology of CeO_2 can affect different properties of the catalysts including the specific surface area. In addition, the catalyst CuO 50 CeO_2 10-0h-65 presented a specific surface area close to that of the CuO 50-0h catalyst, which indicates that a higher coprecipitation temperature has a positive effect on the textural properties of the catalyst, possibly due to the increased kinetics of precipitation and nucleation of the reactants which can increase the interactions between the metal species.

Table 5.11 N_2-physisorption surface area, pore volume and pore size of the catalysts under study.

Sample	BET surface area (m^2/g)	Pore volume (cm^3/g)	Pore size (nm)
CuO 50-0h	70	0.38	24
CuO 50 CeO_2 10-0h	55	0.24	3 and 34
CuO 50 CeO_2 10-0h-65	68	0.30	12 and 34

Figure 5.15 shows the pore size distribution graphs (BJH desorption branch) of the three catalysts investigated in this section. The results show that both catalysts containing CeO_2 presented a complex pore size distribution containing mesopores between 3 and 34nm, while the catalyst CuO 50-0h presented a monomodal pore size distribution with mesopores of 24nm.

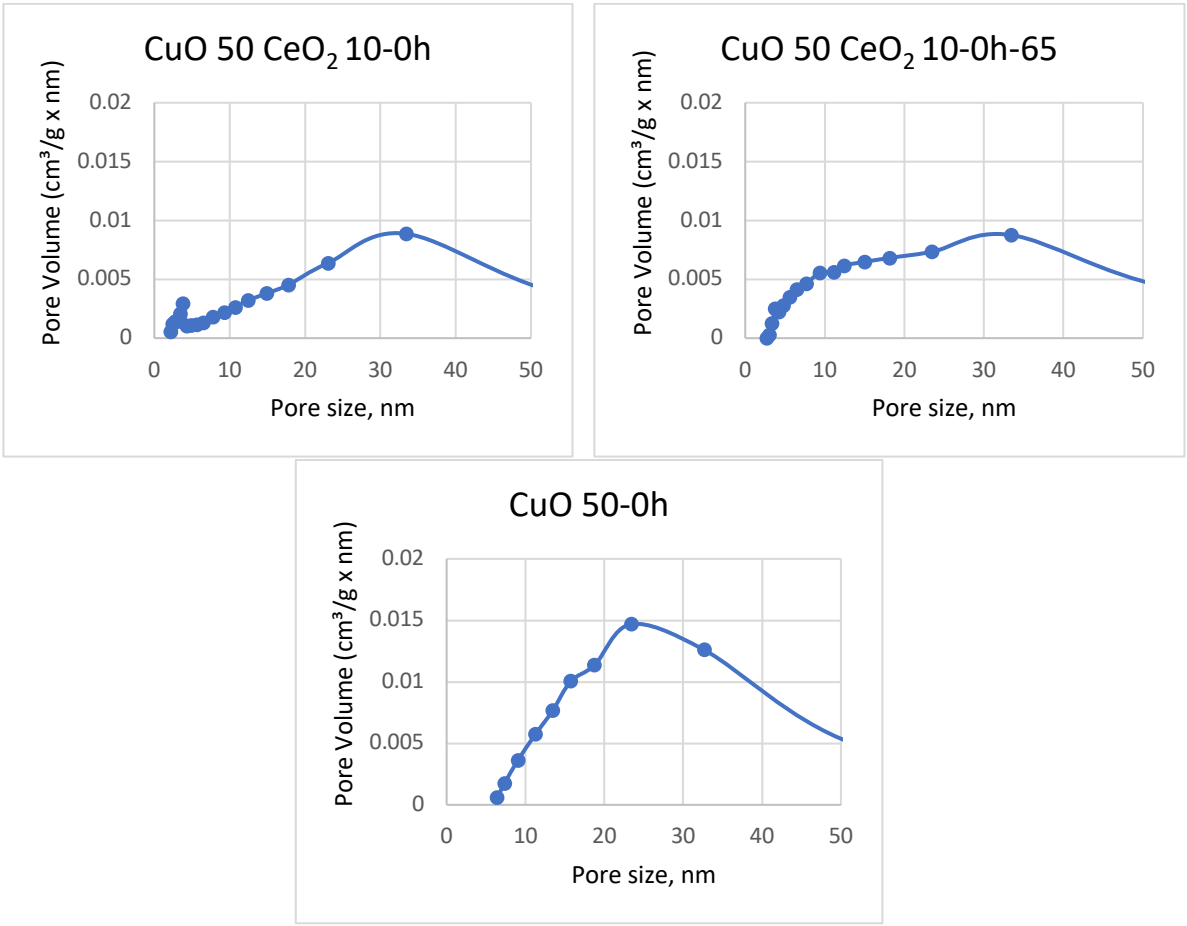

Figure 5.15 BJH pore size distribution of the CuO 50-0h, CuO 50 CeO_2 10-0h and CuO 50 CeO_2 10-0h-65 catalysts.

Figure 5.16 shows the results of the CO_2-TPD analysis for the investigation of the surface basicity of the catalysts CuO 50 CeO_2 10-0h and the CuO 50-0h catalyst. The results show that the addition of ceria caused a change in the surface basicity of the catalyst and in the quantity of strong basic sites. This resulted in a decrease of the

strength of the basic sites, which caused a shift of the peak from a CO_2 desorption temperature of 620ºC in the CuO 50-0h catalyst, to a CO_2 desorption temperature of approximately 500ºC for the catalyst with ceria. This indicates that the replacement of zirconia by ceria in the catalyst causes a change in the surface basicity of the material. More precisely, the replacement of some zirconia by ceria caused a reduction in the strength of the basic sites.

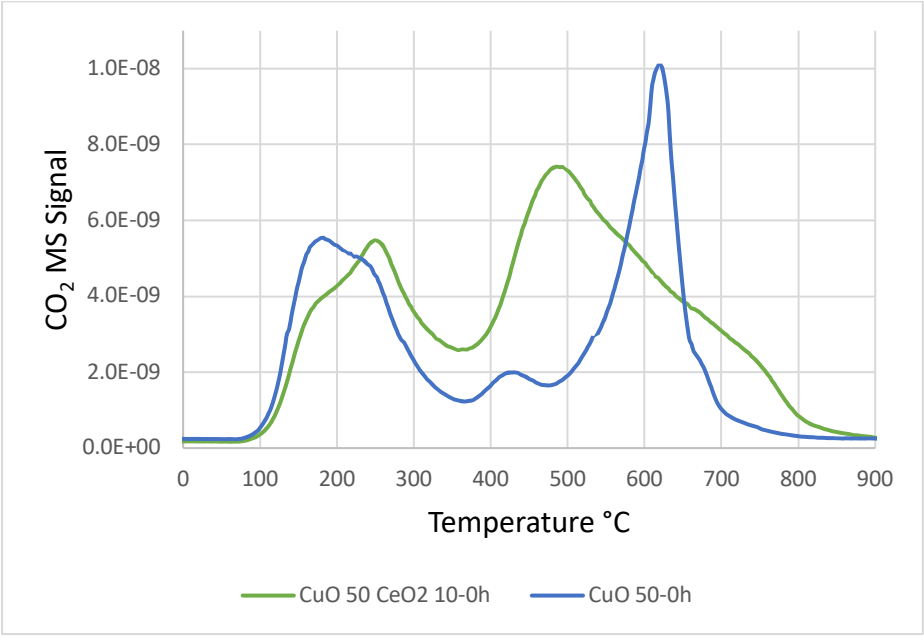

Figure 5.16 CO_2-TPD profiles of the CuO 50 CeO_2 10-0h and the CuO 50-0h catalysts.

Shi *et al*. [51] prepared Cu-Ce, Cu-Zr and Cu-Ce-Zr catalysts by metal nitrates coprecipitation with sodium carbonate and analyzed them with CO_2-TPD analysis. Their results showed that the Cu-Zr catalyst presented a considerable CO_2 desorption peak at approximately 600ºC, corresponding to a strong basic site while the Cu-Ce catalyst presented a smaller peak at the same temperature. This indicates that the strong basic sites are formed preferentially due to the presence of Zr under the conditions of this work and it explains the CO_2 desorption peak shift to a lower temperature occurring in these catalysts. In the work of Khobragade *et al*. [50], the Pd supported on Ce catalysts with the highest surface basicity presented the best catalytic performance for the hydrogenation of CO_2 to methanol, while the catalyst with the lowest surface basicity presented the lowest catalytic performance. In addition, the work of Singh *et al*. [52] suggests that the presence of strong basic sites is favorable for the catalytic activity because the adsorption of CO_2 on these sites occurs as unidentate carbonate species, which produces methanol through the formate pathway [53].

The quantitative results of the basic sites investigation are presented in Table 5.12. The data in this table shows that the catalyst containing CeO_2 presented a higher quantity of total basic sites compared to the CuO 50-0h catalyst. However, as discussed above, the catalyst containing CeO_2 presented less strong basic sites due

to the shift of the CO_2 desorption temperature to a lower value. As mentioned above, ZrO_2 has a higher affinity for CO_2 than CeO_2 [51], which can be appreciated in the higher amount of strong basic sites of the catalyst CuO 50-0h.

Table 5.12 Quantity of weak, moderate strength and strong basic sites and basic sites per unit surface area of the CuO 50-0h and CuO 50 CeO_2 10-0h catalysts.

Sample	Weak basic sites (μmol/g)	Moderate strength basic sites (μmol/g)	Strong basic sites (μmol/g)	Total basic sites (μmol/g)	Basic sites per unit surface area (μmol/m^2)
CuO 50-0h	100.0	20.0	110.0	230.0	3.28
CuO 50 CeO_2 10-0h	110.0	190.0	40.0	340.0	6.18

The results of the H_2-TPR analysis of the two catalysts containing CeO_2 and the CuO 50-0h catalyst are shown in Figure 5.17 and the quantitative results are presented in Table 5.13. The reduction profiles (Figure 5.17) indicate that the catalysts CuO 50 CeO_2 10-0h and CuO 50 CeO_2 10-0h-65 presented a lower reduction temperature (i.e. 153 and 160ºC, respectively) compared to the catalyst CuO 50-0h (i.e. 169ºC). Previous works have shown that the presence of CeO_2 can improve the reducibility of finely dispersed CuO, causing a decrease in the reduction temperature [43]. In fact, the work of Shi *et al*. [51] showed that the Cu based catalysts containing CeO_2 they prepared, presented a lower reduction temperature compared to the catalyst without this oxide. The profiles of the CeO_2 containing catalysts (Figure 5.17) also presented a more uniform and symmetrical shape, which may indicate a more uniform Cu particle size distribution. In contrast, the CuO 50-0h catalyst presented a small shoulder around 178ºC. A previous research work [54] indicates that different CuO species have been identified in ceria containing catalysts, including finely dispersed CuO, bulk CuO and Cu inside a CeO_2 lattice. The reduction temperature of ceria is approximately 327ºC [31], [55], which means that in this case, all the reduction peaks corresponded to the reduction of only CuO, given that the H_2-TPR was done with a maximum temperature of 280ºC. Despite the above, it is possible that some CeO_2 was reduced in a small proportion, which explains the results of CuO contents of the catalysts greater than 50%, as shown in Table 5.13.

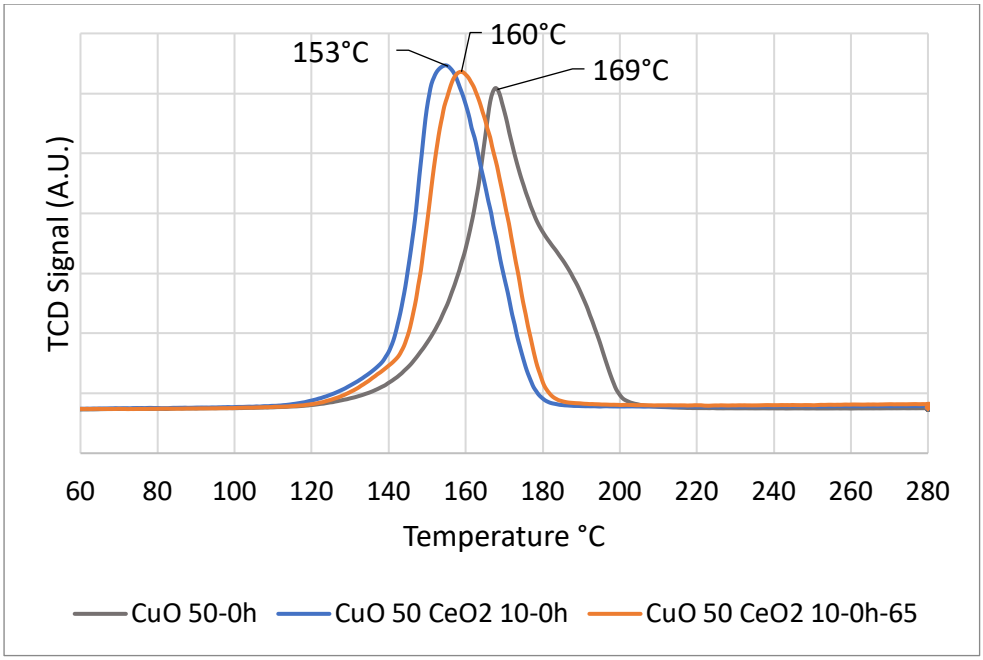

Figure 5.17 H_2-TPR profiles of the catalysts under study.

The calculated CuO contents of the CuO 50 CeO_2 10-0h and CuO 50 CeO_2 10-0h-65 catalysts with the H_2 consumed during the H_2-TPR analysis were close to the theoretical composition, with a difference of only 4.6% and 6.8%, respectively, which indicates an adequate precipitation of the Cu species.

Table 5.13 H_2-TPR quantitative results of the CeO_2 containing catalysts and the Cu 50-0h catalyst.

Sample	H_2 consumption, mmol/g	Catalyst theoretical Cu content, mmol Cu/g	H_2/Cu ratio	Calculated CuO wt% of the catalyst
CuO 50-0h	6.21	6.29	0.99	49.4
CuO 50 CeO_2 10-0h	6.57	6.29	1.04	52.3
CuO 50 CeO_2 10-0h-65	6.70	6.29	1.06	53.4

The copper surface area, copper dispersion % and copper particle size were determined by the N_2O surface reaction technique for the catalysts containing CeO_2 and the CuO 50-0h catalyst. The results presented in Table 5.14 show that both catalysts containing CeO_2 presented a lower Cu surface area (i.e. 10.7 and 9.2 m^2/g) compared to the CuO 50-0h catalyst (i.e. 17 m^2/g). These results indicate that the addition of ceria was not beneficial from the point of view of the active metal surface area. The reason of this behavior may be because of the amorphous character of the ceria in the present work.

As mentioned previously, the morphology of CeO_2 has an important effect on catalyst properties such as the specific surface area and on the catalytic activity, due to the different exposed crystalline planes [50]. It is possible that the presence of amorphous

CeO_2 covered the Cu particles causing a reduction in the Cu surface area and blocking the access of H_2 to the Cu active sites. This idea could be investigated more deeply by the use of analysis techniques such as TEM coupled with EDS to study the metal interactions at a nanometer scale and with XPS to study the surface composition of the catalysts.

Another reason explaining the decrease of the Cu surface area is the replacement of 10.2% ZrO_2 by CeO_2 in the CeO_2 containing catalysts. The work of Bonura *et al*. [48] showed that for catalysts synthesized by metal nitrates coprecipitation, as in the present work, the specific surface area and the copper surface area decrease with increasing CeO_2 content of the catalyst.

Table 5.14 N_2O surface reaction results of the CeO_2 containing catalysts and the CuO 50-0h catalyst.

Sample	Copper surface area m^2/g	Copper dispersion %	Copper particle size nm
CuO 50-0h	17.0	6.5	15.8
CuO 50 CeO_2 10-0h	10.7	4.1	25.0
CuO 50 CeO_2 10-0h-65	9.2	3.5	29.4

In addition, the Cu particle sizes determined by the N_2O surface reaction technique were higher for the catalysts containing ceria compared to the CuO 50-0h catalyst. The presence of amorphous CeO_2 could also reduce the promoting effects of ZnO and ZrO_2, causing a growth of the Cu particles. The size of the Cu nanoparticles can affect importantly the catalytic performance of the catalysts for the CO_2 hydrogenation to methanol [55]. These results suggest that the ceria present in the Cu-containing catalysts did not only help the reduction of copper but also increased the copper particle size creating almost twice bigger active copper particles comparing to the material without CeO_2.

The results obtained indicate that the microfluidic synthesis of CuO-ZnO-ZrO_2 catalysts is not compatible with addition of CeO_2, as the addition of this oxide to the catalysts caused a decrease in the Cu surface area, in the Cu dispersion and an increase in the Cu particle size, which is in contradiction with some of the investigated literature [56]. The conditions applied during the microfluidic synthesis didn't allow the formation of desirable nanocrystalline phases of CeO_2, giving only amorphous CeO_2. This could possibly be addressed by including an aging step after the synthesis of the catalyst precursors by the microfluidic method, by increasing the residence time of the precipitate during the catalyst synthesis or by preparing the CeO_2 support separately under different conditions.

5.3.2. Catalytic tests results

The catalytic tests results including the H_2 and CO_2 conversions, the methanol selectivity against the CO_2 conversion and the methanol productivity are presented in Figure 5.18 and in Table 5.15.

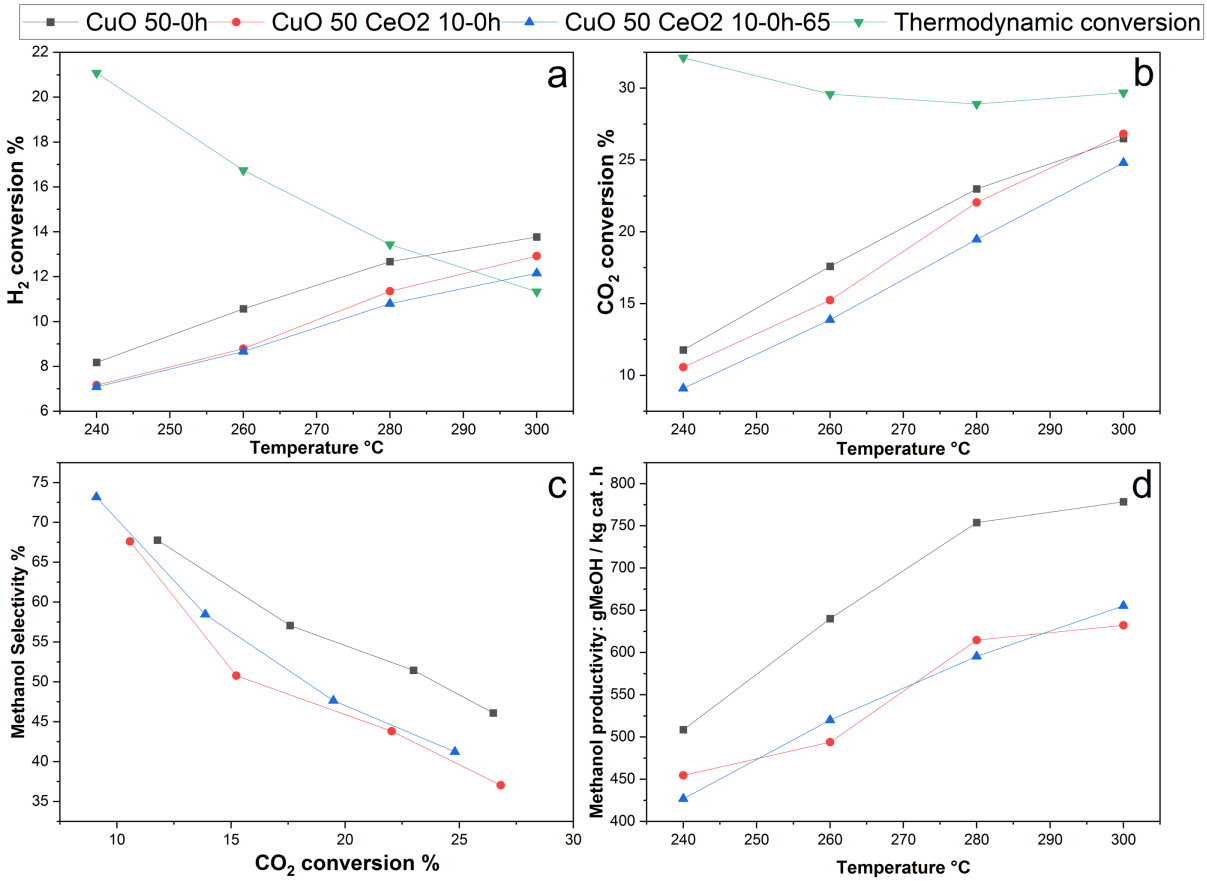

Figure 5.18 H_2 (a) and CO_2 (b) conversions %, methanol selectivity against the CO_2 conversion % (c) and methanol productivity (d) of the catalysts under study. P: 50bar, GHSV: 24000Nml h^{-1} g^{-1}, molar ratio H_2/CO_2: 3.9.

As shown in Figure 5.18a and b, the catalyst CuO 50 CeO_2 10-0h presented lower values of H_2 and CO_2 conversions than the CuO 50-0h catalyst. Furthermore, there were no significant differences between the reactants conversions of the two CeO_2 containing catalysts, indicating that a coprecipitation temperature of 65ºC didn't have an important effect on the catalytic performance. This may be due to the short contact time at 65ºC of the metal nitrates and the precipitating agent. Moreover, it seems that the promoting effect on the catalytic activity by heating the precipitation zone to 65ºC obtained in Chapter 4 was lost, probably by the addition of CeO_2 and its effects on the catalyst due to its amorphous state.

The work of Wang *et al*. [56] suggested that CeO_2 can improve the methanol selectivity in the methanol synthesis reactions. However, this was not the case in the present work, possibly due to the amorphous morphology of CeO_2 in the investigated catalysts.

The lower reactants conversions caused a reduction in the methanol productivity of the CeO_2 containing catalysts as observed in Figure 5.18d. These results can be explained partly by the contribution of different effects, such as the morphology of CeO_2 which was amorphous in this case and may be unfavorable for the properties of the catalysts, and the lower specific and Cu surface areas, as explained in the preceding sections. Different research works support the idea that the morphology of ceria can have an effect on the performance of ceria containing catalysts for the production of methanol [40], [44], [45], [50], [57].

In their work, Khobragade *et al*. [50] prepared a Pd catalyst supported on 4 different morphologies of CeO_2, including polyhedral, rod, cube and polygonal morphologies and obtained catalysts with different properties and catalytic activity. Their characterization results showed that the different morphologies presented different exposed crystalline planes, which affected importantly the specific surface area and the number of oxygen vacancies of the material, affecting the catalytic activity. In their work, the polyhedral morphology presented the best catalytic activity. The work of Tan *et al*. [57] explored the use of Cu-Ni alloy catalysts impregnated on CeO_2 supports with different morphologies for the hydrogenation of CO_2 to methanol. They found that the nanorods morphology gave a better catalytic performance than the nanospheres morphology, mainly due to the higher concentration of oxygen vacancies present in the former, which can adsorb and activate the CO_2 molecule. The results of the work of Ouyang *et al*. [40] also suggest that the morphology of CeO_2 influences importantly the properties and the catalytic performance of Cu based catalysts, where the nanorod morphology presented the best catalytic performance, followed by the nanocubes and nanospheres morphologies. The data presented in the work of Zhu *et al*. [58] also suggests that Cu supported on different ceria morphologies present different catalytic performance.

The reported research results [40], [50], [57], [58] indicate clearly that the morphology of CeO_2 has an important effect on the catalyst properties and performance. The work of Bonura *et al*. [48] also investigated the use of ceria as a promoter of Cu based catalysts prepared by the classical coprecipitation of metallic nitrates. The XRD results of their work showed that the catalysts they synthesized didn't present crystalline peaks of CeO_2, which indicates that it is in an amorphous state or under the detection limits. In this work, the ceria containing catalysts didn't develop ceria crystalline phases either, which may be due to the low ceria content employed, to the zero aging time or due to other conditions such as the calcination temperature.

The results of the work of Bonura *et al*. [48] also indicate that the addition of CeO_2 decreased both the specific and the Cu surface areas of the catalysts, suggesting that amorphous CeO_2 doesn't have a positive promotion effect on the Cu based catalysts for the production of methanol. In addition, the decrease of the strong basic sites of ZrO_2 due to the partial substitution by CeO_2 could be a contributing factor to the lower

catalytic performance of the CeO_2 containing catalysts. The basicity of ZrO_2 provides a high CO_2 chemisorption capacity, exceeding those of other oxides such as Al_2O_3, TiO_2, MgO and SiO_2 [59]. Another work [60] also suggests that ZrO_2 presents a higher basicity compared to CeO_2, which also gives ZrO_2 a higher methanol selectivity. The catalysts containing ceria presented a higher concentration of total basic sites than the CuO 50-0h catalyst. However, they presented a lower concentration of strong basic sites, which may also be a factor contributing to the lower catalytic activity of the ceria containing catalysts. Moreover, the work of van de water *et al*. [61] indicates that the active site and reaction mechanism on Cu/CeO_2 catalysts are different from those of $Cu\text{-}ZnO\text{-}Al_2O_3$ catalysts, with CO being the carbon source for methanol. This theory helps explaining the lower catalytic activity of the ceria containing catalysts, as the gas feed of all the catalytic tests performed in this work was composed of CO_2, H_2 and a small amount of N_2 used as an internal standard. For such reasons, the CeO_2 in the catalysts may participate in the reaction to a lesser extent, causing a reduction in the reactants conversions.

CeO_2 was expected to be a good promoter of $CuO\text{-}ZnO\text{-}ZrO_2$ catalysts, however, as mentioned above the obtained results show that the microfluidic technique is not compatible with the use of CeO_2. In future works, this could possibly be fixed by employing longer aging times or by increasing the residence time of the reactants during the microfluidic technique at temperatures above ambient conditions, in order to increase the crystallization of CeO_2. The use of an ultrasound device would be recommended, as ultrasounds inhibit the agglomeration of the precipitate particles that can cause blockages in the system.

Table 5.15 Results of the catalytic tests of the catalysts containing CeO_2 and the CuO 50-0h catalyst. P: 50bar, GHSV: 24000Nml h^{-1} g^{-1}, molar ratio H_2/CO_2: 3.9.

Catalyst	Temperature ºC	H_2 Conversion %	CO_2 Conversion %	Methanol selectivity %	Methanol productivity g CH_3OH/(kg of catalyst x hour)
CuO 50 CeO_2 10-0h	240	7.2	10.6	67.6	455
	260	8.8	15.2	50.8	494
	280	11.3	22.0	43.8	615
	300	12.9	26.8	37.0	632
CuO 50 CeO_2 10-0h-65	240	7.1	9.1	73.2	427
	260	8.7	13.9	58.5	520
	280	10.8	19.5	47.7	595
	300	12.2	24.8	41.2	655
CuO 50-0h	240	8.2	11.8	67.8	509
	260	10.6	17.6	57.1	640
	280	12.7	23.0	51.4	754
	300	13.8	26.5	46.1	779

5.3.3. Conclusions

Two catalysts containing ceria were prepared by the microfluidic method with immediate filtration (i.e. one with heating of the precipitation zone to 65ºC and the other one without it) and their properties and catalytic performance were compared to those of the CuO 50-0h catalyst containing no CeO_2 and used as a reference.

The characterization results showed that the specific surface area and the metallic Cu surface areas suffered a decrease after the addition of ceria to the catalyst and this could possibly be explained by the covering of Cu nanoparticles by the amorphous CeO_2. The Cu dispersion was also decreased after the addition of CeO_2 and the Cu particle sizes increased, suggesting a decrease of the promoting effects of ZnO and ZrO_2 caused by the presence of amorphous CeO_2. Moreover, the replacement of some ZrO_2 by CeO_2 caused a change in the surface basicity of the catalysts, by reducing the concentration of strong basic sites. The mixed effects of the catalyst properties mentioned above combined with the amorphous state of the CeO_2 caused a decrease in the catalytic performance of the CeO_2 containing catalysts. These findings indicate that the use of the microfluidic technique is not compatible with the use of CeO_2 as a catalyst component, as it doesn't favor the crystallization of this phase. This means that this synthesis method must be adapted to obtain the promoting effects of CeO_2 indicated in the literature.

Regarding the CeO_2 containing catalyst synthesized by heating of the precipitation zone to 65ºC, it was found that a higher coprecipitation temperature had a promoting effect on the specific surface area, but didn't improve other properties such as the reducibility or the Cu surface area. A higher precipitation temperature didn't affect greatly the activity of this catalyst either, which can also be explained by the covering of the Cu particles by CeO_2, decreasing the promoting effects of higher precipitation temperature of 65ºC observed in Chapter 4.

As a perspective, the synthesis of catalysts by the microfluidic method by controlling the crystallinity of ceria via different methods, such as the use of a microfluidic technique with precursors aging might be interesting as a continuation of the present work. In addition, the preparation of CeO_2 separately could also allow to improve the catalytic performance of CuO-ZnO-ZrO_2 catalysts promoted with this oxide and prepared by the microfluidic method.

5.4. Effect of the addition of In_2O_3 to Cu-ZnO-ZrO_2 catalysts prepared by the microfluidic method

Even though there is an emergence of research works about indium-based catalysts for the hydrogenation of CO_2 to methanol, there are no reports about the synthesis of this type of catalysts by coprecipitation using a microfluidic device. The use of the microfluidic method for the synthesis of In_2O_3 containing catalysts for methanol synthesis may have a positive effect on the properties and performance of the catalysts. The high methanol selectivity, the high stability along with reports of promoting effects of In_2O_3 based catalysts [62]–[66] make it an interesting choice for the investigation of alternative catalysts for the production of methanol.

Two catalysts containing In_2O_3 were prepared in this work in order to investigate the use of this oxide as a promoter in a Cu based catalyst (i.e. catalyst named CuZnZrIn) and as an active metal using Zn and Zr as catalyst supports (i.e. catalyst named ZnZrIn). The theoretical compositions of the catalysts were 40wt% CuO, 33.3wt% ZnO, 16.6wt% ZrO_2 and 10wt% In_2O_3 for the CuZnZrIn catalyst and 60wt% ZnO, 30wt% ZrO_2 and 10wt% In_2O_3 for the ZnZrIn catalyst

5.4.1. Determination of the precipitation pH of hydrated indium nitrate $In(NO_3)_3$ $4.6H_2O$.

Knowing the precipitation pH of the hydrated indium nitrate is important to ensure that all of the metal precursors precipitate during a catalyst synthesis by coprecipitation. To do so, 50 ml of a solution of 0.25 M $In(NO_3)_3 \cdot 4.6H_2O$ were prepared, and titrated with a solution of Na_2CO_3 to determine the precipitation pH of the indium nitrate compound. The initial pH of the $In(NO_3)_3 \cdot 4.6H_2O$ solution was 1.9. Sodium carbonate was added progressively to an agitated beaker containing the $In(NO_3)_3 \cdot 4.6H_2O$ solution, and precipitation and redissolution were noticed between pHs of 1.9 and 3. The precipitation without further dissolution of the precipitate occurred between pHs of 3 and 4. This results indicate that above a pH of 4, the coprecipitation should take place without indium staying in solution. A pH between 7 and 8 was used during the catalysts synthesis in this work, which means that all of the indium must precipitate during this process.

5.4.2. Catalysts characterization results and discussion

The catalysts of this section were synthesized by the microfluidic synthesis with immediate filtration and with heating of the precipitation zone to 65ºC, as presented in Chapter 2, section 2.2. This method was selected due to the effects of a higher

coprecipitation temperature on some catalyst properties such as the specific surface area as was shown previously.

The results of the XRD analysis of the precursors and the calcined catalysts are presented in Figure 5.19 on the left and right side, respectively. The results show that the precursor containing both indium and copper (i.e. CuZnZrIn) remained amorphous, while the precursor containing indium but no copper (i.e. ZnZrIn) developed a crystalline phase composed mainly of hydrozincite $Zn_5(CO_3)_2(OH)_6$ (PDF number: 72-1100). The high content of ZnO of the ZnZrIn precursor favored the formation of the hydrozincite phase composed of Zn. No indium containing species were detected in both of the precursors, which may be due to the low concentration of this metal and/or to the amorphous state due to the zero aging after the coprecipitation step.

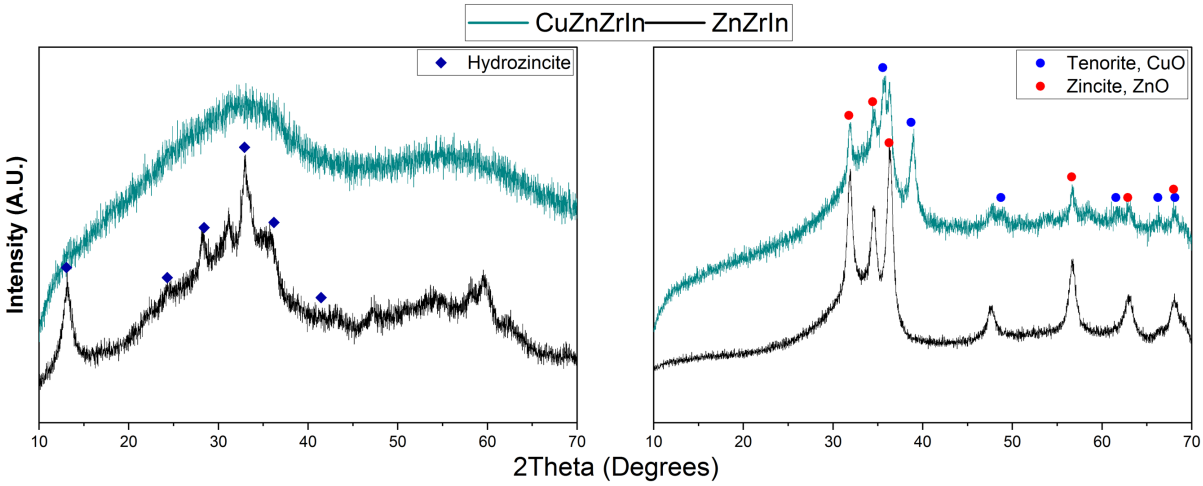

Figure 5.19 X-ray diffractograms of the CuZnZrIn and ZnZrIn precursors on the left and the calcined catalysts on the right.

The X-ray diffractograms of the catalysts after calcination are shown on the right side of Figure 5.19. The CuZnZrIn catalyst developed crystalline phases corresponding to CuO (PDF number: 72-0629) and ZnO (PDF number: 75-1526), while the catalyst ZnZrIn only developed the ZnO phase. ZrO_2 peaks were not detected due to its amorphous state as explained before. In_2O_3 (PDF number: 06-0416) or other In-containing species were not detected either, possibly due to the low content of this component in the catalysts and also due to its amorphous state or low crystallinity due to the zero aging time. Other conditions such as the calcination temperature and the calcination time may also have an effect on the crystallization of In_2O_3.

Using Scherrer's equation, the crystallite sizes of the phases in the precursors and in the calcined catalysts were calculated and are shown in Table 5.16. As mentioned above, only the ZnZrIn precursor developed the hydrozincite phase with a crystallite size of 7.5nm. The catalyst CuZnZrIn was the only to develop the CuO phase due to the evident composition reason, with a crystallite size of 14nm, while both catalysts developed the ZnO phase after calcination with very similar crystallite sizes.

Table 5.16 Crystallite sizes (nm) of the phases identified in the precursors and in the catalysts after calcination calculated with Scherrer's equation.

	Precursor	Calcined catalyst	
Catalyst	Hydrozincite	Tenorite, CuO	Zincite, ZnO
CuZnZrIn	-	14	15
ZnZrIn	7.5	-	14

The TGA results presented in Figure 5.20 show that the two catalyst precursors investigated in this section presented different thermal decomposition profiles attributable to the evident composition differences. The composition differences in both materials are due mostly to the presence of Cu in the CuZnZrIn precursor and the absence of it in the ZnZrIn precursor.

The ZnZrIn catalyst also presented a high relative content of ZnO and ZrO_2 compared to the CuZnZrIn precursor. The higher Zn content in ZnZrIn favored the formation of hydrozincite, which as explained before, decomposes between 150ºC to 350ºC [10]. This explains the derivative peaks developed in this temperature range. After the coprecipitation reaction between $In(NO_3)_3 \cdot 4.6H_2O$ and Na_2CO_3, the formation of indium carbonate $In_2(CO_3)_3$ and also indium hydroxycarbonate are expected as the precipitation products. However, no thermal decomposition data of these compounds was found in the literature. Despite that, the thermal decomposition data of $In(OH)_3$ was available and it was found to decompose between 220 and 250ºC [67], which can explain the decomposition peaks generated in such temperature range. The peak occurring around 500ºC in the decomposition profile of the catalyst CuZnZrIn can be attributed to the decomposition of an amorphous Cu-Zn precursor, as explained before [9].

The final mass losses % of the two catalyst precursors were similar, with values of 21% and 22% for the ZnZrIn and CuZnZrIn catalyst precursors, respectively, at a final decomposition temperature of 700ºC.

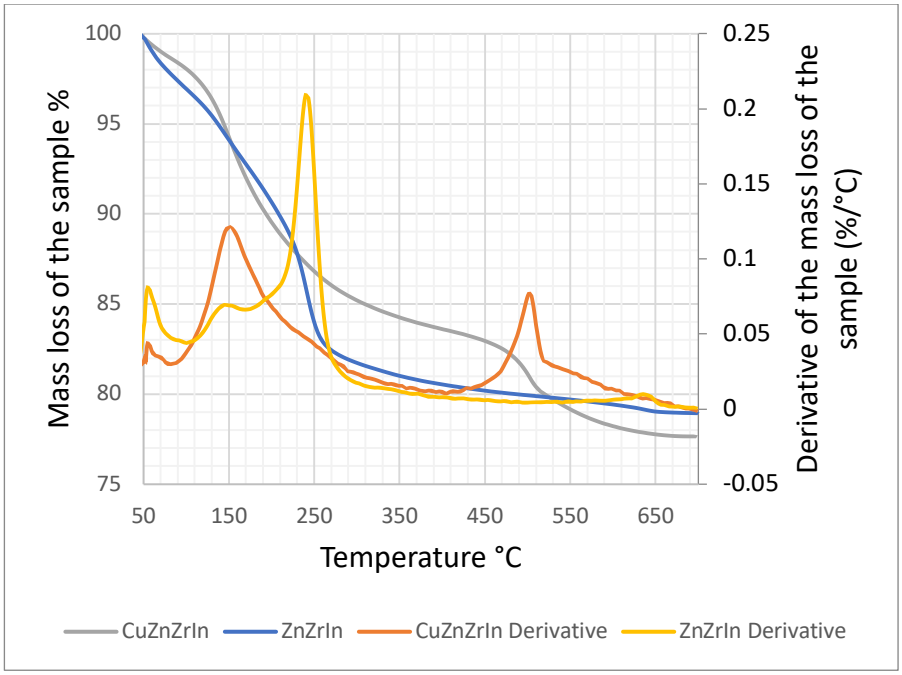

Figure 5.20 TGA results of the CuZnZrIn and ZnZrIn catalyst precursors.

The N_2-physisorption characterization results of the catalysts of this work are presented in Figure 5.21 and in Table 5.17. The adsorption and desorption isotherms presented correspond to isotherms of type IV with a hysteresis loop of type 3. These correspond to mesoporous materials with cylindrical shaped pores and layered solids with narrow pore networks [30], [68].

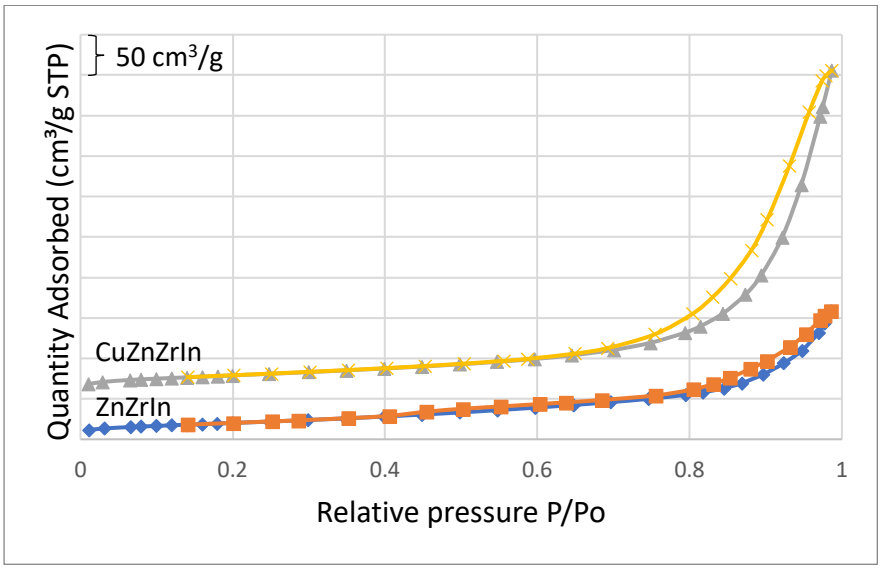

Figure 5.21 N_2-Physisorption isotherms of the CuZnZrIn and the ZnZrIn catalysts.

The results of the specific surface area and pore sizes showed that the catalyst ZnZrIn presented lower values of specific surface area and pore size compared to the CuZnZrIn catalyst. These results can be explained partly due to the important composition differences of both catalysts. The higher specific surface area of the

catalyst CuZnZrIn suggests a promoting effect occurring due to the addition of In_2O_3. As shown in the work of Sadeghinia *et al*. [69], the addition of In_2O_3 to a Cu-ZnO-Al_2O_3 catalyst gave catalysts with higher specific surface areas, suggesting a promoting effect on the catalyst properties. Nevertheless, the effect of the addition of In_2O_3 to Cu-ZnO-Al_2O_3 on the catalytic performance was different and will be discussed in the corresponding section.

Table 5.17 N_2-Physisorption specific, surface area and pore size results of the catalysts ZnZrIn and CuZnZrIn.

Sample	BET surface area (m^2/g)	Pore size (nm)
ZnZrIn	75	3 and 13
CuZnZrIn	103	13

Figure 5.22 shows the CO_2-TPD profiles of the catalysts CuZnZrIn and ZnZrIn and Table 5.18 presents the quantification of the basic sites of both catalysts.

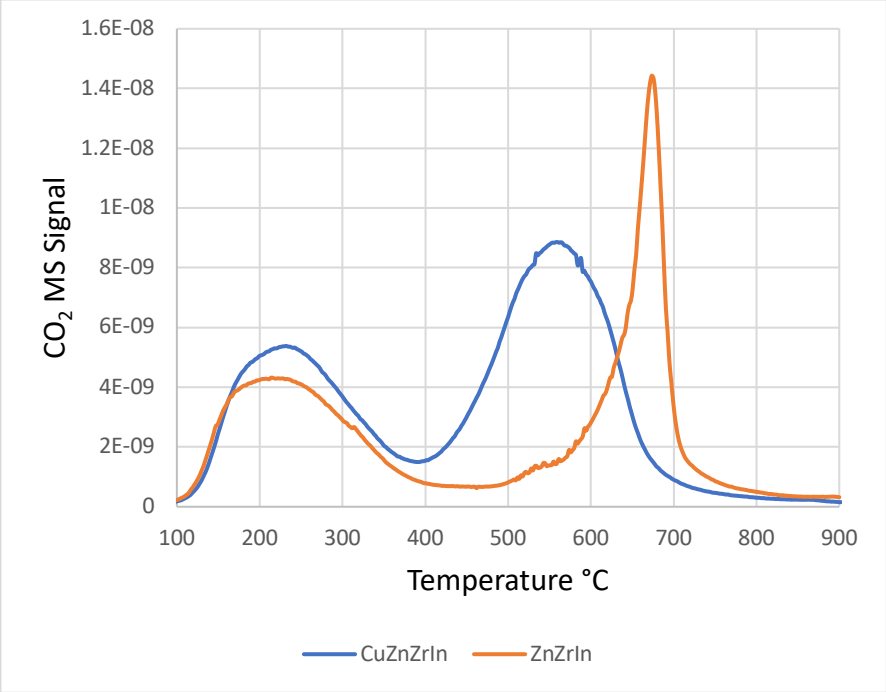

Figure 5.22 CO_2-TPD profiles of the CuZnZrIn and ZnZrIn catalysts.

The results of the CO_2-TPD characterization show that the CuZnZrIn and ZnZrIn catalysts present different CO_2 desorption profiles, indicating different surface basicity and different affinities for CO_2. The CuZnZrIn and ZnZrIn catalysts presented an amount of 93.0 and 74.0 μmol g^{-1} of weak basic sites, respectively. In the case of the moderate strength basic sites, the catalyst CuZnZrIn presented an amount of 70.0 μmol g^{-1} while the catalyst ZnZrIn presented 27.0 μmol g^{-1}. Moreover, in the case of

the strong basic sites, the catalyst CuZnZrIn presented an amount of 150.0 μmol g^{-1}, while the catalyst ZnZrIn presented an amount of 110.0 μmol g^{-1}. The total amount of basic sites was higher for the catalyst CuZnZrIn, with a value of 313.0 μmol g^{-1}, compared to the total amount of basic sites of the catalyst ZnZrIn with a total basicity of 211.0 μmol g^{-1}. This may be due to the increased adsorption of CO_2 on the Cu-support interfaces, which doesn't occur in the catalyst ZnZrIn because of its lack of Cu.

Regarding the role of In_2O_3 in the surface basicity, the oxygen vacancies of this material can facilitate the adsorption of CO_2 [70]. However, in another work [71] it was shown that the CO_2-TPD profile of pure In_2O_3 presented a considerable desorption peak around 100ºC, and another much smaller peak around 450ºC, suggesting that In_2O_3 adsorbs CO_2 mostly physically, while stronger adsorption of CO_2 on this oxide occurred to a lesser extent.

Table 5.18 also shows that the catalyst CuZnZrIn presented a higher basicity per catalyst surface area than the catalyst ZnZrIn, meaning that the CuZnZrIn catalyst presented a higher affinity for CO_2, which could impact positively its catalytic performance.

Table 5.18 Quantity of weak, moderate strength and strong basic sites and basic sites per unit surface area of the CuZnZrIn and ZnZrIn catalysts.

Sample	Weak basic sites (μmol/g)	Moderate strength basic sites (μmol/g)	Strong basic sites (μmol/g)	Total basic sites (μmol/g)	Basic sites per unit surface area (μmol/m^2)
CuZnZrIn	93.0	70.0	150.0	313.0	3.0
ZnZrIn	74.0	27.0	110.0	211.0	2.8

The H_2-TPR profiles of the two catalysts containing indium are shown in Figure 5.23. The catalyst ZnZrIn presented an almost flat shape with two small peaks at 265ºC and at 548ºC which may correspond to the reduction of In_2O_3. The consumption of H_2 at 265ºC and 548ºC corresponded to 0.036 and 0.65 mmol of H_2 per gram of catalyst, respectively, while the theoretical In_2O_3 content of a catalyst composed of 10 wt% In_2O_3 as in the present work is 0.36 mmol of In_2O_3 per gram of catalyst. These values can be used to determine if the In_2O_3 was reduced partially or completely with the aid of the chemical reaction of the reduction of In_2O_3. Such reaction is presented in Equation 5.2 [72]:

Equation 5.2 Reduction reaction of indium oxide In_2O_3.

$$In_2O_3(s) + 3H_2(g) \rightarrow 2In(s) + 3H_2O(g)$$

Assuming that all the consumed H_2 corresponding to the reduction peaks at 265ºC and 548ºC of the catalyst ZnZrIn were consumed in the reduction of In_2O_3, this would mean that 0.012 and 0.22 mmol of In_2O_3 per gram of catalyst would be reduced, respectively. These values are below the theoretical In_2O_3 content of 0.36 mmol of In_2O_3 per gram of catalyst, which basically means that 64% of the In_2O_3 present in the ZnZrIn catalyst was reduced during the H_2-TPR analysis.

In the case of the catalyst CuZnZrIn, a reduction peak close to 200ºC occurred due to the reduction of the copper species present in this catalyst. As shown in Table 5.19, the H_2 consumption of the peak occurring at 199ºC was 4.95 mmol of H_2 per gram of catalyst, which matched very closely the catalyst's theoretical Cu content of 5.0 mmol of Cu per gram of catalyst. This means an experimental value of 39.5 CuO wt%, which is very close to the theoretical value of 40 wt% CuO, indicating that the Cu loading of the catalyst during the coprecipitation reaction was correct. Similarly, as with catalyst ZnZrIn, the H_2-TPR analysis of the catalyst CuZnZrIn evidenced the presence of a reduction peak at 750ºC indicating a hydrogen consumption of 0.9 mmol of H_2 per gram of catalyst. Assuming that this entire amount was used for the reduction of In_2O_3, it would mean the presence of 0.3 mmol of In_2O_3 per gram of catalyst, which is below the In_2O_3 content of 0.36 mmol of In_2O_3 per gram of catalyst, indicating only a partial reduction of the In_2O_3 species (83%).

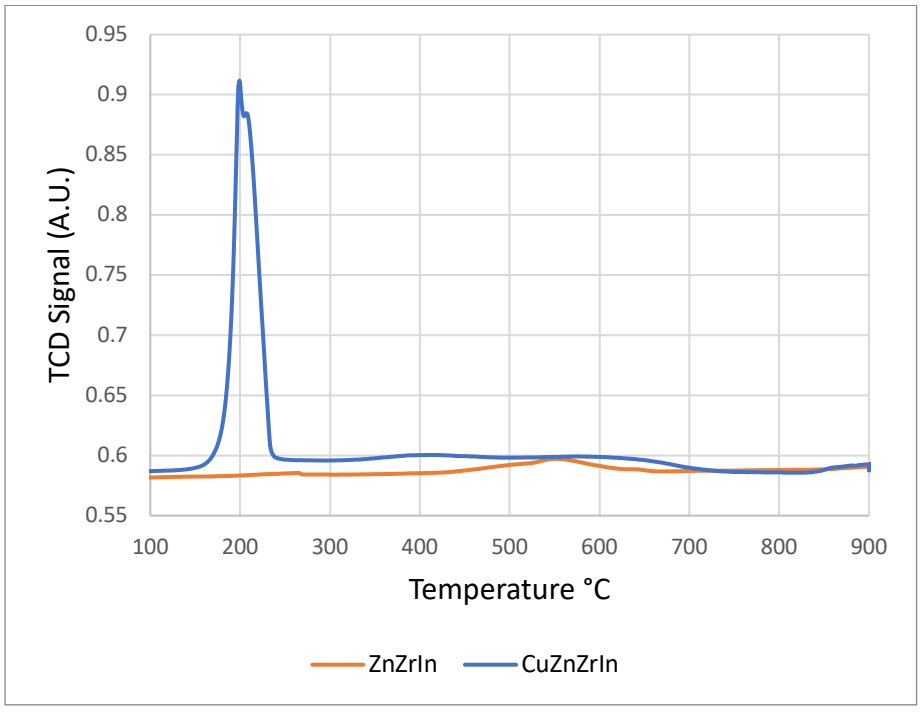

Figure 5.23 H_2-TPR results of the CuZnZrIn and the ZnZrIn catalysts.

Table 5.19 H_2-TPR quantitative results of the CuZnZrIn catalyst.

Sample	H_2 consumption, mmol/g	Catalyst theoretical Cu content, mmol Cu/g	H_2/Cu ratio	Calculated CuO wt% of the catalyst
CuZnZrIn*	4.95	5.0	0.99	39.5

*This sample has a theoretical mass content of 40% CuO.

According to the work of Shi *et al*. [73], the reduction of In_2O_3 can start at temperatures ranging from 300 to 350ºC, forming the $Cu_{11}In_9$ intermetallic compound in the presence of CuO, while the rest of the reduction process of In_2O_3 takes place above 400ºC. Their results also suggest that In_2O_3 is completely reduced at temperatures above 700ºC. Despite the wide reduction temperature range in which the reduction of In_2O_3 occurs, a reduction temperature of 350ºC was considered optimal as it produced a catalyst with high CO_2 conversion, high methanol selectivity and methanol yield [73]. For the above reason, the reduction temperature chosen for the two indium containing catalysts of this work was 350ºC, before the catalytic tests. In their work, Shi *et al*. [73] also found that higher reduction temperatures caused a decrease in the catalyst activity and selectivity [73]. Nevertheless, the catalyst composition that they investigated was 22.4 wt% CuO and 77.6 wt% In_2O_3, which differs from the compositions explored in the current work. Moreover, according to the work of Schoeller *et al.* [72], the reduction reaction of In_2O_3 is thermodynamically favored above approximately 150ºC at H_2 concentrations above 4% and with low moisture contents (i.e. 7ppm H_2O) [72].

5.4.3. Catalytic tests results

Figure 5.24 and Table 5.20 show the H_2 and CO_2 conversions, the methanol selectivity against the CO_2 conversions and the methanol productivities of the catalysts investigated in this work.

The CuZnZrIn catalyst presented a better catalytic performance with higher reactants conversions and better methanol productivities compared to the ZnZrIn catalyst. However, the methanol selectivity of the CuZnZrIn catalyst was lower compared to that of the ZnZrIn catalyst, evidenced by the higher production of carbon monoxide by the RWGS reaction. The literature on the RWGS reaction mechanism on Cu-based catalysts indicates that this reaction is catalyzed by copper [74][75], which explains the higher carbon monoxide production and lower methanol selectivity of the copper containing catalyst CuZnZrIn.

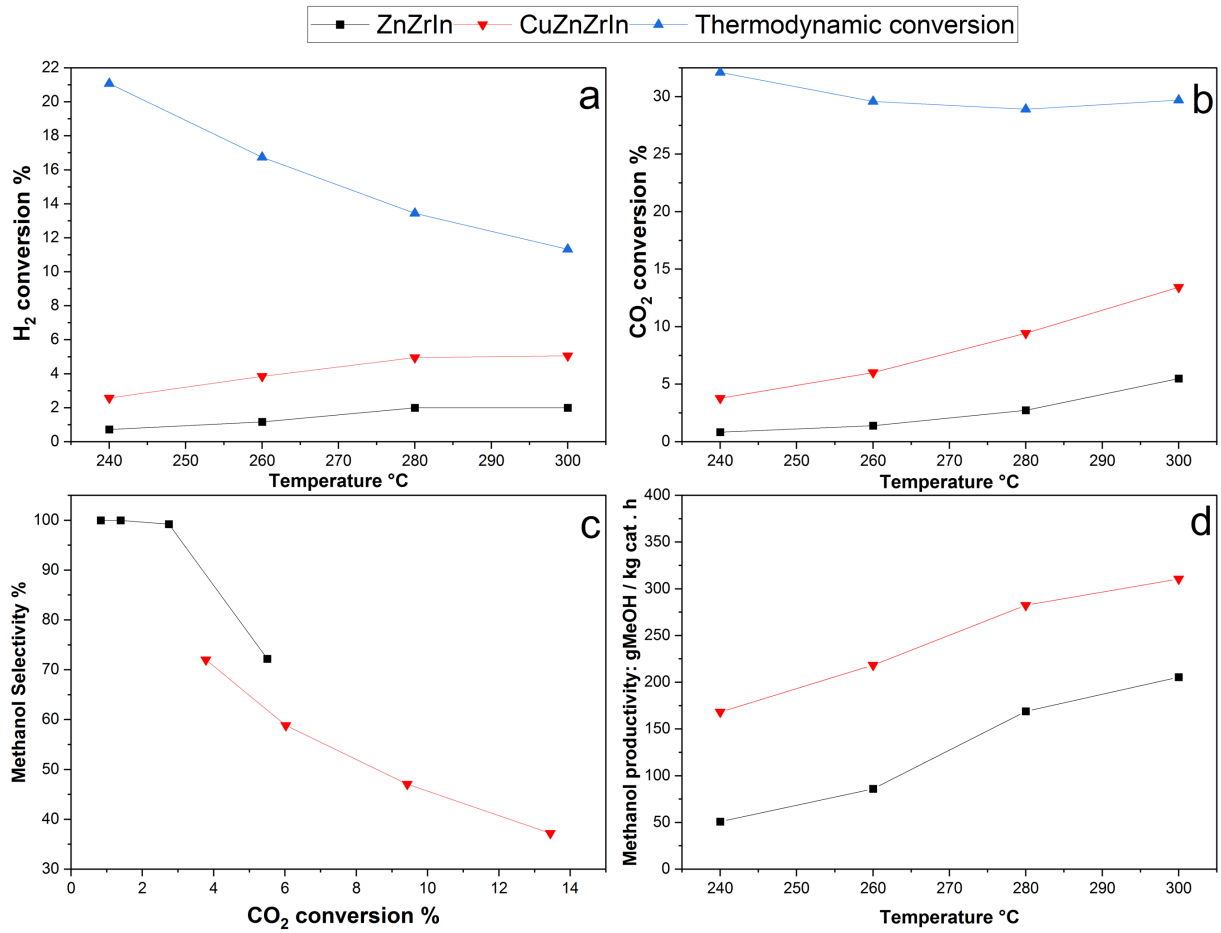

Figure 5.24 Catalytic performance of the CuZnZrIn and ZnZrIn catalysts. H_2 (a) and CO_2 (b) conversions, methanol selectivity against the CO_2 conversion (c) and methanol productivity (d). P: 50bar, GHSV: 24000Nml h^{-1} g^{-1}, molar ratio H_2/CO_2: 3.9.

The quantitative results of the catalytic tests also showed that the decreased catalytic performance of the catalyst CuZnZrIn compared to other catalysts prepared in previous chapters may be due to the differences in composition and possibly due to other factors such as the amorphous state of In_2O_3. As a reminder, the method employed for the synthesis of the catalysts of this section was the microfluidic synthesis with immediate filtration, with zero aging time and a coprecipitation temperature of 65ºC. It is possible that the zero aging time of these catalysts didn't promote the crystallization of In_2O_3, affecting the catalytic performance of these materials. According to Wang *et al*. [76], there are three different crystal structures reported for In_2O_3, which are the cubic bixbyite-type phase (c-In_2O_3), the hexagonal corundum-type phase (h-In_2O_3) and the orthorhombic Rh_2O_3-type phase (o-In_2O_3), where each phase can have different catalytic activity [77]. The two cited research works indicate that h-In_2O_3 can transform into c-In_2O_3 during the CO_2 hydrogenation [76][77]. To promote the crystallization of In_2O_3, longer aging times at temperatures around 65ºC may be desirable. This can be achieved by using the microfluidic continuous coprecipitation method, which consists in sending the coprecipitation products to a stirred beaker at 65ºC for aging. Furthermore, using higher calcination temperatures may also promote the development of crystalline forms of In_2O_3.

In addition, according to the work of Stangeland *et al*. [78], two other research works in which Cu-based catalysts promoted with In_2O_3 were investigated found that the use of In_2O_3 caused a decrease in the catalytic activity. In fact, the work of Sadeghinia *et al*. [69] showed that despite the promotions of In_2O_3 on Cu-ZnO-Al_2O_3 catalysts, including higher specific and Cu surface areas, smaller Cu crystallite sizes and a higher quantity of oxygen vacancies, this compound caused a decrease in the production of methanol, with increasing concentrations of In_2O_3 causing a higher decrease of the methanol productivity. The authors attributed this to a stronger adsorption of CO_2, causing a drop in the catalytic activity [69].

The results of the CO_2-TPD characterization of the two catalysts of this work showed that the CuZnZrIn catalyst presented the highest total surface basicity, as well as a higher amount of weak, moderate and strong basic sites compared to the catalyst ZnZrIn. As explained in previous chapters, the surface basicity is directly correlated to the adsorption of CO_2 on the surface of the catalyst, which has an effect on the reaction kinetics and on the CO_2 conversion and methanol productivity. This explains in part the better catalytic performance obtained with the catalyst CuZnZrIn.

The low H_2 and CO_2 conversions of the ZnZrIn catalyst may also be due to the decreased H_2 adsorption and dissociation capacity due to the lack of copper. So, catalysts with higher contents of In_2O_3 may be necessary to have more active sites that can dissociate H_2. Although it has been shown by theoretical modelling that the oxygen vacancies of In_2O_3 can participate in the CO_2 adsorption and in the H_2 splitting steps [79], the results of the work of Zhang *et al*. [80] indicate that the H_2 splitting ability of In_2O_3 is much weaker than that of metallic Cu. This causes a reduction in the reaction kinetics of hydrogen activation step, which in turn causes a reduction in the reactants conversion of the catalyst ZnZrIn. The work of Tsoukalou *et al*. [81] indicates that the indium species active in the dissociation of H_2 in In_2O_3-ZrO_2 catalysts are affected by the phase of the ZrO_2 support, where monoclinic ZrO_2 gives the highest methanol yield and selectivity.

Also, the 100% methanol selectivity shown by the ZnZrIn catalyst at 240ºC and 260ºC can be attributed in part to the lower RWGS reaction conversion, which is favored at higher temperatures. In the case of the methanol productivity of the ZnZrIn catalyst, it also presented a decrease as a consequence of the lower reactants conversions.

Methanol selectivities of 100% have been reported for cubic In_2O_3 nanomaterials and In_2O_3 supported on monoclinic ZrO_2, with CO_2 conversions of less than 5.5%, at a temperature of 300°C, pressure of 50 bar and H_2/CO_2 molar ratios of 4.74 [62]. The reason of the 100% selectivity of In_2O_3-ZrO_2 catalysts at some temperatures can be explained due to different reaction pathway due to the synergy between the metal species [62]. According to Wang *et al*. [76], many studies have found that the methanol formation route on In_2O_3 occurs on the oxygen vacancies according to the following

pathway: CO_2 → HCOO* → H_2CO* → H_3CO* → CH_3OH. The oxygen vacancies on the surface of In_2O_3 participate in the adsorption of CO_2 and its hydrogenation and can stabilize reaction intermediates such as HCOO, H_2COO and H_2CO during the methanol synthesis reaction [70], [76].

Table 5.20 Results of the catalytic tests of the catalysts CuZnZrIn and ZnZrIn. P: 50bar, GHSV: 24000Nml h^{-1} g^{-1}, molar ratio H_2/CO_2: 3.9.

Catalyst	Temperature ºC	H_2 Conversion %	CO_2 Conversion %	Methanol selectivity %	Methanol productivity g CH_3OH/(kg of catalyst x hour)
CuZnZrIn	240	2.6	3.8	72.0	168
	260	3.8	6.0	58.8	218
	280	4.9	9.4	47.0	282
	300	5.0	13.4	37.2	311
ZnZrIn	240	0.7	0.83	100	51
	260	1.2	1.4	100	86
	280	2.0	2.7	99.2	169
	300	2.0	5.5	72.2	206

In general, the catalytic tests results showed that the use of 10 wt% In_2O_3 supported on ZnO and ZrO_2 as in the ZnZrIn catalyst didn't give an interesting catalytic performance, and suggests that higher In_2O_3 concentrations should be investigated along with longer aging times to study the effect of the crystallinity of In_2O_3 on the catalytic performance. Employing a microfluidic technique that allows the aging of the precipitates at temperatures around 65ºC may be useful to increase the crystallinity of In_2O_3 and possibly obtaining a positive effect on the catalytic performance. In addition, the use of 10 wt% In_2O_3 in a Cu containing catalyst didn't present a promoting effect either, possibly influenced by the amorphous nature of In_2O_3 too. In summary, higher In_2O_3 contents with longer aging times may give catalysts with more interesting catalytic properties. Also, additional investigations about the properties of In_2O_3 should be carried out in order to understand better the catalytic activity of this material for the hydrogenation of CO_2 to methanol, such as determining optimal aging times of the catalyst precursors, determining the optimal calcination temperatures and duration and doing catalytic tests of In_2O_3 with different morphologies, among others.

The results of the H_2-TPR analysis showed that In_2O_3 was not completely reduced in both CuZnZrIn and ZnZrIn catalysts. For this reason, a deeper study of the optimal activation procedure of In_2O_3 before the methanol synthesis reaction should be carried out. It is possible that the reduction treatment applied to the CuZnZrIn and ZnZrIn catalysts (i.e. reduction with pure H_2 at 350ºC for 15 hours) had a negative effect on the catalytic activity. So, reducing this material at different temperatures and for different periods of time would be interesting to investigate in order to determine the reduction conditions that give optimal properties and an optimal catalytic performance.

XRD could be used to determine the presence of metallic In or In_2O_3 after reduction and possibly to determine their quantities by doing quantitative analysis of X-ray diffractograms. An alternative to the activation treatment by reduction with H_2 could be to not reduce the CuO-In_2O_3 catalysts before the reaction, which could cause the formation of intermetallic nanoparticles [73] in situ under the reducing atmosphere employed in the catalytic tests. Also, employing higher contents of In_2O_3 along with ZnO and ZrO_2 may increase the interactions between these metal species improving the catalytic activity.

5.4.4. Catalytic performance of different catalysts containing In_2O_3 available in the literature

The catalytic tests' results of different catalysts containing In_2O_3 available in the literature are presented in Table 5.21. Despite the fact that employing different conditions during the catalytic tests may give different conversions, selectivity and productivity values, some useful information can be extracted from the study of the catalytic tests results of other research works.

Table 5.21 Catalytic performance of different catalysts containing In for the production of methanol.

Catalyst composition	Synthesis method	H_2:CO_2 mole ratio	Pressure, bar	CO_2 Conversion %	Methanol selectivity %	Methanol productivity	GHSV	Ref.
51.7% Cu 23.9% Zn 19.3% Al 5.1% In Mole %	Coprecipitation of hydrotalcite-like compounds.	3:1	30	250°C – 5.8%	250°C – 50%	-	30000 cm^3 g_{cat}^{-1} h^{-1}	[82]
82.2% Cu 16.5% Zn 1.3% In Mole %	Impregnation of Cu/ZnO with In nitrate.	3:1	30	250°C – 7.1%	250°C – 37%	-	10000-100000 cm^3 g_{cat}^{-1} h^{-1}	[82]
22.1% Cu 3.11% In Remaining Zr wt%	One-pot hydrogen bubble assisted method.	3:1	30	270°C – 16.1%	270°C – 35%	270°C – 390 g MeOH kg_{cat}^{-1} h^{-1}	18000 cm^3 g_{cat}^{-1} h^{-1}	[83]
20.8% Cu 6.2% In Remaining Zr wt%	One-pot hydrogen bubble assisted method.	3:1	30	270°C – 10%	270°C – 51%	270°C – 330 g MeOH kg_{cat}^{-1} h^{-1}	18000 cm^3 g_{cat}^{-1} h^{-1}	[83]
82.5% Cu 16.5% Zr 1.0% In Mole %	Coprecipitation and impregnation methods.	3:1	30	230°C – 6.1% 270°C – 5.3%	230°C – 56% 270°C – 44%	230°C – 384.5 270°C – 1249.5 g MeOH kg_{cat}^{-1} h^{-1}	80000 cm^3 g_{cat}^{-1} h^{-1}	[78]
50% In 50% Zr Mole %	Coprecipitation method.	4:1	50	280°C – 4.6 %	280°C – 87%	270 g MeOH kg_{cat}^{-1} h^{-1}	24000 cm^3 g_{cat}^{-1} h^{-1}	[66]
100% In Mole %	Coprecipitation method.	4:1	50	280°C – 3.9%	280°C – 84%	220 g MeOH kg_{cat}^{-1} h^{-1}	24000 cm^3 g_{cat}^{-1} h^{-1}	[66]
CuO 40%, ZnO 33.3%, ZrO_2 16.6, In_2O_3 10%	Coprecipitation with a	3.9:1	50	300ºC – 13.4%	300ºC – 37.2%	311 g MeOH kg_{cat}^{-1} h^{-1}	17552 h^{-1}	This work.

wt%. Catalyst CuZnZrIn.	microfluidic reactor.						24000 Ncm^3 g_{cat}^{-1} h^{-1}	
ZnO 60%, ZrO_2 30%, In_2O_3 10%. Catalyst ZnZrIn.	Coprecipitation with a microfluidic reactor.	3.9:1	50	300ºC – 5.5%	300ºC – 72.2%	206 g MeOH kg_{cat}^{-1} h^{-1}	25823 h^{-1} 24000 Ncm^3 g_{cat}^{-1} h^{-1}	This work.

Stangeland *et al*. [78] synthesized a Cu-ZrO_2 catalyst promoted with In_2O_3 and obtained a high methanol productivity of 1249.5 at 270ºC, much higher than the methanol productivity of the catalysts of this work. They obtained an increase in the methanol productivity from 52.7 to 60.5 mmol per gram of catalyst when 0.3 mole % In was incorporated into the Cu-ZrO_2 catalyst, suggesting that small quantities of this oxide can improve the catalytic activity.

Zhang *et al.* [83] synthesized two Cu catalysts containing different amounts of In_2O_3 and using ZrO_2 as a support, and the two catalysts presented a methanol productivity of 390 and 330 g MeOH kg_{cat}^{-1} h^{-1}, where the catalyst with the lowest content of In_2O_3 presented the highest CO_2 conversion and methanol productivity. The values of the methanol productivity that they obtained were slightly superior to the productivity value of 311 g MeOH kg_{cat}^{-1} h^{-1} at 300ºC of the catalyst CuZnZrIn prepared in this work. However, the GHSV of their work was 18000 cm^3 h^{-1} g_{cat}^{-1} which is lower to the one employed in this work 24000 Ncm^3 h^{-1} g^{-1}.

Frei *et al.* [66] synthesized a pure In_2O_3 and an In_2O_3 plus ZrO_2 catalysts and tested their catalytic activity using a H_2:CO_2 molar ratio of 4, a pressure of 50 bar and a GHSV of 24000 cm^3 g_{cat}^{-1} h^{-1}, which are the same conditions of the catalytic tests of the catalysts of this work. The CuZnZrIn catalyst presented a higher methanol productivity of 311 g MeOH kg_{cat}^{-1} h^{-1} than both of their catalysts, which presented methanol productivities of 220 and 270 g MeOH kg_{cat}^{-1} h^{-1}. Nevertheless, the ZnZrIn catalyst of this work presented a lower methanol productivity of 206 g MeOH kg_{cat}^{-1} h^{-1}, possibly due to the lack of Cu and to the lower surface basicity of this catalyst. These results suggest that the presence of Cu in an In_2O_3 containing catalyst may be beneficial for the methanol productivity due to the improved H_2-splitting capacity, as explained before in the catalytic tests results section. Moreover, other metals such as Ni and Pd have been used together with In_2O_3, improving the catalytic activity and selectivity [76], so the use of other metals may also be beneficial and give a better catalytic performance. Figure 5.25 shows that the catalysts prepared in this work (i.e. CuZnZrIn and ZnZrIn) presented methanol productivity values close to those of other catalysts investigated in the literature. Also, as mentioned before, the conditions of the catalytic tests are different for each material, which makes difficult an appropriate comparison of their catalytic performance.

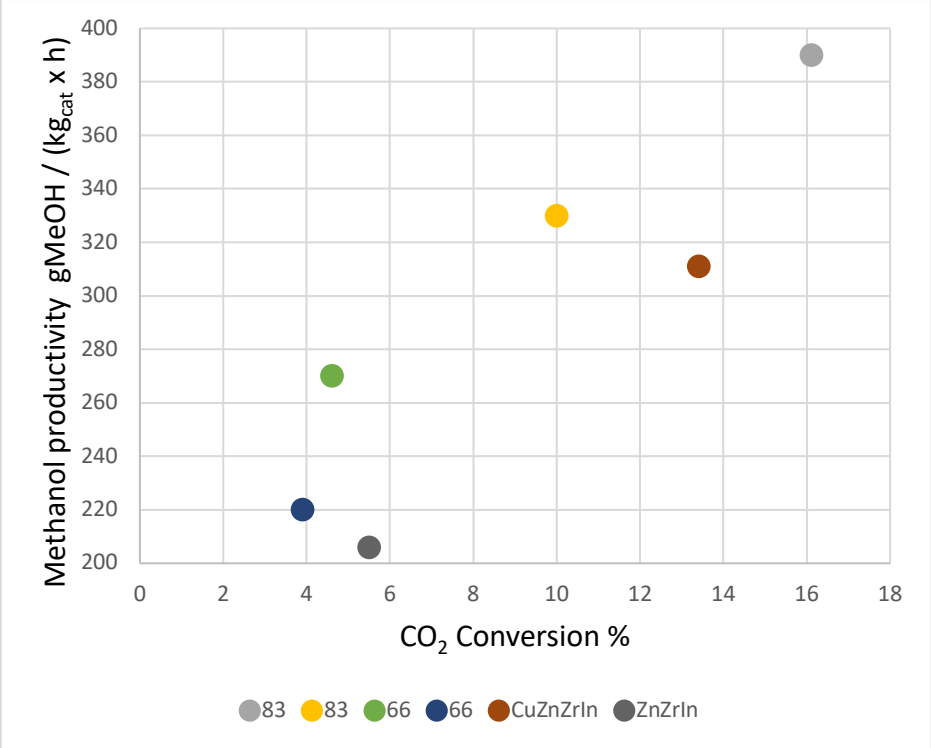

Figure 5.25 Methanol productivity vs. CO_2 conversion % for some of the catalysts included in Table 5.21. Each number corresponds to the reference of the work.

In summary, despite the difficulty in comparing the catalytic tests results done under different conditions and with different catalyst compositions, the CuZnZrIn and the ZnZrIn catalysts of this work presented methanol productivity values of the same order of magnitude of catalysts synthesized in other works. This investigation also showed that using small quantities of In_2O_3 as a promoter, as in the reference [78] can improve the catalytic activity.

5.4.5. Methanol productivity against the Cu surface area of the catalysts

Given the importance of the Cu surface area on the catalytic activity for the production of methanol, a graph of the methanol productivity against the Cu surface area was built. This is shown in Figure 5.26.

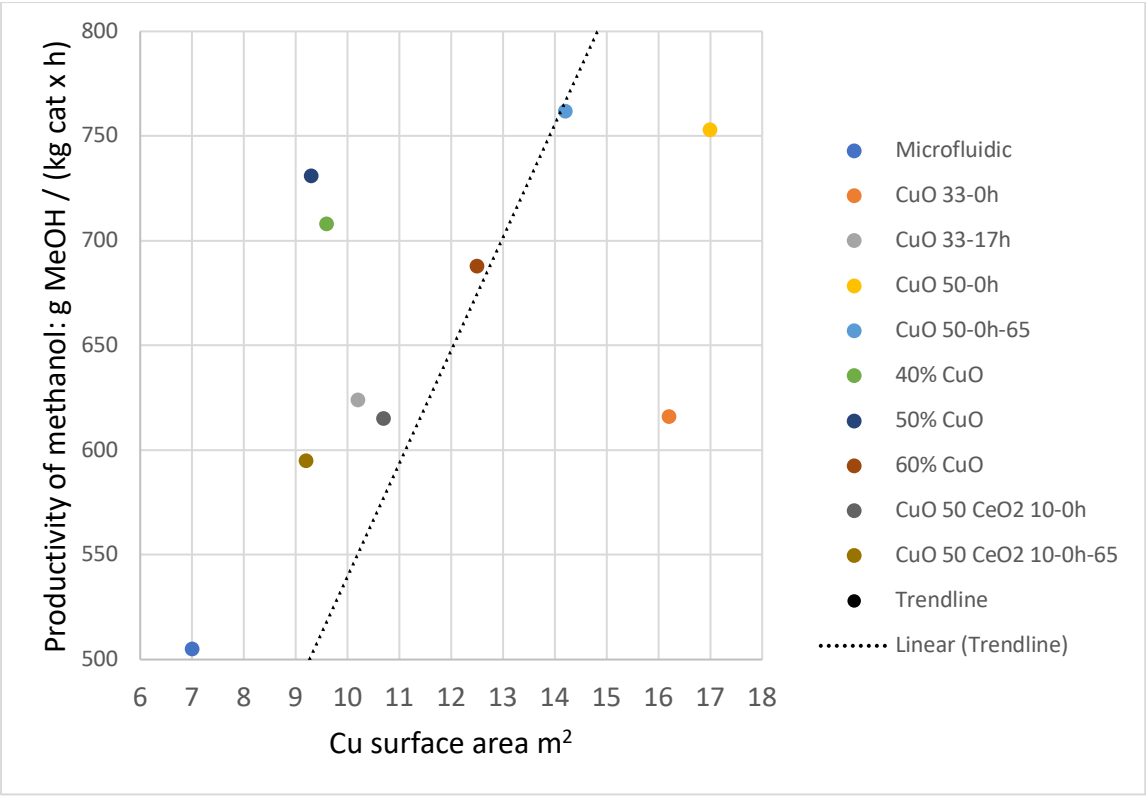

Figure 5.26 Methanol productivity against the Cu surface area at 280ºC.

The results show a correlation between the methanol productivity and the Cu surface area, where some catalysts were closer to the regression line (i.e. Microfluidic, CuO 33-17h, CuO 50-0h-65, 60% CuO, CuO 50 CeO_2 10-0h, CuO 50 CeO_2 10-0h-65), indicating a stronger correlation between these two parameters, while others deviated more importantly from it (i.e. CuO 33-0h, CuO 50-0h, 40% CuO, 50% CuO). The reason of the deviation from the trendline can be attributed to other parameters affecting the methanol productivity, such as the surface basicity, the presence and amount of oxygen vacancies, the metal-support interactions, among others. This means that the Cu surface area is important for the catalytic activity, but the abovementioned parameters are important as well. In the case of catalyst CuO 33-0h, many aspects influenced its catalytic activity besides the Cu surface area, such as the quantity of basic sites per unit surface area, the reducibility, the Cu particle size, among others, indicating a weaker dependence of the catalytic activity on the Cu surface area. In contrast, the catalyst 60% CuO was closer to the trendline, indicating a more important effect of the Cu surface area on the catalytic activity. In fact, this catalyst presented the highest CuO content of all the catalysts investigated, making the Cu surface area more important for its catalytic activity.

5.4.6. Conclusions

Two indium containing catalysts were synthesized by the microfluidic method with immediate filtration and heating of the precipitation zone to 65ºC to investigate their

physicochemical properties and their catalytic performance for the hydrogenation of CO_2 to methanol.

The characterization results show that the two investigated catalysts presented different physicochemical properties attributed to their different compositions. As shown before, the catalyst CuZnZrIn developed CuO and ZnO crystalline phases while the catalyst ZnZrIn developed only the ZnO crystalline phase. In contrast, In_2O_3 was present in both catalysts in an amorphous state, due to the low concentration of this metal or due to the low crystallization due to the synthesis conditions.

Regarding the results of the catalytic tests, it was shown that the CuZnZrIn catalyst presented a higher catalytic activity compared to the ZnZrIn catalyst, which may be due to the presence of copper, which serves as active sites for the H_2 splitting, due to the higher surface basicity of the catalyst and due to the higher specific surface area of the CuZnZrIn catalyst. Despite this, both In_2O_3 containing catalysts presented lower methanol productivities than the other catalysts prepared in this thesis. This suggests that the synthesis of In_2O_3 containing catalysts by the microfluidic method must be optimized in order to get to materials with more attractive properties and catalytic activity. Using the microfluidic technique with an aging step of the precipitates may be helpful to increase the crystallinity of In_2O_3 and to obtain catalysts with better catalytic performance. Moreover, according to the reviewed literature, the amorphous nature of In_2O_3 obtained in this work may be a factor that contributes to the lower catalytic performance presented by the two indium containing catalysts.

More investigations involving the use of higher In_2O_3 contents, longer aging times and the modification of the synthesis technique could help obtain catalysts with more interesting properties and superior catalytic activity. Also, the optimal synthesis and pretreatment conditions of In_2O_3 must be determined, to gain more knowledge about its properties as a catalyst and promoter and to improve the catalytic activity of In_2O_3 containing catalysts.

5.5. Bibliography of chapter 5

[1] T. Witoon, N. Kachaban, W. Donphai, P. Kidkhunthod, K. Faungnawakij, M. Chareonpanich, and J. Limtrakul, “Tuning of catalytic CO_2 hydrogenation by changing composition of CuO-ZnO-ZrO_2 catalysts,” *Energy Convers. Manag.*, vol. 118, pp. 21–31, 2016, doi: 10.1016/j.enconman.2016.03.075.

[2] K. Chang, T. Wang, and J. G. Chen, “Methanol Synthesis from CO_2 Hydrogenation over CuZnCeTi Mixed Oxide Catalysts,” *Ind. Eng. Chem. Res.*, vol. 58, no. 19, pp. 7922–7928, 2019, doi: 10.1021/acs.iecr.9b00554.

[3] V. L’hospital, L. Angelo, Y. Zimmermann, K. Parkhomenko, and A. C. Roger, “Influence of the Zn/Zr ratio in the support of a copper-based catalyst for the synthesis of methanol from CO_2,” *Catal. Today*, vol. 369, no. April 2020, pp. 95–104, 2021, doi: 10.1016/j.cattod.2020.05.018.

[4] M. Behrens, D. Brennecke, F. Girgsdies, S. Kißner, A. Trunschke, N. Nasrudin, S. Zakaria, N. F. Idris, S. B. A. Hamid, B. Kniep, R. Fischer, W. Busser, M. Muhler, and R. Schlögl, “Understanding the complexity of a catalyst synthesis: Co-precipitation of mixed Cu,Zn,Al hydroxycarbonate precursors for Cu/ZnO/Al_2O_3 catalysts investigated by titration experiments,” *Appl. Catal. A Gen.*, vol. 392, no. 1–2, pp. 93–102, 2011, doi: 10.1016/j.apcata.2010.10.031.

[5] Y. Ma, Q. Sun, D. Wu, W. H. Fan, Y. L. Zhang, and J. F. Deng, “A practical approach for the preparation of high activity Cu/ZnO/ZrO_2 catalyst for methanol synthesis from CO_2 hydrogenation,” *Appl. Catal. A Gen.*, vol. 171, no. 1, pp. 45–55, 1998, doi: 10.1016/S0926-860X(98)00079-9.

[6] R. Raudaskoski, M. V. Niemelä, and R. L. Keiski, “The effect of ageing time on co-precipitated Cu/ZnO/ZrO_2 catalysts used in methanol synthesis from CO_2 and H_2,” *Top. Catal.*, vol. 45, no. 1–4, pp. 57–60, 2007, doi: 10.1007/s11244-007-0240-9.

[7] C. Huang, S. Chen, X. Fei, D. Liu, and Y. Zhang, “Catalytic hydrogenation of CO_2 to methanol: Study of synergistic effect on adsorption properties of CO_2 and H_2 in CuO/ZnO/ZrO_2 system,” *Catalysts*, vol. 5, no. 4, pp. 1846–1861, 2015, doi: 10.3390/catal5041846.

[8] N. Mota, R. Guil-Lopez, B. G. Pawelec, J. L. G. Fierro, and R. M. Navarro, “Highly active Cu/ZnO-Al catalyst for methanol synthesis: Effect of aging on its structure and activity,” *RSC Adv.*, vol. 8, no. 37, pp. 20619–20629, 2018, doi: 10.1039/c8ra03291b.

[9] V. L’Hospital, “Développement et optimisation de catalyseurs à base de cuivre pour la synthèse de méthanol et de diméthyléther à partir de CO_2,” University of Strasbourg, 2018.

[10] V. Vágvölgyi, M. Hales, W. Martens, J. Kristóf, E. Horváth, and R. L. Frost, “Dynamic and controlled rate thermal analysis of hydrozincite and smithsonite,” *J. Therm. Anal. Calorim.*, vol. 92, no. 3, pp. 911–916, 2008, doi: 10.1007/s10973-007-8846-5.

[11] V. Vágvölgyi, A. Locke, M. Hales, J. Kristóf, R. L. Frost, E. Horváth, and W. N. Martens, “Mechanism for decomposition of aurichalcite-A controlled rate thermal analysis study,” *Thermochim. Acta*, vol. 468, no. 1–2, pp. 81–86, 2008, doi: 10.1016/j.tca.2007.11.024.

[12] T. Phongamwong, U. Chantaprasertporn, T. Witoon, T. Numpilai, Y. Poo-arporn, W. Limphirat, W. Donphai, P. Dittanet, M. Chareonpanich, and J. Limtrakul, “CO_2 hydrogenation to methanol over CuO–ZnO–ZrO_2–SiO_2 catalysts: Effects of SiO_2 contents,” *Chem. Eng. J.*, vol. 316, pp. 692–703, 2017, doi:

10.1016/j.cej.2017.02.010.
[13] N. Koga, J. M. Criado, and H. Tanaka, “Apparent kinetic behavior of the thermal decomposition of synthetic malachite,” *Thermochim. Acta*, vol. 340–341, pp. 387–394, 1999, doi: 10.1016/s0040-6031(99)00289-0.
[14] T. M. Yurieva, “Catalyst for methanol synthesis: Preparation and activation,” *React. Kinet. Catal. Lett.*, vol. 55, no. 2, pp. 513–521, 1995, doi: 10.1007/BF02073088.
[15] G. J. Millar, I. H. Holm, P. J. R. Uwins, and J. Drennan, “Characterization of precursors to methanol synthesis catalysts Cu/ZnO system,” *J. Chem. Soc. - Faraday Trans.*, vol. 94, no. 4, pp. 593–600, 1998, doi: 10.1039/a703954i.
[16] J. Xiao, D. Mao, X. Guo, and J. Yu, “Effect of TiO_2, ZrO_2, and TiO_2-ZrO_2 on the performance of CuO-ZnO catalyst for CO_2 hydrogenation to methanol,” *Appl. Surf. Sci.*, vol. 338, pp. 146–153, 2015, doi: 10.1016/j.apsusc.2015.02.122.
[17] I. W. M. Brown, K. J. D. Mackenzie, and G. J. Gainsford, “Thermal decomposition of the basic copper carbonates malachite and azurite,” *Thermochim. Acta*, vol. 75, no. 1–2, pp. 23–32, 1984, doi: 10.1016/0040-6031(84)85003-0.
[18] J. Gorzynski, *Organic Chemistry*, 3rd e. New York: McGraw-Hill Education, 2011.
[19] P. J. Smith, S. A. Kondrat, P. A. Chater, B. R. Yeo, G. M. Shaw, L. Lu, J. K. Bartley, S. H. Taylor, M. S. Spencer, C. J. Kiely, G. J. Kelly, C. W. Park, and G. J. Hutchings, “A new class of Cu/ZnO catalysts derived from zincian georgeite precursors prepared by co-precipitation,” *Chem. Sci.*, vol. 8, no. 3, pp. 2436–2447, 2017, doi: 10.1039/c6sc04130b.
[20] I. Abbas, H. Kim, C. H. Shin, S. Yoon, and K. D. Jung, “Differences in bifunctionality of ZnO and ZrO_2 in Cu/ZnO/ZrO_2/Al_2O_3 catalysts in hydrogenation of carbon oxides for methanol synthesis,” *Appl. Catal. B Environ.*, vol. 258, no. December 2018, 2019, doi: 10.1016/j.apcatb.2019.117971.
[21] D. Waller, D. Stirling, F. S. Stone, and M. S. Spencer, “Copper-zinc oxide catalysts: Activity in relation to precursor structure and morphology,” *Faraday Discuss. Chem. Soc.*, vol. 87, pp. 107–120, 1989, doi: 10.1039/DC9898700107.
[22] V. Deerattrakul, P. Dittanet, M. Sawangphruk, and P. Kongkachuichay, “CO_2 hydrogenation to methanol using Cu-Zn catalyst supported on reduced graphene oxide nanosheets,” *J. CO_2 Util.*, vol. 16, pp. 104–113, 2016, doi: 10.1016/j.jcou.2016.07.002.
[23] T. Witoon, T. Permsirivanich, W. Donphai, A. Jaree, and M. Chareonpanich, “CO_2 hydrogenation to methanol over Cu/ZnO nanocatalysts prepared via a chitosan-assisted co-precipitation method,” *Fuel Process. Technol.*, vol. 116, pp. 72–78, 2013, doi: 10.1016/j.fuproc.2013.04.024.
[24] A. Virdian, C. D. Satrya, E. Nurfani, and Y. Darma, “The effect of surface morphology in copper oxide nanostructure to photo detector characteristics,” *J. Phys. Conf. Ser.*, vol. 877, no. 1, 2017, doi: 10.1088/1742-6596/877/1/012024.
[25] M. Ahamed, H. A. Alhadlaq, M. A. M. Khan, P. Karuppiah, and N. A. Al-Dhabi, “Synthesis, Characterization, and Antimicrobial Activity of Copper Oxide Nanoparticles,” *J. Nanomater.*, vol. 2014, p. 637858, 2014, doi: 10.1155/2014/637858.
[26] I. Z. Luna, L. N. Hilary, A. M. S. Chowdhury, M. A. Gafur, N. Khan, and R. A. Khan, “Preparation and Characterization of Copper Oxide Nanoparticles Synthesized via Chemical Precipitation Method,” *OALib*, vol. 02, no. 03, pp. 1–8, 2015, doi: 10.4236/oalib.1101409.

[27] S. Jadhav, S. Gaikwad, M. Nimse, and A. Rajbhoj, “Copper Oxide Nanoparticles: Synthesis, Characterization and Their Antibacterial Activity,” *J. Clust. Sci.*, vol. 22, no. 2, pp. 121–129, 2011, doi: 10.1007/s10876-011-0349-7.
[28] L. Lin, G. Wang, and F. Zhao, “CO2 Hydrogenation to Methanol on ZnO/ZrO_2 Catalysts: Effects of Zirconia Phase,” *ChemistrySelect*, vol. 6, no. 9, pp. 2119–2125, 2021, doi: 10.1002/slct.202002108.
[29] M. Thommes, K. Kaneko, A. V. Neimark, J. P. Olivier, F. Rodriguez-Reinoso, J. Rouquerol, and K. S. W. Sing, “Physisorption of gases, with special reference to the evaluation of surface area and pore size distribution (IUPAC Technical Report),” *Pure Appl. Chem.*, vol. 87, no. 9–10, pp. 1051–1069, 2015, doi: 10.1515/pac-2014-1117.
[30] E. S. Borovinskaya, S. Trebbin, F. Alscher, and C. Breitkopf, “Synthesis, Modification, and Characterization of CuO/ZnO/ZrO_2 Mixed Metal Oxide Catalysts for CO_2/H_2 Conversion,” *Catalysts*, vol. 9, no. 12, p. 1037, Dec. 2019, doi: 10.3390/catal9121037.
[31] S. Navarro-Jaén, M. Virginie, J. Thuriot-Roukos, R. Wojcieszak, and A. Y. Khodakov, “Structure–performance correlations in the hybrid oxide-supported copper–zinc SAPO-34 catalysts for direct synthesis of dimethyl ether from CO_2,” *J. Mater. Sci.*, vol. 57, no. 5, pp. 3268–3279, 2022, doi: 10.1007/s10853-022-06890-w.
[32] F. C. F. Marcos, L. Lin, L. E. Betancourt, S. D. Senanayake, J. A. Rodriguez, J. M. Assaf, R. Giudici, and E. M. Assaf, “Insights into the methanol synthesis mechanism via CO_2 hydrogenation over Cu-ZnO-ZrO_2 catalysts: Effects of surfactant/Cu-Zn-Zr molar ratio,” *J. CO_2 Util.*, vol. 41, no. May, 2020, doi: 10.1016/j.jcou.2020.101215.
[33] H. Jeong, C. H. Cho, and T. H. Kim, “Effect of Zr and pH in the preparation of Cu/ZnO catalysts for the methanol synthesis by CO_2 hydrogenation,” *React. Kinet. Mech. Catal.*, vol. 106, no. 2, pp. 435–443, 2012, doi: 10.1007/s11144-012-0441-5.
[34] T. Witoon, J. Chalorngtham, P. Dumrongbunditkul, M. Chareonpanich, and J. Limtrakul, “CO_2 hydrogenation to methanol over Cu/ZrO_2 catalysts: Effects of zirconia phases,” *Chem. Eng. J.*, vol. 293, pp. 327–336, 2016, doi: 10.1016/j.cej.2016.02.069.
[35] W. Wang, Z. Qu, L. Song, and Q. Fu, “Effect of the nature of copper species on methanol synthesis from CO_2 hydrogenation reaction over CuO/$Ce_{0.4}Zr_{0.6}O_2$ catalyst,” *Mol. Catal.*, vol. 493, no. June, p. 111105, 2020, doi: 10.1016/j.mcat.2020.111105.
[36] S. Tada, S. Kayamori, T. Honma, H. Kamei, A. Nariyuki, K. Kon, T. Toyao, K. I. Shimizu, and S. Satokawa, “Design of Interfacial Sites between Cu and Amorphous ZrO_2 Dedicated to CO_2-to-Methanol Hydrogenation,” *ACS Catal.*, vol. 8, no. 9, pp. 7809–7819, 2018, doi: 10.1021/acscatal.8b01396.
[37] S. Dang, H. Yang, P. Gao, H. Wang, X. Li, W. Wei, and Y. Sun, “A review of research progress on heterogeneous catalysts for methanol synthesis from carbon dioxide hydrogenation,” *Catal. Today*, vol. 330, no. March 2018, pp. 61–75, 2019, doi: 10.1016/j.cattod.2018.04.021.
[38] B. Liang, J. Ma, X. Su, C. Yang, H. Duan, H. Zhou, S. Deng, L. Li, and Y. Huang, “Investigation on Deactivation of Cu/ZnO/Al_2O_3 Catalyst for CO_2 Hydrogenation to Methanol,” *Ind. Eng. Chem. Res.*, vol. 58, no. 21, pp. 9030–9037, 2019, doi: 10.1021/acs.iecr.9b01546.
[39] A. Pintar, J. Batista, and S. Hoevar, “TPR, TPO and TPD Examination of

$Cu_{0.15}Ce_{0.85}O_{2-y}$ Mixed Oxide Catalyst Prepared by Co-precipitation Synthesis," *Micromeritics*, vol. 2, pp. 1–4, 2011.

[40] B. Ouyang, W. Tan, and B. Liu, "Morphology effect of nanostructure ceria on the Cu/CeO_2 catalysts for synthesis of methanol from CO_2 hydrogenation," *Catal. Commun.*, vol. 95, pp. 36–39, 2017, doi: 10.1016/j.catcom.2017.03.005.

[41] L. Lin, S. Yao, Z. Liu, F. Zhang, N. Li, D. Vovchok, A. Martínez-Arias, R. Castañeda, J. Lin, S. D. Senanayake, D. Su, D. Ma, and J. A. Rodriguez, "In Situ Characterization of Cu/CeO_2 Nanocatalysts for CO_2 Hydrogenation: Morphological Effects of Nanostructured Ceria on the Catalytic Activity," *J. Phys. Chem. C*, vol. 122, no. 24, pp. 12934–12943, Jun. 2018, doi: 10.1021/acs.jpcc.8b03596.

[42] J. Zhong, X. Yang, Z. Wu, B. Liang, Y. Huang, and T. Zhang, "State of the art and perspectives in heterogeneous catalysis of CO_2 hydrogenation to methanol," *Chem. Soc. Rev.*, vol. 49, no. 5, pp. 1385–1413, 2020, doi: 10.1039/c9cs00614a.

[43] B. Yang, W. Deng, L. Guo, and T. Ishihara, "Copper-ceria solid solution with improved catalytic activity for hydrogenation of CO_2 to CH_3OH," *Chinese J. Catal.*, vol. 41, no. 9, pp. 1348–1359, 2020, doi: 10.1016/S1872-2067(20)63605-1.

[44] X. Jiang, X. Nie, X. Guo, C. Song, and J. G. Chen, "Recent Advances in Carbon Dioxide Hydrogenation to Methanol via Heterogeneous Catalysis," *Chem. Rev.*, vol. 120, no. 15, pp. 7984–8034, 2020, doi: 10.1021/acs.chemrev.9b00723.

[45] K. Chang, H. Zhang, M. J. Cheng, and Q. Lu, "Application of Ceria in CO_2 Conversion Catalysis," *ACS Catal.*, vol. 10, no. 1, pp. 613–631, 2020, doi: 10.1021/acscatal.9b03935.

[46] F. Heidari and A. Irankhah, "Effect of surfactants and digestion time on nano crystalline cerium oxide characteristics synthesized by differential precipitation," *Ceram. Int.*, vol. 40, no. 8 PART B, pp. 12655–12660, 2014, doi: 10.1016/j.ceramint.2014.04.112.

[47] P. Sripada, J. Kimpton, A. Barlow, T. Williams, S. Kandasamy, and S. Bhattacharya, "Investigating the dynamic structural changes on Cu/CeO_2 catalysts observed during CO_2 hydrogenation," *J. Catal.*, vol. 381, pp. 415–426, 2020, doi: 10.1016/j.jcat.2019.11.017.

[48] G. Bonura, F. Arena, G. Mezzatesta, C. Cannilla, L. Spadaro, and F. Frusteri, "Role of the ceria promoter and carrier on the functionality of Cu-based catalysts in the CO_2-to-methanol hydrogenation reaction," *Catal. Today*, vol. 171, no. 1, pp. 251–256, 2011, doi: 10.1016/j.cattod.2011.04.038.

[49] X. Hu, W. Qin, Q. Guan, and W. Li, "The Synergistic Effect of $CuZnCeO_x$ in Controlling the Formation of Methanol and CO from CO_2 Hydrogenation," *ChemCatChem*, vol. 10, no. 19, pp. 4438–4449, Oct. 2018, doi: 10.1002/cctc.201800668.

[50] R. Khobragade, M. Roškarič, G. Žerjav, M. Košiček, J. Zavašnik, N. Van de Velde, I. Jerman, N. N. Tušar, and A. Pintar, "Exploring the effect of morphology and surface properties of nanoshaped Pd/CeO_2 catalysts on CO_2 hydrogenation to methanol," *Appl. Catal. A Gen.*, vol. 627, no. September, 2021, doi: 10.1016/j.apcata.2021.118394.

[51] Z. Shi, Q. Tan, and D. Wu, "Ternary copper-cerium-zirconium mixed metal oxide catalyst for direct CO_2 hydrogenation to methanol," *Mater. Chem. Phys.*, vol. 219, no. July, pp. 263–272, 2018, doi: 10.1016/j.matchemphys.2018.08.038.

[52] R. Singh, K. Tripathi, and K. K. Pant, "Investigating the role of oxygen vacancies

and basic site density in tuning methanol selectivity over Cu/CeO_2 catalyst during CO_2 hydrogenation," *Fuel*, vol. 303, no. March, p. 121289, 2021, doi: 10.1016/j.fuel.2021.121289.

[53] N. J. Azhari, D. Erika, S. Mardiana, T. Ilmi, M. L. Gunawan, I. G. B. N. Makertihartha, and G. T. M. Kadja, "Methanol synthesis from CO_2: A mechanistic overview," *Results Eng.*, vol. 16, no. October, p. 100711, 2022, doi: 10.1016/j.rineng.2022.100711.

[54] M.-F. Luo, Y.-P. Song, J.-Q. Lu, X.-Y. Wang, and Z.-Y. Pu, "Identification of CuO Species in High Surface Area CuO−CeO_2 Catalysts and Their Catalytic Activities for CO Oxidation," *J. Phys. Chem. C*, vol. 111, no. 34, pp. 12686–12692, Aug. 2007, doi: 10.1021/jp0733217.

[55] S. Li, L. Guo, and T. Ishihara, "Hydrogenation of CO_2 to methanol over Cu/AlCeO catalyst," *Catal. Today*, vol. 339, no. July 2018, pp. 352–361, 2020, doi: 10.1016/j.cattod.2019.01.015.

[56] W. Wang, Z. Qu, L. Song, and Q. Fu, "CO_2 hydrogenation to methanol over Cu/CeO_2 and Cu/ZrO_2 catalysts: Tuning methanol selectivity via metal-support interaction," *J. Energy Chem.*, vol. 40, no. xxxx, pp. 22–30, 2020, doi: 10.1016/j.jechem.2019.03.001.

[57] Q. Tan, Z. Shi, and D. Wu, "CO_2 hydrogenation over differently morphological CeO_2-supported Cu-Ni catalysts," *Int. J. Energy Res.*, vol. 43, no. 10, pp. 5392–5404, 2019, doi: 10.1002/er.4636.

[58] J. Zhu, Y. Su, J. Chai, V. Muravev, N. Kosinov, and E. J. M. Hensen, "Mechanism and Nature of Active Sites for Methanol Synthesis from CO/CO_2 on Cu/CeO_2," *ACS Catal.*, vol. 10, no. 19, pp. 11532–11544, 2020, doi: 10.1021/acscatal.0c02909.

[59] Y. Nitta, O. Suwata, Y. Ikeda, Y. Okamoto, and T. Imanaka, "Copper-zirconia catalysts for methanol synthesis from carbon dioxide: Effect of ZnO addition to Cu-ZrO_2 catalysts," *Catal. Letters*, vol. 26, no. 3–4, pp. 345–354, 1994, doi: 10.1007/BF00810608.

[60] A. R. Richard and M. Fan, "Rare earth elements: Properties and applications to methanol synthesis catalysis via hydrogenation of carbon oxides," *J. Rare Earths*, vol. 36, no. 11, pp. 1127–1135, 2018, doi: 10.1016/j.jre.2018.02.012.

[61] L. G. A. van de Water, S. K. Wilkinson, R. A. P. Smith, and M. J. Watson, "Understanding methanol synthesis from CO/H_2 feeds over Cu/CeO_2 catalysts," *J. Catal.*, vol. 364, pp. 57–68, 2018, doi: 10.1016/j.jcat.2018.04.026.

[62] P. Gao, L. Zhang, S. Li, Z. Zhou, and Y. Sun, "Novel Heterogeneous Catalysts for CO_2 Hydrogenation to Liquid Fuels," *ACS Cent. Sci.*, vol. 6, no. 10, pp. 1657–1670, Oct. 2020, doi: 10.1021/acscentsci.0c00976.

[63] K. Stangeland, H. Li, and Z. Yu, "CO_2 hydrogenation to methanol: the structure–activity relationships of different catalyst systems," *Energy, Ecol. Environ.*, vol. 5, no. 4, pp. 272–285, 2020, doi: 10.1007/s40974-020-00156-4.

[64] F. Salomone, E. Sartoretti, S. Ballauri, M. Castellino, C. Novara, F. Giorgis, R. Pirone, and S. Bensaid, "CO_2 hydrogenation to methanol over Zr- and Ce-doped indium oxide," *Catal. Today*, vol. 423, no. January, p. 114023, 2023, doi: 10.1016/j.cattod.2023.01.030.

[65] S. K. Sharma, B. Paul, R. S. Pal, P. Bhanja, A. Banerjee, C. Samanta, and R. Bal, "Influence of Indium as a Promoter on the Stability and Selectivity of the Nanocrystalline Cu/CeO_2 Catalyst for CO_2 Hydrogenation to Methanol," *ACS Appl. Mater. Interfaces*, vol. 13, no. 24, pp. 28201–28213, 2021, doi: 10.1021/acsami.1c05586.

[66] M. S. Frei, C. Mondelli, A. Cesarini, F. Krumeich, R. Hauert, J. A. Stewart, D. Curulla Ferré, and J. Pérez-Ramírez, “Role of Zirconia in Indium Oxide-Catalyzed CO_2 Hydrogenation to Methanol,” *ACS Catal.*, vol. 10, no. 2, pp. 1133–1145, Jan. 2020, doi: 10.1021/acscatal.9b03305.

[67] P. Kampe, A. Wesner, P. Schühle, F. Hess, and J. Albert, “Effect of Conversion, Temperature and Feed Ratio on In_2O_3/$In(OH)_3$ Phase Transitions in Methanol Synthesis Catalysts: A Combined Experimental and Computational Study,” *Chempluschem*, vol. 88, no. 9, 2023, doi: 10.1002/cplu.202300425.

[68] Y. Liang, D. Mao, X. Guo, J. Yu, G. Wu, and Z. Ma, “Solvothermal preparation of CuO-ZnO-ZrO_2 catalysts for methanol synthesis via CO_2 hydrogenation,” *J. Taiwan Inst. Chem. Eng.*, vol. 121, pp. 81–91, 2021, doi: 10.1016/j.jtice.2021.03.049.

[69] M. Sadeghinia, M. Rezaei, A. Nemati Kharat, M. Namayandeh Jorabchi, B. Nematollahi, and F. Zareiekordshouli, “Effect of In_2O_3 on the structural properties and catalytic performance of the CuO/ZnO/Al_2O_3 catalyst in CO_2 and CO hydrogenation to methanol,” *Mol. Catal.*, vol. 484, no. January, p. 110776, 2020, doi: 10.1016/j.mcat.2020.110776.

[70] C. Y. Chou and R. F. Lobo, “Direct conversion of CO_2 into methanol over promoted indium oxide-based catalysts,” *Appl. Catal. A Gen.*, vol. 583, no. February, p. 117144, 2019, doi: 10.1016/j.apcata.2019.117144.

[71] C. Y. Regalado Vera, N. Manavi, Z. Zhou, L. C. Wang, W. Diao, S. Karakalos, B. Liu, K. J. Stowers, M. Zhou, H. Luo, and D. Ding, “Mechanistic understanding of support effect on the activity and selectivity of indium oxide catalysts for CO_2 hydrogenation,” *Chem. Eng. J.*, vol. 426, no. May, p. 131767, 2021, doi: 10.1016/j.cej.2021.131767.

[72] H. Schoeller and J. Cho, “Oxidation and reduction behavior of pure indium,” *J. Mater. Res.*, vol. 24, no. 2, pp. 386–393, 2009, doi: 10.1557/jmr.2009.0040.

[73] Z. Shi, Q. Tan, C. Tian, Y. Pan, X. Sun, J. Zhang, and D. Wu, “CO_2 hydrogenation to methanol over Cu-In intermetallic catalysts: Effect of reduction temperature,” *J. Catal.*, vol. 379, pp. 78–89, 2019, doi: 10.1016/j.jcat.2019.09.024.

[74] S. I. Fujita, M. Usui, and N. Takezawa, “Mechanism of the reverse water gas shift reaction over Cu/ZnO catalyst,” *J. Catal.*, vol. 134, no. 1, pp. 220–225, 1992, doi: 10.1016/0021-9517(92)90223-5.

[75] M. J. L. Ginés, A. J. Marchi, and C. R. Apesteguía, “Kinetic study of the reverse water-gas shift reaction over CuO/ZnO/Al_2O_3 catalysts,” *Appl. Catal. A Gen.*, vol. 154, no. 1–2, pp. 155–171, 1997, doi: 10.1016/S0926-860X(96)00369-9.

[76] J. Wang, G. Zhang, J. Zhu, X. Zhang, F. Ding, A. Zhang, X. Guo, and C. Song, “CO_2 Hydrogenation to Methanol over In_2O_3-Based Catalysts: From Mechanism to Catalyst Development,” *ACS Catal.*, vol. 11, no. 3, pp. 1406–1423, 2021, doi: 10.1021/acscatal.0c03665.

[77] J. Wang, C. Y. Liu, T. P. Senftle, J. Zhu, G. Zhang, X. Guo, and C. Song, “Variation in the In_2O_3 Crystal Phase Alters Catalytic Performance toward the Reverse Water Gas Shift Reaction,” *ACS Catal.*, vol. 10, no. 5, pp. 3264–3273, 2020, doi: 10.1021/acscatal.9b04239.

[78] K. Stangeland, H. H. Navarro, H. L. Huynh, W. M. Tucho, and Z. Yu, “Tuning the interfacial sites between copper and metal oxides (Zn, Zr, In) for CO_2 hydrogenation to methanol,” *Chem. Eng. Sci.*, vol. 238, p. 116603, 2021, doi: 10.1016/j.ces.2021.116603.

[79] M. S. Frei, M. Capdevila-Cortada, R. García-Muelas, C. Mondelli, N. López, J.

A. Stewart, D. Curulla Ferré, and J. Pérez-Ramírez, “Mechanism and microkinetics of methanol synthesis via CO_2 hydrogenation on indium oxide,” *J. Catal.*, vol. 361, pp. 313–321, 2018, doi: 10.1016/j.jcat.2018.03.014.

[80] G. Zhang, G. Fan, L. Yang, and F. Li, “Tuning surface-interface structures of ZrO_2 supported copper catalysts by in situ introduction of indium to promote CO_2 hydrogenation to methanol,” *Appl. Catal. A Gen.*, vol. 605, no. July, p. 117805, 2020, doi: 10.1016/j.apcata.2020.117805.

[81] A. Tsoukalou, A. I. Serykh, E. Willinger, A. Kierzkowska, P. M. Abdala, A. Fedorov, and C. R. Müller, “Hydrogen dissociation sites on indium-based ZrO_2-supported catalysts for hydrogenation of CO_2 to methanol,” *Catal. Today*, vol. 387, pp. 38–46, 2022, doi: 10.1016/j.cattod.2021.04.010.

[82] K. Stangeland, F. Chamssine, W. Fu, Z. Huang, X. Duan, and Z. Yu, “CO_2 hydrogenation to methanol over partially embedded Cu within Zn-Al oxide and the effect of indium,” *J. CO_2 Util.*, vol. 50, no. March, p. 101609, 2021, doi: 10.1016/j.jcou.2021.101609.

[83] G. Zhang, G. Fan, L. Yang, and F. Li, “Tuning surface-interface structures of ZrO_2 supported copper catalysts by in situ introduction of indium to promote CO_2 hydrogenation to methanol,” *Appl. Catal. A Gen.*, vol. 605, no. August, p. 117805, 2020, doi: 10.1016/j.apcata.2020.117805.

Chapter 6 General conclusions and perspectives

6.1. General conclusions and perspectives

In this research work the effects of different synthesis parameters on the properties and activity of Cu-ZnO-ZrO_2 catalysts for the synthesis of methanol were investigated. The synthesis parameters studied included the catalyst synthesis method (i.e. batch or microfluidic) and different variables involved in the microfluidic synthesis by coprecipitation, including the aging time, the coprecipitation temperature and the composition of the catalysts. The main objective of this work was to study the abovementioned synthesis parameters to optimize the microfluidic synthesis technique by coprecipitation and obtain catalysts with improved catalytic performance.

The characterization results and the catalytic tests showed that the catalyst synthesized by the microfluidic method presented a higher surface basicity, a more uniform copper particle size distribution and a higher copper surface area than the catalyst synthesized by the batch method, giving the catalyst synthesized by the microfluidic method superior conversions and methanol productivity per mass of catalyst. This catalyst also presented a higher density of basic sites per unit surface area, which indicates a higher affinity of this catalyst for CO_2.

Regarding the effect of aging time, it was found that it plays an important role in the development of crystalline phases and on other catalyst properties such as the specific surface area, the surface basicity, the reducibility, the Cu surface area and the Cu particle size. The catalyst CuO 33-0h prepared without any aging step presented a higher specific surface area, a higher surface basicity, a lower reduction temperature and a higher Cu surface area, which explains the superior results in terms of reactants conversions and methanol productivity of this catalyst. This catalyst also presented a higher concentration of basic sites per unit surface area of catalyst, suggesting the presence of more active sites for the CO_2 activation, and lower distances between active sites, causing an increase in the catalytic activity. The investigation of the coprecipitation temperature during the microfluidic synthesis by coprecipitation showed that carrying out the coprecipitation reaction at 65ºC during short contact times had a positive effect on the catalytic activity of the catalyst investigated, however, this effect was lost when applying this synthesis technique to a catalyst containing CeO_2.

Moreover, the composition of the catalysts was investigated by exploring the effects of different CuO contents and the effects of the use of CeO_2 and In_2O_3 on the catalyst properties and on the catalytic activity. It was found that the variation of the CuO content of the catalysts from a CuO content of 40% to a content of 60%, didn't affect greatly the crystallinity of the catalysts, but did have an effect on the morphology and the porosity of the catalysts. Higher contents of CuO caused an increase in the Cu surface area, which improved the reactants conversions and the methanol productivity.

In the case of ceria, it was found that the replacement of 10.2% of ZrO_2 of a Cu-ZnO-ZrO_2 catalyst by CeO_2 caused a decrease in the catalytic performance under the conditions of these experiments. This can be explained by the decrease of the specific surface area and Cu surface area caused by CeO_2. According to the obtained results and the reviewed literature, the amorphous state of the ceria may be a contributing factor to the lower performance of the catalysts, as different studies indicate that the morphology of CeO_2 has an important effect on its catalytic performance. A covering effect by CeO_2 of the Cu nanoparticles can also explain the decrease in the Cu surface area and the decrease of the catalytic activity of the CeO_2 containing catalysts. The microfluidic synthesis by coprecipitation and the use of CeO_2 as a catalyst component can be considered incompatible. However, modifying the microfluidic synthesis by allowing aging of the precursors could allow to obtain the promoting effects of CeO_2 that are reported in the literature.

Lastly, it was found that the addition of In_2O_3 to the Cu based catalysts didn't improve the properties and catalytic performance as was expected, probably due to the amorphous nature of the In_2O_3 and also due to the lower H_2 splitting capacity of In_2O_3 compared to that of metallic Cu. The catalytic performance of the catalyst containing In_2O_3 but no copper also presented a low catalytic performance explained possibly by the same reasons. Also, more studies about the activation of In_2O_3 before the CO_2 hydrogenation reaction could be useful to increase the promoting effects of this oxide.

In future works, a deeper study of the morphology and the crystalline structure of the catalysts synthesized by the microfluidic method employing transmission electron microscopy (TEM) would allow to understand better the differences with catalysts synthesized by other methods and the microscopic features of catalysts prepared without an aging step, like catalyst CuO 33-0h, which presented an excellent catalytic performance. Also, performing an elemental mapping of the microscopy images would allow to better understand the composition of the different structures developed on the surface of the catalysts. Moreover, doing H_2-TPD analysis to the catalysts of this work would allow to study the H_2 adsorption and desorption mechanisms with temperature, which could complement the results of the CO_2-TPD analysis used to characterize the mechanisms of adsorption of CO_2 on the catalysts surface. In addition, using the X-ray photoelectron spectroscopy (XPS) technique could allow to study more deeply the different interactions that could occur between the metal species, such as alloying, formation of intermetallic compounds, solid solutions, among others. This study would also benefit from the use of TEM. Finally, the study of the effects of the crystallinity of CeO_2 and In_2O_3 on the catalytic performance would be interesting and it would allow to find optimal catalyst compositions and optimal synthesis conditions for the coprecipitation by the microfluidic method.

Diego RUA GONZALEZ

Synthèse de matériaux catalytiques de type oxydes mixtes pour la production de méthanol par la précipitation en flux continu en système microfluidique

Résumé

Le réchauffement climatique est une préoccupation pour les générations actuelles et futures en raison de l'augmentation des émissions de gaz à effet de serre (GES) dans l'atmosphère, principalement dues à la dépendance aux combustibles fossiles. L'utilisation de carburants alternatifs tels que le méthanol durable produit à partir de H_2 renouvelable et de CO_2 contribuerait à réduire les émissions de GES et les effets du changement climatique. La synthèse du méthanol à partir de matières premières riches en CO_2 se fait préférentiellement en utilisant un catalyseur solide composé de CuO, ZnO et ZrO_2. Ce type de catalyseur peut être produit par coprécipitation des espèces métalliques à l'aide d'un dispositif microfluidique, avec des avantages qui ont été démontrés par rapport aux catalyseurs synthétisés par coprécipitation discontinue. Dans ce travail, différents catalyseurs pour l'hydrogénation du CO_2 en méthanol ont été synthétisés en utilisant la technique microfluidique dans différentes conditions, afin d'explorer différents paramètres de synthèse pouvant conduire au développement de catalyseurs plus actifs. Les différences de propriétés et d'activité entre un catalyseur synthétisé par la méthode microfluidique et un autre synthétisé par la méthode batch ont été étudiées, suivies d'une exploration des effets du temps de vieillissement et de la température de coprécipitation sur les catalyseurs. Enfin, l'effet de différentes compositions de catalyseurs sur les propriétés et l'activité a été déterminé, en étudiant différentes teneurs en CuO, l'utilisation de CeO_2 comme promoteur et l'utilisation de In_2O_3 comme promoteur et comme métal actif.

Mots clés: Méthanol, valorisation du CO_2, coprécipitation, méthode microfluidique, catalyseurs solides, conditions de synthèse, composition, performances catalytiques.

Abstract

Global warming is a concern for the current and future generations due to the increasing greenhouse gases (GHG) emissions to the atmosphere, mainly due to the dependence on fossil fuels. The use of alternative fuels such as sustainable methanol produced from renewable H_2 and from CO_2 would contribute to reduce the GHG emissions and the effects of climate change. The synthesis of methanol using CO_2 rich feedstock is preferentially done by using a solid catalyst composed of CuO, ZnO and ZrO_2. This type of catalyst can be produced by coprecipitation of the metal species using a microfluidic device, with advantages that have been demonstrated over catalysts synthesized by batch coprecipitation. In this work, different catalysts for the hydrogenation of CO_2 to methanol were synthesized using the microfluidic technique under different conditions, in order to explore different synthesis parameters that could lead to the development of more active catalysts. The differences in the properties and activity between a catalyst synthesized by the microfluidic method and another synthesized by the batch method were investigated, followed by an exploration of the effects of the aging time and the coprecipitation temperature on the catalysts. Lastly, the effect of different compositions of catalysts on the properties and activity were determined, by investigating different CuO contents, the use of CeO_2 as a catalyst promoter, and the use of In_2O_3 as a catalyst promoter and as active metal.

Keywords: Methanol, CO_2 valorization, coprecipitation, microfluidic method, solid catalysts, synthesis conditions, composition, catalytic performance.